Platinum- and Palladium-Based Single-Atom Alloy Catalysts for Selective Hydrogenation and Dehydrogenation Reactions

A dissertation submitted by

Jilei Liu

in partial fulfillment of the requirements for the degree of

Doctor of Philosophy

in

Chemical Engineering

Tufts University

May 2018

Advisor:

Maria Flytzani-Stephanopoulos, Ph.D.

Abstract

Approximately 80% of all chemical, materials and fuel production in the modern industry use heterogeneous catalysts during some phases in the process. Platinum group metals, especially Pt or Pd are often used in heterogeneous catalysts but susceptible to unselective reactivity, deactivation, and poisoning. The industrial Pt and Pd catalysts, although very successful in many cases, are basically "black boxes" without well controlled structural and compositional properties. Different additives are used to modify the metal nanoparticle catalysts on the support to form the multiple metallic catalysts with high precious metal loading. Some toxic poisons, such as Pb or V, are often used to improve the selectivity of these catalysts. Due to these drawbacks, a rational catalyst design approach to make Pt and Pd catalysts more efficient and cleaner is of great interest.

The major challenges in Pt and Pd catalysts are their high price, unselective reactivity, carbon deposition and CO poisoning. This thesis addresses these problems with a novel *single-atom alloy* approach, where isolated Pt atoms, stabilized in Cu nanoparticle surface, are identified as the active sites for key elementary reactions. The Pt metal was predesigned with minimum atomic ensembles and loaded in the surface of cheaper metal nanoparticles to achieve the best possible selectivity, stability and reactivity and reduced concentration of precious metals. This class of single-atom alloy catalysts were applied in catalyzing industrially important selective hydrogenation and dehydrogenation reactions and thoroughly studied for their surface chemistry and structural and compositional properties.

Pt-Cu single-atom alloy nanoparticle catalysts were prepared with the galvanic replacement method and supported on alumina and silica. With comprehensive characterization, the formation of single-atom alloy nanoparticles was for the first time demonstrated in the field. This class of catalysts showed excellent performance in selective hydrogenation of 1,3-butadiene, selective dehydrogenation of butane and CO tolerant hydrogen activation reactions. By depositing a small amount of Pt single-atoms in the surface of Cu nanoparticles, the reactivity in selective hydrogenation and dehydrogenation reactions is improved more than one order of magnitude. Notably, close to 100% selectivity to desired partial hydrogenation and dehydrogenation products are also achieved. The PtCu single-atom alloy catalysts are stable in reaction conditions without carbon deposition or sintering.

In these processes, the single-atom Pt is efficient in catalyzing key elementary reactions including H_2 dissociation and C-H activation, while the highly selective nature of Cu remains unaffected. The energy barriers of these elementary reaction steps are significantly lowered with the single-atom Pt sites. But single-atom Pt sites bind CO and the product molecules weakly compared to monometallic Pt nanoparticles, which results in CO tolerance and high selectivity.

The suitability of the single-atom approach in PdAu catalysts was also studied. The PdAu single-atom alloy nanoparticle catalysts were successfully synthesized with sequential reduction methods and demonstrated to be highly selective, stable and reactive in partial hydrogenation of 1-hexyne in the liquid phase.

This thesis work uses an integrated approach, including catalyst preparation, advanced characterization, catalyst evaluation under realistic conditions. Collaborative surface science information and DFT calculations complement the catalyst. This provides the platform materials that bridge the materials gap between catalysis and surface science studies. Moreover, it highlights a rational catalyst design approach to optimize the catalytic performance at the single-atom limit.

Acknowledgements

"A journey of a thousand miles begins with a single step."

-Tao Te Ching, 500 B.C.

My graduate study at Tufts would not have been so enjoyable and productive without the mentors, teachers, co-workers, collaborators, friends and family I have had the pleasure of working or living with. I am very grateful to all of them.

First, I would like to express my deep appreciation to my advisor, Prof. Maria Flytzani-Stephanopoulos, for offering me the opportunity to engage in this lab and for being an outstanding mentor and teacher. The reason I came to Tufts University was to work with her. Six years ago, I knocked on her door with no experience on heterogeneous catalysis but just the passion to explore. She accepted me to the lab and gave me the time to learn. Professor Flytzani-Stephanopoulos inspired me with brilliant ideas and taught me to incorporate creative thinking in my research. Her perspective on identifying and addressing important problems is critical to my PhD study. I highly cherish her guidance and advice that would always serve as inspiration for the personal and professional development in my life. It has been my great privilege and pleasure working with a P.I. with so much passion and enthusiasm for research and holding such a high standard for work ethic.

Professor Charles Sykes is a great mentor and collaborator who played an important role in my PhD research, for which I am truly grateful. I gained the critical fundamental chemistry insight through collaborating with him. I benefited a lot from his

unbelievable understanding of chemical and physical phenomena on surfaces in the last five years.

I would also like to thank Professor Terry Haas. The collaboration with him on XAS and XRD data analysis has been essential. I owe a great deal to my committee for providing critical insight into my work. Professor Charles Sykes, Professor Terry Haas, Professor Chia-Kuang (Frank) Tsung and Professor Matthew Panzer helped me a lot with their expertise in chemical engineering, chemistry and heterogeneous catalysis, and have given me valuable feedbacks. I want to thank Professor Howard Saltsburg for his valuable critique and comments on my early work.

I have been lucky to work with many exceptional graduate students during my PhD. I would like to thank Dr. Ioannis Valsamakis and Dr. Matthew Boucher for teaching and training me with the catalyst techniques when I joined the group. Dr. Ming Yang has been the model of hard working and critical thinking that has become a strong motivating force. Dr. Felicia Lucci, Dr. Matthew Marcinkowski, Dr. Andrew Therrien, Matthew Uhlman, Matthew Darby and Dr. Matthew Montemore were key to the collaboration with Sykes, Stamatakis and Kaxiras labs. I had the privilege of working with many great lab mates: Dr. Branko Zugic, Dr. Chongyang Wang, Dr. Junjun Shan, Mengwei Li, Sufeng Cao, Georgios Giannakakis, Dr. Antonios Trimpalis, Joshua Wimble, George Cladaras, Matthew Rutter, Dr. Nan Yi, Mengyao Ouyang, Yuan Wang. Without them, NCEL would not have been be such as a pleasant place to work in.

Many thanks to my undergraduate and high school students, Tingyi Dong, Nicholas Cicchetti, Ahmad Sukkar, Karen Li and Wesley Viola. Great appreciation to Beth

Frasso, Margaret DeChiaro and Emily Edward, whose tireless behind the scenes effort kept my research going smoothly.

Last, but foremost I want to thank my wife, Jin and my little daughter, my parents and in-laws. Thank you for being my support through the process, being the cheerleader when I felt difficult to carry on and being the most enthusiastic audiences for every little progress. I love you all.

Table of Contents

1. Chapter 1. Introduction 1
   1.1 Heterogeneous catalysis 1
   1.2 Selective hydrogenation of alkynes and dienes to alkenes 2
      1.2.1 Selective hydrogenation catalysts 3
      1.2.2 Hydrogenation reactions with Pd and Pt catalysts 4
      1.2.3 Pt and Pd based bimetallic catalysts for selective hydrogenation 8
      1.2.4 Selective hydrogenation on non Pd or Pt catalysts 15
   1.3 CO tolerant Pt catalysts 16
   1.4 Selective dehydrogenation of light alkanes 18
      1.4.1 Alkane to alkene processes 18
      1.4.2 Catalytic selective dehydrogenation reactions 19
      1.4.3 Pt alloy catalysts for selective dehydrogenation 21
   1.5 Thesis objectives: 23
      1.5.1 Specific aim 1 24
      1.5.2 Specific aim 2 26
      1.5.3 Specific aim 3 27
      1.5.4 Specific aim 4 27
   1.6 References 28
2. Chapter 2 Experimental methods and procedures 56
   2.1 Catalyst preparation 56
      2.1.1 Materials and Chemicals 56
      2.1.2 Pt-Cu catalysts 56
      2.1.3 Pd-Au catalysts 57
   2.2 Catalyst characterization and activity measurements 58
      2.2.1 Catalyst characterization 58
         2.2.1.1 Surface Area 58
         2.2.1.2 High-resolution transmission electron microscopy (HR-TEM) 59
         2.2.1.3 Materials compositions 59
         2.2.1.4 Ultraviolet and visible light (UV-Vis) absorption spectroscopy 59
         2.2.1.5 X-ray photoelectron spectroscopy (XPS) 60
         2.2.1.6 X-ray powder diffraction (XRD) 60

2.2.1.7 X-ray absorption spectroscopy (XAS) 60
2.2.1.8 Scanning transmission electron microscopy (STEM) 61
2.2.1.9 Fourier-transformed infrared spectroscopy (FTIR) 61
2.2.2 Catalytic activity measurements 62
2.2.2.1 Flow reactor studies 62
2.2.2.2 Batch reactor studies 65
2.3 References 66
3. Chapter 3. PtCu single-atom alloy nanoparticle catalysts for selective hydrogenation of 1,3-butadiene 67
3.1 Introduction 67
3.2 Experimental methods 68
3.3 Results and Discussion 70
3.3.1 Characterization of PtCu NP catalysts 70
3.3.2 Selective hydrogenation of 1,3-butadiene 82
3.4 Collaboration: surface science studies on Pt-Cu(111) SAAs 92
3.6 Summary 92
3.7 References 94
4. Chapter 4. Tackling CO poisoning with single-atom alloy catalysts 98
4.1 Introduction 98
4.2 Experimental methods 99
4.3 Results and Discussion 100
4.3 Collaboration: CO-TPD and STM on Pt-Cu(111) SAA 114
4.4 Summary 115
4.4 References 115
5. Chapter 5. PtCu single-atom alloy catalysts for coke resistant C-H activation and selective dehydrogenation of n-butane 120
5.1 Introduction 120
5.2 Experimental methods 121
5.3 Results and discussion 123
5.4 Collaboration: surface science and DFT studies on the C-H activation over PtCu SAA catalysts 142
5.5 Summary 143
5.6 References 144

6. Chapter 6. PdAu single-atom alloy catalysts for selective hydrogenation of 1-hexyne to 1-hexene 152
6.1 Introduction 152
6.2 Experimental methods 155
6.2.1 Catalyst Synthesis 155
6.2.2 Catalyst characterization 156
6.2.3 H_2-D_2 exchange 157
6.2.4 Partial hydrogenation of 1-hexyne 157
6.3 Results and discussion 158
6.4 Summary 193
6.5 References 194
7. Chapter 7. Conclusions and Recommendations 205
7.1 Conclusions 205
7.2 Recommendations 209

List of Figures

Figure 1.1. STM images of SAAs of PtAu(111), PdAu(111), PtCu(111) and PdCu(111)[135]. 15
Figure 1.2. Equilibrium conversion of C2−C4 paraffins to olefins as a function of temperature at 1 bar (left) and pressure dependence of the dehydrogenation of propane as a function of temperature (right).[155] 19
Figure 3.1. (A) TEM images of unsupported Cu NPs, inset is particle size distribution (scale bar=50 nm). (B) TEM image of ϒ-Al_2O_3 supported Cu NPs (calcined). 71
Figure 3.2. (A) HR-TEM images of supported Cu NPS. (B) An enlarged region from (A)..... 72
Figure 3.3. UV-Vis spectra of $PtCl_6^{2-}$ standards compared to the filtrate from GR preparation of $Pt_{0.1}Cu_{14}/Al_2O_3$..... 73
Figure 3.4. (A) STEM image and elemental mapping (EDS) of $Pt_{0.1}Cu_{14}/Al_2O_3$. (B) Al, (C) O, (D) Cu and (E) Pt maps obtained from the same region on the sample. 75
Figure 3.5. *In situ* Pt L_{III} EXAFS of selected samples and Pt foil plotted in k space..... 76
Figure 3.6. Characterization of Pt/Cu SAA NPs. (A-D) HAADF-STEM images with (C) colored intensity map from selected region, and (E) EXAFS k^3 – weighted Fourier transforms. (A, D) typical regions of the sample $Pt_{0.1}Cu_{14}/Al_2O$, showing Cu metal particles with isolated Pt atoms. Isolated Pt atoms are highlighted by red arrows. The lattice spacing of Cu(111) is 0.21 nm. (B) Enlarged image and (c) colorized intensity map of highlighted region showing isolated Pt atoms. (E) EXAFS data was collected *in situ* at Pt-L_{III} edge at room temperature from Pt foil, $Pt_{0.1}Cu_{14}/Al_2O_3$, $Pt_{0.2}Cu_{12}/Al_2O_3$ and Pt_2Cu_6/Al_2O_3. 78
Figure 3.7. Typical HAADF-STEM images of $Pt_{0.1}Cu_{14}/Al_2O_3$. The samples were pre-reduced in H_2 at 350 °C. Isolated Pt atoms are highlighted by white circles. 79
Figure 3.8. XRD analysis of selected samples including a fresh and $Pt_{0.2}Cu_{12}/Al_2O_3$ used for butadiene hydrogenation. All catalysts, except the sample used in the hydrogenation reaction, were reduced in H_2 prior to XRD. (Cu JCPDS No. 85-1326, Cu_3Pt JCPDS No. 65-3247, CuPt JCPDS No. 48-1549)..... 80
Figure 3.9. Normalized *in situ* XANES spectra of selected samples collected at room temperature in H_2 (except where otherwise noted). The Pt/Cu samples were pre-reduced in H_2 at 350 °C *in situ*, while the $Pt_{0.1}/Al_2O_3$ was pre-reduced in H_2 at 400 °C *in situ.* 81
Figure 3.10. Selective hydrogenation of butadiene as a function of temperature over Cu_{15}/Al_2O_3, $Pt_{0.1}Cu_{14}/Al_2O_3$, and $Pt_{0.2}Cu_{12}/Al_2O_3$ NPs (1,3-butadiene (1.25 %), H_2 (20 %) and He (balance), GHSV=1,200 h^{-1}). 83
Figure 3.11. Conversion and product yields in the selective hydrogenation of butadiene corresponding to Figure 6. (0.4 g catalyst, flow rate = 20 mL/min; 1, 3-butadiene (1.25 %), H_2 (20 %) and He (balance), GHSV=1,200 h^{-1}.) 84
Figure 3.12. Long-time hydrogenation steady-state activity test over $Pt_{0.1}Cu_{14}/Al_2O_3$ at 160 °C. (~ 0.1 g catalyst, flow rate = 50 mL/min. 2% 1, 3-butadiene, 20% H_2 and balance He. GHSV=12,000 h^{-1}. Conversion of butadiene in one hour is around 98 %)..... 85
Figure 3.13. Selective hydrogenation of butadiene as a function of temperature over $Pt_{0.1}Cu_{14}/Al_2O_3$. (0.1 g catalyst, flow rate = 50 mL/min. 2 % 1,3-butadiene, 20 % H_2 and balance He. GHSV=12,000 h^{-1}) (A) Conversion of butadiene and selectivity to butene with increasing and decreasing temperature ramps. (B) Conversion of butadiene in cyclic hydrogenation

experiments, the catalysts were treated in H_2 at 350 °C between each cycle. The conversion of the first cycle is shown in (A). 87
Figure 3.14. Butadiene conversion in the presence of excess propylene. Conversion and selectivity in long-time steady state selective hydrogenation of butadiene at 160 and 145 °C (~ 0.1 g catalyst $Pt_{0.1}Cu_{14}/Al_2O_3$, flow rate = 50 mL/min. 2 % 1, 3-butadiene, 20 % propylene, 16 % H_2 and balance He. GHSV=12,000 h^{-1}). 88
Figure 3.15. Conversion and selectivity in the selective hydrogenation of butadiene over $Pt_{0.1}Cu_{14}/Al_2O_3$ as a function of temperature. (~ 0.1 g catalyst, flow rate = 50 mL/min. 2 % 1, 3-butadiene, 20 % propylene, 16 % H_2 and balance He. GHSV=12,000 h^{-1}). 89
Figure 3.16. TPO profile of spent $Pt_{0.1}Cu_{14}/Al_2O_3$ catalyst used for the long-time activity test in (a) 2 % 1, 3-butadiene, 20 % propylene, 16 % H_2 and balanced He for around 48 h; (b) 2 % 1, 3-butadiene, 20 % H_2 and balanced He for around 30 h. (TPO condition: 20 % O_2/He, 50 mL/min, 3 °C/min) Scale bar corresponds to 0.05 % CO_2 in the gas stream. 91
Figure 4.1. Fourier transform of k^3-weighted Pt L_{III} EXAFS of Pt foil and $Pt_{0.008}$Cu-SAA in CO and H_2 gases mixture plotted in R-space. 102
Figure 4.2. IR spectra in the carbonyl range of pre-reduced Pt-NP. 104
Figure 4.3. IR spectra in the carbonyl range of pre-reduced $Pt_{0.39}$Cu-bimetallic. 105
Figure 4.4. IR spectra in the carbonyl range of pre-reduced $Pt_{0.008}$Cu-SAA. 107
Figure 4.5. IR spectra in the carbonyl range of pre-reduced (A) $Pt_{0.008}$Cu-SAA and (B) Cu-NP. .. 107
Figure 4.6. Temperature effects on IR intensity of the linearly adsorbed CO on Pt sites of (A) $Pt_{0.008}$Cu-SAA, (B) $Pt_{0.39}$Cu-bimetallic and (C) Pt-NP. The vertical axis is the ratio of the peak absorbance at the given temperature to the peak absorbance at 25 °C. The peak vibrational frequency of each carbonyl is (A) 2088 cm^{-1}, (B) 2045-2031 cm^{-1} and (C) 2033-2018 cm^{-1}. 108
Figure 4.7. Isothermal H_2-D_2 exchange over Pt-NP (A, B, C) and $Pt_{0.008}$Cu-SAA (D, E, F) at 120, 150 and 200 °C. CO was turned on and off during the experiments. Gas composition: 33% H_2, 33% D_2, 3.3% CO, balance Argon. Total flow rate=50 mL/min. 90 mg catalysts. 111
Figure 4.8. H_2-D_2 exchange as a function of temperature. Gas composition: 33% H_2, 33% D_2, 667ppm CO (A), or 3.3% CO (B) balance Argon. Total flow rate=50 mL/min. 80 mg catalysts. .. 112
Figure 4.9. Ratio of retained reaction rate of acetylene hydrogenation in CO over $Pt_{0.008}$Cu-SAA and Pt-NP at different temperatures. Rate retained = reaction rate with CO/rate without CO in the reaction gas. Gas composition: 20% H_2, 2.2% C_2H_2, 200 ppm CO, 10% Argon, balance He. 114
Figure 5.1. FTIR spectra of chemisorbed CO molecule on $Pt_{0.01}$Cu-SAA catalyst. The time values on the graph indicate the time of helium gas purge after CO exposure. 125
Figure 5.2. FTIR spectra of chemisorbed CO molecule on the $Pt_{0.03}$Cu-SAA catalyst. The time values on the graph indicate the time of helium gas purge after CO exposure. 126
Figure 5.3. *In situ* Pt L_{III} EXAFS of (a) $Pt_{0.01}$Cu-SAA, (b) $Pt_{0.03}$Cu-SAA and (c) Pt foil plotted in k space. 127
Figure 5.4. Fourier transform of k^3-weighted Pt L_{III} EXAFS of (a) $Pt_{0.01}$Cu-SAA, (b) $Pt_{0.03}$Cu-SAA and (c) Pt foil plotted in R space. 128
Figure 5.5. Reactor studies of B-D scrambling. TPSR data for the B-D scrambling reaction over $Pt_{0.03}$Cu-SAA, $Pt_{0.01}$Cu-SAA and Cu-NP catalysts, followed by mass spectrometry. (Temperature ramp 5 °C/min). The 59/58 mass ratio indicates the C_4H_9D level. The data are from the second reaction cycle. Gas composition: 5% butane, 2% deuterium and balance argon. 50 mL/min, 100 mg catalysts. 129

Figure 5.6. Temperature programmed surface reaction data for the B-D scrambling reaction over Cu-NP catalyst. 130
Figure 5.7. Reactor studies of B-D scrambling. TPSR data for the B-D scrambling reaction over Pt-NP catalysts, followed by mass spectrometry. (Temperature ramp 5 °C/min). The 59/58 mass ratio indicates the C_4H_9D level. First, second and third cycles of TPSR are shown. Gas composition: 5% butane, 2% deuterium and balance argon. 50 mL/min, 100 mg catalysts..... 131
Figure 5.8. Reactor studies of B-D scrambling. 12-hour stability test for the $Pt_{0.01}Cu$-SAA catalyst at 360 °C. The catalyst was at room temperature at the beginning and end of the test. Gas composition: 5% butane, 2% deuterium and balance argon. 50 mL/min, 100 mg catalysts..... 132
Figure 5.9. Determination of carbon deposition**.** Temperature programmed oxidation (TPO) of (a) Pt-NP, (b) $Pt_{0.012}Cu$-SAA and (c) silica. (a) and (b) were treated in butane-D2 exchange reaction condition at 360 °C for 12 hours. (a), (b) and (c) were treated in argon flow at 300 °C for 2 hours before TPO to desorb the hydrocarbon adsorbates. 133
Figure 5.10. B-D scrambling rate as a function of Pt loading in the catalysts. Gas composition: 5% butane, 2% deuterium and balance argon. 50 mL/min, 100 mg catalysts..... 134
Figure 5.11. Reactor studies of B-D scrambling. TPSR data for the B-D scrambling reaction over $Pt_{0.39}Cu$ followed by mass spectrometry. (5 °C/min) Gas composition: 5% butane, 2% deuterium and balance argon. 50 mL/min, 100 mg sample. 135
Figure 5.12. Arrhenius- type plot. The reaction rate of butane dehydrogenation was measured between 450 and 390 °C with conversion below 10%. Reaction condition: 2.5% butane, 5% H_2, bal. He. 50 mL/min, 30-80 mg sample. 137
Figure 5.13. Long-term butane dehydrogenation reaction over $Pt_{0.01}Cu$-SAA catalyst. Reaction condition: 2.5% butane, 5% H_2, bal. He. 50 mL/min, 0.1 g catalysts, 400 °C. 138
Figure 5.14. Comparing the degree of coking in Pt NP vs PtCu SAA catalysts. Temperature–programmed-oxidation (TPO) of (a) Pt-NP and (b) $Pt_{0.01}Cu$-SAA. (a) and (b) are spent catalysts after butane dehydrogenation reaction. (a) and (b) were treated in a He flow at 300 °C for 1 h before TPO to desorb the hydrocarbon adsorbates. TPO conditions: 10% O_2/N_2, 50 mL/min, 3 °C/min, 100 mg sample. 139
Figure 5.15. TEM images and particle size distribution (insets) of (a) fresh $Pt_{0.01}Cu$-SAA and (b) spent $Pt_{0.01}Cu$-SAA after butane dehydrogenation reaction at 400 °C. 140
Figure 5.16. FTIR spectra of chemisorbed CO molecule on the used the $Pt_{0.01}Cu$-SAA. The time values on the graph indicate the time of helium gas purge after CO exposure. 141
Figure 5.17. FTIR spectra of chemisorbed CO molecule on the used $Pt_{0.03}Cu$-SAA catalyst. The time values on the graph indicate the time of helium gas purge after CO exposure. 142
Figure 6.1. (a) Photograph of PdAu-SAA NP solution. (b, d) TEM images and (c) particle size distribution of PdAu-SAA NPs..... 159
Figure 6.2. Powder XRD of PdAu-SAA/SiO_2. 160
Figure 6.3. Dark field STEM image and Au and Pd EDX maps of PdAu-SAA..... 161
Figure 6.4. Powder XRD of PdAu samples with different Pd/Au ratios..... 162
Figure 6.5. ATR-IR spectra of the CO stretch on Pd-NP, Au-NP and PdAu-SAA samples. Spectra were collected at 30 °C with pure CO flowing in the gas phase for Au-NP and PdAu-SAA. The spectra for Pd-NP were collected in H_2/He (20%) gas after CO adsorption..... 163
Figure 6.6. Leaching test: 1-hexene/1-hexyne ratio as a function of time. The liquid phase was separated from the reaction mixture after 6-hour reaction. Fresh 1-hexyne was injected and the

typical hydrogenation reaction conditions used in this work were applied. (5 bar H_2, 600 rpm, 25 ^oC) The 1-hexene/1-hexyne ratio is plotted here. No conversion of 1-hexyne was observed. .. 164
Figure 6.7. Time-resolved batch reactor data for the hydrogenation of 1-hexyne over (a) 10 wt% Pd/C catalysts and (b) PdAu-SAA/SiO_2 catalysts. (c) selectivity to 1-hexene as a function of conversion. Reaction condition: 1% hexyne-ethanol solution, 5 bar H_2, 600 rpm, 25 ^oC. Same 1-hexyne/Pd ratio was used for hydrogenation reaction with 10wt% Pd/C and PdAu-SAA/SiO_2.. 165
Figure 6.8. Initial reaction rate of hydrogenation of 1-hexyne normalized by amount of surface Pd. (Batch reactor, 1% 1-hexyne-ethanol solution, 5 Bar H_2, 600 rpm, 25 ^oC)..... 167
Figure 6.9. Time- resolved batch reactor data of partial hydrogenation of 1-hexyne to hexene over PdAu-SAA/SiO_2 catalysts. 1% hexyne-ethanol solution, 5 bar H_2, 600 rpm, 70 ^oC..... 168
Figure 6.10. Stability test for PdAu-SAA/SiO_2 catalyst. The reaction rate of hydrogenation of 1-hexyne (bars) and selectivity to 1-hexene at 50% conversion (squares) was compared between the first, second and third cycles. (Batch reactor, 1% Hexyne-ethanol solution, 5 bar H_2, 600 rpm, 25 ^oC. ~3h each cycle)..... 169
Figure 6.11. (a, c) TEM image and (b) particle size distribution of used PdAu-SAA NPs..... 170
Figure 6.12. Characterization of used PdAu-SAA/SiO_2 catalysts. (a) XRD, (b) XPS and (c) CO-DRIFTS. The tests were performed on spent catalysts without further treatment at ambient temperature. 172
Figure 6.13. XPS of $Pd_{0.2}Au$ bimetallic catalysts. 173
Figure 6.14. DRIFTS spectra recorded when 1-hexyne and H_2 are carried over PdAu-SAA/SiO_2 catalyst. 174
Figure 6.15. DRIFTS spectra between 3130 and 3120 cm^{-1} recorded when 1-hexyne and H_2 are carried over PdAu-SAA/SiO_2 catalyst..... 175
Figure 6.16. IR spectra of liquid 1-hexyne collected with ATR accessory. 176
Figure 6.17. DRIFTS spectra between 3800 and 3450 cm^{-1} recorded when 1-hexyne and H_2 are carried over PdAu-SAA/SiO_2 catalyst..... 177
Figure 6.18. DRIFTS spectra between 3450 and 2000 cm^{-1} recorded when 1-hexyne and H_2 are carried over silica..... 178
Figure 6.19. DRIFTS spectra between (A) 3800 and 3450 cm^{-1} and (B) 3360 and 3250 cm^{-1} recorded when 1-hexyne and H_2 are carried over silica. 179
Figure 6.20. ATR-IR collected with 1-hexyne and 120 psi H_2 applied on $Pd_{0.004}Au$-SAA catalysts in the batch mode at room temperature. 180
Figure 6.21. ATR-IR collected with 1-hexyne and 120 psi H_2 applied on $Pd_{0.004}Au$-SAA catalysts in the batch mode at room temperature. 180
Figure 6.22. ATR-IR collected with 1-hexyne and 120 psi H_2 applied on $Pd_{0.01}Au$ catalysts in the batch mode at room temperature. 181
Figure 6.23. ATR-IR collected with 1-hexyne and 120 psi H_2 applied on $Pd_{0.2}Au$ catalysts in the batch mode at room temperature. 182
Figure 6.24. 1-hexyne adsorption isotherm at 30 and 60 °C. 183
Figure 6.25. Hydrogenation of 1-hexyne. (A) Reaction rate of PdAu-SAA/SiO_2 and Au/SiO_2. Reaction condition: 1% hexyne-ethanol solution, 5 bar H_2, 600 rpm, 25 ^oC. (B) H_2-D_2 exchange TPSR of PdAu-SAA/SiO_2 and Au/SiO_2 catalysts. H_2-D_2 exchange: 10% H_2, 10% D_2, balance Argon, 50 mL/min, 5 °C/min. 184

Figure 6.26. 1-hexyne hydrogenation reaction rate and the selectivity to 1-hexene at 100% conversion of 1-hexyne with Pd-NP (5% Pd/SiO_2) and PdAu-SAA/SiO_2 catalysts. Reaction condition: 1% hexyne-ethanol solution, 5 bar H_2, 600 rpm, 25 ^oC. 185
Figure 6.27. Arrhenius type plot of 1-hexyne selective hydrogenation over 5% Pd/SiO_2 and PdAu-SAA/SiO_2 catalysts. Reaction conditions: 1% hexyne-ethanol solution, 5 bar H_2, 600 rpm, 6-70 ^oC. 186
Figure 6.28. KIE measurements. The conversion vs. reaction time for 1-hexyne hydrogenation with PdAu-SAA/SiO_2 catalysts. The initial rate is calculated from the slope of the conversion-time curve. Reaction condition: 1% hexyne-ethanol solution, 5 bar H_2 or D_2, 600 rpm, 25 ^oC. 187
Figure 6.29. Reaction order to H_2 and 1-hexyne. (A) The reaction rate was measured with 1% 1-hexyne and 3-7.5 bar H_2, 600 rpm, 25 ^oC. (B) The reaction rate was measured with 0.5-1.5% 1-hexyne, 5 bar H_2, 600 rpm, 25 ^oC..... 188
Figure 6.30. Arrhenius type plot of H_2-D_2 exchange over PdAu-SAA/SiO_2 catalysts. The RGA intensity of HD is corrected background signal and is proportional to the concentration of HD. Reaction condition: H_2-D_2 exchange: 10% H_2, 10% D_2, balance Argon, 50 mL/min, 170-110 ^oC. 189
Figure 6.31. Reaction rate ratio of 1-hexyne hydrogenation over 1-hexene hydrogenation of PdAu-SAA/SiO_2 and Pd/SiO_2 catalysts. Reaction condition: 1% hexane -or hexene-ethanol solution, 5 bar H_2, 600 rpm, 25 ^oC. 191
Figure 6.32. Arrhenius type plot of 1-hexene hydrogenation over PdAu-SAA/SiO_2 catalysts. Reaction condition: 1% hexene-ethanol solution, 5 bar H_2, 600 rpm. 192

Chapter 1. Introduction

1.1 Heterogeneous catalysis

Catalysts are the substances that increase the rate of chemical reactions and maintain their physical and chemical properties in reaction conditions. Approximately 90% of all chemical, materials and fuel production in the modern industry use catalysts during some phases in the process. The majority of these processes (~ 85%) use a heterogeneous catalyst, where the catalysts are in the solid phase and the reactants are in the liquid or gas phases.[1] The heterogeneous catalysts are complex in their makeup and the specific role of each component in the reaction conditions. Understanding the structure-function relationships have been the focus of a large portion of the ongoing research in heterogeneous catalysis.[2] The multidisciplinary collaboration of ambient/above ambient pressure catalysis studies with surface science and DFT techniques is a powerful approach to fill this gap.[3]

The major motivation of understanding the structure-function relationships in heterogeneous catalysis is to guide the rational design of the catalysts. Catalysts with high activity, selectivity and durability are always desired. Catalysis is called to address the new challenges caused by the rapid development of human society. For example, the fast growth of the middle-class population in the world make the chemical processes that are more efficient, cleaner and environmentally benign more and more attractive, which requires the catalysts to be highly selective to target products and can be used in not too severe conditions.[4,5] Additionally, the emerging “hydrogen economy” requires efficient fuel cells, which makes the

development of high performance and CO- tolerant fuel cell catalysts crucial. Moreover, the recent “shale gas boom” has put catalysts for coke resistant C-H activation and conversion into the center of the stage. For these cases, the selectivity in forming desired products is very important, if not the most important, as pointed out by Somorjai and McCrea 16 years ago[5]: “In the past, the focus of research in catalysis science was activity to optimize turnover rates. In the future, selectivity to form the desired product without the formation of byproducts will be the major research challenge.”

1.2 Selective hydrogenation of alkynes and dienes to alkenes

Selective hydrogenations lie in the heart of chemical industry. They are the key reactions in the production of bulk feed stocks for the polymer industry and the production of fine and specialty chemicals including food additives, pharmaceuticals, fragrances and agrochemicals. Specifically, the selective hydrogenation of alkyne and dienes to alkenes is important for the polymer industry. The alkene feedstock produced from cracking processes usually consists 1-8% highly unsaturated hydrocarbons, such as alkynes and dienes. However, the alkyne and diene concentration should be reduced to ppm level to avoid poisoning the polymerization catalysts. One attractive approach is to selectively hydrogenate these molecules to alkenes without further converting alkenes to alkanes.

1.2.1 Selective hydrogenation catalysts

Selective hydrogenations of both double and triple carbon-carbon bonds are important for a wide range of industrial processes. Pd, Pt, Ni, and Ru based systems are commonly employed for hydrogenation of alkenes and alkynes due to their high catalytic activity.[6–8] However, they are not always selective to the desired products. Among these metals, Pd and Pt are the most selective, but typically exhibit a decrease in alkene selectivity with alkyne conversion. Therefore, Pd and Pt catalysts are commonly used with promoters to improve alkene selectivity; transition metals such as Ag, Rh, Au, Cu, Zn, Cr, and V have been reported to be effective selectivity promoters.[9]

Industrial selective hydrogenation reactions are carried out on Pd- based catalysts with additives. For gas phase selective hydrogenation, Pd is alloyed with Au, Cu or Ag to improve the selectivity and durability and is supported on low-acidic support to avoid side reactions. For liquid phase selective hydrogenation, Pd is modified with Pb or Bi to form the Lindlar catalyst.[10] To further improve the selectivity, CO or quinoline are mixed with the reactant in many processes. However, the wide use of Pd in the catalyst significantly increases the cost and the lead additives draw environmental concerns. New designs of Pt and Pd catalysts with high catalytic performance and minimal usage of precious Pt group metals are highly desired.

Pd and Pt have been extensively studied looking at reaction mechanisms, active intermediates, effect of nanoparticle size, effect of carbon deposits, effect of forming alloys with another metal, effect of additives, etc.[6,11] In recent years, group IB metals Au and Cu, especially Au, have received attention for selective hydrogenation and were found to be very selective. However, they are much less active than group VIII metals in hydrogenation, lacking

in the activation of hydrogen.[11–14] Even though Pd and Pt show high selectivity in hydrogenation, their selectivity is suppressed in the presence of excess alkenes, which are present under industrial hydrogenation conditions. Take butadiene hydrogenation for instance, in order to improve the selectivity, people have been investigating the hydrogenation activity and selectivity of bimetallic group VIII – IB metals, including Pd-Cu, Pd-Ag, Pd-Au, Pt-Cu, Pt-Au, etc.[15–18] The change of the hydrogenation chemistry was attributed to the limited hydrogen chemisorption capability of the bimetallic catalysts, the change in adsorption strength of reactants and intermediates caused by electronic effects, and ensemble effects. [15–20]

1.2.2 Hydrogenation reactions with Pd and Pt catalysts

The general reaction pathway of alkynes and diene hydrogenation is shown in scheme 1.1. The selectivity to alkenes is attributed to their relatively weak adsorption on the catalyst surface ($k_1/k_{-1} >> k_3/k_{-3}$). The well-known Horiuti-Polanyi mechanism assumes the hydrogenation of di-σ-bonded alkenes takes place in two steps through an adsorbed half-hydrogenated alkyl intermediate with atomic hydrogen.[21] Years later, Cremer and Somorjai suggested that π-bonded and di-σ-bonded species co-exist on Pt (111) and the hydrogenation through π-bonded alkenes was dominant.[22,23] With development of *in situ* and *in operando* techniques including IR, ^{14}C labeling and NMR, evidence emerged to suggest a hydrocarbon fragment layer is formed on the Pt surface after hydrocarbon exposure.[24–26] The previous model of a molecule on clean Pt surface is too simple compared to the real case. The experimental results suggested that adsorbed hydrocarbons were involved in the

hydrogenation through transferring hydrogen to the adsorbed alkenes.[27] In recent years, the role of hydrocarbon fragments has been debated.[28] It is generally believed now that adsorbed hydrocarbons do not directly participate in the hydrogenation reactions but act as site blockers.[28–30] However, the adsorbed hydrocarbons have a significant effect on the hydrogenation reactions. It is found that the hydrogenation activity can be significantly enhanced when the alkylidyne layer is removed.[31] The type of hydrocarbon molecules is also a factor that can influence the hydrogenation activity. Testing the hydrogenation of ethylene with different adsorbed hydrocarbon species, Zaera and coworkers identified the trend of hydrogenation activity as alkylidyne > benzyl > C_nH > graphite.[32] Under ethylene hydrogenation condition, the alkylidyne surface coverage is in the sub-saturation regime.[33] The reaction is through a stepwise hydrogen addition pathway with adsorbed ethylene. Utilizing deuterium and hydrogen in ethylene hydrogenation reactions, Zaera and coworkers identified a second reaction pathway which might involve a "reverse" Eley–Rideal step by which gas-phase ethylene reacts with two deuterium atoms adsorbed on adjacent sites of the platinum surface.[34]

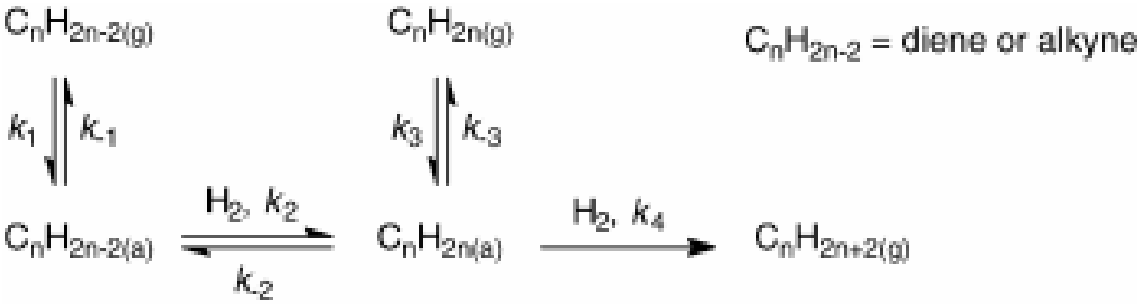

Scheme 1.1.

For the selective hydrogenation of butadiene, the butadiene molecules bind onto the catalytic surface more strongly than alkenes.[35,36] The kinetics of hydrogenation of butadiene on Pd show negative reaction order with respect to butadiene. [35,36] Butadiene hydrogenation can occur through 1, 2 or 1, 4 additions to yield 1-butene or 2-butenes, respectively. Joice and coworkers proposed a butadiene hydrogenation mechanism through π-allyl, as shown in scheme 1.2.[37] They associated the variance in the yield of 1-butene and 2-butenes with relative stability of 1-methyl-2-allyl intermediates, as cis-isomer formed from *intermediate a* and trans-isomer formed from *intermediate b*.

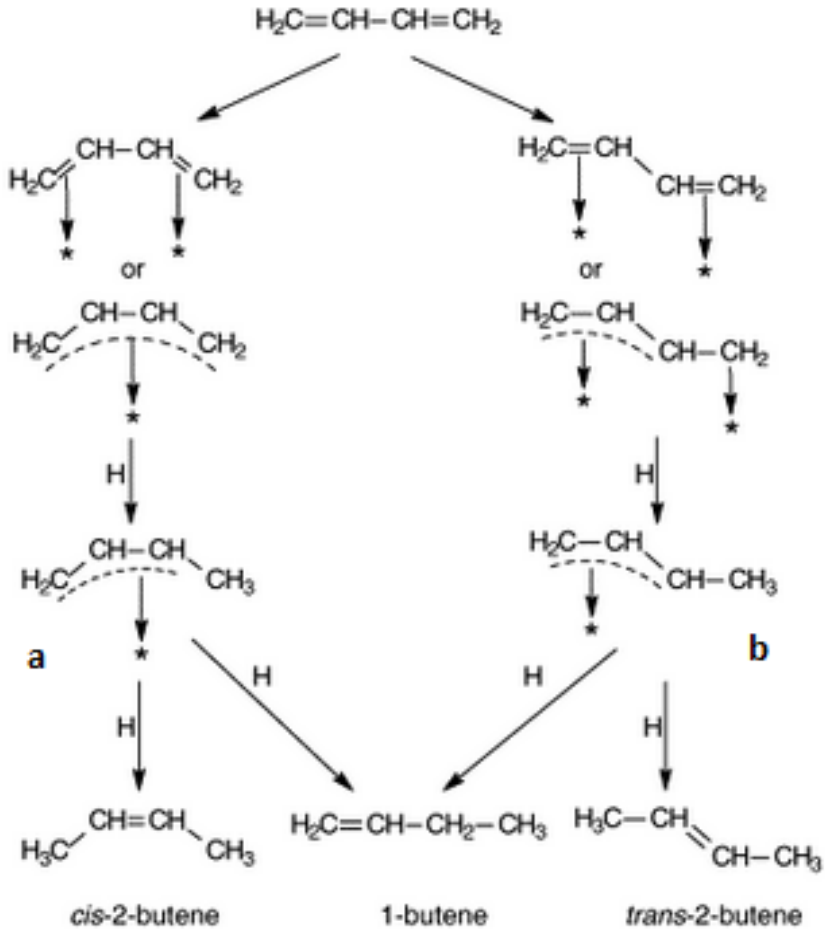

Scheme 1.2.

In order to explain the direct formation of butane and its correlation with 2-butenes, Boitiaux and coworkers proposed another butadiene hydrogenation mechanism that involves carbene formation.[38] They suggested that metals that do not favor carbene formation will not allow direct hydrogenation of butadiene. Moreover, Nishimura and coworkers proposed a hydrogenation mechanism with only one double bond associated with the surface to account for the low yield to 2-butenes in hydrogenation of butadiene on Cu.[36]

Pd and Pt catalysts are poisoned by the adsorbed hydrocarbons at the reaction conditions. When the Pd and Pt surfaces are exposed to hydrocarbon and hydrogen molecules, the dissociative adsorption and polymerization of the unsaturated hydrocarbons lead to a carbonaceous layer on the metal surface.[39–41] Moreover, surface carbides are formed with the dissolution of carbon in the metal lattices.[42] The metal carbides formed in the reaction condition result in higher selectivity and lower reactivity through poisoning. Moreover, hydrogen atoms can dissolve in Pd and Pt metal to form hydrides. Hydrogen activation on these metals is facile under ambient conditions. The hydrides, especially the beta hydrides in Pd, contribute to the full hydrogenation of alkynes to alkanes. In the low hydrogen partial pressure regime, the hydride formation is avoided but the carbon deposition becomes a problem.

Ni catalysts are also known for their high catalytic activity in hydrogenation reactions and relatively low cost. Raney nickel is widely used in the industrial hydrogenation processes. However, additives such as Cr are needed to improve its selectivity in partial hydrogenation

reactions. Recently, NiZn has been identified as a promising selective acetylene hydrogenation catalyst, which will be discussed in this chapter.

1.2.3 Pt and Pd based bimetallic catalysts for selective hydrogenation

The modification of Pd and Pt with another metal has been examined extensively for the selective hydrogenation of alkynes and dienes. Through electronic and ensemble effects, the bimetallic alloys of Pt and Pd modify the hydrogen activation and molecule adsorption to reduce the undesired reactions. The additive metals studied include Ag, Au, Bi, Cu, Ga, Sn and Zn.[43] Pd-Ag and Pd-Pb catalysts are applied in the commercial selective hydrogenation processes. In these systems, Pt and Pd are still the bulk phases. The ensemble sizes have been reduced in alloys but they are typically small domains greater than single atoms.

One approach to improve the selectivity of Pt and Pd catalysts is through the partial poisoning of the active sites. The Lindlar catalyst is a notable example, in which Pd is modified with Pb additives and supported on calcium carbonates. It shows high selectivity to the partial hydrogenation products and cis-isomers of alkenes. However, the high use of Pd in the catalyst significantly increases the cost and the Pb additives draw environmental concerns. Pd-Bi and Pd-Sn catalysts were investigated as non-lead alternatives to Lindlar catalysts.[44,45] Bi and Pd can form stable alloy phase as PdBi or $PdBi_2$.[46] Bi was believed to partially poison the most active low-coordinated Pd atoms in the catalysts and disperse the Pd ensembles.[44,45,47] So the Pd-Bi catalysts showed high selectivity to alkenes and low alkane formation. However, Anderson and coworkers found that Pd-Bi was less selective in 2-hexyne hydrogenation compared to 1-hexyne

hydrogenation.[45] Similarly, the Pd-Sn is more selective than monometallic Pd catalysts in 1,3-butadiene hydrogenation to butene. Through the addition of Sn, Pd domains were broken by Sn ensembles which reduces the beta Pd-H formation.[48–50] The dilution of Pd also likely leads to lower hydrogen and hydrocarbon adsorption strength on the catalytic surfaces.[51] Overall, the Pd-Sn showed lower reactivity and higher selectivity compared to Pd catalysts.

Another class of Pd and Pt alloys is with additives such as Cu, Ag, Au, Ga and Zn. In these alloys, significant electronic effects induce decreased binding energy of alkynes and alkenes and lessen the formation of beta Pd-H. Pd-Ag alloy is the active phase in industrial acetylene selective hydrogenation catalysts[52,53], so the Pd-Ag system is one of the most studied catalysts for selective hydrogenation[54–58]. Unlike monometallic Pd, beta Pd-H and subsurface carbon are not formed in Pd-Ag catalysts.[55] On bare Pd surface, adsorbed ethylidyne partially poisons the catalysts and leads to higher selectivity. The Ag ensembles have similar effects. They reduce the availability of hydrogen and weaken the adsorption of alkenes, leading to high selectivity .[56,59]

The Pd-Ga and Pd-Zn catalysts have also been studied for their improved selectivity to partial hydrogenation products. Ga and Zn break the Pd domains and induce changes in the electronic properties of Pd, both of which favor the selective hydrogenation over the over hydrogenation.[60] Moreover, intermetallic Pd-Zn nanoparticles (NPs) were formulated and used in selective hydrogenation reactions.[61,62] DFT calculations suggest the Pd-Zn intermetallic surface binds ethylene through pi-bonding on the single Pd sites.[62]

Cu based alloys

Cu is relatively inert compared to Pt or Pd for hydrogenation reactions. This is because of its higher hydrogen activation barrier. However, Cu is intrinsically very selective in the partial hydrogenation reactions.[63] Pt-Cu and Pd-Cu alloys were used to improve the selectivity of Pd and Pt catalysts in selective hydrogenation reactions.

A variety of hydrogenation reactions catalyzed by Pd-Cu have been studied.[64–67] By adding 30% Cu to the Pd/Al_2O_3 catalysts, Leviness et al. found Pd-Cu catalysts had higher selectivity to ethylene but lower activity in hydrogenation of acetylene. This was attributed to the ensemble effects that lower the adsorption strength of ethylene molecules and decrease the formation of Pd-H.[64] Guzzi et al. investigated the hydrogenation of phenylacetylene and 1-butene with Pd-Cu catalysts supported on pumice. They correlated the high selectivity of Pd-Cu in partial hydrogenation of phenylacetylene to the electronic effect with the presence of CuOx, while the fully reduced Pd-Cu catalyze the isomerization of 1-butene.[66]

The electron transfer between Cu and Pd (or Pt) largely affects the hydrogenation chemistry of Pd (or Pt). Through theoretical calculation, Fernandez-Garcia et al. identified the charge transfer between Pd and Cu in Pd_8Cu_{92} (111) and $Pd_{40}Cu_{60}$(111) surfaces and found surface Pd atoms are negatively charged.[68,69] This has been debated in the literature. Skoda et al. suggest there is no significant charge transfer based on the CO-FTIR results.[65] However, other researchers have used Auger spectroscopy[70,71], CO chemisorption[71] and XPS[72] to show there is charge transfer on both Cu and Pd, which affets the binding strength of molecules.

Pt-Cu has been synthesized and studied for the selective hydrogenation of alkynes, hydrogenolysis of pentane, hydrogenation of acrylonitrile and hydrodechlorination of 1,2-dichloroethane.[73–77] Chen and coworkers have studied the alkene and alkyne hydrogenation on Pt-Cu, Pt-Fe, Pt-Co and Pt-Ni catalysts with ambient pressure catalysis studies, surface science techniques and DFT calculations.[78–82] Pt-Ni, Pt-Co and Pt-Fe show better activity compared to monometallic Pt, which is due to the weaker binding of H atoms and hydrocarbon molecules on the bimetallic surfaces compared to Pt.[80] This is mainly an electronic effect as subsurface Pt-Ni-Pt catalysts showed even higher hydrogenation activity.[80,81] Pt-Cu also binds H and hydrocarbon molecules more weakly than Pt, but shows lower activity than Pt-Ni, Pt-Co and Pt-Fe.[78,79,82] A flow reactor study of 1,3-butadiene hydrogenation was performed with these catalysts, finding Pt-Cu has the lowest reactivity but highest selectivity to butenes.[82] This suggests Pt-Cu might be a candidate for selective hydrogenation reactions. However, more understanding of Pt-Cu catalysts is needed for rational catalyst design.

The ensemble effects in bimetallic catalysts can have considerable influence on their catalytic behavior and efforts have been made to study the surface structure of Pt-Cu alloys. Lucci et al. examined the Pt-Cu surfaces with sub-monolayer Pt coverage with variable temperature STM and identified a few metastable surface structures at different Pt coverages.[83] At low Pt coverage (0.01 and 0.03 monolayer), isolated Pt atoms are uniformly distributed on the Cu(111) terraces and populated with higher density in the vicinity of step edges. When more Pt (0.1ML) is deposited into the Cu(111) surface, finger-like protrusions were observed near step edges.[83] And at even higher Pt loadings, 3D islands were formed on the Cu surface.[84]

Au based alloys

Gold, like copper, is a group I metal, and is well known for its selective hydrogenation activity.[85–89] High selectivity to ethylene at 100% acetylene conversion were reported for Au/Al_2O_3[85] and Au/TiO_2[89] catalysts, while the catalytic activity was correlated with Au particle size. Lopez-Sanchez and co-workers reported that the Au/TiO_2 catalysts were totally selective to propene in propyne hydrogenation with progressive deactivation.[13] More than 95% selectivity to butene was also demonstrated for the hydrogenation of 2-butyne catalyzed by Au/Al_2O_3 and Au/SiO_2.[87] The results of DFT simulations suggested that the highly selective character of Au NPs catalysts was related to the preferential adsorption of carbon-carbon triple bonds on the edge of Au NPs, while the binding energy of carbon-carbon double bonds on Au was lower which leads to lower surface coverage.[90] However, the hydrogen dissociation ability of Au is limited, due to its full d-band.[91]

Bimetallic Pd-Au catalysts were employed to improve the selectivity of Pd in selective hydrogenation reactions. Louis and coworkers have prepared Pd-Au catalysts with different methods including co-deposition-precipitation, co-impregnation in excess of solution, colloids stabilized by polyvinyl alcohol (PVA) and colloids stabilized by tetrakis(hydroxypropyl) phosphonium chloride and studied their performance in hydrogenation of 1,3-butadiene to butenes.[92,93] They found the selectivity of the catalysts was correlated with the distribution of Pd in the Au surface and the Pd/Au ratio. With CO-IR techniques, they demonstrated that Pd atoms can be mostly atomically dispersed in Au surface when the Pd/Au ratio is smaller than

1/20. At this condition, the selectivity of the catalysts is optimum. In other work on PdAu catalysts for selective hydrogenation reactions, Zhang et al.[94], Szumelda et al.[95], and Pei et al.[96] drew similar conclusion, namely, that the best possible selectivity is achieved when the size of Pd ensembles is the smallest. Varied approaches were used to obtain different Pd distributions; Szumelda et al. and Pei et al. changed the Pd/Au ratio in catalysts supported on carbon and silica, while Zhang et al. used different pretreatment methods. Recently, Xu et al. studied the structural rearrangement of Pd-Au nanoparticles in different atmospheres with DFT calculations[97]. They found Pd atoms could be stabilized in the surface of PdAu when hydrogen was present.

Bimetallic PdAu materials of various compositions have been studied extensively for a number of reactions, including selective oxidation[98–101], selective hydrogenation[16,102–108], the Ullmann reaction[109], vinyl acetate synthesis[110], formic acid decomposition[111], and the direct synthesis of hydrogen peroxide[112–114]. Generally, it is difficult to elucidate the roles of Pd and Au in the catalytic cycles and their alloying effects due to the presence of many Pd and Au ensembles on the catalyst surfaces. In a few reports, the effect of preparing isolated Pd or Au atoms in the bimetallic PdAu catalysts has been attributed to providing exceptional activity or selectivity because of the unique chemistry of single-atom sites, which also allows for more conclusive mechanistic studies.[98,110,115–117] Pioneering work from the Goodman[110] and Toshima[118] groups has identified Pd or Au single- atom active sites in vinyl acetate synthesis and glucose oxidation, respectively, on catalytic surfaces with well-defined single Pd or Au atom structures. The Mullins group has demonstrated that the PdAu alloy surfaces catalyze the

dehydrogenation of formic acid while the extended Pd surfaces catalyze the dehydration of formic acid.[111]

Single-atom Alloys

Single-atom alloy (SAA) is a class of alloys where the active metal is atomically dispersed and isolated in the surface of the host (inert) metal. The early work on SAA was focused on the Pd-Cu system. The Sykes group demonstrated that fully isolated Pd atoms are stable in the surface of Cu(111)[119]. These isolated Pd atoms can dissociate H_2 and facilitate spillover of H to the Cu surface, and the weakly adsorbed H on the Cu can participate in the selective hydrogenation reactions. As the hydrogen activation is the rate limiting step for selective hydrogenation reactions with Cu catalysts, SAA becomes an attractive approach to activate Cu and preserve its high selectivity. Boucher et al. prepare a nanoparticle analog of the model SAA catalysts by putting a small amount of Pd in the surface of Cu nanoparticles[120]. This Pd-Cu catalyst shows good selectivity and activity compared to its monometallic counterparts. Ma et al. studied the PdCu(111) SAA surface for selective hydrogenation of acetylene with DFT calculations. They reported that PdCu(111) SAA has moderate H_2 activation capability and low desorption barrier of ethylene, which results in its high selectivity.[121]

The hydrogen activation and possible spillover has been studied with Pd-Au, Ni-Cu and Co-Ag, as well. Pd, Ni and Co exist as isolated atoms in the host metals in these systems. In many of these studies, the term of “single-atom alloy” was not used.[122–127] Other catalytic reactions including dehydrogenation, oxidation, hydrogenolysis, and Uhlman coupling have been investigated for the SAA catalysts with DFT and experimental approaches.[128–134]

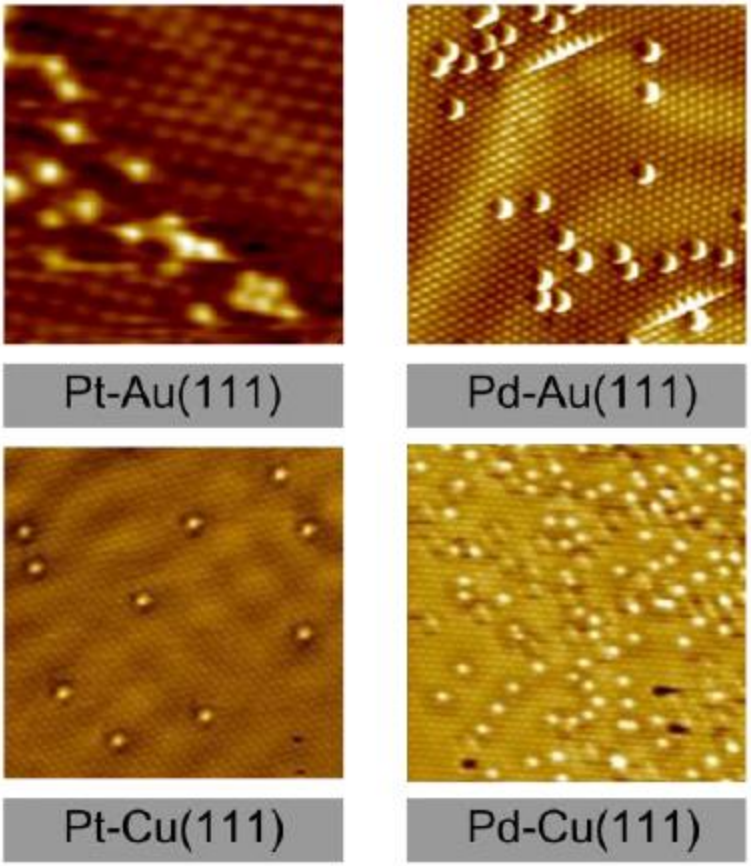

Figure 1.1. STM images of SAAs of PtAu(111), PdAu(111), PtCu(111) and PdCu(111)[135].

1.2.4 Selective hydrogenation on non Pd or Pt catalysts

With the consideration of the cost of Pd and Pt, development of non Pd or Pt catalysts has been investigated. One of the promising non-precious metal catalysts is bimetallic Ni-Zn. Norskov and coworkers screened different bimetallic and monometallic catalysts in terms of their methyl heat of adsorption and identified NiZn as the potential non-precious metal selective acetylene hydrogenation catalyst.[63] Furthermore, oxide catalysts have drawn attention in recent years. Pérez-Ramírez and coworkers have demonstrated ceria catalysts with

high acetylene and propyne hydrogenation selectivity. However, relative high H_2/C_3H_4 ratio and high temperature are required to achieve the desired performance.[136,137]

1.3 CO tolerant Pt catalysts

Pt metal is highly active for H_2 dissociation, which is the most important reason that Pt is widely used for fuel cell anodes and hydrogenation. However, Pt is very susceptible to carbon monoxide (CO) poisoning.[138] Due to the strong binding of CO onto Pt, even trace amounts of CO impurity, which is always present in H_2 -rich fuel gas produced from fuel reforming, can diminish H_2 activation and the overall reactivity.[138,139] It is reported that 20 ppm of CO at temperatures less than 100 °C can cause a significant activity drop of fuel cells.[140] Current research has been focused on the development of CO- tolerant Pt electrocatalysts.

The mechanism of H_2 activation in the presence of CO at the fuel cell anode with Pt catalysts can be expressed as follows:[141]

$$H_2 + 2Pt \rightarrow 2Pt - H$$

$$CO + Pt \rightarrow Pt - CO$$

$$2CO + 2Pt - H \rightarrow 2Pt - CO + H_2$$

$$2Pt - H \rightarrow 2Pt + 2H^+ + 2e^-$$

The dissociative adsorption of hydrogen is the rate limiting step in this process. Thus, the adsorption of CO on the Pt sites largely affects the anode reactions on Pt catalysts. Forming an alloy of Pt is the most-studied approach in improving its CO tolerance.[142–147] Pt-Ru and Pt-Sn anode catalysts have shown enhanced CO tolerance at fuel cell operating conditions. The effect

of Ru on Pt is twofold: it facilitates the CO electro-oxidation and weakens the Pt-CO bonds. Watanabe et al.[146] and Venkataraman et al.[142] demonstrated by *in situ* experiments that the Ru sites lowered the CO oxidation barrier and improved the efficiency of CO conversion. It was also found that the Pt-CO binding strength is decreased with the addition of Ru.[143,145,147] Moreover, Pt-Au, Pd-Au and Ni-Cu weakly adsorb CO due to electronic effects by the alloy formation, which can be potentially used in fuel cells.[122,144,148,149] Ensemble effects have been shown to increase CO binding strength at extended catalytic metal sites, therefore, from a fundamental perspective, metal alloys which alter the adsorption geometry of CO should exhibit weaker binding and enhanced CO tolerance.

The strong CO adsorption also hinders the fast conversion of CO to CO_2 at low temperatures (< 200 ^{o}C), and becomes a technical challenge for efficient emission control and the water-gas shift (WGS) reaction for hydrogen upgrading. Recently, atomically dispersed Pt_1 (or Pd_1) -O_x- stabilized on a variety of supports, such as silica[150], titania[151], KLTL-Zeolite[151,152], MCM-41[151], alumina[153] and iron oxide[154], were found to be highly active in WGS and CO oxidation reactions. The single platinum atom sites have a cationic nature that results in weak CO adsorption[150], thus becoming the exclusive sites for the low temperature CO conversion. Although single-atom catalytic sites in Pt_1 (or Pd_1)-O_x-oxides possess the desired property of weaker CO adsorption, they may not be stable enough under hydrogenation conditions. Single site catalysts that can activate hydrogen molecules and are electronically conductive are desired for CO-tolerant fuel cell catalysts.

1.4 Selective dehydrogenation of light alkanes

1.4.1 Alkane to alkene processes

Light alkenes including ethylene, propylene and butene are important feedstocks for the chemical industry to produce a wide variety of chemicals. The major processes to produce light alkenes are steam cracking and fluid catalytic cracking, which make lighter alkenes from naphtha and other feedstocks. However, the high demand of propylene in polymer industry has exceeded the production of propylene from these processes. This has created so-called "propylene gap".

The recent "shale gas boom" in North America provides low price and abundant light alkanes, which makes direct dehydrogenation of light alkanes to alkenes an economically reasonable process. There are several commercial plants in the world operating with dehydrogenation techniques to produce light alkenes. The high selectivity and lower energy demand makes the direct dehydrogenation more and more favorable for the production of light alkenes, especially with low shale gas price. One of the major technologies is the Olefex (UOP) process using Pt based catalysts. However, coke deposition is a big challenge for the commercial dehydrogenation catalysts and special designs of the reactor and regeneration process are needed to reduce coke deposition and to remove the coke. Indeed, in the industrial dehydrogenation processes, a significant portion of the catalysts are in the regeneration stage and the dehydrogenation process is often dominated by the need to control the coke formation.[155,156]

The industrial light alkane dehydrogenation processes typically run between 450 and 650 °C. At lower temperatures, the selective dehydrogenation reactions are largely limited by

thermodynamics, making the equilibrium alkene concentration low. Figure 1.2 shows the equilibrium conversion of alkanes at different temperatures. Effective alkene production at lower temperature is possible with lower alkane partial pressure.

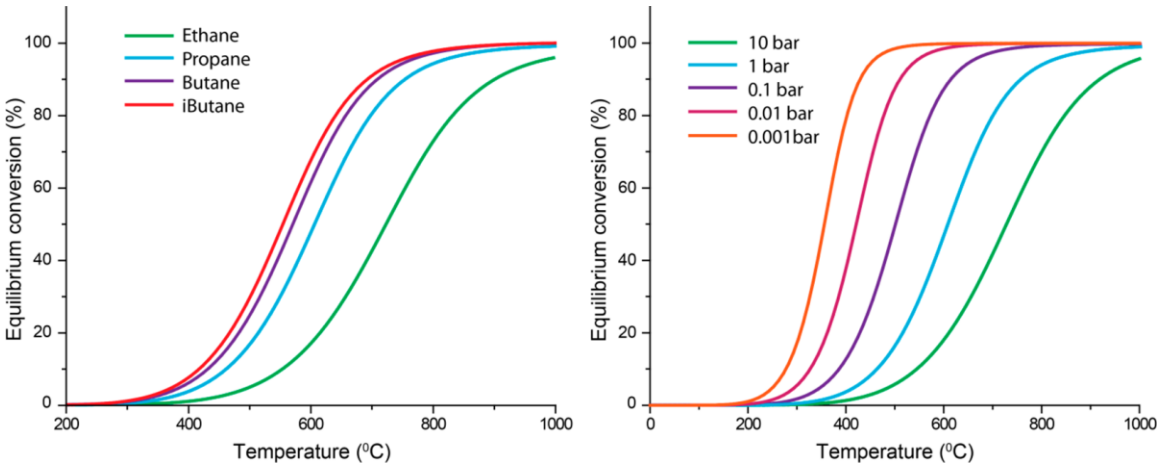

Figure 1.2. Equilibrium conversion of C2−C4 paraffins to olefins as a function of temperature at 1 bar (left) and pressure dependence of the dehydrogenation of propane as a function of temperature (right).[155] Adapted with permission. Copyright (2014) American Chemical Society.

1.4.2 Catalytic selective dehydrogenation reactions

Pt group metals are known for their reactivity in light alkane dehydrogenation and have been extensively studied. As shown in Scheme 1.3, a Langmuir-Hinshelwood mechanism was proposed for selective dehydrogenation of propane on Pt catalysts. The C-H bond scission happens consecutively followed by the desorption of butene and hydrogen molecules. The rate limiting step is the dissociative adsorption of propane molecule. [157,158]

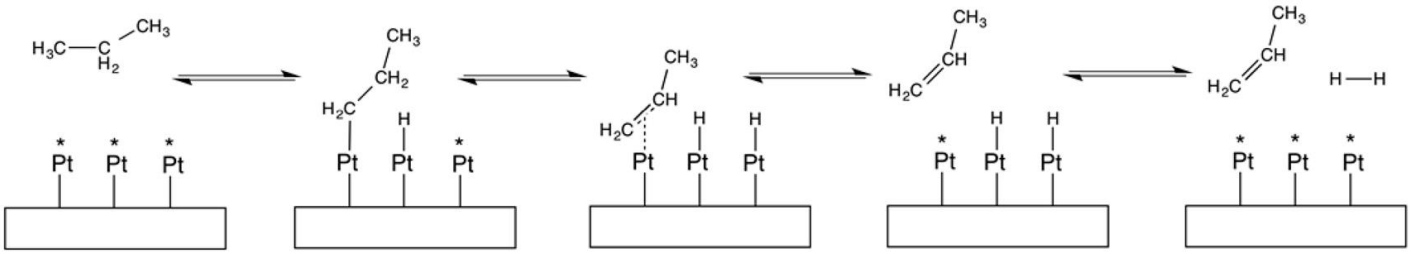

Scheme 1.3. Dehydrogenation mechanism on Pt catalysts.[155]

Thus far, Pt is the most often used metal catalyst for light alkane dehydrogenation, which is due to its high activity in C-H activation and relatively low activity in C-C cleavage.[155] It is widely believed that the selective dehydrogenation of light alkanes is structurally insensitive. Thus, higher dehydrogenation activity can be reached with smaller particle size. However, the side reactions in this process are structurally sensitive. For most of the side reactions, especially coke formation, undercoordinated sites and extended Pt surface are the active sites.[159–163]

Understanding the deactivation of the catalysts is crucial for the design of alkane dehydrogenation catalysts. Carbon deposition is the most important deactivation pathway. To tackle this challenge, both the Pt metal and the catalyst support must be optimized. Another crucial factor in deactivation is the sintering of metal nanoparticles. In the current industrial processes, catalysts are regenerated with oxidation and metal redispersion steps. Coke is burned in oxygen and Pt particles can be fragmented and redispersed with a small amount of oxygen and chlorine at a temperature around 500 °C.[164,165]

1.4.3 Pt alloy catalysts for selective dehydrogenation

One of the most commonly applied approaches to reduce the carbon deposition in dehydrogenation reaction is to add a second metal to the Pt catalysts. These modifiers can improve the selectivity and control the coking through ensemble and electronic effects**.**

Pt-Sn, Pt-Zn, Pt-Ga and Pt-In alloys have been studied as catalysts for selective alkane dehydrogenation. Sn is the most studied and industrially widely used secondary metal for alkane dehydrogenation reactions. The addition of Sn reduces the side reactions including hydrogenolysis and isomerization, and decreases the acidity of the support. Hydrogenolysis and isomerization are the precursors of coke formation, while the surface acid sites can catalyze polymerization leading to carbon deposition. Sn is also capable of impeding the sintering of Pt at the reaction conditions.[166,167] Moreover, the segregation of Sn in the regeneration process is believed to reduce the sintering of Pt.[166] In the alkane dehydrogenation condition, where H_2 is present, Sn is in metallic state and alloyed with Pt. Both geometric and electronic effects contribute to the catalytic performance of Pt-Sn catalysts.

The geometric effects of alloying Pt with Sn are essentially the decoration of the low coordination Pt sites and the reduction of the size of Pt ensembles. FTIR as well as TPR and STEM-EDS studies have been conducted by Vironvskaia et al.[168] and Nagaraja et al.[167], respectively, to study the structural evolution of Pt-Sn catalysts in alkane dehydrogenation reaction conditions. They found Sn alloyed with Pt with diffusion of Sn species taking place under reaction conditions. The coke formation on Pt-Sn catalysts was considerably reduced due to the blocking of the low coordination sites of Pt nanoparticles, which are responsible for cracking and hydrogenolysis, by Sn species. Moreover, Sn breaks the Pt ensembles. The

ensemble effect on alkane dehydrogenation is minimal as this reaction is structurally insensitive. However, the ensemble effect on the side reactions including hydrogenolysis and cracking is significant.[169–171] Furthermore, Lieske et al. suggested Sn sites facilitated the diffusion of coke precursors to the oxide support, resulting in reduction of the coke formation.[170,172]

Sn also alters the electronic properties of Pt upon alloying. Electrons can be transferred to Pt 5d band leading to the weakening of the adsorption of alkene molecules.[158,173] Through FTIR and adsorption microcalorimetry studies, Dumesic and coworkers found the adsorption of ethylene and isobutene on Pt-Sn is weaker compared to Pt.[174–176] Moreover, the formation of alkylidyne is reduced with the formation of Pt-Sn alloys. Alkylidyne is believed to be the precursor for undesired coke and hydrogenolysis. DFT studies indicated the dehydrogenation barrier of alkane on Pt-Sn is higher than on Pt, while the alkene desorption barrier on Pt-Sn is lower. Thus, the addition of Sn to Pt decreases the activity of Pt but increases the selectivity.[157,158,177]

Pt-Ga, Pt-In and Pt-Ge have been investigated for alkane dehydrogenation as well. Knowing that acidity is one of the major causes of coke formation[178], the addition of Ga and In can reduce the Bronsted acidity of the catalysts, which in turn reduces the coke formation[179,180]. Ge has similar effect as Sn, but its electron donation effect is smaller than Sn.[181] Moreover, Li, Na and K can poison the acid sites on the metal oxide support, decreasing the coke formation.[182,183] Zn and Mg were doped into the support to induce the phase change, leading to lower acidity support materials.[184,185]

Single-atom catalysts for selective dehydrogenation reactions

Recently, Luo and co-workers proposed a single Pd atom doped in a Cu_{55} cluster and conducted DFT calculations for propane dehydrogenation to propylene.[128] They found single Pd atom at the edge site of Cu_{55} cluster can lower the energy barrier for the first C-H cleavage, and single Pd atom favors the C-H bond scission over the C-C one. Wasserscheid and coworkers reported a supported liquid phase Pd-Ga catalyst that is highly stable in the butane dehydrogenation reaction at 445 °C. This is due to the Ga diluting the Pd domains to make Pd ensembles smaller or even down to single atoms and the liquid nature of the active phases.[186]

Non-Pt catalysts have been studied for alkane dehydrogenation as well. Single site Zn(II) stabilized with three -O-Si on the amorphous silica surface is stable at 550 °C and catalyzes the heterolytic cleavage of C-H bonds, but is unfavorable for C-C bond cleavage.[187] Gong and coworkers showed the effect of TiO_2 addition on the stability of Pt/Al_2O_3 catalysts and demonstrated a 10% optimal TiO_2 loading.[188]

1.5 Thesis objectives:

In previous work from our lab, single-atom catalysts of Au and Pt on metal oxides and carbon supports have been designed and synthesized. The Au_1-O_x-OH_y and Pt_1-O_x-OH_y have been shown to be the active sites for various reactions. However, the single atoms in metal hosts were not investigated. In 2012, Sykes, Flytzani-Stephanopoulos and coworkers demonstrated isolated Pd atoms can be stabilized in the surface of Cu(111) in ultra-high vacuum condition to form "*Single-atom Alloy (SAA)*". Sykes et al. postulated that SAAs are

potentially good catalysts for selective hydrogenation reactions. Inspired by the surface science studies on SAAs, Boucher et al. prepared bimetallic $Pd_{0.18}Cu_{15}$ nanoparticles as an analog of PdCu(111) SAA and showed $Pd_{0.18}Cu_{15}$ NPs were highly selective in hydrogenation of phenylacetylene to styrene. Lacking direct evidence to confirm its structural properties at the atomic level, this catalyst still cannot be categorized as SAA.

Following the inspirational work from the Flytzani-Stephanopoulos and Sykes groups, this thesis aimed to investigate the feasibility of designing catalytically active and stable SAA NPs and apply the SAA strategy in the rational design of practical catalysts. Through combined studies by catalytic and surface science techniques, the latter by the Sykes group at Tufts, as well as collaborative DFT calculations, this thesis also aimed to extend the understanding of structure-function relationship in SAA catalysis. A few industrially important probe reactions/processes were studied: selective hydrogenation and selective dehydrogenation reactions, and the CO tolerance of Pt catalysts. Moreover, the fundamentally important key elementary reactions involved in these reactions/processes, including hydrogen activation, C-H activation and adsorption/desorption of CO, were investigated.

1.5.1 Specific aim 1

The first part of the specific aim 1 was **to investigate approaches to form PtCu SAA NP catalysts and to confirm the isolated atomic dispersion of Pt in the host metal**. To date, most of the bimetallic catalysts reported in the literature are prepared with co-reduction or co-precipitation methods containing comparable compositions of the two elements. These

methods cannot avoid the formation of monometallic NPs. And the high Pt or Pd loading can result in the formation of Pt or Pd nanoclusters in the catalysts. Recent studies by Boucher et al. showed the effectiveness of galvanic replacement in the preparation of PdCu bimetallic catalysts.[120] In other work, sequential reduction methods have been applied in the formation of core-shell structured bimetallic catalysts with very well-defined structures.[189] Herein, both galvanic replacement and sequential reduction methods were used in the preparation of SAA NPs. Moreover, it is challenging to characterize the single-atom sites in the surface of another metal. In this thesis, *in situ* IR, *in situ* X-ray absorption spectroscopy and STEM characterization were employed to investigate the structural and chemical properties of SAA catalysts combined with other characterization techniques.

The close collaboration with surface science groups and DFT groups have also contributed to the rational catalyst design in this thesis work. The feasibility of formation of SAAs and their surface chemistry were studied by the collaborators in UHV conditions experimentally and with DFT calculations. The results are compared among all investigators to extend the understanding of the SAA catalysts.

The second part of the specific aim 1 was **to design highly selective catalysts for hydrogenation of butadiene to butene and to extend the understanding of PtCu SAA catalysts in selective hydrogenation reactions**. Pt alloys with the smallest possible Pt ensemble, single atoms, has not been studied in ambient pressure selective hydrogenation reactions. The SAA configuration is intrinsically selective in partial hydrogenation reactions as the side reactions that require more than one Pt atoms are avoided. The electronic effects in PtCu alloys also contribute to high selectivity. In this thesis, the selective hydrogenation of 1,3-butadiene in the

presence of excess propylene is studied with supported PtCu SAA catalysts. This is an industrially important reaction and the performance of SAA catalysts is of great interest. This thesis aimed at extending the understanding of selective hydrogenation with SAA catalysts and answer one important fundamental question: are isolated Pt single atoms enough to activate Cu for selective hydrogenation reactions?

1.5.2 Specific aim 2

The specific aim 2 of this thesis was **to gain an improved understanding of the nature of active sites of PtCu SAA with CO as probe molecule and to investigate an approach to improve the CO tolerance of Pt catalysts**. CO is an important probe molecule to characterize the catalytic surfaces. Its interaction with the surface-active sites can effectively reflect the surface chemistry of the catalysts. For bimetallic alloys, the electronic and ensemble effects can influence the binding strength of CO and the vibrational frequency of adsorbed CO molecules. Thus, studying the interaction of CO with SAA catalysts is of fundamental interest. Moreover, CO poisoning is one of the major practical challenges for Pt catalysts, especially the Pt fuel cell catalysts. Based on the literature of other Pt alloys, the small Pt ensembles and electronic effects in Pt-Cu are beneficial for the CO tolerance of Pt catalysts. Thus, we investigated PtCu SAA as a promising CO tolerant catalyst. Its high performance in hydrogen activation would also contribute to its further application in various reactions.

1.5.3 Specific aim 3

C-H activation is the key elementary step in many important chemical reactions, including the conversion of light alkanes and alcohols. The light alkanes conversion to chemicals is more and more attractive with the recent "shale gas boom". Pt is one of the most important catalytic metals for alkane dehydrogenation reactions, however, it suffers from instability due to coking. The specific aim 3 of this thesis was **to investigate an approach to overcome the challenges of coking in alkane dehydrogenation reactions. Specifically, the use of PtCu SAA catalysts compared to monometallic Pt catalysts was studied. And to investigate the C-H activation reactions with SAA catalysts.** C-H activation barrier on Cu is relatively high and the coke formation is unlikely. This thesis determines what is the smallest possible Pt ensemble in Cu that can catalyze the C-H activation reaction. The selective dehydrogenation catalyst is designed with this smallest possible Pt ensemble to avoid the coke formation.

1.5.4 Specific aim 4

The last specific aim of this thesis was **to explore the potential of SAAs for the design of selective hydrogenation catalysts with PdAu for hydrogenation reactions in the liquid phase, and to extend the understanding of selective hydrogenation reactions with PdAu SAA catalysts.** To date, Cu based SAA catalysts, especially PtCu, have been extensively studied for various selective hydrogenation and dehydrogenation reactions, which are reported in this thesis and in others' work. Beyond that, this thesis aimed to explore the feasibility of applying the SAA strategy to Au based catalysts, especially PdAu, an important bimetallic catalyst with surface chemistry different from Cu in many ways. The performance of SAA catalysts in liquid

phase selective hydrogenation is also of great interest. Moreover, a sequential reduction preparation approach, adapted from the literature was developed as an effective method to form SAA NPS with Au.[189] By investigating PdAu SAA systems, this thesis shows that the SAA approach is not limited to a specific class of bimetallic catalysts; indeed it can be a general design approach for many bimetallic catalysts for different reactions.

1.6 References

1. Bowker M. *The Basis and Applications of Heterogeneous Catalysis*. Oxford University Press; 1998.

2. Meunier FC. Bridging the Gap between Surface Science and Industrial Catalysis. *ACS Nano*. 2008;2(12):2441-2444. doi:10.1021/nn800787e.

3. Besenbacher F, Chorkendorff I, Clausen BS, et al. Design of a Surface Alloy Catalyst for Steam Reforming. *Science*. 1998;279(5358):1913-1915. doi:10.1126/science.279.5358.1913.

4. Thomas JM, Harris KDM. Some of tomorrow's catalysts for processing renewable and non-renewable feedstocks, diminishing anthropogenic carbon dioxide and increasing the production of energy. *Energy Environ Sci*. 2016;9(3):687-708. doi:10.1039/C5EE03461B.

5. Somorjai GA, McCrea K. Roadmap for catalysis science in the 21st century: a personal

view of building the future on past and present accomplishments. *Appl Catal A Gen*. 2001;222(1-2):3-18. doi:10.1016/S0926-860X(01)00825-0.

6. Arnold H, Döbert F, Gaube J. Selective Hydrogenation of Hydrocarbons. In: *Handbook of Heterogeneous Catalysis*. ; 2008:3266-3283.

7. Silvestre-Albero J, Sepulveda-Escribano A, Rodriguez-Reinoso F, Anderson JA. Influence of Zn on the characteristics and catalytic behavior of TiO2-supported Pt catalysts. *J Catal*. 2004;223:179-190. doi:10.1016/j.jcat.2004.01.019.

8. Molnár Á, Sárkány A, Varga M. Hydrogenation of carbon-carbon multiple bonds: Chemo-, regio- and stereo-selectivity. *J Mol Catal A Chem*. 2001;173(1-2):185-221.

9. Chen B, Dingerdissen U, Krauter JGE, et al. New developments in hydrogenation catalysis particularly in synthesis of fine and intermediate chemicals. *Appl Catal A Gen*. 2005;280(1):17-46. doi:10.1016/j.apcata.2004.08.025.

10. Lindlar H, Dubuis R. Palladium Catalyst for Partial Reduction of Acetylenes. *Org Synth*. 1966;46:89. doi:10.15227/orgsyn.046.0089.

11. Molnar A, Sarkany A, Varga M. Hydrogenation of carbon – carbon multiple bonds : chemo-, regio- and stereo-selectivity. *J Mol Catal A Chem*. 2001;173:185-221. doi:10.1016/S1381-1169(01)00150-9.

12. McEwan L, Julius M, Roberts S, Fletcher JCQ. A review of the use of gold catalysts in selective hydrogenation reactions. *Gold Bull*. 2010;43(4):298-306.

13. Lopez-Sanchez JA, Lennon D. The use of titania- and iron oxide-supported gold catalysts

for the hydrogenation of propyne. In: *Applied Catalysis A: General*. Vol 291. ; 2005:230-237.

14. Jia J, Haraki K, Kondo J. Selective hydrogenation of acetylene over Au/Al2O3 catalyst. *J Phys Chem B*. 2000;2(1):11153-11156. http://pubs.acs.org/doi/abs/10.1021/jp001213d.

15. Hightower JW, Furlong B, Sárkány A, Guczi L. 1,3-Butadiene Hydrogenation in 1-Butene Over Alumina Supported Pd-Ag Catalysts. *Stud Surf Sci Catal*. 1993;75:2305-2308.

16. Miura H, Terasaka M, Oki K, Matsuda T. Preparation of Egg-Shell Type Pd-Ag and Pd-Au Catalysts by Selective Deposition and Hydrogenation of 1,3-Butadiene. *Stud Surf Sci Catal*. 1993;75:2379-2382.

17. Phillips J, Auroux A, Bergeret G, Massardier J, Renouprez A. Phase behavior of palladium-silver particles supported on silica. *J Phys Chem*. 1993;97(14):3565-3570. http://pubs.acs.org/doi/abs/10.1021/j100116a021.

18. Furlong BK, Hightower JW, Chan TY-L, Sarkany A, Guczi L. 1,3-Butadiene selective hydrogenation over Pd/alumina and CuPd/alumina catalysts. *Appl Catal A Gen*. 1994;117(1):41-51.

19. Lianos L, Debauge Y, Massardier J, Jugnet Y, Bertolini JC. 1,3-butadiene hydrogenation on Pd50Cu50 single crystals. *Catal Letters*. 1997;44:211-216.

20. Constant L, Ruiz P, Abel M, Robach Y, Porte L, Bertolini JC. Pd deposited on Cu(110): a highly performant catalyst for the 1,3-butadiene hydrogenation reaction. *Top Catal*. 2000;14:125-129.

21. Horiuti I, Polanyi M. Exchange reactions of hydrogen on metallic catalysts. *Trans Faraday Soc*. 1934;30:1164. doi:10.1039/tf9343001164.

22. Cremer PS, Somorjai GA. Surface science and catalysis of ethylene hydrogenation. *J Chem Soc Faraday Trans*. 1995;91(20):3671.

23. Cremer PS, Su XC, Shen YR, Somorjai GA. Ethylene hydrogenation on Pt(111) monitored in situ at high pressures using sum frequency generation. *J Am Chem Soc*. 1996;118(12):2942-2949.

24. Taylor G, Thomson SJ, Webb G. Radiochemical studies of chemisorption and catalysis VIII. The behavior of 14C-ethylene and tritium adsorbed on alumina-supported palladium, rhodium, and platinum catalysts. *J Catal*. 1968;12(2):191-197. doi:10.1016/0021-9517(68)90094-8.

25. Sheppard N. Vibrational Spectroscopic Studies of the Structure of Species Derived From the Chemisorption of Hydrocarbons on Metal Single-Crystal Surfaces. *Annu Rev Phys Chem*. 1988;39(1):589-644. doi:10.1146/annurev.pc.39.100188.003105.

26. Wang PK, Slichter CP, Sinfelt JH. Structures and reactions of ethylene (C2H4) adsorbed on small platinum clusters. *J Phys Chem*. 1985;89(17):3606-3609. doi:10.1021/j100263a007.

27. Thomson SJ, Webb G. Catalytic hydrogenation of olefins on metals: a new interpretation. *J Chem Soc Chem Commun*. 1976;(13):526. doi:10.1039/c39760000526.

28. Zaera F. Surface Chemistry of Hydrocarbon Fragments on Transition Metals: Towards Understanding Catalytic Processes. *Catal Letters*. 2003;91(1/2):1-10.

doi:10.1023/B:CATL.0000006310.50290.ba.

29. Tilekaratne A, Simonovis JP, López Fagúndez MF, Ebrahimi M, Zaera F. Operando Studies of the Catalytic Hydrogenation of Ethylene on Pt(111) Single Crystal Surfaces. *ACS Catal*. 2012;2(11):2259-2268. doi:10.1021/cs300411p.

30. Zaera F. The Surface Chemistry of Metal-Based Hydrogenation Catalysis. *ACS Catal*. 2017;7(8):4947-4967. doi:10.1021/acscatal.7b01368.

31. Ebrahimi M, Simonovis JP, Zaera F. Near-Unity Reaction Probability in Olefin Hydrogenation Promoted by Heterogeneous Metal Catalysts. *J Phys Chem Lett*. 2014;5(12):2121-2125. doi:10.1021/jz500954g.

32. Simonovis J, Tillekaratne A, Zaera F. The Role of Carbonaceous Deposits in Hydrogenation Catalysis Revisited. *J Phys Chem C*. 2017;121(4):2285-2293. doi:10.1021/acs.jpcc.6b12517.

33. Tillekaratne A, Simonovis JP, Zaera F. Ethylene hydrogenation catalysis on Pt(111) single-crystal surfaces studied by using mass spectrometry and in situ infrared absorption spectroscopy. *Surf Sci*. 2016;652:134-141. doi:10.1016/j.susc.2015.11.005.

34. Dong Y, Ebrahimi M, Tillekaratne A, Simonovis JP, Zaera F. Hydrogenation vs. H–D isotope scrambling during the conversion of ethylene with hydrogen/deuterium catalyzed by platinum under single-collision conditions. *Phys Chem Chem Phys*. 2016;18(28):19248-19258. doi:10.1039/C6CP04157D.

35. Bond GC, Webb G, Wells PB, Winterbottom JM. The hydrogenation of alkadienes. Part I.

The hydrogenation of buta-1,3-diene catalysed by the Noble Group VIII metals. *J Chem Soc*. 1965:3218-3227.

36. Nishimura E, Inoue Y, Yasumori I. The Mechanism of the Selective Hydrogenation of 1,3-Butadiene on Copper Surfaces. *Bull Chem Soc Jpn*. 1975;48:803-807.

37. Joice BJ, Rooney JJ, Wells PB, Wilson GR. Nature and reactivity of intermediates in hydrogenation of buta-1,3-diene catalyzed by cobalt and palladium-gold alloys. *Discuss Faraday Soc*. 1966;41:223-236.

38. Boitiaux JP, Cosyns J, Robert E. Additive effects in the selective hydrogenation of unsaturated hydrocarbons on platinum and rhodium catalysts: II. Influence of various compounds containing phosphorus, oxygen, sulphur and chlorine on the catalytic performance of platinum catalyst. *Appl Catal*. 1989;49:235-246.

39. Bond GC. The role of carbon deposits in metal-catalysed reactions of hydrocarbons. *Appl Catal A Gen*. 1997;149(1):3-25. doi:10.1016/S0926-860X(96)00249-9.

40. Webb G. The formation and role of carbonaceous residues in metal-catalysed reactions of hydrocarbons. *Catal Today*. 1990;7(2):139-155. doi:10.1016/0920-5861(90)85013-E.

41. Battiston GC, Dalloro L, Tauszik GR. Performance and aging of catalysts for the selective hydrogenation of acetylene: a micropilot-plant study. *Appl Catal*. 1982;2(1-2):1-17. doi:10.1016/0166-9834(82)80170-X.

42. Teschner D, Vass E, Havecker M, et al. Alkyne hydrogenation over Pd catalysts: A new paradigm. *J Catal*. 2006;242(1):26-37. doi:10.1016/j.jcat.2006.05.030.

43. Chen B, Dingerdissen U, Krauter JGE, et al. New developments in hydrogenation catalysis particularly in synthesis of fine and intermediate chemicals. *Appl Catal A Gen*. 2005;280(1):17-46. doi:10.1016/j.apcata.2004.08.025.

44. Sá J, Montero J, Duncan E, Anderson JA. Bi modified Pd/SnO2 catalysts for water denitration. *Appl Catal B Environ*. 2007;73(1-2):98-105. doi:10.1016/j.apcatb.2006.06.012.

45. Anderson J, Mellor J, Wells R. Pd catalysed hexyne hydrogenation modified by Bi and by Pb. *J Catal*. 2009;261(2):208-216. doi:10.1016/j.jcat.2008.11.023.

46. López N, Vargas-Fuentes C. Promoters in the hydrogenation of alkynes in mixtures: insights from density functional theory. *Chem Commun*. 2012;48(10):1379-1391. doi:10.1039/C1CC14922A.

47. Kimura H, Kimura A, Kokubo I, Wakisaka T, Mitsuda Y. Palladium based multi-component catalytic systems for the alcohol to car□ylate oxidation reaction. *Appl Catal A Gen*. 1993;95(2):143-169. doi:10.1016/0926-860X(93)85071-V.

48. Pattamakomsan K, Ehret E, Morfin F, et al. Selective hydrogenation of 1,3-butadiene over Pd and Pd–Sn catalysts supported on different phases of alumina. *Catal Today*. 2011;164(1):28-33. doi:10.1016/j.cattod.2010.10.013.

49. Choi SH, Lee JS. XAFS Study of Tin Modification of Supported Palladium Catalyst for 1,3-Butadiene Hydrogenation in the Presence of 1-Butene. *J Catal*. 2000;193(2):176-185. doi:10.1006/jcat.2000.2893.

50. Breinlich C, Haubrich J, Becker C, Valcarcel A, Delbecq F, Wandelt K. Hydrogenation of 1,3-butadiene on Pd(111) and PdSn/Pd(111) surface alloys under UHV conditions. *J Catal*. 2007;251(1):123-130. doi:10.1016/j.jcat.2007.07.003.

51. Verdier S. Pd–Sn/Al2O3 catalysts from colloidal oxide synthesis II. Surface characterization and catalytic properties for buta-1,3-diene selective hydrogenation. *J Catal*. 2003;218(2):288-295. doi:10.1016/S0021-9517(03)00064-2.

52. Cheung T-TP, Johnson MM, Brown SH, Zisman SA, Kimble JB. Selective acetylene hydrogenation. 1996.

53. Cheung T-TP, Johnson MM. Alkyne hydrogenation process. 1996.

54. Pachulski A, Schödel R, Claus P. Performance and regeneration studies of Pd–Ag/Al2O3 catalysts for the selective hydrogenation of acetylene. *Appl Catal A Gen*. 2011;400(1-2):14-24. doi:10.1016/j.apcata.2011.03.019.

55. Khan NA, Uhl A, Shaikhutdinov S, Freund H-J. Alumina supported model Pd–Ag catalysts: A combined STM, XPS, TPD and IRAS study. *Surf Sci*. 2006;600(9):1849-1853. doi:10.1016/j.susc.2006.02.016.

56. Mei D, Neurock M, Smith CM. Hydrogenation of acetylene–ethylene mixtures over Pd and Pd–Ag alloys: First-principles-based kinetic Monte Carlo simulations. *J Catal*. 2009;268(2):181-195. doi:10.1016/j.jcat.2009.09.004.

57. Jin Y, Datye AK, Rightor E, et al. The Influence of Catalyst Restructuring on the Selective Hydrogenation of Acetylene to Ethylene. *J Catal*. 2001;203(2):292-306.

doi:10.1006/jcat.2001.3347.

58. Studt F, Abild-Pedersen F, Bligaard T, Sørensen RZ, Christensen CH, Nørskov JK. On the Role of Surface Modifications of Palladium Catalysts in the Selective Hydrogenation of Acetylene. *Angew Chemie Int Ed*. 2008;47(48):9299-9302. doi:10.1002/anie.200802844.

59. Huang DC, Chang KH, Pong WF, Tseng PK, Hung KJ, Huang WF. Effect of Ag-promotion on Pd catalysts by XANES. *Catal Letters*. 1998;53(3/4):155-159. doi:10.1023/A:1019022326090.

60. Armbrüster M, Kovnir K, Behrens M, Teschner D, Grin Y, Schlögl R. Pd−Ga Intermetallic Compounds as Highly Selective Semihydrogenation Catalysts. *J Am Chem Soc*. 2010;132(42):14745-14747. doi:10.1021/ja106568t.

61. Zhou H, Yang X, Li L, et al. PdZn Intermetallic Nanostructure with Pd–Zn–Pd Ensembles for Highly Active and Chemoselective Semi-Hydrogenation of Acetylene. *ACS Catal*. 2016;6(2):1054-1061. doi:10.1021/acscatal.5b01933.

62. Mashkovsky IS, Markov P V., Bragina GO, Rassolov A V., Baeva GN, Stakheev AY. Intermetallic Pd1–Zn1 nanoparticles in the selective liquid-phase hydrogenation of substituted alkynes. *Kinet Catal*. 2017;58(4):480-491. doi:10.1134/S0023158417040139.

63. Studt F, Abild-Pedersen F, Bligaard T, Sorensen RZ, Christensen CH, Norskov JK. Identification of Non-Precious Metal Alloy Catalysts for Selective Hydrogenation of Acetylene. *Science*. 2008;320(5881):1320-1322. doi:10.1126/science.1156660.

64. Leviness S, Nair V, Weiss AH, Schay Z, Guczi L. Acetylene hydrogenation selectivity

control on PdCu/Al2O3 catalysts. *J Mol Catal*. 1984;25(1-3):131-140. doi:10.1016/0304-5102(84)80037-1.

65. Skoda F, Astier MP, Pajonk GM, Primet M. Surface characterization of palladium-copper bimetallic catalysts by FTIR spectroscopy and test reactions. *Catal Letters*. 1994;29(1-2):159-168. doi:10.1007/BF00814262.

66. Guczi L, Schay Z, Stefler G, Liotta LF, Deganello G, Venezia AM. Pumice-Supported Cu–Pd Catalysts: Influence of Copper on the Activity and Selectivity of Palladium in the Hydrogenation of Phenylacetylene and But-1-ene. *J Catal*. 1999;182(2):456-462. doi:10.1006/jcat.1998.2344.

67. Trawczyński J, Gheek P, Okal J, Zawadzki M, Gomez MJI. Reduction of nitrate on active carbon supported Pd-Cu catalysts. *Appl Catal A Gen*. 2011;409-410:39-47. doi:10.1016/j.apcata.2011.09.020.

68. Fernández-García M, Conesa JC, Clotet A, Ricart JM, López N, Illas F. Study of the Heterometallic Bond Nature in PdCu(111) Surfaces. *J Phys Chem B*. 1998;102(1):141-147. doi:10.1021/jp971973x.

69. Cole RJ, Brooks NJ, Weightman P. Determination of charge transfer in the CuxPd1-x alloy system. *Phys Rev B*. 1997;56(19):12178-12182. doi:10.1103/PhysRevB.56.12178.

70. Mårtensson N, Nyholm R, Calén H, Hedman J, Johansson B. Electron-spectroscopic studies of the CuxPd1-x alloy system: Chemical-shift effects and valence-electron spectra. *Phys Rev B*. 1981;24(4):1725-1738. doi:10.1103/PhysRevB.24.1725.

71. Pope TD, Griffiths K, Norton PR. Surface and interfacial alloys of Pd with Cu(100): structure, photoemission and CO chemisorption. *Surf Sci*. 1994;306(3):294-312. doi:10.1016/0039-6028(94)90073-6.

72. Liu G, St. Clair TP, Goodman DW. An XPS Study of the Interaction of Ultrathin Cu Films with Pd(111). *J Phys Chem B*. 1999;103(40):8578-8582. doi:10.1021/jp991843j.

73. Wei X, Wang A-Q, Yang X-F, Li L, Zhang T. Synthesis of Pt-Cu/SiO2 catalysts with different structures and their application in hydrodechlorination of 1,2-dichloroethane. *Appl Catal B Environ*. 2012;121-122:105-114. doi:10.1016/j.apcatb.2012.03.020.

74. Toshima N, Wang Y. Preparation and Catalysis of Novel Colloidal Dispersions of Copper/Noble Metal Bimetallic Clusters. *Langmuir*. 1994;10(12):4574-4580. doi:10.1021/la00024a031.

75. Borovkov VY, Luebke DR, Kovalchuk VI, D'Itri JL. Hydrogen-Assisted 1,2-Dichloroethane Dechlorination Catalyzed by Pt−Cu/SiO 2 : Evidence for Different Functions of Pt and Cu Sites. *J Phys Chem B*. 2003;107(23):5568-5574. doi:10.1021/jp0300389.

76. Dejongste H. Role of Cu in the hydrogenolysis of pentane on Cu alloy catalysts. *J Catal*. 1980;63(2):389-394. doi:10.1016/0021-9517(80)90092-5.

77. Vadlamannati LS, Kovalchuk VI, D'Itri JL. Dechlorination of 1,2-dichloroethane catalyzed by Pt–Cu/C: unraveling the role of each metal. *Catal Letters*. 1999;58(4):173-178. doi:10.1023/A:1019015009078.

78. Guo Z, Chen Y, Li L, Wang X, Haller GL, Yang Y. Carbon nanotube-supported Pt-based

bimetallic catalysts prepared by a microwave-assisted polyol reduction method and their catalytic applications in the selective hydrogenation. *J Catal*. 2010;276(2):314-326. doi:10.1016/j.jcat.2010.09.021.

79. Qi S, Yu W, Lonergan WW, Yang B, Chen JG. General Trends in the Partial and Complete Hydrogenation of 1,4-Cyclohexadiene over Pt-Co, Pt-Ni and Pt-Cu Bimetallic Catalysts. *ChemCatChem*. 2010;2(6):625-628. doi:10.1002/cctc.201000082.

80. Humbert M, Chen J. Correlating hydrogenation activity with binding energies of hydrogen and cyclohexene on M/Pt(111) (M = Fe, Co, Ni, Cu) bimetallic surfaces. *J Catal*. 2008;257(2):297-306. doi:10.1016/j.jcat.2008.05.013.

81. Khan NA, Murillo LE, Chen JG. Observation of Novel Low-Temperature Hydrogenation Activity on Co/Pt(111) Surfaces. *J Phys Chem B*. 2004;108(40):15748-15754. doi:10.1021/jp0479419.

82. Lonergan WW, Xing X, Zheng R, Qi S, Huang B, Chen JG. Low-temperature 1,3-Butadiene Hydrogenation over Supported Pt/3d/γ-Al2O3 Bimetallic Catalysts. *Catal Today*. 2011;160:61-69. doi:10.1016/j.cattod.2010.05.014.

83. Lucci FR, Lawton TJ, Pronschinske A, Sykes ECH. Atomic Scale Surface Structure of Pt/Cu(111) Surface Alloys. *J Phys Chem C*. 2014;118(6):3015-3022. doi:10.1021/jp405254z.

84. Liu J, Lucci FR, Yang M, et al. Tackling CO Poisoning with Single-Atom Alloy Catalysts. *J Am Chem Soc*. 2016;138(20):6396-6399. doi:10.1021/jacs.6b03339.

85. Jia J, Haraki K, Kondo JN, Domen K, Tamaru K. Selective Hydrogenation of Acetylene over Au/Al2O3 Catalyst. *J Phys Chem B*. 2000;104(47):11153-11156. doi:10.1021/jp001213d.

86. Lopez-Sanchez JA, Lennon D. The use of titania- and iron oxide-supported gold catalysts for the hydrogenation of propyne. *Appl Catal A Gen*. 2005;291(1-2):230-237. doi:10.1016/j.apcata.2005.01.048.

87. Hugon A, Delannoy L, Krafft JM, Louis C. Selective Hydrogenation of 1,3-Butadiene in the Presence of an Excess of Alkenes over Supported Bimetallic Gold−Palladium Catalysts. *J Phys Chem C*. 2010;114:10823-10835. doi:10.1021/jp100479b.

88. Mukherjee P, Patra CR, Ghosh A, Kumar R, Sastry M. Characterization and Catalytic Activity of Gold Nanoparticles Synthesized by Autoreduction of Aqueous Chloroaurate Ions with Fumed Silica. *Chem Mater*. 2002;14(4):1678-1684. doi:10.1021/cm010372m.

89. Choudhary TV, Sivadinarayana C, Datye AK, Kumar D, Goodman DW. Acetylene Hydrogenation on Au-Based Catalysts. *Catal Letters*. 2003;86(1/3):1-8. doi:10.1023/A:1022694505504.

90. Segura Y, López N, Pérez-Ramírez J. Origin of the superior hydrogenation selectivity of gold nanoparticles in alkyne + alkene mixtures: Triple- versus double-bond activation. *J Catal*. 2007;247(2):383-386.

91. Bond G, Thompson DT. Catalysis by Gold. *Catal Rev*. 1999;41(3-4):319-388. doi:10.1081/CR-100101171.

92. Kolli N El, Delannoy L, Louis C. Bimetallic Au–Pd catalysts for selective hydrogenation of

butadiene: Influence of the preparation method on catalytic properties. *J Catal*. 2013;297:79-92. doi:10.1016/j.jcat.2012.09.022.

93. Hugon A, Delannoy L, Krafft J-M, Louis C. Selective Hydrogenation of 1,3-Butadiene in the Presence of an Excess of Alkenes over Supported Bimetallic Gold−Palladium Catalysts. *J Phys Chem C*. 2010;114(24):10823-10835. doi:10.1021/jp100479b.

94. Zhang S, Chen C-Y, Jang BW-L, Zhu A-M. Radio-frequency H2 plasma treatment of AuPd/TiO2 catalyst for selective hydrogenation of acetylene in excess ethylene. *Catal Today*. 2015;256:161-169. doi:10.1016/j.cattod.2015.04.002.

95. Szumełda T, Drelinkiewicz A, Kosydar R, Gurgul J. Hydrogenation of cinnamaldehyde in the presence of PdAu/C catalysts prepared by the reverse “water-in-oil” microemulsion method. *Appl Catal A Gen*. 2014;487:1-15. doi:10.1016/j.apcata.2014.08.036.

96. Pei GX, Liu XY, Wang A, et al. Promotional Effect of Pd Single Atoms on Au Nanoparticles Supported on Silica for the Selective Hydrogenation of Acetylene in Excess Ethylene. *New J Chem*. 2014;38:2043-2051. doi:10.1039/c3nj01136d.

97. Xu C-Q, Lee M-S, Wang Y-G, et al. Structural Rearrangement of Au–Pd Nanoparticles under Reaction Conditions: An ab Initio Molecular Dynamics Study. *ACS Nano*. 2017;11(2):1649-1658. doi:10.1021/acsnano.6b07409.

98. Zhang H, Watanabe T, Okumura M, Haruta M, Toshima N. Catalytically highly active top gold atom on palladium nanocluster. *Nat Mater*. 2011;11(1):49-52.

99. Xie S, Tsunoyama H, Kurashige W, Negishi Y, Tsukuda T. Enhancement in Aerobic Alcohol

Oxidation Catalysis of Au 25 Clusters by Single Pd Atom Doping. *ACS Catal*. 2012;2(7):1519-1523. doi:10.1021/cs300252g.

100. Ab Rahim MH, Forde MM, Jenkins RL, et al. Oxidation of Methane to Methanol with Hydrogen Peroxide Using Supported Gold-Palladium Alloy Nanoparticles. *Angew Chemie*. 2013;125(4):1318-1322. doi:10.1002/ange.201207717.

101. Personick ML, Madix RJ, Friend CM. Selective Oxygen-Assisted Reactions of Alcohols and Amines Catalyzed by Metallic Gold: Paradigms for the Design of Catalytic Processes. *ACS Catal*. 2017;7(2):965-985. doi:10.1021/acscatal.6b02693.

102. Choudhary TV, Sivadinarayana C, Datye AK, Kumar D, Goodman DW. Acetylene Hydrogenation on Au-Based Catalysts. *Catal Letters*. 2003;86(1):1-8. doi:10.1023/A:1022694505504.

103. Pawelec B, Venezia AM, La Parola V, Cano-Serrano E, Campos-Martin JM, Fierro JLG. AuPd alloy formation in Au-Pd/Al2O3 catalysts and its role on aromatics hydrogenation. *Appl Surf Sci*. 2005;242(3-4):380-391. doi:10.1016/j.apsusc.2004.09.004.

104. Sárkány A, Horváth A, Beck A. Hydrogenation of acetylene over low loaded Pd and Pd-Au/SiO2 catalysts. *Appl Catal A Gen*. 2002;229(1-2):117-125. doi:10.1016/S0926-860X(02)00020-0.

105. Piccolo L, Piednoir A, Bertolini J-C. Pd–Au single-crystal surfaces: Segregation properties and catalytic activity in the selective hydrogenation of 1,3-butadiene. *Surf Sci*. 2005;592(1-3):169-181. doi:10.1016/j.susc.2005.07.005.

106. Kittisakmontree P, Pongthawornsakun B, Yoshida H, Fujita S, Arai M, Panpranot J. The liquid-phase hydrogenation of 1-heptyne over Pd–Au/TiO2 catalysts prepared by the combination of incipient wetness impregnation and deposition–precipitation. *J Catal*. 2013;297:155-164. doi:10.1016/j.jcat.2012.10.007.

107. Sárkány A, Geszti O, Sáfrán G. Preparation of Pdshell–Aucore/SiO2 catalyst and catalytic activity for acetylene hydrogenation. *Appl Catal A Gen*. 2008;350(2):157-163. doi:10.1016/j.apcata.2008.08.012.

108. Zhang Y, Diao W, Williams CT, Monnier JR. Selective hydrogenation of acetylene in excess ethylene using Ag- and Au–Pd/SiO2 bimetallic catalysts prepared by electroless deposition. *Appl Catal A Gen*. 2014;469:419-426. doi:10.1016/j.apcata.2013.10.024.

109. Zhang L, Wang A, Miller T, et al. E ffi cient and Durable Au Alloyed Pd Single-Atom Catalyst for the Ullmann Reaction of Aryl Chlorides in Water. *ACS Catal*. 2014;4:1546-1553.

110. Chen M, Kumar D, Yi C-W, Goodman DW. The promotional effect of gold in catalysis by palladium-gold. *Science*. 2005;310(5746):291-293. doi:10.1126/science.1115800.

111. Yu W-Y, Mullen GM, Flaherty DW, Mullins CB. Selective Hydrogen Production from Formic Acid Decomposition on Pd–Au Bimetallic Surfaces. *J Am Chem Soc*. 2014;136(31):11070-11078. doi:10.1021/ja505192v.

112. Edwards J, Solsona B, Landon P, et al. Direct synthesis of hydrogen peroxide from H2 and O2 using TiO2-supported Au–Pd catalysts. *J Catal*. 2005;236(1):69-79.

doi:10.1016/j.jcat.2005.09.015.

113. Jirkovský JS, Panas I, Ahlberg E, Halasa M, Romani S, Schiffrin DJ. Single Atom Hot-Spots at Au–Pd Nanoalloys for Electrocatalytic H 2 O 2 Production. *J Am Chem Soc*. 2011;133(48):19432-19441. doi:10.1021/ja206477z.

114. Edwards JK, Solsona B, N EN, et al. Switching Off Hydrogen Peroxide Hydrogenation in the Direct Synthesis Process. *Science*. 2009;323(5917):1037-1041. doi:10.1126/science.1168980.

115. Gao F, Goodman DW. Pd–Au bimetallic catalysts: understanding alloy effects from planar models and (supported) nanoparticles. *Chem Soc Rev*. 2012;41(24):8009. doi:10.1039/c2cs35160a.

116. Hutchings GJ. Nanocrystalline gold and gold palladium alloy catalysts for chemical synthesis. *Chem Commun*. 2008;(10):1148-1164. doi:10.1039/B712305C.

117. Zhang L, Xie Z, Gong J. Shape-controlled synthesis of Au–Pd bimetallic nanocrystals for catalytic applications. *Chem Soc Rev*. 2016;45(14):3916-3934. doi:10.1039/C5CS00958H.

118. Zhang H, Watanabe T, Okumura M, Haruta M, Toshima N. Catalytically highly active top gold atom on palladium nanocluster. *Nat Mater*. 2011;11(1):49-52. doi:10.1038/nmat3143.

119. Kyriakou G, Boucher MB, Jewell a. D, et al. Isolated Metal Atom Geometries as a Strategy for Selective Heterogeneous Hydrogenations. *Science*. 2012;335(6073):1209-1212.

120. Boucher MB, Zugic B, Cladaras G, et al. Single atom alloy surface analogs in Pd0.18Cu15

nanoparticles for selective hydrogenation reactions. *Phys Chem Chem Phys*. 2013;15(29):12187-12196. doi:10.1039/c3cp51538a.

121. Ma L-L, Lv C-Q, Wang G-C. A DFT study and micro-kinetic analysis of acetylene selective hydrogenation on Pd-doped Cu(111) surfaces. *Appl Surf Sci*. 2017;410:154-165. doi:10.1016/j.apsusc.2017.01.084.

122. Ruff M, Takehiro N, Liu P, Nørskov JK, Behm RJ. Size-specific chemistry on bimetallic surfaces: A combined experimental and theoretical study. *ChemPhysChem*. 2007;8:2068-2071. doi:10.1002/cphc.200700070.

123. Takehiro N, Liu P, Bergbreiter A, Nørskov JK, Behm RJ. Hydrogen adsorption on bimetallic PdAu(111) surface alloys: minimum adsorption ensemble, ligand and ensemble effects, and ensemble confinement. *Phys Chem Chem Phys*. 2014;16:23930-23943. doi:10.1039/c4cp02589j.

124. Ramos M, Martínez AE, Busnengo HF. H2 Dissociation on Individual Pd Atoms Deposited on Cu(111). *Phys Chem Chem Phys*. 2012;14:303-310. doi:10.1039/c1cp22163a.

125. Yao Y, Goodman DW. Direct Evidence of Hydrogen Spillover from Ni to Cu on Ni-Cu Bimetallic Catalysts. *J Mol Catal A Chem*. 2014;383-384:239-242. doi:10.1016/j.molcata.2013.12.013.

126. Serrate D, Moro-Lagares M, Piantek M, Pascual JI, Ibarra MR. Enhanced Hydrogen Dissociation by Individual Co Atoms Supported on Ag(111). *J Phys Chem C*. 2014;118:5827-5832. doi:10.1021/jp411860b.

127. Yu W-Y, Mullen GM, Mullins CB. Hydrogen Adsorption and Absorption with Pd–Au Bimetallic Surfaces. *J Phys Chem C*. 2013;117(38):19535-19543. doi:10.1021/jp406736b.

128. Cao X, Ji Y, Luo Y. Dehydrogenation of Propane to Propylene by a Pd/Cu Single-Atom Catalyst: Insight from First-Principles Calculations. *J Phys Chem C*. 2015;119(2):1016-1023. doi:10.1021/jp508625b.

129. Qiu M, Fang Z, Li Y, et al. First-Principles Investigation of the Activation of CO2 Molecule on TM/Cu (TM=Fe, Co and Ni) Surface Alloys. *Appl Surf Sci*. 2015;353:902-912. doi:10.1016/j.apsusc.2015.06.165.

130. Linke R, Schneider U, Busse H, et al. Interaction of Hydrogen with Cu3Pt(111): Dissociation via Isolated Platinum Atoms. *Surf Sci*. 1994;307-309:407-411.

131. Zhang H, Kawashima K, Okumura M, Toshima N. Colloidal Au single-Atom Catalysts Embedded on Pd Nanoclusters. *J Mater Chem A*. 2014;2:13498-13508. doi:10.1039/c4ta01696c.

132. Cheng X, Zhao Y, Li F, Liu Y. Catalytic Mechanisms of Au11 and Au11-nPtn (n=1-2) clusters: a DFT Investigation on the Oxidation of CO by O2. *J Mol Model*. 2015;21:230. doi:10.1007/s00894-015-2780-4.

133. Yao Y, Goodman DW. New Insights into Structure–Activity Relationships for Propane Hydrogenolysis over Ni–Cu Bimetallic Catalysts. *RSC Adv*. 2015;5:43547-43551. doi:10.1039/C5RA07433A.

134. Zhang L, Wang A, Miller JT, et al. Efficient and Durable Au Alloyed Pd Single-Atom

Catalyst for the Ullmann Reaction of Aryl Chlorides in Water. *ACS Catal*. 2014;4(5):1546-1553. doi:10.1021/cs500071c.

135. Lucci FR. Surface Reactivity of Single Atom Alloys: Model Studies Guiding the Design of Atom Efficient Nanoparticle Catalysts. 2016.

136. Vilé G, Bridier B, Wichert J, Pérez-Ramírez J. Ceria in Hydrogenation Catalysis: High Selectivity in the Conversion of Alkynes to Olefins. *Angew Chemie Int Ed*. 2012;51(34):8620-8623. doi:10.1002/anie.201203675.

137. Carrasco J, Vilé G, Fernández-Torre D, Pérez R, Pérez-Ramírez J, Ganduglia-Pirovano MV. Molecular-Level Understanding of CeO 2 as a Catalyst for Partial Alkyne Hydrogenation. *J Phys Chem C*. 2014;118(10):5352-5360. doi:10.1021/jp410478c.

138. Cheng X, Shi Z, Glass N, et al. A review of PEM hydrogen fuel cell contamination: Impacts, mechanisms, and mitigation. *J Power Sources*. 2007;165(2):739-756.

139. Baschuk JJ, Li X. Carbon monoxide poisoning of proton exchange membrane fuel cells. *Int J Energy Res*. 2001;25(8):695-713.

140. Zhang J, Xie Z, Zhang J, et al. High temperature PEM fuel cells. *J Power Sources*. 2006;160(2):872-891. doi:10.1016/j.jpowsour.2006.05.034.

141. Stonehart P, Ross PN. The Commonality of Surface Processes in Electrocatalysis and Gas-Phase Heterogeneous Catalysis. *Catal Rev*. 1975;12(1):1-35. doi:10.1080/01614947508067520.

142. Venkataraman R, Kunz HR, Fenton JM. Development of New CO Tolerant Ternary Anode

Catalysts for Proton Exchange Membrane Fuel Cells. *J Electrochem Soc*. 2003;150(3):A278-A284. doi:10.1149/1.1543567.

143. Avgouropoulos G, Ioannides T. CO tolerance of Pt and Rh catalysts: effect of CO in the gas-phase oxidation of H2 over Pt and Rh supported catalysts. *Appl Catal B Environ*. 2005;56(1-2):77-86. doi:10.1016/j.apcatb.2004.07.016.

144. Zhou S, McIlwrath K, Jackson G, Eichhorn B. Enhanced CO tolerance for hydrogen activation in Au-Pt dendritic heteroaggregate nanostructures. *J Am Chem Soc*. 2006;128(6):1780-1781. doi:10.1021/ja056924+.

145. Liu Z, Jackson GS, Eichhorn BW. PtSn intermetallic, core-shell, and alloy nanoparticles as CO-tolerant electrocatalysts for H2 oxidation. *Angew Chem Int Ed Engl*. 2010;49(18):3173-3176. doi:10.1002/anie.200907019.

146. Watanabe M, Motoo S. Electrocatalysis by ad-atoms: Part III. Enhancement of the oxidation of carbon monoxide on platinum by ruthenium ad-atoms. *J Electroanal Chem Interfacial Electrochem*. 1975;60(3):275-283. doi:10.1016/S0022-0728(75)80262-2.

147. Koper MTM, Shubina TE, van Santen RA. Periodic Density Functional Study of CO and OH Adsorption on Pt−Ru Alloy Surfaces: Implications for CO Tolerant Fuel Cell Catalysts. *J Phys Chem B*. 2002;106(3):686-692. doi:10.1021/jp0134188.

148. Pedersen MO, Helveg S, Ruban A, et al. How a Gold Substrate can Increase the Reactivity of a Pt Overlayer. *Surf Sci*. 1999;426:395-409. doi:10.1016/S0039-6028(99)00385-4.

149. Kirstein W, Krüger B, Thieme F. CO adsorption studies on pure and Ni-covered Cu(111)

surfaces. *Surf Sci*. 1986;176:505-529.

150. Zhai Y, Pierre D, Si R, et al. Alkali-Stabilized Pt-OHx Species Catalyze Low-Temperature Water-Gas Shift Reactions. *Science*. 2010;329:1633-1636. doi:10.1126/science.1192449.

151. Yang M, Liu J, Lee S, et al. A common single-site Pt(II)-O(OH)x- species stabilized by sodium on “active” and “inert” supports catalyzes the water-gas shift reaction. *J Am Chem Soc*. 2015;137(10):3470-3473. doi:10.1021/ja513292k.

152. Kistler JD, Chotigkrai N, Xu P, et al. A single-site platinum CO oxidation catalyst in zeolite KLTL: microscopic and spectroscopic determination of the locations of the platinum atoms. *Angew Chem Int Ed Engl*. 2014;53(34):8904-8907. doi:10.1002/anie.201403353.

153. Peterson EJ, DeLaRiva AT, Lin S, et al. Low-temperature carbon monoxide oxidation catalysed by regenerable atomically dispersed palladium on alumina. *Nat Commun*. 2014;5:4885. doi:10.1038/ncomms5885.

154. Qiao B, Wang A, Yang X, et al. Single-atom catalysis of CO oxidation using Pt1/FeOx. *Nat Chem*. 2011;3(8):634-641. doi:10.1038/nchem.1095.

155. Sattler JJHB, Ruiz-Martinez J, Santillan-Jimenez E, Weckhuysen BM. Catalytic Dehydrogenation of Light Alkanes on Metals and Metal Oxides. *Chem Rev*. 2014;114(20):10613-10653. doi:10.1021/cr5002436.

156. Meyers RA. *Handbook of Petroleum Refining Processes*. Third Edit. McGraw-Hill Education; 2004.

157. Nykänen L, Honkala K. Density Functional Theory Study on Propane and Propene

Adsorption on Pt(111) and PtSn Alloy Surfaces. *J Phys Chem C*. 2011;115(19):9578-9586. doi:10.1021/jp1121799.

158. Yang M-L, Zhu Y-A, Zhou X-G, Sui Z-J, Chen D. First-Principles Calculations of Propane Dehydrogenation over PtSn Catalysts. *ACS Catal*. 2012;2(6):1247-1258. doi:10.1021/cs300031d.

159. Rioux RM, Song H, Hoefelmeyer JD, Yang P, Somorjai GA. High-Surface-Area Catalyst Design: Synthesis, Characterization, and Reaction Studies of Platinum Nanoparticles in Mesoporous SBA-15 Silica †. *J Phys Chem B*. 2005;109(6):2192-2202. doi:10.1021/jp048867x.

160. Song H, Rioux RM, Hoefelmeyer JD, et al. Hydrothermal Growth of Mesoporous SBA-15 Silica in the Presence of PVP-Stabilized Pt Nanoparticles: Synthesis, Characterization, and Catalytic Properties. *J Am Chem Soc*. 2006;128(9):3027-3037. doi:10.1021/ja057383r.

161. Spivey JJ, Roberts GW, Jr. JGG, Kim S, Rhodes WD. Turnover frequencies in metal catalysis: Meanings, functionalities and relationships. In: ; :320-348. doi:10.1039/9781847553294-00320.

162. Cortright RD, Dumesic JA. Microcalorimetric, Spectroscopic, and Kinetic Studies of Silica Supported Pt and Pt/Sn Catalysts for Isobutane Dehydrogenation. *J Catal*. 1994;148(2):771-778. doi:10.1006/jcat.1994.1263.

163. Yang M-L, Zhu Y-A, Fan C, Sui Z-J, Chen D, Zhou X-G. DFT study of propane dehydrogenation on Pt catalyst: effects of step sites. *Phys Chem Chem Phys*.

2011;13(8):3257. doi:10.1039/c0cp00341g.

164. Lieske H, Lietzb G, Spindler H, Völterb J. Reactions of platinum in oxygen- and hydrogen-treated Pt/$gamma;-Al2O3 catalysts I. Temperature-programmed reduction, adsorption, and redispersion of platinum. *J Catal*. 1983;81(1):8-16. doi:10.1016/0021-9517(83)90142-2.

165. Monzón A, Garetto TF, Borgna A. Sintering and redispersion of Pt/γ-Al2O3 catalysts: a kinetic model. *Appl Catal A Gen*. 2003;248(1-2):279-289. doi:10.1016/S0926-860X(03)00300-4.

166. Iglesias-Juez A, Beale AM, Maaijen K, Weng TC, Glatzel P, Weckhuysen BM. A combined in situ time-resolved UV-Vis, Raman and high-energy resolution X-ray absorption spectroscopy study on the deactivation behavior of Pt and PtSn propane dehydrogenation catalysts under industrial reaction conditions. *J Catal*. 2010;276:268-279. doi:10.1016/j.jcat.2010.09.018.

167. Nagaraja BM, Shin C-H, Jung K-D. Selective and stable bimetallic PtSn/θ-Al2O3 catalyst for dehydrogenation of n-butane to n-butenes. *Appl Catal A Gen*. 2013;467:211-223. doi:10.1016/j.apcata.2013.07.022.

168. Virnovskaia A, Morandi S, Rytter E, Ghiotti G, Olsbye U. Characterization of Pt,Sn/Mg(Al)O Catalysts for Light Alkane Dehydrogenation by FT-IR Spectroscopy and Catalytic Measurements. *J Phys Chem C*. 2007;111(40):14732-14742. doi:10.1021/jp074686u.

169. Cortright RD, Hill JM, Dumesic JA. Selective dehydrogenation of isobutane over supported Pt/Sn catalysts. *Catal Today*. 2000;55(3):213-223. doi:10.1016/S0920-5861(99)00249-7.

170. Lieske H, Sárkány A, Völter J. Hydrocarbon adsorption and coke formation on Pt/Al2O3 and Pt-Sn/Al2O3 catalysts. *Appl Catal*. 1987;30(1):69-80. doi:10.1016/S0166-9834(00)81012-X.

171. Wu J, Peng Z, Bell AT. Effects of composition and metal particle size on ethane dehydrogenation over PtxSn100−x/Mg(Al)O (70⩽x⩽100). *J Catal*. 2014;311:161-168. doi:10.1016/j.jcat.2013.11.017.

172. Boudart M, Aldag A, Benson JE, Dougharty NA, Girvin Harkins C. On the specific activity of platinum catalysts. *J Catal*. 1966;6(1):92-99. doi:10.1016/0021-9517(66)90113-8.

173. Cardona-Martinez N, Dumesic JA. Applications of Adsorption Microcalorimetry to the Study of Heterogeneous Catalysis. In: ; 1992:149-244. doi:10.1016/S0360-0564(08)60007-3.

174. Cortright RD, Dumesic JA. Effects of Potassium on Silica-Supported Pt and Pt/Sn Catalysts for Isobutane Dehydrogenation. *J Catal*. 1995;157(2):576-583. doi:10.1006/jcat.1995.1322.

175. Shen J, Hill JM, Watwe RM, Spiewak BE, Dumesic JA. Microcalorimetric, Infrared Spectroscopic, and DFT Studies of Ethylene Adsorption on Pt/SiO 2 and Pt−Sn/SiO 2 Catalysts. *J Phys Chem B*. 1999;103(19):3923-3934. doi:10.1021/jp9902452.

176. Natal-Santiago MA, Podkolzin SG, Cortright RD, Dumesic JA. Microcalorimetric studies of interactions of ethene, isobutene, and isobutane with silica-supported Pd, Pt, and PtSn. *Catal Letters*. 1997;45(3/4):155-163. doi:10.1023/A:1019004720871.

177. Gao J, Zhao H, Yang X, Koel BE, Podkolzin SG. Geometric Requirements for Hydrocarbon Catalytic Sites on Platinum Surfaces. *Angew Chemie Int Ed*. 2014;53(14):3641-3644. doi:10.1002/anie.201309043.

178. Zhang Y, Zhou Y, Shi J, et al. Comparative study of bimetallic Pt-Sn catalysts supported on different supports for propane dehydrogenation. *J Mol Catal A Chem*. 2014;381:138-147. doi:10.1016/j.molcata.2013.10.007.

179. Silvestre-Albero J, Serrano-Ruiz JC, Sepúlveda-Escribano A, Rodríguez-Reinoso F. Modification of the catalytic behaviour of platinum by zinc in crotonaldehyde hydrogenation and iso-butane dehydrogenation. *Appl Catal A Gen*. 2005;292:244-251. doi:10.1016/j.apcata.2005.06.005.

180. Vu BK, Song MB, Ahn IY, et al. Pt–Sn alloy phases and coke mobility over Pt–Sn/Al2O3 and Pt–Sn/ZnAl2O4 catalysts for propane dehydrogenation. *Appl Catal A Gen*. 2011;400(1-2):25-33. doi:10.1016/j.apcata.2011.03.057.

181. Ballarini AD, de Miguel SR, Castro AA, Scelza OA. n-Decane dehydrogenation on Pt, PtSn and PtGe supported on spinels prepared by different methods of synthesis. *Appl Catal A Gen*. 2013;467:235-245. doi:10.1016/j.apcata.2013.07.030.

182. Casella ML, Siri GJ, Santori GF, Ferretti OA, Ramírez-Corredores MM. Surface

Characterization of Li-Modified Platinum/Tin Catalysts for Isobutane Dehydrogenation. *Langmuir*. 2000;16(13):5639-5643. doi:10.1021/la991437r.

183. Siri GJ, Bertolini GR, Casella ML, Ferretti OA. PtSn/γ-Al2O3 isobutane dehydrogenation catalysts: The effect of alkaline metals addition. *Mater Lett*. 2005;59(18):2319-2324. doi:10.1016/j.matlet.2005.03.013.

184. Aguilar-Ríos G, Valenzuela MA, Armendariz H, et al. Metal-support effects and catalytic properties of platinum supported on zinc aluminate. *Appl Catal A Gen*. 1992;90(1):25-34. doi:10.1016/0926-860X(92)80245-8.

185. Lai Y, He S, Li X, Sun C, Seshan K. Dehydrogenation of n-dodecane over PtSn/MgAlO catalysts: Investigating the catalyst performance while monitoring the products. *Appl Catal A Gen*. 2014;469:74-80. doi:10.1016/j.apcata.2013.09.042.

186. Taccardi N, Grabau M, Debuschewitz J, et al. Gallium-rich Pd–Ga phases as supported liquid metal catalysts. *Nat Chem*. 2017;9(9):862-867. doi:10.1038/nchem.2822.

187. Schweitzer NM, Hu B, Das U, et al. Propylene Hydrogenation and Propane Dehydrogenation by a Single-Site Zn 2+ on Silica Catalyst. *ACS Catal*. 2014;4(4):1091-1098. doi:10.1021/cs401116p.

188. Jiang F, Zeng L, Li S, Liu G, Wang S, Gong J. Propane Dehydrogenation over Pt/TiO2-Al2O3 Catalyst. *ACS Catal*. 2015;5:438-447. doi:10.1021/ie800848c.

189. Tedsree K, Li T, Jones S, et al. Hydrogen production from formic acid decomposition at room temperature using a Ag-Pd core-shell nanocatalyst. *Nat Nanotechnol*.

2011;6(5):302-307.

Chapter 2. Experimental methods and procedures

2.1 Catalyst preparation

2.1.1 Materials and Chemicals

For the preparation of nanoparticles, metal precursors chloroplatinic acid hydrate ($H_2PtCl_6 \cdot x\ H_2O$, ~38% Pt basis, Sigma-Aldrich), and copper nitrate trihydrate ($Cu(NO_3)_2 \cdot 3\ H_2O$, Johnson Matthey) were used. Aluminum oxide (ϒ-Al_2O_3, ultra-pure grade 99.99%, surface area 70-100 m^2/g, Inframat Advanced Materials) was used as catalyst support. Poly(vinylpyrrolidone) (PVP, MW= 58,000, Alfa Aesar) was used as stabilizing agent for colloidal nanoparticles. L-ascorbic acid (Sigma-Aldrich) was used as anti-oxidizing agent. The copper precursor was reduced with sodium borohydride ($NaBH_4$, Sigma-Aldrich) to form the nanoparticles (NPs).

2.1.2 Pt-Cu catalysts

Pt-Cu bimetallic samples were synthesized by galvanic replacement (GR) reaction as described below. Briefly, an aqueous solution of $Cu(NO_3)_2$ and PVP (200:1 molar ratio of Cu to PVP, 1:1 wt/wt) was degassed in vacuum and in nitrogen gas sequentially. A 0.1 M solution of ascorbic acid was added to the Cu/PVP solution, followed by the addition of $NaBH_4$ solution (0.1 M) dropwise. The solution turned to an opaque brown suspension after the addition of $NaBH_4$. Aluminum oxide (2 g) was suspended in 100 ml of DI water under magnetic stirring and added to the Cu NPs colloidal solution dropwise. The solution was kept under flowing nitrogen and constant stirring for 30 min before it was filtered and washed with DI water 3 times. The

resulting materials were dried in vacuum for 24 h, calcined in air to 350 °C at 2 °C/min and held for 4 h.

GR reaction took place in aqueous solution under nitrogen protection with constant stirring and refluxing at 100 °C. The desired amount of Pt precursor ($H_2PtCl_6 \cdot x\ H_2O$, Sigma - Aldrich) was added to the suspension of Cu NPs (pre-reduced in 100% H_2 at 300 °C) containing HCl (2mM). The Pt precursor was reduced by Cu host via the displacement reaction shown in Scheme 1. After 20 min, the resulting material was filtered, washed and dried in vacuum.

$PtCl_6^{2-} + 4\ e^- \rightarrow Pt + 6\ Cl^-$ ($\Delta E° = 0.74$ V)

$Cu \rightarrow Cu^{2+} + 2\ e^-$ ($\Delta E° = -0.34$ V)

Scheme 1. Galvanic replacement reaction.

2.1.3 Pd-Au catalysts

PdAu-SAA NPs were prepared using sequential reduction methods as reported in Tedsree et al. with some modifications.[1] First, Au NPs were prepared as follows: 0.3 g $HAuCl_4 \cdot 3H_2O$ and 1.2 g poly(vinylpyrrolidinone) (PVP, MW= 58,000) were mixed in 50 mL ethylene glycol (EG) in a round bottom flask with vigorous stirring. The solution was purged with N_2 for one hour before 0.3 g $NaHCO_3$ was added. The solution was then heated to 90 °C at 5 °C/min with N_2 flowing through the round bottom flask. The solution was held at 90 °C for half an hour before cooling to ambient temperature. The Au NPs were thus obtained. To prepare PdAu-SAA NPs, the desired amount of $Pd(NO_3)_2 \cdot xH_2O$ was dissolved in 1 mL EG and added to

the round bottom flask containing the EG-dispersed Au NPs. Under N_2 purge and vigorous stirring, the solution was heated to 90 °C at 5 °C/min and held for 8 h. After the solution was cooled to ambient temperature, 300 mL of acetone was added in order to precipitate the NPs. The acetone-EG solution was centrifuged at 3000 rpm for 10 minutes to separate the NPs. The retrieved NPs were then washed with ethanol and hexane thrice and dried in vacuum overnight. To obtain silica supported Au and PdAu NPs, fumed silica (heat treated in air at 650 °C for 3 h) was introduced into the NP gold and PdAu-SAA solutions in water and stirred overnight. The slurry carrying the supported NPs was centrifuged and dried in vacuum for 24 h. The supported NPs were calcined in air at 300 °C for 1 hour followed by reduction in H_2 at 250 °C for 1 hour. The unsupported Pd-NPs were prepared by the same method with $Pd(NO_3)_2$ precursor.

2.2 Catalyst characterization and activity measurements

2.2.1 Catalyst characterization

2.2.1.1 Surface Area

The BET surface areas of the samples were measured by single-point N_2 adsorption/desorption cycles in a Micromeritics AutoChem II 2920 apparatus. Each sample was degassed in He at 250-350°C for 60 min before the adsorption. A 30 % N_2-He gas mixture was used in the BET measurement.

2.2.1.2 High-resolution transmission electron microscopy (HR-TEM)

HR-TEM was conducted on a JEOL 2010 electron microscope with 200 kV and 107 µA beam emission. The specimens were obtained by drying one drop of colloidal solution of NPs in ethanol onto a carbon film with nickel or copper covered microgrid.

2.2.1.3 Materials compositions

The elemental composition of the catalysts was measured by inductively coupled plasma atomic emission spectrometry (ICP-AES). The samples were dissolved in HCl-H_2O_2 or HCl-HNO_3 mixture overnight. The solution was further diluted before the ICP tests for all elemental concentrations to be within the 1-100 ppm range.

The Pt and Cu loading on each sample was measured by ICP-AES on a Leeman Labs PS1000 instrument. The solid samples were digested in concentrated HCl and H_2O_2 prior to the testing. No Pt or Cu was detected by XPS on the solid alumina support after digestion. The collected wash solution from GR and Cu NP preparation was used without additional treatments.

2.2.1.4 Ultraviolet and visible light (UV-Vis) absorption spectroscopy

UV-Vis absorption spectra were collected in the range of 200 - 800 nm using an Evolution^{TM} 300 UV-Vis Spectrophotometer (Thermo Scientific). The diluted solution of the samples was placed in a quartz cuvette. Standard solution was prepared with $HPtCl_6$ and $Cu(NO_3)_2$.

2.2.1.5 X-ray photoelectron spectroscopy (XPS)

XPS data were obtained by using a Thermo Scientific K-Alpha system equipped with an Al source and a double focusing hemispherical analyzer with a 128-channel detector at a pass energy of 50-100 eV. To prepare the XPS samples, the powders were deposited on the copper tapes or silver plates. The copper tapes and silver plates were fixed on a glass slide with the carbon tapes before being transferred into the XPS chamber.

2.2.1.6 X-ray powder diffraction (XRD)

XRD analysis was performed on a PANalytical X'Pert Pro instrument. Cu Kα radiation was used with a power setting of 40 mA, 45 kV. Data was collected for 2θ between 10° and 80°. The catalysts were reduced in 100% H_2 at 350 °C (Pt-Cu samples) or 300 °C (Cu monometallic samples) prior to the XRD measurements.

2.2.1.7 X-ray absorption spectroscopy (XAS)

XAS was performed at beamline X18B at Brookhaven National Laboratory and beamline 12-BM at Argonne National Laboratory. The Pt-Cu and Pt NPs were reduced in 100% H_2 at 350 °C (Pt-Cu bimetallic samples) or 400 °C (Pt monometallic samples) *in situ* prior to the tests. PdAu samples were treated in H_2 at ambient temperature to 150 °C. The X-ray absorption near edge structure (XANES) spectra were collected in H_2 or He atmospheres. Extended X-ray

absorption fine structure (EXAFS) was measured in H_2 or He. The spectra were recorded in the fluorescence mode at room temperature.

XAS data were processed and analyzed using Athena and Artemis.[2] The XANES spectra were background corrected and normalized. And the EXAFS data were fitted in r-space with the models based on metallic Pt, $PtCu_3$, and PtO.[3]

2.2.1.8 Scanning transmission electron microscopy (STEM)

Aberration-corrected high-angle annular dark-field (HAADF) STEM images of Pt-Cu NPs were obtained at a nominal resolution of 0.07 nm using a JEOL 2200FS-AC STEM/TEM equipped with a hexapole corrector (CEOS GmbH, Heidelberg, Germany) at Oak Ridge National Laboratory. Energy-dispersive X-ray spectroscopy (EDS) imaging was conducted with a Bruker-AXS 30 mm^2 silicon-drift detector system and Pt, Cu, Al and O elemental maps were collected. The instrument was operated at 200 kV for all imaging and EDS work.

HAADF-STEM images of Pd/Au NPs were obtained at a nominal resolution of 0.078 nm using a JEOL ARM200 STEM/TEM at center for nanoscale systems at Harvard University. EDS imaging was conducted, and elemental maps were collected. The instrument was operated at 200 kV for all imaging and EDS work.

2.2.1.9 Fourier-transformed infrared spectroscopy (FTIR)

FTIR spectra were collected using a Nicolet Nexus 470 spectrometer equipped with a MCT-B detector in the single beam absorbance mode at a resolution of 2 cm^{-1}. Prior to the IR

experiments, the samples were reduced in pure H_2 at 300 (Cu-NP), 350 ($Pt_{0.008}$Cu-SAA and $Pt_{0.39}$Cu-bimetallic) or 400 (Pt-NP) °C in a quartz microreactor and sealed in the glass vials. The powder sample of 0.02 g was made into a thin pellet (~ 1cm in diameter). The sample was then loaded into a flow cell sealed with NaCl windows and allows the CO flow through the catalyst pellet. In a typical CO adsorption IR experiment, the sample was first reduced in 50 mL/min 5 % H_2-He for 1 hr at 200 ^oC followed with the He purge to cool down to 25 ^oC. Baseline was collected at 25 ^oC under He purge after the catalyst has been swept for at least 30 min. The sample was then exposed to 1 % CO-He flow at the same temperature for 45 min and was purged again with He for at least another 30 min until the gas phase CO signal was fully diminished (rather quickly within 5 min of purge) and the catalyst surface adsorption spectra has minimal difference between the IR scans. The IR spectra shown in the main text were collected afterwards at 25, 40, 60, 80, and 100 °C. A ramping rate of 5 ^oC/min was used. The corresponding spectra at each temperature were collected after the sample was stabilized at the target temperature for 10 min.

2.2.2 Catalytic activity measurements

2.2.2.1 Flow reactor studies

The selective hydrogenation activity of the catalysts was tested in a quartz-bed flow reactor for 1,3-butadiene hydrogenation with 400 mg of catalyst diluted by 1.5 g of quartz particles. The as synthesized Pt-Cu catalysts were reduced in H_2 at 350 °C for 4 h prior to the reaction, the Cl-residues were removed in H_2 as well. A gas mixture of 1.25 % 1,3-butadiene, 20 % H_2 and balance He (flow rate=20 mL/min, GHSV=1,200 h^{-1}) was introduced at 120 °C,

followed by descending temperature testing. Gas chromatograph (GC) injections were done at each temperature after the temperature was stabilized for at least 10 min. The exit gas stream was analyzed by a HP-6890 GC equipped with a 30 ft. column (1/8 in., filled with Sebaconitrile 20 % Chromosorb Paw 80/100).

The hydrogenation activity of the catalysts was tested in a packed-bed flow microreactor (L=22 inch, O.D.=1/2 inch) with 100 mg of catalyst diluted by 0.5 g of quartz particles. The samples were pre-reduced in 100% H_2 at 25 mL/min (300 °C for Cu_{15}/Al_2O_3, 350 °C for Pt-Cu samples and 400 °C for $Pt_{0.1}/Al_2O_3$) with a heating rate of 2 °C/min, and then cooled to 30 °C before the reaction gas mixture (2 % 1,3-butadiene, 20 % H_2 and balance He. GHSV=12,000 h^{-1}) was introduced. The tests were started at 30 °C and the temperature was raised to higher values (60, 90, 120, 150 and 170 °C) at 5 °C/min and held at each temperature for 30 min. After reaching 170 °C, the samples were cooled back to RT, collecting data at selected intermediate temperatures to check for (de)activation. Gas chromatograph (GC) injections were done by sampling the gas at various temperatures after stabilizing the temperature for 10 min. Moreover, long-time stability tests were conducted isothermally at 160 °C for 46 h following the activity tests (2 % 1,3-butadiene, 20 % H_2 and balance He. GHSV=12,000 h^{-1}). The exit gas stream was analyzed by a HP6890 GC equipped with a flame ionization detector (FID). A 30 ft. column (1/8 in. dia.) filled with Sebaconitrile 20 % Chromosorb Paw 80/100 supplied by Sigma-Aldrich was used to separate the gas species.

The activity tests with added propylene were conducted in a similar fashion with a gas mixture of 2 % 1,3-butadiene, 20 % propylene, 16 % H_2 and balance He. The total flow rate was 50 mL/min, and the catalyst load was 100mg (GHSV=12,000 h^{-1}). The steady-state stability tests

were conducted isothermally at 160 °C and 145 °C, for 12 h at each temperature. The exit gas stream composition was determined by GC as described above.

Cyclic hydrogenation tests were performed to probe the stability of the catalysts. The first cycle was performed as described for the activity tests. Then the sample was treated in 100 % H_2 at 350 °C for 1 h. The reaction gas mixture (2 % 1,3-butadiene, 20 % H_2 and balance He. GHSV=12,000 h^{-1}) was introduced at 170 °C followed by cooling down to other temperatures. GC injections were done at specified temperatures after the temperature was held stable for at least 10 min.

H_2-D_2 exchange was conducted in a packed-bed flow microreactor (L=22 inch, O.D.=1/2 inch) with 80-90 mg of catalyst diluted by 0.5 g of quartz particles. The samples were pre-reduced in 100% H_2 (at 350 °C for $Pt_{0.008}$Cu-SAA and 400 °C for Pt-NP) and then cooled to desired temperature before the reaction gas mixture (33% H_2, 33% D_2, 3.3% CO and balance Ar. Flow rate=50mL/min) was introduced. For the isothermal H_2-D_2 exchange, CO was introduced to the gas phase and turned off at the certain time points while H_2 and D_2 were flowing. To do temperature programmed H_2-D_2 exchange, a gas mixture of 33% H_2, 33% D_2, 3.3% (or 667ppm) CO and balance Ar (flow rate=50 mL/min) was introduced at 120 °C and temperature was increased to 200 °C at 5 °C/min. The gas effluent from the reactor was analyzed by mass spectrometry (SRS RGA 200). Acetylene hydrogenation was performed in a packed-bed flow microreactor (L=22 inch, O.D.=1/2 inch) at 70 and 80 °C isothermally (20% H_2, 2.2% C_2H_2, 200 ppm CO, 10% Argon, balance He, flow rate=24-48 mL/min). 50-500 mg catalysts were used. The exit gas stream was analyzed by mass spectrometry.

Temperature- programmed oxidation (TPO) was conducted in a Micromeritics AutoChem II 2920 instrument equipped with a mass spectrometer. The spent catalyst (33 mg) used in the long-time stability testing with or without addition of propylene was loaded to the microreactor for the TPO test. The sample was degassed with He, flowing at a rate of 50 mL/min, with a heating rate of 10 °C/min up to 100 °C, and cooled to 25 °C in He. Next, 20 % O_2 in He at the same flowrate was introduced. The sample was stabilized at 25 °C for 5 min followed by raising the temperature to 800 °C at 3 °C/min. The CO_2 in the gas stream was analyzed online by a mass spectrometer (Pfeiffer, TCP270). Temperature- programmed desorption in He (He-TPD) was performed with a similar setup. The spent catalyst (33 mg) from the long-time stability testing with or without addition of propylene was loaded to the micro reactor for the He-TPD test. After degassing in pure He flow (50 mL/min) for 20 min at ambient temperature, the sample was heated in the He gas (50 mL/min) to 800 °C at 3 °C/min. The exit gas stream was analyzed online by a mass spectrometer in histogram-spectrum mode scanning mass-to-charge ratio (m/z) between 1 and 120.

2.2.2.2 Batch reactor studies

A stainless-steel Parr reactor was used for the hydrogenation of 1-hexyne. The desired amount of sample was added to 20-80 mL ethanol. The mixture was stirred for half an hour and sonicated for 15 minutes before being loaded into the reactor. Pure hydrogen was bubbled through the solution while stirring for 1 h. 1-hexyne was injected into the solution to reach 1% vol/vol concentration in ethanol. The reactor was then pressurized with pure hydrogen to the

desired pressure (5 bar) under stirring at 600 rpm. Liquid-phase specimens were taken from the reactor at different time points.

Leaching test: the catalyst sample was put in the typical hydrogenation reaction condition (5 bar H_2, 600 rpm, 25 °C) for 6 hours before centrifugation to separate the solid sample from the liquid solution. The liquid solution was purged with pure H_2 for one hour before adding fresh 1-hexyne with 1/100 (vol/vol) ratio. The solution was transferred into the reactor and held under reaction condition for 60 min. Liquid-phase specimens were taken from the reactor at different time points.

2.3 References

1. Tedsree K, Li T, Jones S, et al. Hydrogen production from formic acid decomposition at room temperature using a Ag-Pd core-shell nanocatalyst. *Nat Nanotechnol*. 2011;6(5):302-307. doi:10.1038/nnano.2011.42.

2. Ravel B, Newville M. ATHENA, ARTEMIS, HEPHAESTUS: Data analysis for X-ray absorption spectroscopy using IFEFFIT. In: *Journal of Synchrotron Radiation*. Vol 12. ; 2005:537-541.

3. Ravel B. ATOMS: Crystallography for the X-ray absorption spectroscopist. *J Synchrotron Radiat*. 2001;8(2):314-316.

Chapter 3. PtCu single-atom alloy nanoparticle catalysts for selective hydrogenation of 1,3-butadiene

3.1 Introduction

Pt is one of the most widely used transition metal catalysts due to its superior catalytic performance for both oxidation and hydrogenation reactions. It is used extensively in electrochemical and heterogeneous catalysts with applications in fuel cells, automotive catalytic converters, and industrial hydrocarbon cracking processes.[1,2]

This chapter reports the very low concentrations of individual, isolated Pt atoms in a Cu surface catalyze the industrially important reaction of butadiene hydrogenation with high selectivity to butene. Butadiene poisons polymerization catalysts even at low concentrations (< 10 ppm) in industrial alkene streams.[3] Of particular interest is the butadiene impurity in propene feedstocks used to produce 42.3 million tons of polypropylene annually.[4] The selective hydrogenation of butadiene to butene serves to increase the purity of alkene feedstocks without reducing their overall concentration. Therefore, catalysts that selectively hydrogenate butadiene to butene and prevent the hydrogenation of butene to butane are of great interest. It has been proposed that the observed product distribution is controlled by the adsorption energy of butadiene to the catalytic surface and weaker bonding is known to direct the product distribution in favor of butene formation.[5,6] We designed and prepared highly diluted Pt-Cu nanoparticles using the single-atom alloy (SAA) principle.[7,8] Nominal amounts of Pt (2 at. %) in

Cu nanoparticle catalysts were found to exhibit high activity and selectivity for butadiene hydrogenation to butene under relatively mild conditions.

3.2 Experimental methods

Pt-Cu nanoparticles (NPs) with different Pt-loadings were synthesized using the galvanic replacement (GR) method on the pre-reduced Cu NPs as described by Boucher et al.[8] The Cu NPs were pre-formed and supported on ϒ-Al_2O_3, followed by calcination in air at 350 °C. GR took place in aqueous solution under nitrogen protection with constant stirring and refluxing at 100 °C. Desired amounts of Pt precursor ($H_2PtCl_6 \cdot xH_2O$, Sigma - Aldrich) were added to a suspension of Cu NPs in an aqueous solution containing HCl (2mM). After 20 min, the resulting material was filtered, washed and dried in vacuum. The sample information is listed in Table 3.1.

Table 3.1. Sample composition

Sample	Composition[a]	Preparation Method
Cu_{15}/Al_2O_3	14.9 at.% Cu	Colloidal
$Pt_{0.1}/Al_2O_3$	0.12 at.% Pt	IWI[b]
$Pt_{0.1}Cu_{14}/Al_2O_3$	0.11 at.% Pt, 13.7 at.% Cu	GR
$Pt_{0.2}Cu_{14}/Al_2O_3$	0.25 at.% Pt, 12.3 at.% Cu	GR
Pt_2Cu_6/Al_2O_3	2.2 at.% Pt, 5.6 at.% Cu	GR

[a] Determined by ICP-AES.

[b] Incipient wetness impregnation (IWI).

HAADF-STEM imaging and EDS elemental mapping were conducted as described in chapter 2. XAS measurements at the Pt L_{III}-edge were made at Argonne National Laboratory and Brookhaven National Laboratory in fluorescence mode at room temperature. As described in chapter 2, all samples were reduced in H_2 *in situ* prior to the measurements. XAS data were processed and analyzed using Athena and Artemis.[9] The XANES spectra were background corrected and normalized. And the EXAFS data were fitted in r-space with the models based on metallic Pt, $PtCu_3$, and PtO.[10]

The selective hydrogenation activity of the catalysts was tested in a quartz-bed flow reactor for 1,3-butadiene hydrogenation with 400 mg of catalyst diluted by 1.5 g of quartz particles. The as synthesized Pt-Cu catalysts were reduced in H_2 at 350 °C for 4 h prior to the

reaction, the Cl-residues were removed in H_2 as well. A gas mixture of 1.25 % 1,3-butadiene, 20 % H_2 and balance He (flow rate=20 mL/min, GHSV=1,200 h^{-1}) was introduced at 120 °C, followed by descending temperature testing. Gas chromatograph (GC) injections were done at each temperature after the temperature was stabilized for at least 10 min. The exit gas stream was analyzed by a HP6890 GC equipped with a 30 ft. column (1/8 in., filled with Sebaconitrile 20 % Chromosorb Paw 80/100).

The activity tests with added propylene were conducted with a gas mixture of 2 % 1,3-butadiene, 20 % propylene, 16 % H_2 and balance He at a flow rate of 50 mL/min (100mg catalyst, GHSV=12,000 h^{-1}). After the activity tests with ascending temperature up to 170 °C, the stability tests were performed isothermally at 160 °C and 145 °C for 12 h at each temperature.

3.3 Results and Discussion

3.3.1 Characterization of PtCu NP catalysts

Similar to Boucher et al.,[11] the Cu NPs were prepared without a support. The average particle size of colloidal Cu NPs is 4.24 ± 1.00 nm with a narrow particle size distribution (Figure 3.1). The Al_2O_3 powder were subsequently introduced to the Cu@PVP colloidal solution to effect Cu@PVP deposition on the support. The alumina supported Cu@PVP were calcined in air to 350 °C to burn off the PVP surfactant. A typical TEM image of the calcined Cu_{15}/Al_2O_3 is shown in Figure 3.1B. Figure 3.2 shows the high resolution TEM (HRTEM) images of Cu_{15}/Al_2O_3. The lattice spacing of Cu facets is consistent with that of metallic Cu (Figure 3.2B). Additionally,

we found the average crystalline size of Cu NPs increased to 13 nm upon the heat treatments, as determined from the X-ray diffractograms in Figure 3.8 by Scherrer equation. Boucher et al. reported the sintering of Cu NP during the similar heat treatment in air, and they showed the particle size of Cu NP was more than double as a result of this process.[11]

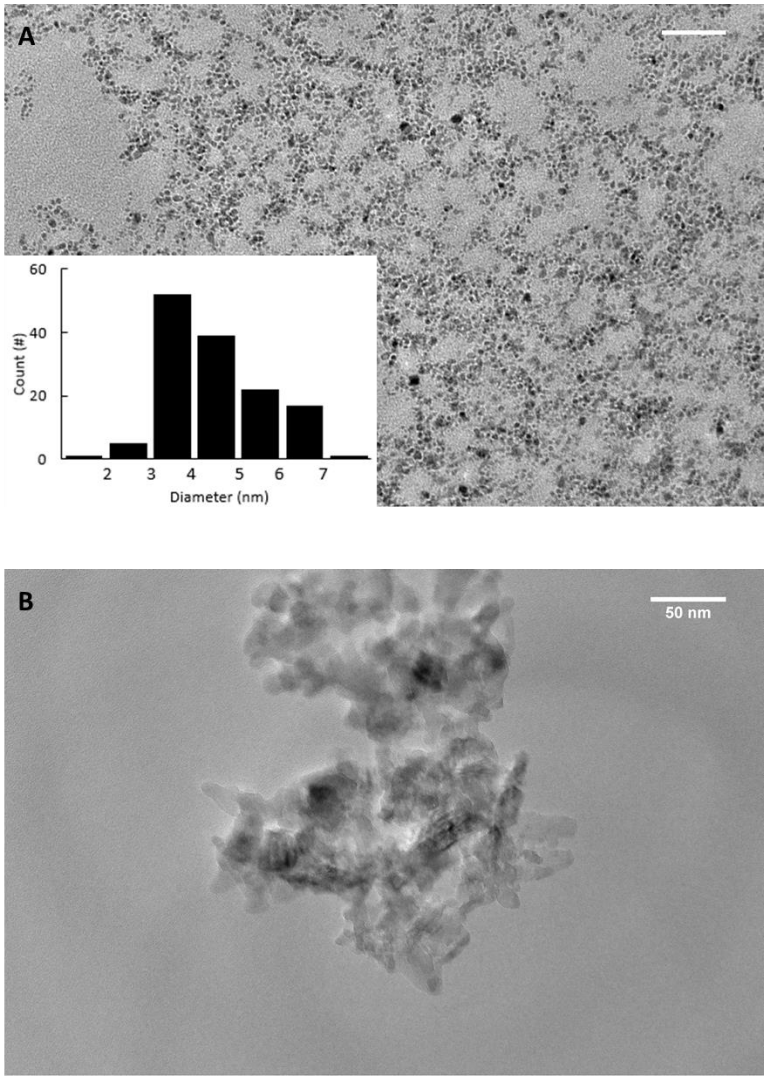

Figure 3.1. (A) TEM images of unsupported Cu NPs, inset is particle size distribution (scale bar=50 nm). (B) TEM image of ϒ-Al_2O_3 supported Cu NPs (calcined).

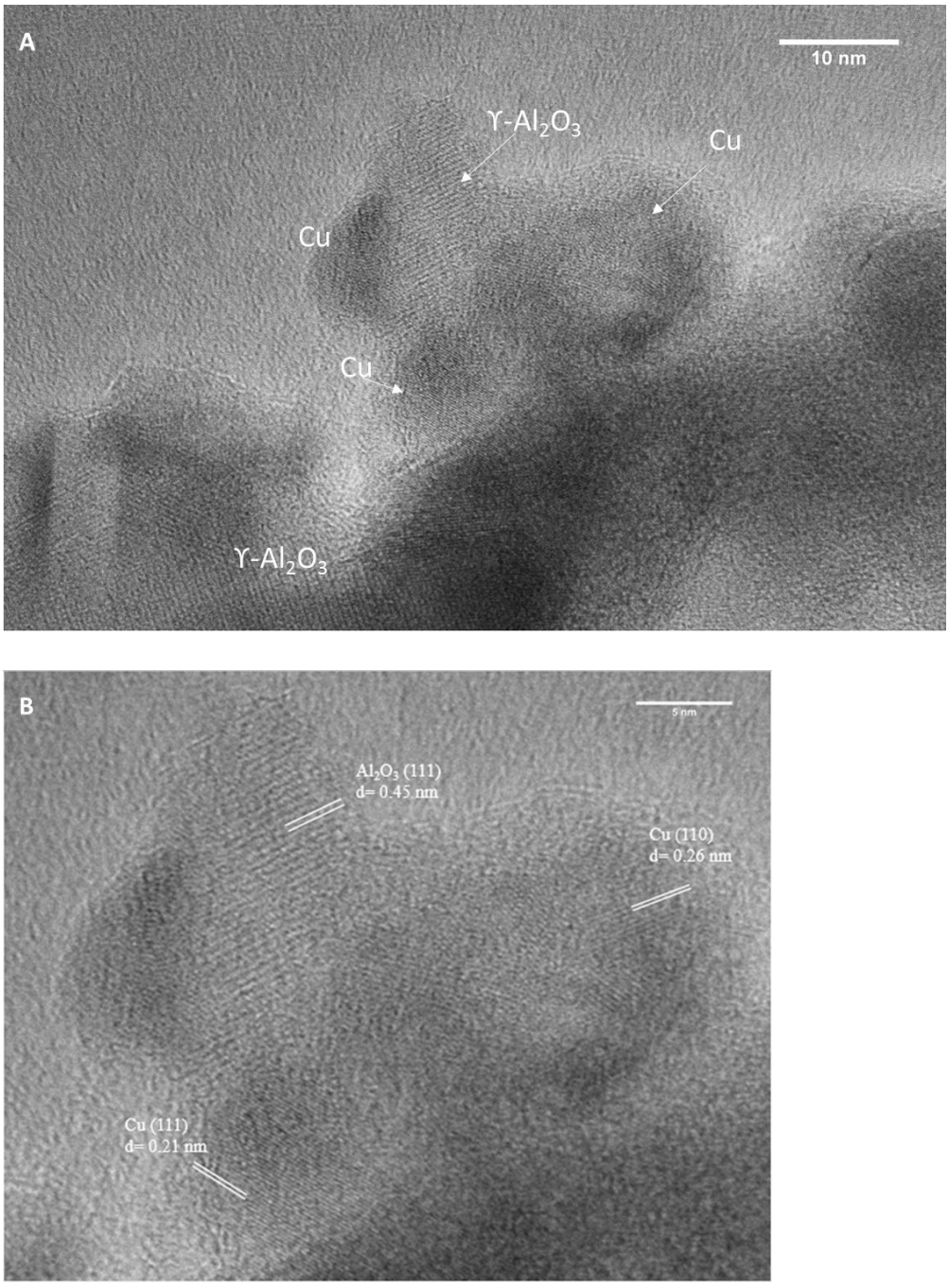

Figure 3.2. (A) HR-TEM images of supported Cu NPS. (B) An enlarged region from (A).

Complete Pt uptake was verified by UV-Vis spectroscopy of the GR filtrates after replacement of Cu with Pt, as shown in Figure 3.3. In contrast to $PtCl_6^{2-}$ standard, the GR wash solution did not show any absorption band at 260 nm. The broader band in the range of 600 –

800 nm indicates the presence of Cu^{2+} in the GR wash solution.[12] The $PtCl_6^{2-}$ absorption peaks at 260 nm of the standard solutions are consistent with those reported in the literature.[13] ICP-AES was used to quantify Pt in the wash solution and no Pt was detected. The observed concentration of Cu^{2+} is (around 4 times) more than the Cu^{2+} produced in GR process. The extra Cu^{2+} is a result of some dissolution of surface CuO in acidic solution ($CuO + 2H^+ \rightarrow Cu^{2+} + H_2O$).[14] The Cu NPs were shortly exposed to the air when transferred from the reduction furnace (100% H_2, 300 °C) to GR solution. The surface CuO layer that would otherwise impede the GR process was removed by the acid in the solution.

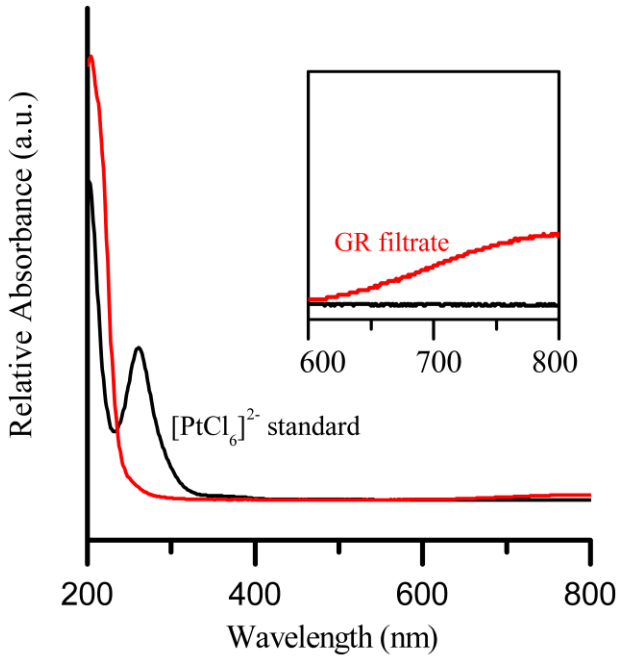

Figure 3.3. UV-Vis spectra of $PtCl_6^{2-}$ standards compared to the filtrate from GR preparation of $Pt_{0.1}Cu_{14}/Al_2O_3$

Three different Pt-Cu NPs were prepared by the galvanic replacement (GR) method, in which a controlled amount of Pt was exchanged with Cu on pre-formed Cu NPs supported on ϒ-Al_2O_3. Low concentrations of Pt in solution form SAA $Pt_{0.1}Cu_{14}/Al_2O_3$ and $Pt_{0.2}Cu_{12}/Al_2O_3$ NPs, while higher concentrations of Pt form Pt_2Cu_6/Al_2O_3.

Elemental mapping by energy dispersive X-ray spectroscopy (EDS) indicates that the Pt-Cu NPs are all bimetallic. Pt, Cu, Al, and O elemental mapping by EDS shows that Pt is distributed over the Cu NPs and is not deposited on the ϒ-Al_2O_3 support (Figure 3.4). *In situ* EXAFS performed at room temperature at the Pt-L_{III} edge reveals the coordination of Pt in Pt-Cu alloys (Figure 3.5 and Table 3.1). No Pt-Pt bonds are detected in $Pt_{0.1}Cu_{14}/Al_2O_3$ and $Pt_{0.2}Cu_{12}/Al_2O_3$, which provides direct evidence for individual, isolated Pt atoms in the Pt-Cu bimetallic NPs. The Pt-Cu first shell interaction distance is 2.61 Å which is between Pt-Pt (2.77 Å) and Cu-Cu bond lengths (2.56 Å),[15] further supporting SAA formation. The finding of Pt-Pt bonds in Pt_2Cu_6/Al_2O_3 suggests that Pt islands and/or clusters are formed in the NPs with higher Pt loading.

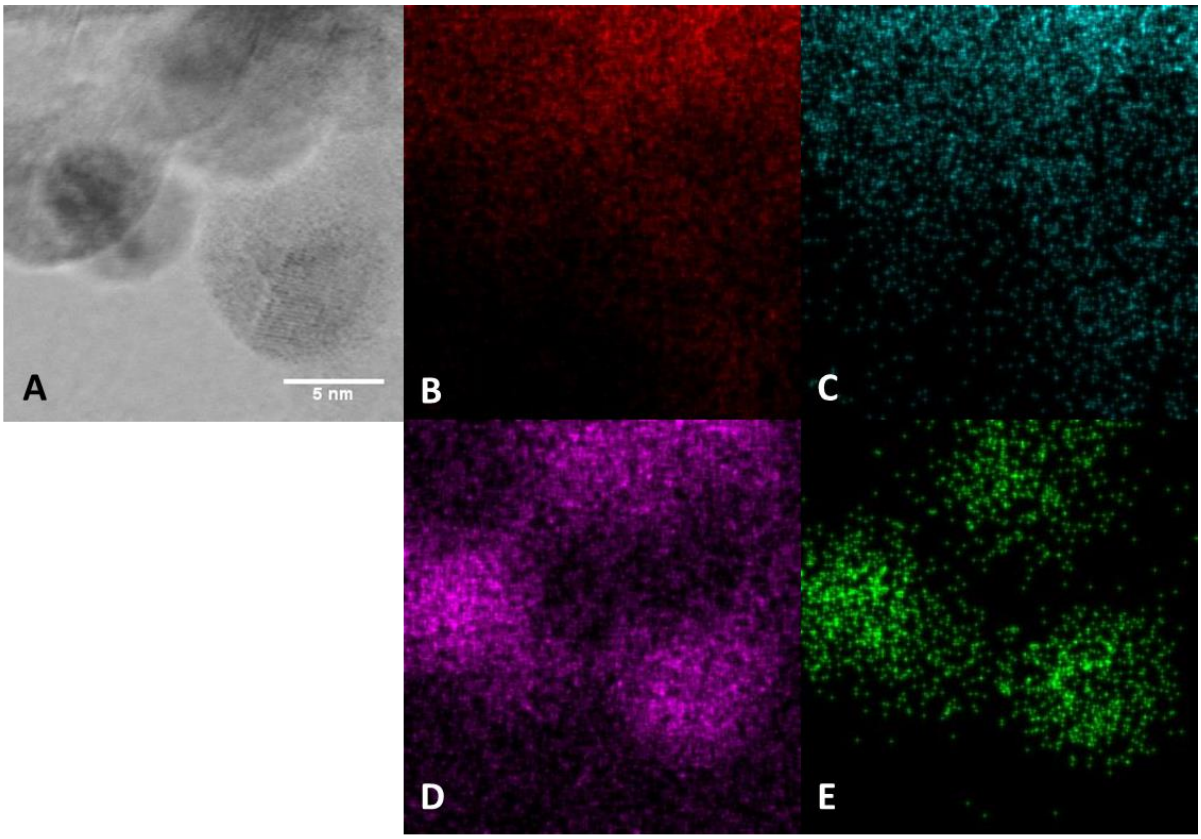

Figure 3.4. (A) STEM image and elemental mapping (EDS) of $Pt_{0.1}Cu_{14}/Al_2O_3$. (B) Al, (C) O, (D) Cu and (E) Pt maps obtained from the same region on the sample.

The *in situ* EXAFS of Pt-Cu bimetallic samples and Pt foil are plotted in k- and Fourier transform spaces (Figure 3.5 and 3.6E). EXFAS of $Pt_{0.1}Cu_{14}/Al_2O_3$ and $Pt_{0.2}Cu_{12}/Al_2O_3$ are significantly distinct from that of Pt foil and Pt_2Cu_6/Al_2O_3. Indeed, no Pt-Pt bonds were formed in $Pt_{0.2}Cu_{12}/Al_2O_3$ or $Pt_{0.1}Cu_{14}/Al_2O_3$. Also, no Pt-O bonds were detected in the Pt-Cu NPs samples (Table 3.1).

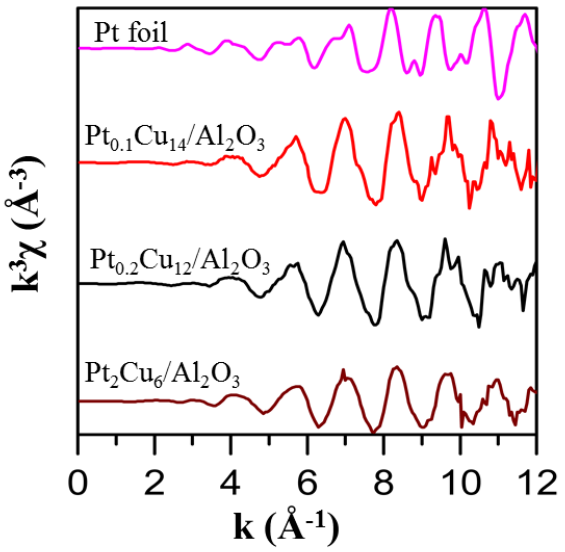

Figure 3.5. *In situ* Pt L_{III} EXAFS of selected samples and Pt foil plotted in k space.

Table 3.1. EXAFS model fitting

Sample	Shell	CN[a]	R[b] (A)	σ^2 (A^2)	R-factor
Pt foil	Pt-Pt	12	2.77	0.0052	0.015
$Pt_{0.1}Cu_{14}/Al_2O_3$	Pt-Pt	N/A			
	Pt-Cu	11.2 ± 1.93	2.61	0.0066	0.006
$Pt_{0.2}Cu_{12}/Al_2O_3$	Pt-Pt	N/A			
	Pt-Cu	11.77 ± 2.31	2.64	0.0078	0.016
Pt_2Cu_6/Al_2O_3	Pt-Pt	4.30 ± 1.44	2.70	0.0050	
	Pt-Cu	7.95 ± 1.51	2.61	0.0087	0.009

[a] CN, coordination number; [b] R, distance between absorber and backscattered atoms. R-factor, closeness of the fit. σ^2 is the disorder in the neighbor distance.

Figure 3.6 shows ac-HAADF-STEM images of $Pt_{0.1}Cu_{14}/Al_2O_3$. Aberration-corrected STEM can distinguish isolated atoms due to differences in Z-contrast.[16,17] In this work, we observed a number of bright, atom-sized features within the Cu lattice (Figure 3.6). Our EXAFS results indicate that these features are isolated Pt atoms in Cu. Additionally, the lattice spacing of Pt-Cu is comparable to the pure Cu lattice spacing which also supports dilute dispersion of Pt atoms (Figure 3.6D). Variations in the background structure of the Cu NPs make imaging of isolated atoms difficult, but in Figure 3.6D the single Pt atoms are more apparent due to the uniform background.[17] STEM and EXAFS analysis demonstrate the formation Pt-Cu SAA NPs, which provides a new catalytic system to study selective hydrogenation reactions.

The Pt-Cu SAA NPs in $Pt_{0.1}Cu_{14}/Al_2O_3$ is imaged by the ac-HAADF-STEM after reduction in H_2 at 350 °C. The isolated Pt atoms are brighter than the Cu areas in the dark field STEM images. Thus, we are able to identify the isolated Pt atoms from its higher brightness comparing to its surrounding area. As shown in Figure 3.7, the isolated Pt atoms are dispersed on the Cu NPs. The white circles highlight some of the isolated Pt atoms. The background from Cu NPs in the ac-HAADF-STEM images is not uniform. Assuming a spherical shape of the NPs, the center region appears brighter due to the greater contribution from the Cu as highlighted by black circles. However, within localized regions, the background remains constant and we observe the bright Pt atoms surrounded by dark Cu regions, which is the evidence for the formation of isolated Pt atoms. Besides that, we do not observe any single atoms or fine clusters of Pt atoms on the alumina.

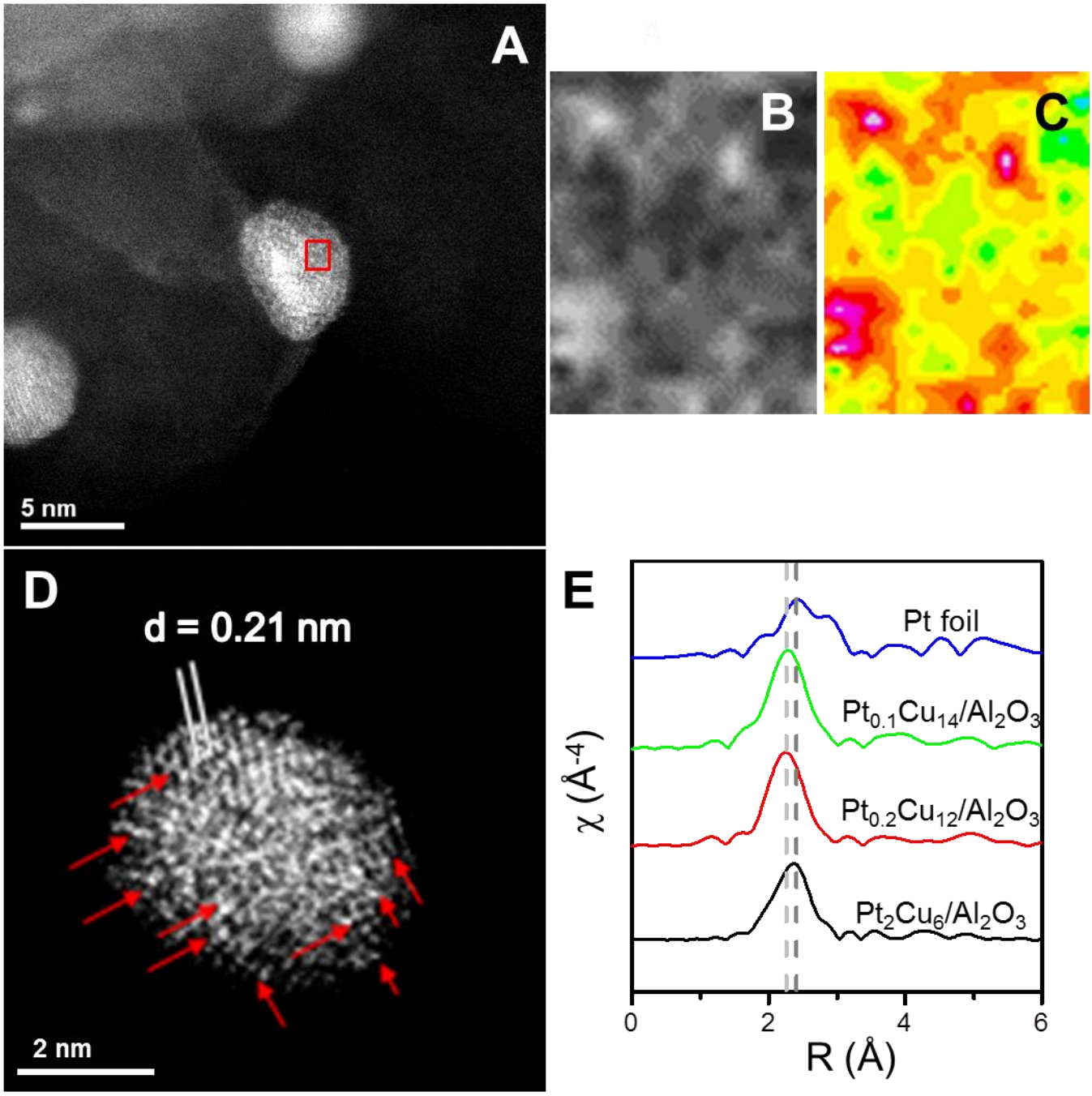

Figure 3.6. Characterization of Pt-Cu SAA NPs. (A-D) HAADF-STEM images with (C) colored intensity map from selected region, and (E) EXAFS k^3 – weighted Fourier transforms. (A, D) typical regions of the sample $Pt_{0.1}Cu_{14}/Al_2O$, showing Cu metal particles with isolated Pt atoms. Isolated Pt atoms are highlighted by red arrows. The lattice spacing of Cu(111) is 0.21 nm. (B)

Enlarged image and (c) colorized intensity map of highlighted region showing isolated Pt atoms.

(E) EXAFS data was collected *in situ* at Pt-L_{III} edge at room temperature from Pt foil, $Pt_{0.1}Cu_{14}/Al_2O_3$, $Pt_{0.2}Cu_{12}/Al_2O_3$ and Pt_2Cu_6/Al_2O_3.

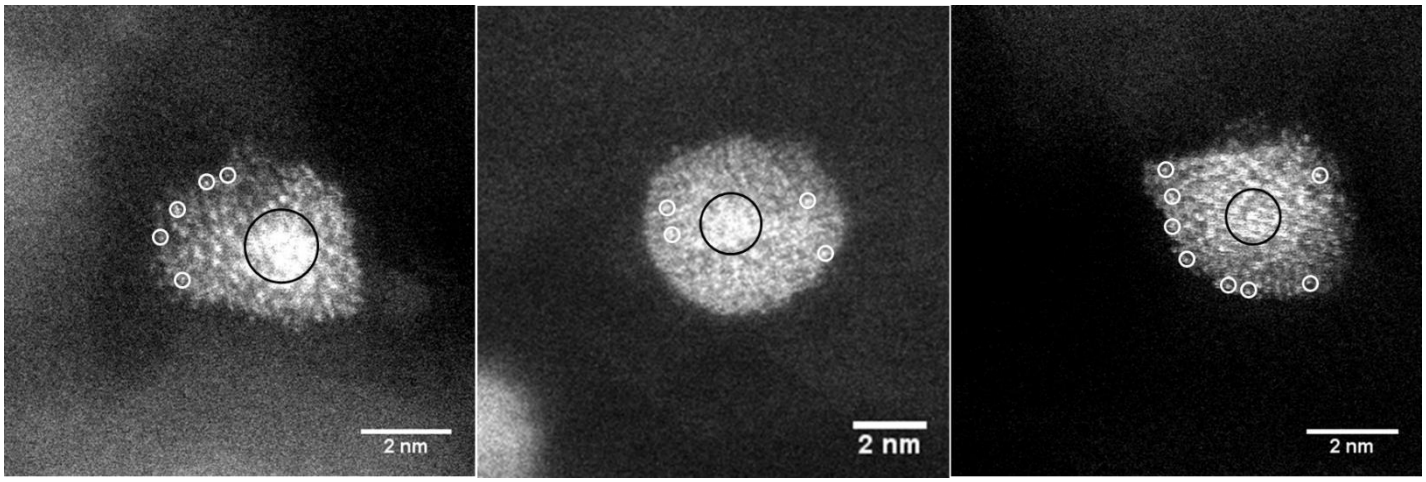

Figure 3.7. Typical HAADF-STEM images of $Pt_{0.1}Cu_{14}/Al_2O_3$. The samples were pre-reduced in H_2 at 350 °C. Isolated Pt atoms are highlighted by white circles.

XRD patterns of selected samples are shown in Figure 3.8. Fresh $Pt_{0.2}Cu_{12}/Al_2O_3$ and $Pt_{0.2}Cu_{12}/Al_2O_3$ were used in the hydrogenation of butadiene have similar XRD patterns as Cu_{15}/Al_2O_3. Only the metallic Cu phase was detected in $Pt_{0.2}Cu_{12}/Al_2O_3$ and used $Pt_{0.2}Cu_{12}/Al_2O_3$. Any CuO skin formed by exposure of the samples to air upon transfer for analysis was too little to show by XRD. No shift in the Cu-peaks was observed between $Pt_{0.2}Cu_{12}/Al_2O_3$ and used $Pt_{0.2}Cu_{12}/Al_2O_3$ or Cu_{15}/Al_2O_3. This suggests the addition of small amounts of Pt did not change the lattice structure of Cu, which is consistent with the lattice spacing determined by STEM

(Figure 3.6). No CuO or Pt phases were observed by XRD. However, Pt-Cu alloy phases were present in Pt_2Cu_6/Al_2O_3 and the Cu phase diminishes, which indicates the formation of bulk Pt-Cu alloys. Furthermore, no significant change in the XRD spectra was found between fresh and used catalysts. The average crystallite size of Cu_{15}/Al_2O_3 was estimated to be 13 nm based on FWHM of Cu peaks as determined by the Scherrer equation.

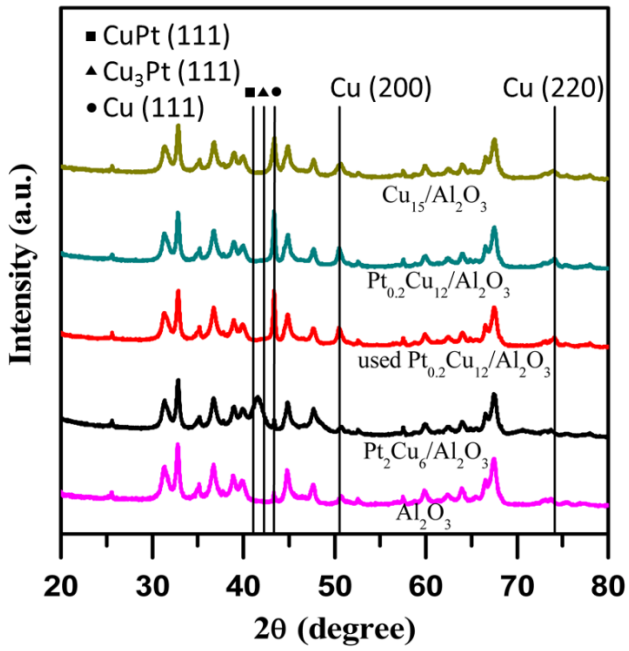

Figure 3.8. XRD analysis of selected samples including a fresh and $Pt_{0.2}Cu_{12}/Al_2O_3$ used for butadiene hydrogenation. All catalysts, except the sample used in the hydrogenation reaction, were reduced in H_2 prior to XRD. (Cu JCPDS No. 85-1326, Cu_3Pt JCPDS No. 65-3247, CuPt JCPDS No. 48-1549)

To gain insight into the electronic states of the Pt species, XANES spectra were collected for Pt monometallic and Pt-Cu bimetallic samples at Pt-L_{III} edge (Figure 3.9). The Pt-Cu

bimetallic and Pt monometallic samples were reduced in 100% H_2 *in situ* prior to the XANES scans. The white line intensity of Pt-Cu samples is significantly lower than that of Pt^{4+}, Pt^{2+}, Pt foil and Pt NPs indicating that the electronic states of Pt are altered in the Pt-Cu bimetallic NPs. Lee and co-workers have reported the decrease in Pt-L_{III} white line intensity of CuPt alloys compared to pure Pt. The change was attributed to changes in Pt $d_{5/2}$ density of state upon alloying.[18] Since Pt-L_{III} edge characterizes the Pt d states, the decrease in white line intensity of Pt-Cu samples compared to $Pt_{0.1}/Al_2O_3$ and Pt foil indicates the Pt d states were affected in the Pt-Cu alloy samples.[19]

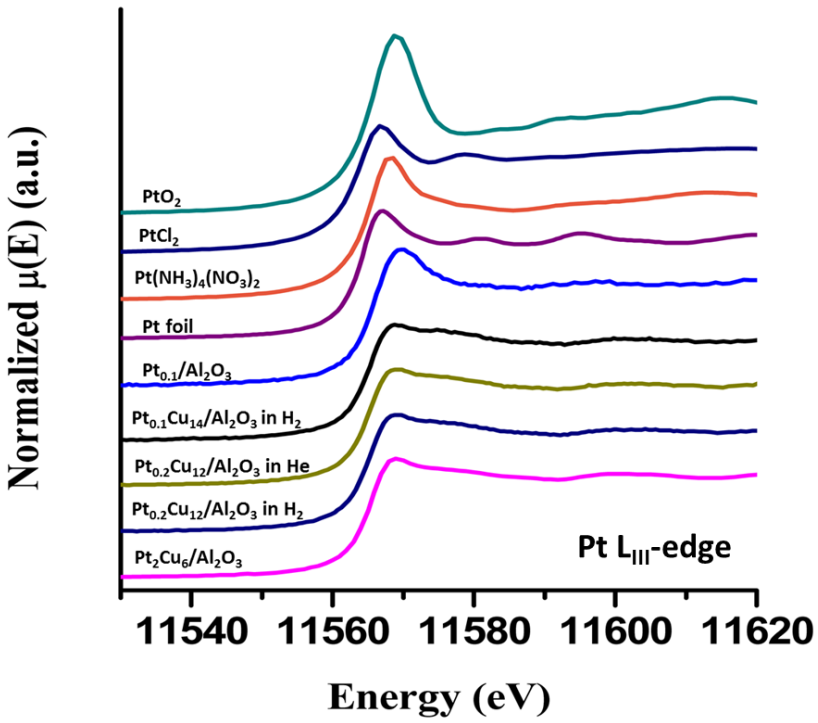

Figure 3.9. Normalized *in situ* XANES spectra of selected samples collected at room temperature in H_2 (except where otherwise noted). The Pt-Cu samples were pre-reduced in H_2 at 350 °C *in situ*, while the $Pt_{0.1}/Al_2O_3$ was pre-reduced in H_2 at 400 °C *in situ.*

3.3.2 Selective hydrogenation of 1,3-butadiene

Our catalytic data reveals that adding a trace amount of Pt to Cu NPs significantly enhances hydrogenation. The butadiene hydrogenation activity and selectivity as a function of temperature on $Pt_{0.1}Cu_{14}/Al_2O$, $Pt_{0.2}Cu_{12}/Al_2O_3$, and Cu_{15}/Al_2O_3 NPs is shown in Figure 3.10. Under the conditions employed, $Pt_{0.1}Cu_{14}/Al_2O_3$ has a hydrogenation reaction onset at 40 °C, which is 40 ^oC lower than that of the monometallic Cu catalyst. The reaction rate over the $Pt_{0.1}Cu_{14}/Al_2O_3$ at 60 ^oC is an order of magnitude higher than the monometallic Cu catalyst. $Pt_{0.2}Cu_{12}/Al_2O_3$ exhibits greater hydrogenation activity than $Pt_{0.1}Cu_{14}/Al_2O_3$ due to a higher Pt atom surface amount due to the increased Pt loading. However, the selectivity remains unaffected because the Pt atoms exist as isolated species in $Pt_{0.2}Cu_{12}/Al_2O_3$ as indicated by EXAFS model fitting. The monometallic $Pt_{0.1}/Al_2O_3$ catalyst is reactive for 1,3-butadiene hydrogenation at ambient temperature. At 60 °C, the activity of $Pt_{0.1}/Al_2O_3$ is around 3 times higher than that of the PtCu SAA catalysts, while the selectivity to butenes is significantly lower than that of the PtCu SAA catalysts.

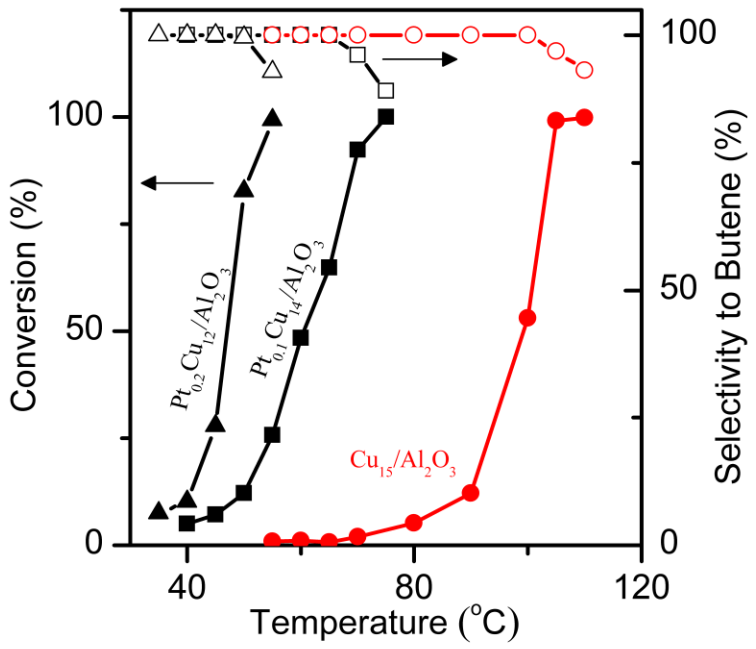

Figure 3.10. Selective hydrogenation of butadiene as a function of temperature over Cu_{15}/Al_2O_3, $Pt_{0.1}Cu_{14}/Al_2O_3$, and $Pt_{0.2}Cu_{12}/Al_2O_3$ NPs (1,3-butadiene (1.25 %), H_2 (20 %) and He (balance), GHSV=1,200 h^{-1}).

Notably, the SAA catalysts maintain the high selectivity to butenes exhibited by Cu. At full conversion, there is over 90% selectivity towards butene isomers. The selectivity of SAA NPs ($Pt_{0.1}Cu_{14}/Al_2O_3$ and $Pt_{0.2}Cu_{12}/Al_2O_3$) was comparable to Cu_{15}/Al_2O_3 whereas Pt monometallic catalysts fully converted butadiene to butane under these conditions. Monometallic Pt is known for over-hydrogenating dienes and alkynes.[20,21] Therefore, by combining the hydrogen activation ability of Pt with the weak binding of butadiene on Cu and the latter's selectivity to butenes, Pt-Cu SAA catalysts exhibit superior performance for this important industrial reaction. Various other alloy surfaces, including Pd-Au and Sn-Pt, have been shown to improve partial

hydrogenation reactions.[22,23] However, this is the first report that single Pt atoms can enhance selective hydrogenation reactions on a less active metal, such as copper.

The yields of different products are shown in Figure 3.11. Under the conditions employed, the yield to butane over $Pt_{0.1}/Al_2O_3$ and Pt_2Cu_6/Al_2O_3 was close to zero.

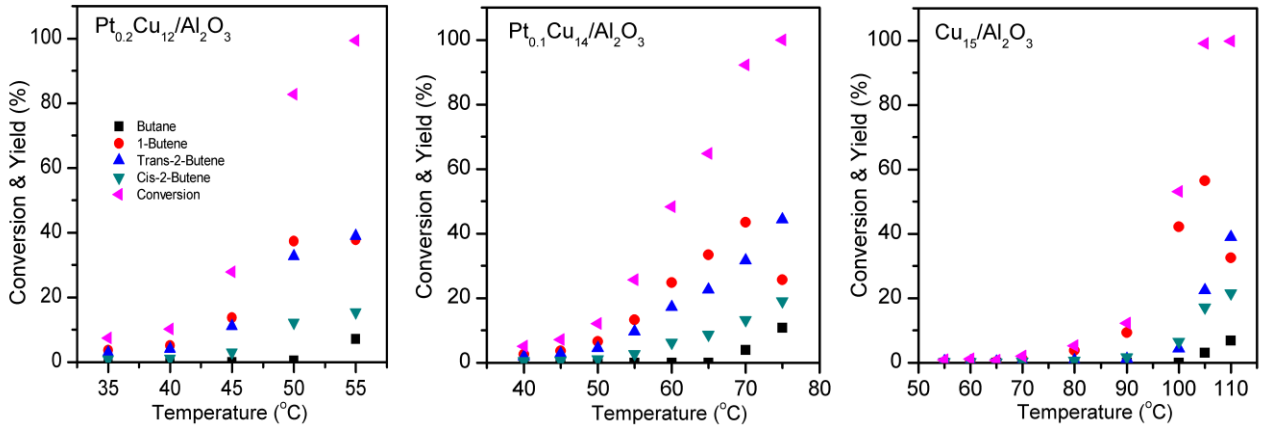

Figure 3.11. Conversion and product yields in the selective hydrogenation of butadiene corresponding to Figure 6. (0.4 g catalyst, flow rate = 20 mL/min; 1, 3-butadiene (1.25 %), H_2 (20 %) and He (balance), GHSV=1,200 h^{-1}.)

The stability of Pt-Cu SAA catalysts in butadiene hydrogenation reaction is demonstrated at 160 °C. As shown in Figure 3.12, the production rates of butene isomers (the desired products) and the selectivity to butene are stable for at least 46 hours. The space velocity here is greater (12,000 h^{-1} versus 1,200 h^{-1}) than that of Figure 3.10; thus an accelerated deactivation rate was expected. The spent catalyst used for the stability test was

tested in He-TPD and TPO whereby no desorption of hydrocarbons took place and a negligible amount of CO_2 was produced (see below, Figure 3.16), respectively.

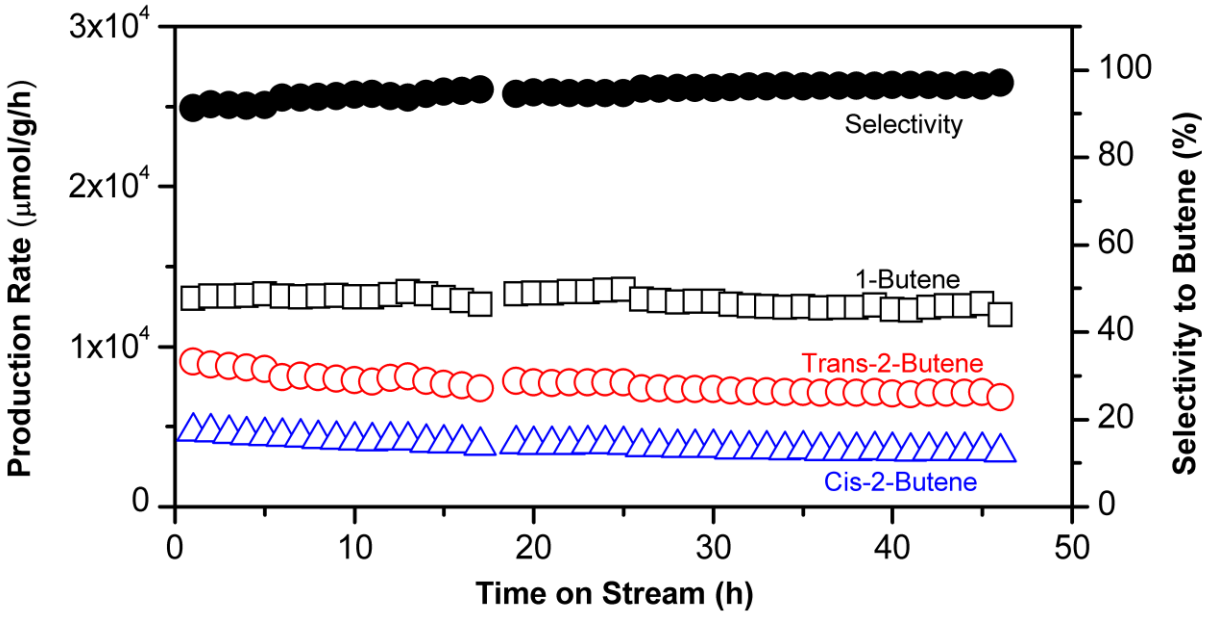

Figure 3.12. Long-time hydrogenation steady-state activity test over $Pt_{0.1}Cu_{14}/Al_2O_3$ at 160 °C. (~ 0.1 g catalyst, flow rate = 50 mL/min. 2% 1, 3-butadiene, 20% H_2 and balance He. GHSV=12,000 h^{-1}. Conversion of butadiene in one hour is around 98 %).

Under the same reaction conditions, the PtCu SAAs samples were tested in consecutive ascending and descending temperature cycles. Figure 3.13A shows the conversion of butadiene in a cycle over $Pt_{0.1}Cu_{14}/Al_2O_3$. The comparison of conversion at 150 °C and 120 °C between the increasing and decreasing temperature ramps shows that the hydrogenation activity was recovered during the decreasing temperature ramp. But at near ambient temperatures, the activity in the cooling part of the cycle is lower. The same was true with all the Pt-Cu alloyed

samples. The results suggest the hydrogenation activity was reduced at lower temperatures but recovered at higher temperatures. Considering that oligomer formation adversely affects the metal-based catalysts in the hydrogenation of hydrocarbons at mild temperatures,[24] we hypothesize the oligomers partially blocked the surface sites at lower temperature and desorbed with increasing temperature.

To check this, after the first temperature heating-cooling cycle (Figure 3.13A), the catalyst was treated at 350 °C in H_2 to fully desorb the weakly adsorbed hydrocarbons on the surface. We found the selective hydrogenation activity was fully recovered after the high temperature treatment for at least 4 cycles, as shown in Figure 3.13B. This result suggests the active sites were maintained in the cyclic reaction tests.

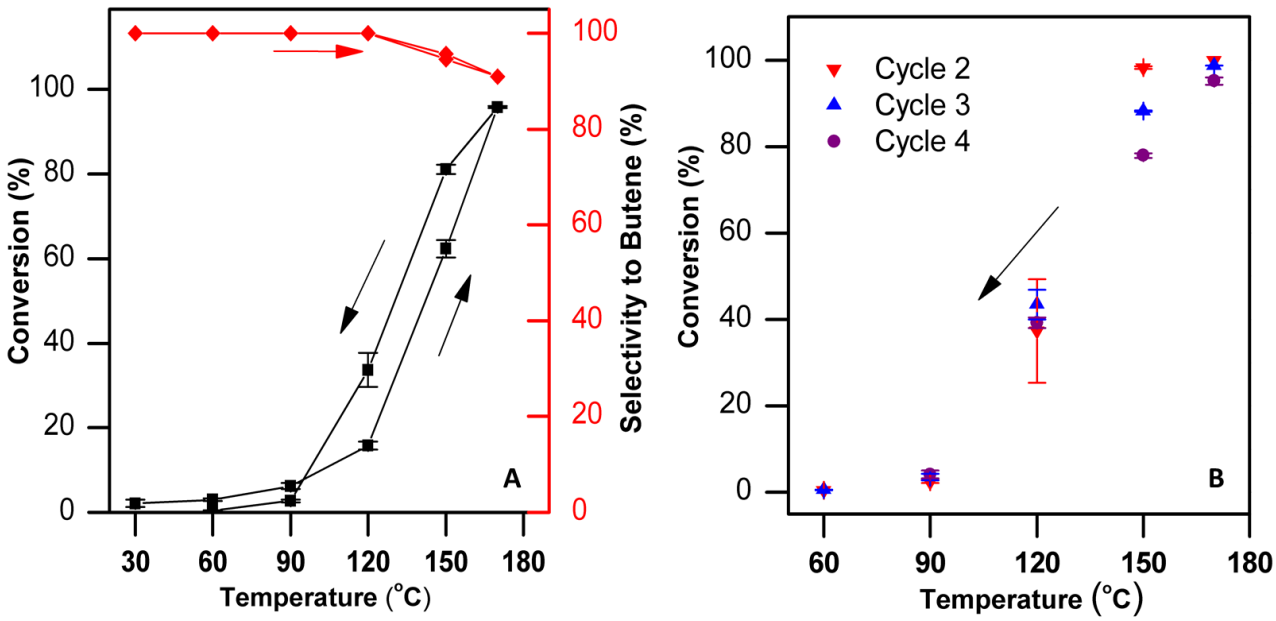

Figure 3.13. Selective hydrogenation of butadiene as a function of temperature over $Pt_{0.1}Cu_{14}/Al_2O_3$. (0.1 g catalyst, flow rate = 50 mL/min. 2 % 1,3-butadiene, 20 % H_2 and balance He. GHSV=12,000 h^{-1}) (A) Conversion of butadiene and selectivity to butene with increasing and decreasing temperature ramps. (B) Conversion of butadiene in cyclic hydrogenation experiments, the catalysts were treated in H_2 at 350 °C between each cycle. The conversion of the first cycle is shown in (A).

To demonstrate the ability of Pt-Cu SAAs to selectively hydrogenate alkadiene impurities in alkene feedstocks,[25] we tested the selective hydrogenation activity of $Pt_{0.1}Cu_{14}/Al_2O_3$ catalysts in the presence of excess propylene and found that butadiene is preferentially hydrogenated on the Pt-Cu SAA NPs (Figure 3.15). Below 120 °C, conversion of propylene was not observed. At

100% conversion of butadiene, less than 1 % of propylene was converted to propane. Comparing these results to the hydrogenation activity of $Pt_{0.1}Cu_{14}/Al_2O_3$ in propylene-free condition, we found the propylene has no effect on the activity and selectivity of Pt-Cu SAAs for the hydrogenation of butadiene. At 160 °C and 145 °C, butadiene is fully converted and >95% converted, respectively, over $Pt_{0.1}Cu_{14}/Al_2O_3$ without significant propylene hydrogenation (1.2 % at 160 °C and 0.5 % at 145 °C) for >12 h on-stream at each temperature (Figure 3.14).

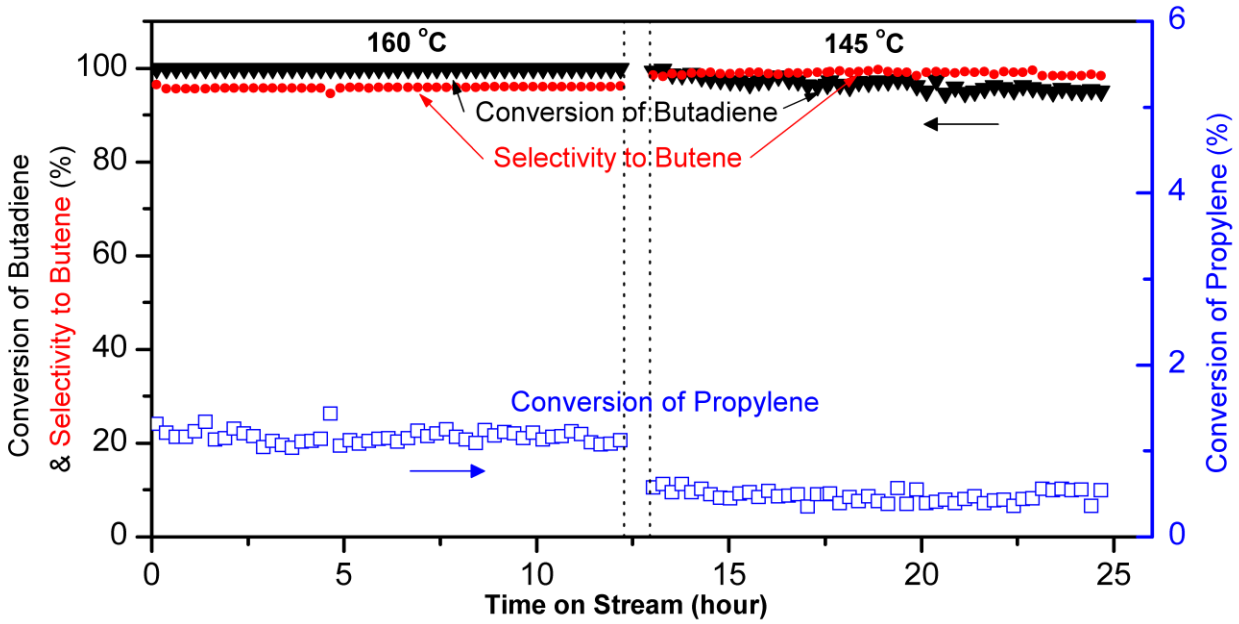

Figure 3.14. Butadiene conversion in the presence of excess propylene. Conversion and selectivity in long-time steady state selective hydrogenation of butadiene at 160 and 145 °C (~ 0.1 g catalyst $Pt_{0.1}Cu_{14}/Al_2O_3$, flow rate = 50 mL/min. 2 % 1, 3-butadiene, 20 % propylene, 16 % H_2 and balance He. GHSV=12,000 h^{-1}).

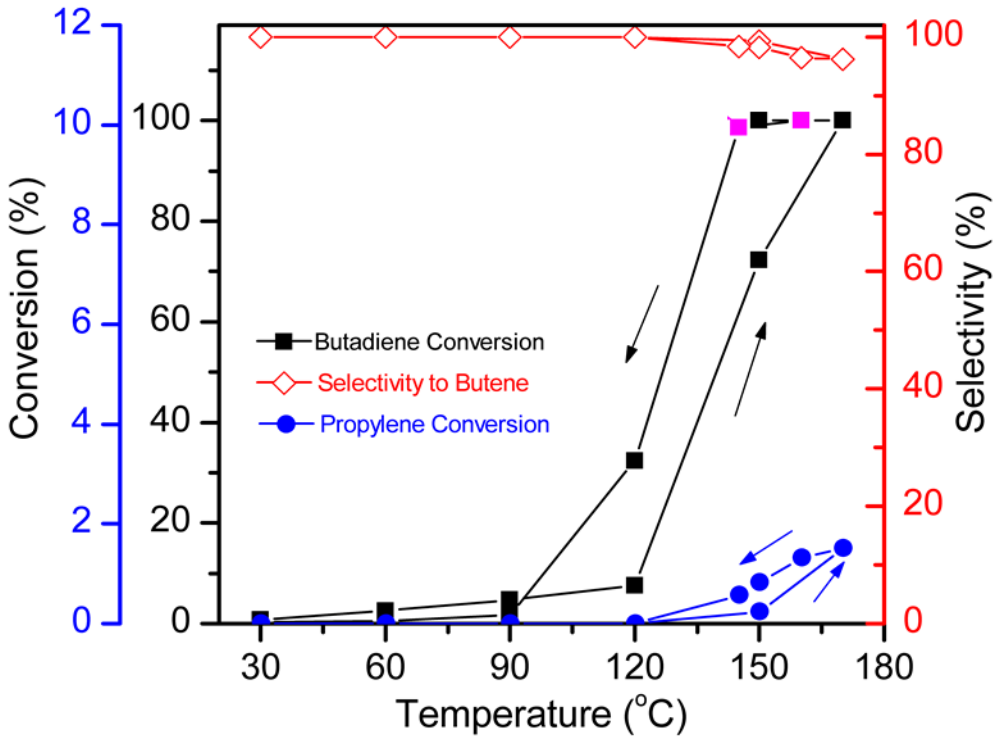

Figure 3.15. Conversion and selectivity in the selective hydrogenation of butadiene over $Pt_{0.1}Cu_{14}/Al_2O_3$ as a function of temperature. (~ 0.1 g catalyst, flow rate = 50 mL/min. 2 % 1, 3-butadiene, 20 % propylene, 16 % H_2 and balance He. GHSV=12,000 h^{-1}).

Although the catalytic activity of Pt-Cu SAA catalyst is stable at 145 °C, deactivation of the catalysts was observed at the lower temperatures. The hysteresis phenomenon in Figure 3.15 indicates some weakly adsorbed species poison the catalysts at the temperatures lower than 90 °C but desorbed at the higher temperatures. These weakly adsorbed molecules are very likely to be the oligomer of 1,3-butadiene formed through the side reactions.

Our experiments reveal that Pt-Cu SAAs exhibit high stability under realistic hydrogenation conditions. The Pt-Cu SAAs maintain stable butadiene conversion for more than 46 h at 160 °C (Figure 3.12). Temperature-programmed oxidation (TPO) studies of the catalysts after hydrogenation show negligible CO_2 formation (Figure 3.16) demonstrating the robustness of SAA catalysts to decomposition, oligomerization, and coke formation. Based on our model catalyst studies, the increase in the selectivity of SAAs is due to the inhibition of hydrocarbon decomposition commonly observed with Pt catalysts because SAAs do not offer extended Pt ensembles where these unfavorable reactions occur. On the other hand, by running at higher temperatures, there are no issues of instability. It is well known that Cu or Pd catalysts for diene and alkyne hydrogenation are affected by oligomer formation at mild temperatures, which leads to instability in their hydrogenation activity.[24] We found that after reaction at near ambient temperatures, the hydrogenation activity of Pt-Cu SAAs can be fully recovered by treatments at higher temperature, effectively desorbing the adsorbed hydrocarbons (Figure 3.13). Running at the higher temperatures shown Figure 3.12 preserved the catalyst activity without affecting its selectivity.

TPO and He-TPD were performed on both of the spent catalysts that have been used in 48 h hydrogenation of butadiene (Figure 3.12) and 30 h hydrogenation in the presence of propylene (Figure 3.14). In TPO test, CO_2 produced by the combustion of carbon species on the catalyst was monitored by mass spectrometry (m/z=44), as shown in Figure 3.16. We found that carbon deposition on the catalyst was negligible. The CO_2 concentration was below 0.02 % with TPO performed up to 800 °C. Moreover, for the catalysts used in the hydrogenation of butadiene, the total CO_2 production corresponds to less than 1/26,000 of the amount of

butadiene converted over the catalysts. For another spent catalyst, the CO_2 production in TPO corresponds to less than 1/90,000 of the amount of hydrocarbon flowed through the catalysts during the hydrogenation of butadiene in the presence of propylene. Similarly, He-TPD shows no desorption of hydrocarbons up to 800 °C as indicated by the lack of hydrocarbon fragments in the range of m/z=1-120 for both spent catalysts.

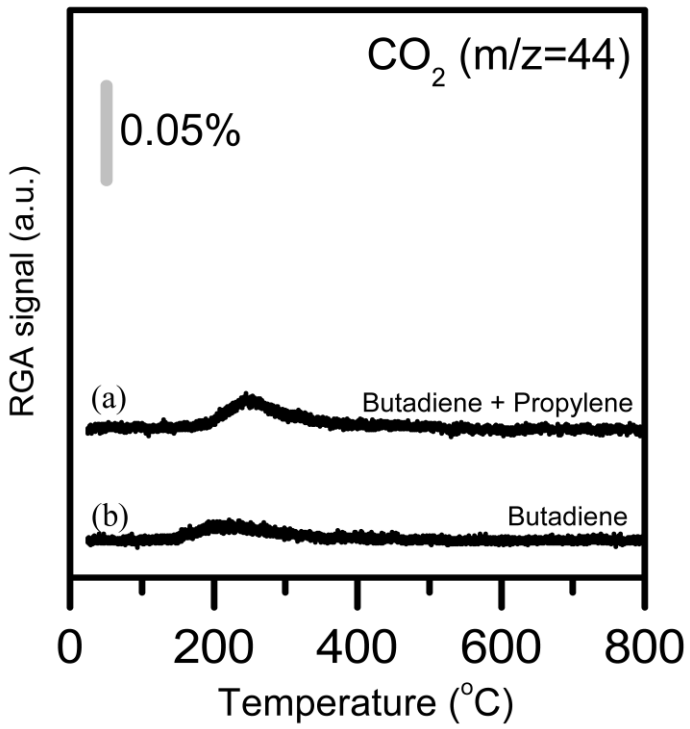

Figure 3.16. TPO profile of spent $Pt_{0.1}Cu_{14}/Al_2O_3$ catalyst used for the long-time activity test in (a) 2 % 1, 3-butadiene, 20 % propylene, 16 % H_2 and balanced He for around 48 h; (b) 2 % 1, 3-butadiene, 20 % H_2 and balanced He for around 30 h. (TPO condition: 20 % O_2/He, 50 mL/min, 3 °C/min) Scale bar corresponds to 0.05 % CO_2 in the gas stream.

3.4 Collaboration: surface science studies on Pt-Cu(111) SAAs

Surface science studies were conducted by Lucci et al. as one part of the collaborative effort in investigating PtCu SAA for selective hydrogenation of 1,3-butadiene.[26,27] At low loadings, Pt exists as individual, isolated atoms substituted into the Cu surface. These single Pt atoms activate the dissociation and spillover of H to Cu. The weak binding of butadiene to Cu allows for the highly selective hydrogenation to butenes. Thus, a bifunctional mechanism for hydrogenation of butadiene is confirmed. No decomposition or poisoning of these alloys was observed which can be attributed to the lack of extended Pt surface sites. At higher Pt content in Pt-Cu alloy surfaces, we directly visualized extended Pt surface sites responsible for the reduced selectivity.

3.6 Summary

This chapter reports a novel SAA catalyst design for selective hydrogenation reactions. This is the first such kind of work in the field. A careful galvanic replacement reaction was conducted to prepare PtCu SAA NPs. With comprehensive characterization approaches including EDS, STEM, EXAFS, XANES, XRD, TEM and UV-Vis, the compositional and structural properties of the NP catalysts were thoroughly investigated.

In selective hydrogenation of 1,3-butadiene, PtCu SAA catalysts show activity at near-to-ambient temperature. By adding a small amount of Pt single atoms to the surface of Cu NPs, the onset of hydrogenation activity is lowered for 40 °C. This is due to the single-atom Pt lower the hydrogenation activation barrier on the Cu surface. PtCu SAA catalysts are highly selective

to partial hydrogenation products compared to monometallic Pt. With the presence of excess propylene, butadiene was converted to butenes at more than 95% selectivity with less than 1% conversion of propylene. The activity of SAA is highly stable under the hydrogenation condition. The work reveals the highly selective nature of the SAA catalysts in hydrogenation reactions and demonstrates the single-atom Pt sites can activate the otherwise inert Cu for selective hydrogenation. Furthermore, in addition to their promising selective hydrogenation properties, single-atom alloys provide the ultimate limit for the efficient use of costly catalytic elements like Pt.

3.7 References

1. Stamenkovic VR, Mun BS, Arenz M, et al. Trends in electrocatalysis on extended and nanoscale Pt-bimetallic alloy surfaces. *Nat Mater*. 2007;6(3):241-247. doi:10.1038/nmat1840.

2. Weitkamp J, Jacobs PA. No Title. 1983;8:123-141.

3. Derrien ML. *Catalytic Hydrogenation*. Vol 27. Elsevier; 1986. doi:10.1016/S0167-2991(08)65364-1.

4. GBI Research. *Polypropylene Global Market to 2020 - Developing Regions of Asia-Pacific and Middle East and Africa to Drive Polypropylene Market Growth*.; 2013.

5. Mittendorfer F, Thomazeau C, Raybaud P, Toulhoat H. Adsorption of Unsaturated Hydrocarbons on Pd(111) and Pt(111): A DFT Study. *J Phys Chem B*. 2003;107(44):12287-12295. doi:10.1021/jp035660f.

6. Valca A, Clotet A, Ricart JM. Selectivity Control for the Catalytic 1 , 3-Butadiene Hydrogenation on Pt (111) and Pd (111) Surfaces : Radical versus Closed-Shell Intermediates. 2005;(111):14175-14182.

7. Kyriakou G, Boucher MB, Jewell AD, et al. Isolated Metal Atom Geometries as a Strategy for Selective Heterogeneous Hydrogenations. *Science*. 2012;335:1209-1212. doi:10.1126/science.1215864.

8. Boucher MB, Zugic B, Cladaras G, et al. Single atom alloy surface analogs in Pd0.18Cu15 nanoparticles for selective hydrogenation reactions. *Phys Chem Chem Phys*.

2013;15:12187-12196. doi:10.1039/c3cp51538a.

9. Ravel B, Newville M. ATHENA, ARTEMIS, HEPHAESTUS: Data analysis for X-ray absorption spectroscopy using IFEFFIT. In: *Journal of Synchrotron Radiation*. Vol 12. ; 2005:537-541.

10. Ravel B. ATOMS: Crystallography for the X-ray absorption spectroscopist. *J Synchrotron Radiat*. 2001;8(2):314-316.

11. Boucher MB, Zugic B, Cladaras G, et al. Single atom alloy surface analogs in Pd0.18Cu15 nanoparticles for selective hydrogenation reactions. *Phys Chem Chem Phys*. 2013;15(29):12187-12196. doi:10.1039/c3cp51538a.

12. Sun Z, Masa J, Xia W, et al. Rapid and surfactant-free synthesis of bimetallic Pt-Cu nanoparticles simply via ultrasound-assisted redox replacement. *ACS Catal*. 2012;2(8):1647-1653.

13. Hikosaka K, Kim J, Kajita M, Kanayama A, Miyamoto Y. Platinum nanoparticles have an activity similar to mitochondrial NADH:ubiquinone oxidoreductase. *Colloids Surf B Biointerfaces*. 2008;66(2):195-200. doi:10.1016/j.colsurfb.2008.06.008.

14. Iwai M, Majima H, Awakura Y. Dissolution of Copper in Hydrochloric Acid Solutions with Dissolved Molecular Oxygen. *Hydrometallurgy*. 1988;20:87-95.

15. Yamamoto T a., Nakagawa T, Seino S, Nitani H. Bimetallic nanoparticles of PtM (M=Au, Cu, Ni) supported on iron oxide: Radiolytic synthesis and CO oxidation catalysis. *Appl Catal A Gen*. 2010;387(1-2):195-202. doi:10.1016/j.apcata.2010.08.020.

16. Yang M, Allard LF, Flytzani-Stephanopoulos M. Atomically dispersed Au-(OH)x species

bound on titania catalyze the low-temperature water-gas shift reaction. *J Am Chem Soc*. 2013;135(10):3768-3771.

17. Peterson EJ, DeLaRiva AT, Lin S, et al. Low-temperature carbon monoxide oxidation catalysed by regenerable atomically dispersed palladium on alumina. *Nat Commun*. 2014;5:4885. doi:10.1038/ncomms5885.

18. Lee Y, Lim K, Chung Y, Whang C, Jeon Y. XPS core-level shifts and XANES studies of Cu – Pt and Co – Pt alloys. 2000;478(July 1999):475-478.

19. Mansour AN, Cook JW, Sayers DE. Quantitative Technique for the Determination of the Number of Unoccupied d-Electron States in a Platinum Catalyst Using the L2 , 3 X-ray Absorption Edge Spectra. *J Phys Chem*. 1984;88:2330-2334.

20. Dobrovolna Z, Kacer P, Cerveny L. Competitive hydrogenation in alkene – alkyne – diene systems with palladium and platinum catalysts. *J Mol Catal A Chem*. 1998;130:279-284.

21. Boitiaux JP, Cosyns J, Robert E. Liquid Phase Hydrogenation of Unsaturatued Hydrogcarbons on Palladium, Platinum and Rodium Catalysts. Part I: Kinetic Study of 1-Butene, 1,3-Butadiene and 1-Butyne Hydrogenation on Platinum. *Appl Catal*. 1987;32:145-168.

22. Kolli N El, Delannoy L, Louis C. Bimetallic Au–Pd catalysts for selective hydrogenation of butadiene: Influence of the preparation method on catalytic properties. *J Catal*. 2013;297:79-92. doi:10.1016/j.jcat.2012.09.022.

23. Zhao H, Koel BE. Adsorption and reaction of 1,3-butadiene on Pt(111) and Sn/Pt(111)

surface alloys. *Surf Sci*. 2004;572(2-3):261-268. doi:10.1016/j.susc.2004.08.039.

24. Delannoy L, Thrimurthulu G, Reddy PS, et al. Selective hydrogenation of butadiene over TiO2 supported copper, gold and gold-copper catalysts prepared by deposition-precipitation. *Phys Chem Chem Phys*. 2014;16(48):26514-26527. doi:10.1039/c4cp02141j.

25. Derrien ML. Selective hydrogenation applied to the refinging of petrochemical raw materials produced by steam cracking. *Stud Surf Sci Catal*. 1986;27:613-666. doi:10.1016/S0167-2991(08)65364-1.

26. Lucci FR, Liu J, Marcinkowski MD, et al. Selective hydrogenation of 1,3-butadiene on platinum – copper alloys at the single-atom limit. *Nat Commun*. 2015;6:8550. doi:10.1038/ncomms9550.

27. Lucci FR. Surface Reactivity of Single Atom Alloys: Model Studies Guiding the Design of Atom Efficient Nanoparticle Catalysts. 2016.

Chapter 4. Tackling CO poisoning with single-atom alloy catalysts

4.1 Introduction

Pt metals are highly active for H_2 dissociation, but are very susceptible to carbon monoxide (CO) poisoning.[1] Due to its strong binding to Pt, even trace amounts of CO impurity, which is always present in H_2 gas produced from fuel reforming, can diminish H_2 activation and reactivity.[2]

As the natural expansion of the SAA concept, we tackled the CO poisoning issue of platinum catalysts with Pt-based SAAs . The situation for isolated Pt atoms may be different than traditional bimetallic alloys, where ensemble effects have been shown to increase the CO binding strength at extended catalytic metal sites[3–5]. From a fundamental perspective, metal alloys that alter the adsorption geometry of CO can exhibit weaker CO binding and enhanced CO tolerance. Isolated Pt atoms enable exclusively atop adsorption configuration of CO, which we show is weaker than CO adsorption on extended Pt sites. In this chapter, we investigated the interaction between CO and Pt sites on a Pt-Cu SAA and demonstrate improved CO tolerance of Pt-Cu SAA catalysts under realistic working conditions for H_2 activation and acetylene hydrogenation reaction.

4.2 Experimental methods

Pt-Cu SAA NPs were prepared with the same galvanic replacement method described in the chapter 3. XAS studies were performed at beamline 12-BM at Argonne National Laboratory. The experiments and data analysis were conducted as described in chapter 3.

FTIR spectra were collected using a Nicolet Nexus 470 spectrometer equipped with a MCT-B detector in the single beam absorbance mode at a resolution of 2 cm^{-1}. Prior to the IR experiments, the samples were reduced in pure H_2 at 300 (Cu-NP), 350 ($Pt_{0.008}$Cu-SAA and $Pt_{0.39}$Cu-bimetallic) or 400 (Pt-NP) °C in a quartz microreactor and sealed in the glass vials. The powder sample of 0.02 g was made into a thin pellet (~ 1cm in diameter). The sample was then loaded into a flow cell sealed with NaCl windows and allows the CO flow through the catalyst pellet. In a typical CO adsorption IR experiment, the sample was first reduced in 50 mL/min 5 % H_2-He for 1 hr at 200 ^oC followed with the He purge to cool down to 25 ^oC. Baseline was collected at 25 ^oC under He purge after the catalyst has been swept for at least 30 min. The sample was then exposed to 1 % CO-He flow at the same temperature for 45 min, and was purged again with He for at least another 30 min until the gas phase CO signal was fully diminished (rather quickly within 5 min of purge) and the catalyst surface adsorption spectra has minimal difference between the IR scans. The IR spectra shown in the main text were collected afterwards at 25, 40, 60, 80, and 100 °C. A ramping rate of 5 ^oC/min was used. The corresponding spectra at each temperature were collected after the sample was stabilized at the target temperature for 10 min.

H_2-D_2 exchange was conducted in a packed-bed flow microreactor (L=22 inch, O.D.=1/2 inch) with 80-90 mg of catalyst diluted by 0.5 g of quartz particles. The samples were pre-

reduced in 100% H_2 (at 350 °C for $Pt_{0.008}Cu$-SAA and 400 °C for Pt-NP) and then cooled to desired temperature before the reaction gas mixture (33% H_2, 33% D_2, 3.3% CO and balance Ar. Flow rate=50mL/min) was introduced. For the isothermal H_2-D_2 exchange, CO was introduced to the gas phase and turned off at the certain time points while H_2 and D_2 are flowing. To do temperature programmed H_2-D_2 exchange, a gas mixture of 33% H2, 33% D_2, 3.3% (or 667ppm) CO and balance Ar (flow rate=50mL/min) was introduced at 120 °C and temperature was increased to 200 °C at 5 °C/min. The gas effluent from the reactor was analyzed by a mass-spectrometer. Acetylene hydrogenation was performed in a packed-bed flow microreactor (L=22 inch, O.D.=1/2 inch) at 70 and 80 °C isothermally (20% H_2, 2.2% C_2H_2, 200 ppm CO, 10% Argon, balance He, flow rate=24-48 mL/min). 50-500 mg catalysts were used. The exit gas stream was analyzed by a mass-spectrometer.

4.3 Results and Discussion

PtCu alloy nanoparticles (NPs) were prepared by galvanic replacement (GR) of Pt for Cu on preformed Cu NPs (Table 4.1)[6,7]. $Pt_{0.008}Cu$ supported on γ-Al_2O_3 is a SAA as confirmed by aberration-corrected high angle annular dark field scanning transmission electron microscopy and extend X-ray absorption fine structure (EXAFS) studies[7]. Importantly, with CO in the gas phase, no Pt-Pt interactions were found by EXAFS in $Pt_{0.008}Cu$-SAA (Table 4.2, Figure 4.1), which demonstrates the stability of the isolated Pt atoms in the presence of CO.

Table 4.1. Sample information.

Sample	Composition[a]	Preparation Method	Pt Species
Cu-NP	14.9 at.% Cu on Al_2O_3	Colloidal	---
Pt-NP	0.12 at.% Pt on Al_2O_3	IWI[b]	Single atom, clusters and NPs
$Pt_{0.008}$Cu-SAA	0.11at.% Pt, 13.7 at.% Cu on Al_2O_3	GR	Single atoms in Cu surface[c]
$Pt_{0.39}$Cu-bimetallic	2.2 at.% Pt, 5.6 at.% Cu on Al_2O_3	GR	Single atom, clusters and NPs [d]

[a] Determined by ICP-AES.

[b] Incipient wetness impregnation (IWI).

[c] Determined by STEM, EXAFS and CO-IR.

[d] Determined by EXAFS and CO-IR.

XAS studies

The EXAFS of $Pt_{0.008}Cu$-SAA is plotted in Figure 4.1 and the EXAFS Model fitting results are summarized in Table 4.2. The EXAFS of $Pt_{0.008}Cu$-SAA with CO in the Fourier transform space is different from that of Pt foil. The peak position is at significant lower R value compared to that of Pt. This is peak is similar to that of PtCu-SAA without CO in the gas phase. Indeed, no Pt-Pt bonds were formed with CO in the gas phase, which demonstrated the stability of the single Pt atoms. The Pt-Cu coordination number (CN) is 10.54 for $Pt_{0.008}Cu$-SAA. The Pt-Cu interaction distance is 2.601 Å, which is smaller than that of Pt-Pt but greater than that of Cu-Cu.[7,8]

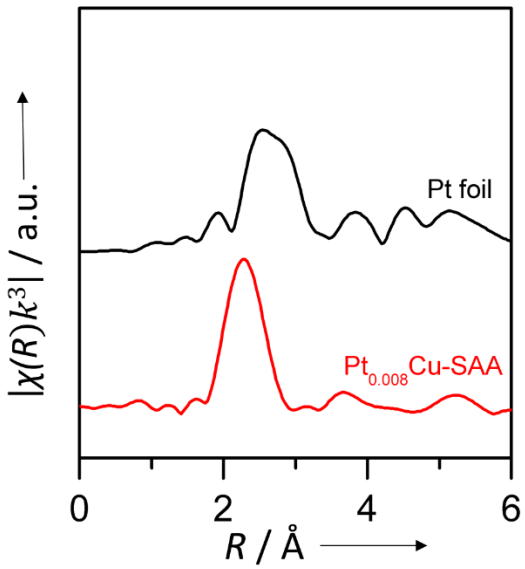

Figure 4.1. Fourier transform of k^3-weighted Pt L_{III} EXAFS of Pt foil and $Pt_{0.008}Cu$-SAA in CO and H_2 gases mixture plotted in R-space.

Table 4.2. EXAFS model fitting.

Sample	Shell	CN[a]	R[b] (Å)	σ^2 (Å^2)	R-factor
Pt foil	Pt-Pt	12	2.764±0.002	0.004	0.001
$Pt_{0.008}$Cu-SAA	Pt-Pt	0			0.015
H_2+CO	Pt-Cu	10.54±2.28	2.601±0.006	0.007	

[a] CN, coordination number. [b] R, distance between absorber and backscattered atoms. R-factor, closeness of the fit, if < 0.05, consistent with broadly correct models.

FTIR studies on adsorbed CO

The adsorption of CO on Pt-Cu alloys and their monometallic counterparts in NP forms was investigated at ambient pressure by IR spectroscopy. CO-FTIR for Pt-NP is shown in Figure 4.2. The absorption peak centered at around 2033-2020 cm^{-1} is assigned to linearly CO adsorbed on Pt, while the broad band centered at around 1808 cm^{-1} is attributed to the bridge CO on Pt. This is in agreement with the typical CO-IR spectra for supported Pt nanoparticles.[9,10]

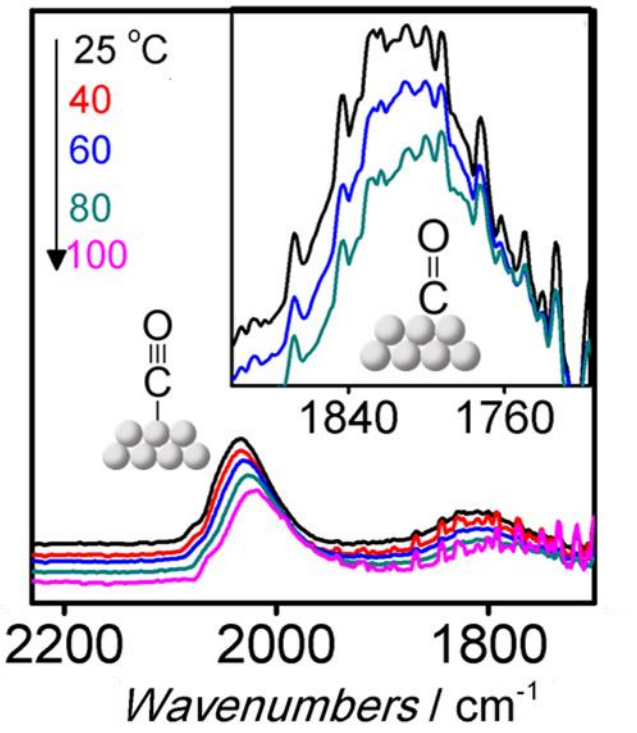

Figure 4.2. IR spectra in the carbonyl range of pre-reduced Pt-NP.

Figure 4.3 reveals the CO-FTIR of $Pt_{0.39}Cu$-bimetallic. The peaks centered at 2110 cm^{-1} are ascribed to linearly adsorbed CO on Cu sites, and the peak at 2043-2029 cm^{-1} is assigned to linearly adsorbed CO on Pt sites in the bimetallic catalysts.[11–15] The CO-Pt peak is slightly blue shifted compared to Pt-NP, which might be due to the CO surface coverage effect or the alloying effect[16]. The FWHM of the atop CO peak on $Pt_{0.008}Cu$-SAA is around 25 cm^{-1}, which indicates the relatively non-uniform distribution of the Pt sites.[17,18] The bridge CO peak appears at around 1800 cm^{-1}.[19,20] The existence of bridge adsorbed CO indicates there are CO clusters or extended Pt ensembles in $Pt_{0.39}Cu$-bimetallic, which is in agreement with the aforementioned EXAFS data fitting results.

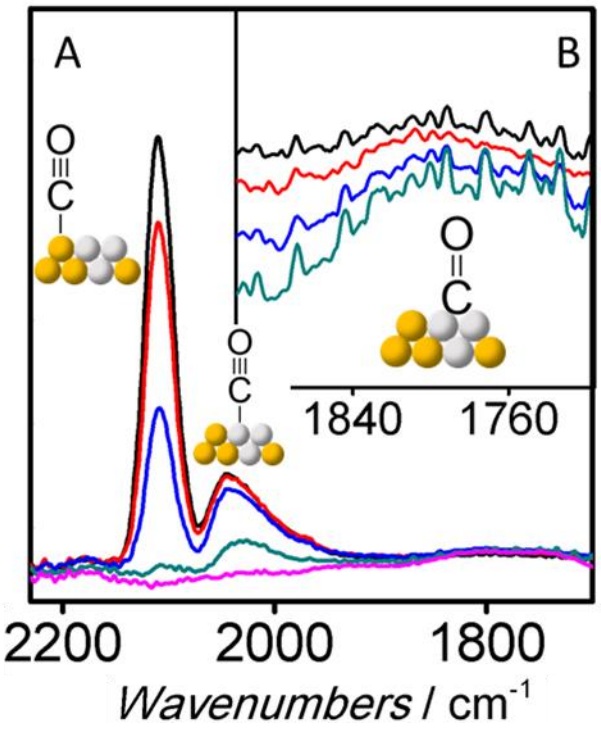

Figure 4.3. IR spectra in the carbonyl range of pre-reduced $Pt_{0.39}Cu$-bimetallic.

In CO-IR of $Pt_{0.008}Cu$-SAA (Figure 4.4), we do not see the bridge CO peaks between 1900 and 1700 cm^{-1}, as observed on the Pt-NP and $Pt_{0.39}Cu$-bimetallic. This indicates the highly dispersed Pt atoms in the surface of Cu, which is consistent with the fact that exclusively isolated Pt atoms are in the surface of $Pt_{0.008}Cu$-SAA, unlike the existence of a mixed phase of Pt atoms, clusters and particles on the Pt-NP and $Pt_{0.39}Cu$-bimetallic. Overlapping peaks between 2150 and 2060 cm^{-1} are seen for $Pt_{0.008}Cu$-SAA, as indicated by the asymmetric absorption band (Figure 4.5 B). The unique absorption band centered at ca. 2088 cm^{-1} is distinct from atop CO on the Cu or Pt NPs, and is assigned to the linearly adsorbed CO on the isolated single Pt atoms. The absorption band of linearly adsorbed CO is at ca. 2020 cm^{-1} on Pt-NP, 2031 cm^{-1} on the Pt ensembles on $Pt_{0.39}Cu$-bimetallic and 2093 cm^{-1} on Cu-NP (Figure 4.3, 4.4 and 4.5). As for the

different Pt species characterized by CO-IR, their formal charges and coordination numbers are essentially the same, and dipole-dipole coupling has little effect on $Pt_{0.008}Cu$-SAA due to the weak CO-metal bonds on isolated Pt atoms and Cu surfaces[21]. Hence, the vibrational frequency of adsorbed CO indicates the electronic properties of the Pt atoms in the surface of catalysts. The change of electronic states of Pt atoms is also observed by aforementioned XANES studies. The change in electronic states will affect the binding strength to CO. In principle, the higher v(CO) indicates less back donation from Pt to CO molecule. Moreover, the ensemble effect of isolated Pt atoms can lower the CO adsorption strength by eliminating the more strongly adsorbed bridge CO. So PtCu SAA is a promising catalyst with low CO binding strength. Indeed, it has been shown by DFT calculation that the adsorption strength of CO on the $Cu_3Pt(111)$ alloy is lower than Pt(111)[22].

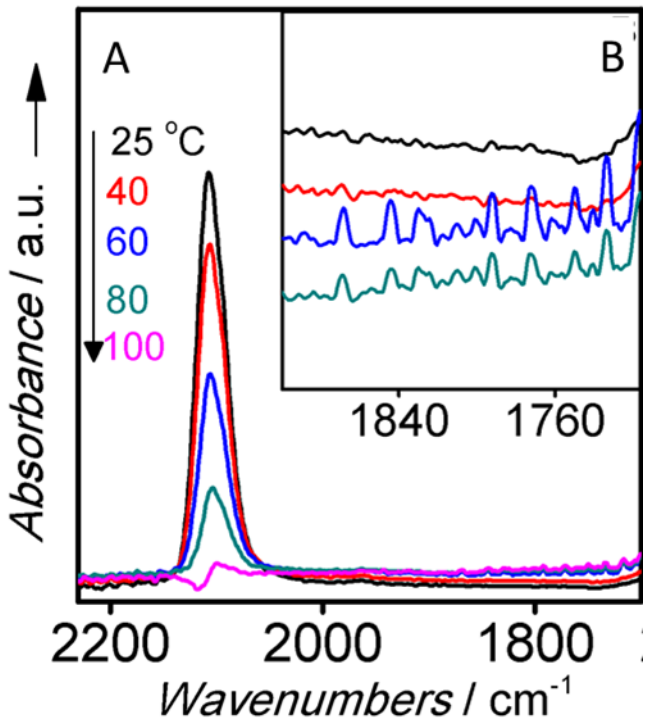

Figure 4.4. IR spectra in the carbonyl range of pre-reduced $Pt_{0.008}Cu$-SAA.

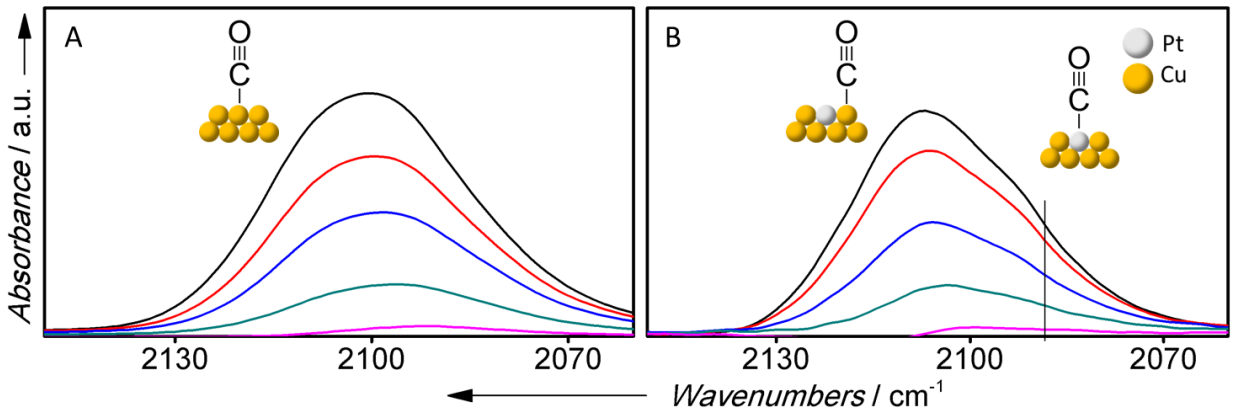

Figure 4.5. IR spectra in the carbonyl range of pre-reduced (A) $Pt_{0.008}Cu$-SAA and (B) Cu-NP.

The temperature effects on the adsorption of CO on $Pt_{0.008}$Cu-SAA, $Pt_{0.39}$Cu-bimetallic and Pt-NP catalysts were investigated. Figure 4.6 summarizes the IR absorption intensity of atop CO at Pt sites for different samples was compared as temperature is increased from 20 to 60 °C. The intensities of the CO adsorption peaks decreased with increased temperature. $Pt_{0.008}$Cu-SAA shows most significant temperature effect as the CO peak intensity decreases to half of the initial value with temperature increases from 20 to 60 °C. While the CO peak intensity on $Pt_{0.39}$Cu-bimetallic decreases to 80%. The CO peak decrease to a further less value on Pt-NP. These results indicate that the CO-Pt bond is the weakest on the $Pt_{0.008}$Cu-SAA compared to Pt-NP and $Pt_{0.39}$Cu-bimetallic.

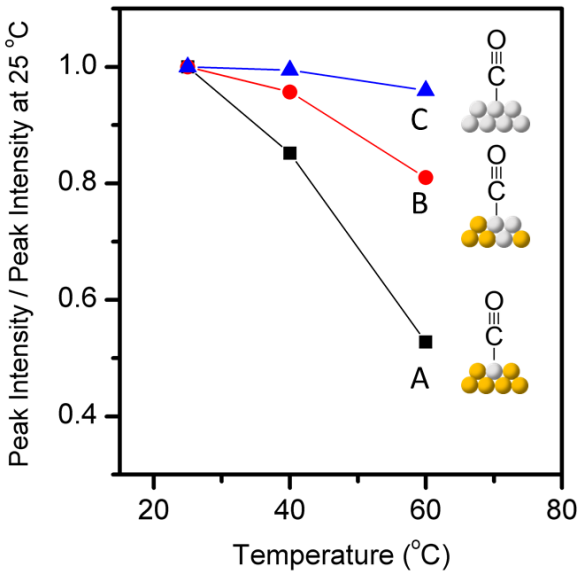

Figure 4.6. Temperature effects on IR intensity of the linearly adsorbed CO on Pt sites of (A) $Pt_{0.008}$Cu-SAA, (B) $Pt_{0.39}$Cu-bimetallic and (C) Pt-NP. The vertical axis is the ratio of the peak absorbance at the given temperature to the peak absorbance at 25 °C. The peak vibrational frequency of each carbonyl is (A) 2088 cm^{-1}, (B) 2045-2031 cm^{-1} and (C) 2033-2018 cm^{-1}.

Table 4.3. CO-IR peak assignments

Peak position (cm^{-1})	Assignments	References
2092-2110	Atop CO on Cu species (Cu-NP, $Pt_{0.39}Cu$-bimetallic, $Pt_{0.008}Cu$-SAA)	[11,12,16,23]
ca. 2088	Atop CO on isolated Pt atoms in the surface of Cu NPs ($Pt_{0.008}Cu$-SAA)	
2018-2043	Atop CO on extended Pt species (Pt-NP, $Pt_{0.39}Cu$-bimetallic)	[14,16,19,20,24]
1788-1812	Bridging CO on two adjacent Pt sites (Pt-NP, $Pt_{0.39}Cu$-bimetallic)	[19,20]

H_2-D_2 exchange in the presence of CO

H_2-D_2 exchange was employed to characterize the H_2 dissociation activity on the corresponding nanocatalysts at ambient pressure in a flow reactor setup.[25] As described in chapter 3, the H_2 activation barrier on Cu surface is significantly higher than that of on extended Pt surface or Pt single atoms. So the H_2 dissociation sites on PtCu-SAA is Pt single atoms. At the meantime, the H_2 desorption barrier on single Pt atoms is lower than that of Cu surface. So the single-atom Pt sites also act as the exit of the H_2 molecule. Thus, the H_2-D_2 exchange characterizes

the activity and availability of the Pt atoms in the surface of PtCu-SAA under practical reaction conditions.

As shown in Figure 4.7, HD is initially produced when H_2 and D_2 are co-fed into the reactor at a certain temperature. Once CO (3.3%) is introduced, the HD production decreases, which indicates the CO poisoning of the Pt sites. With the same CO concentration in the gas phase, $Pt_{0.008}$Cu-SAA yields 12 times more HD than Pt-NP at 150 °C. Since the CO coverage is a function of binding strength, and we have shown that CO binds to Pt-Cu SAAs more weakly compared to pure Pt, the reduced binding strength of CO to $Pt_{0.008}$Cu-SAA yields more CO-free sites that are available for H_2 activation and hence HD production. In other words, $Pt_{0.008}$Cu-SAA is one order of magnitude more CO tolerant compared to monometallic Pt catalysts under the reaction conditions employed.

The temperature effects on the CO tolerance of Pt catalysts are also investigated. As shown in Figure 4.7, the H_2-D_2 exchange in the presence of CO was studied at 120, 150 and 200 °C. At higher temperatures, the CO effect on HD production decreases. Moreover, $Pt_{0.008}$Cu-SAA shows significantly higher HD production at different temperatures with the presence of 3.3% CO. This further confirms the CO tolerance of $Pt_{0.008}$Cu-SAA catalysts at different operating conditions.

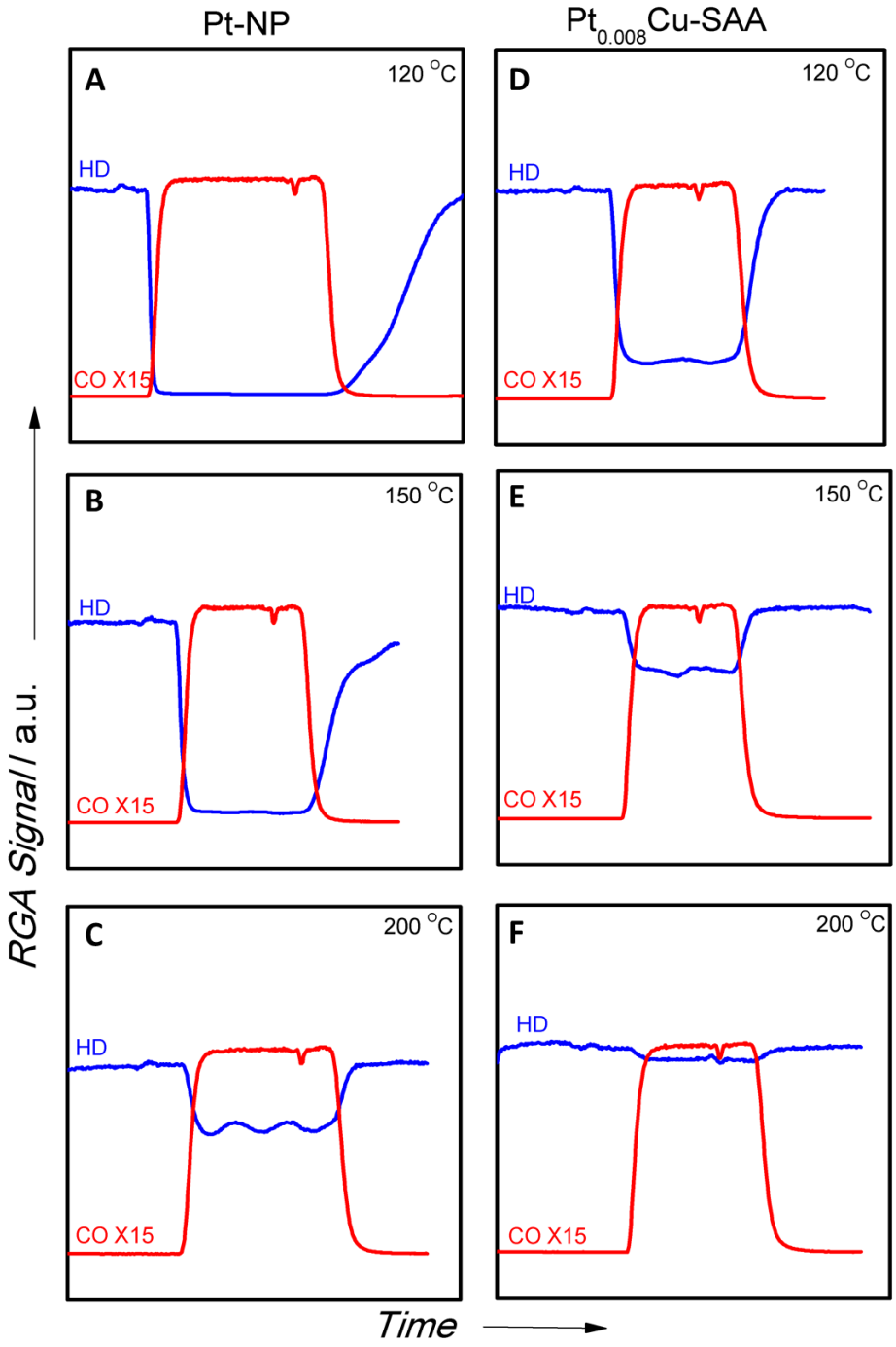

Figure 4.7. Isothermal H_2-D_2 exchange over Pt-NP (A, B, C) and $Pt_{0.008}$Cu-SAA (D, E, F) at 120, 150 and 200 °C. CO was turned on and off during the experiments. Gas composition: 33% H_2, 33% D_2, 3.3% CO, balance Argon. Total flow rate=50 mL/min. 90 mg catalysts.

The CO tolerance of $Pt_{0.008}$Cu-SAA was studied in temperature-programed H_2-D_2 experiments, over a wide temperature range (120 to 200 °C) with CO concentrations from 667 ppm to 3.3% (Figure 4.8). At this temperature range, $Pt_{0.008}$Cu-SAA shows higher HD production compared to that of Pt-NP. Moreover, $Pt_{0.008}$Cu-SAA outperforms Pt-NPs at lower CO concentration (667 ppm) as well, which demonstrates the broad operation window of Pt-Cu SAA as a CO-tolerant catalyst.

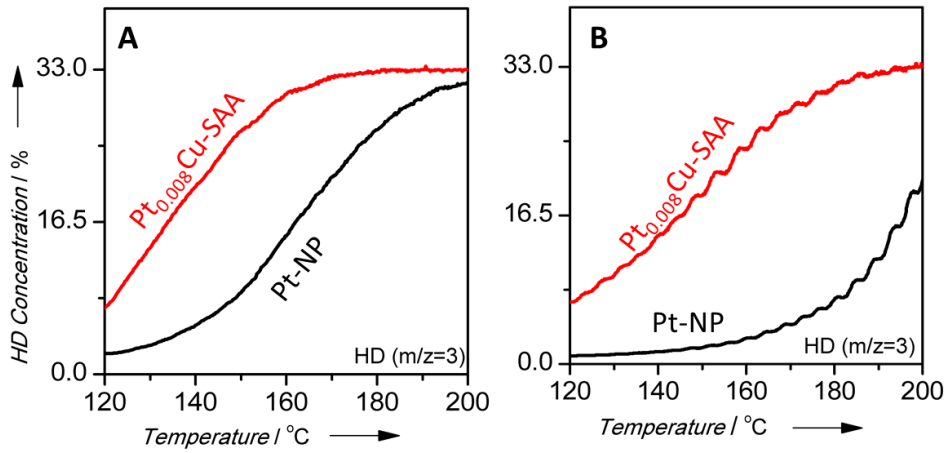

Figure 4.8. H_2-D_2 exchange as a function of temperature. Gas composition: 33% H_2, 33% D_2, 667ppm CO (A), or 3.3% CO (B) balance Argon. Total flow rate=50 mL/min. 80 mg catalyst loading.

H_2 activation is the rate limiting step for hydrogenation reactions and the key elementary step the anode reaction of H_2 fuel cells. The H_2-D_2 exchange with and without CO indicates Pt-Cu

SAA as a class of promising CO-tolerant catalysts for fuel cells and other applications in the chemical industry.

To investigate the CO-tolerance of Pt-Cu SAA under realistic catalytic reaction conditions, we conducted the selective hydrogenation of acetylene over $Pt_{0.008}$Cu-SAA and Pt-NP with and without CO in a flow reactor. Figure 4.9 plots the ratio between reaction rate with 200ppm CO in the gas phase and rate without CO. The reactions were performed at temperatures lower than 80 °C and with 200 ppm CO, which are very close to the operating conditions of the hydrogen fuel cells. We found about half of the reaction rate was retained for $Pt_{0.008}$Cu-SAA. However, the hydrogenation activity of Pt-NP decreased 15-fold with 200 ppm CO. The H_2-D_2 exchange and acetylene hydrogenation activity of Cu-NP was at least one order of magnitude lower than that of $Pt_{0.008}$Cu-SAA at these temperatures. Our results demonstrate that Pt-Cu SAAs offer a new approach to design CO-tolerant materials for industrial applications.

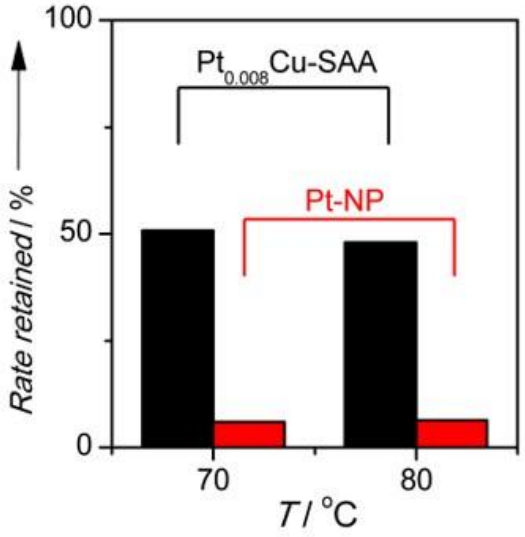

Figure 4.9. Ratio of retained reaction rate of acetylene hydrogenation in CO over $Pt_{0.008}$Cu-SAA and Pt-NP at different temperatures. Rate retained = reaction rate with CO/rate without CO in the reaction gas. Gas composition: 20% H_2, 2.2% C_2H_2, 200 ppm CO, 10% Argon, balance He. Flow rate = 24 mL/min.

4.3 Collaboration: CO-TPD and STM on Pt-Cu(111) SAA

In agreement with the Pt surface structure observed by scanning tunneling microscopy (STM)[26,27], the CO desorption profiles reveal the development of 3 distinct Pt-Cu alloyed structures with increasing Pt coverage. With atomic resolution, the Pt atoms image ~20 pm taller than the surrounding Cu lattice and appear as brighter protrusions. At low Pt coverages, CO desorbs from isolated Pt atoms (peak at 350 K) and at intermediate coverages, CO desorbs from extended ensembles of Pt atoms (peak at 480 K). At 5 ML Pt, the surface layer is composed primarily of continuous ordered Pt atoms and CO desorbs at 410 K. At low CO

coverages, CO desorption from Pt(111) is reported at 450 K and with increasing CO coverage desorption is observed at 400 K due to the repulsion between co-adsorbed CO molecules[28]. In Pt-Cu alloys, CO adsorbs weakest on the Pt-Cu SAA and strongest on the extended Pt clusters.

The mobility of H atoms on Pt-Cu SAAs was demonstrated in UHV by co-adsorption of H_2 and D_2 onto SAA Pt-Cu(111). We observed desorption of HD (m/z = 3) which provides evidence of the dissociation of H_2 and migration of H atoms away from the dissociation site. When equal amounts of H and D atoms are adsorbed on the surface, we observe complete scrambling of H and D with ratio of H_2:HD:D_2 of 1:2:1 due to H atom spillover and its facile diffusion on Cu.

4.4 Summary

In this chapter, we investigated the fundamentals of CO adsorption on Pt-Cu alloys using a variety of catalysis techniques. We found that CO binds weaker to single Pt atoms in Cu compared to larger Pt ensembles or monometallic Pt. Thus, when CO is present in the gas phase, more CO-free Pt sites are available on the SAA than the monometallic Pt, yielding higher hydrogenation activity under realistic conditions. We postulate that this SAA approach in other metal combinations can be used for the design of novel CO-tolerant catalysts for other industrially important reactions such as hydrocarbon and alcohol oxidation reactions, and for the present generation, low-temperature hydrogen fuel cells where the platinum electrocatalyst is prone to CO-poisoning.

4.4 References

1. Cheng X, Shi Z, Glass N, et al. A review of PEM hydrogen fuel cell contamination: Impacts, mechanisms, and mitigation. *J Power Sources*. 2007;165(2):739-756.

2. Baschuk JJ, Li X. Carbon monoxide poisoning of proton exchange membrane fuel cells. *Int J Energy Res*. 2001;25(8):695-713.

3. Pedersen MØ, Helveg S, Ruban A, et al. How a gold substrate can increase the reactivity of a Pt overlayer. *Surf Sci*. 1999;426:395-409.

4. Ruff M, Takehiro N, Liu P, Nørskov JK, Behm RJ. Size-specific chemistry on bimetallic surfaces: A combined experimental and theoretical study. *ChemPhysChem*. 2007;8:2068-2071. doi:10.1002/cphc.200700070.

5. Kirstein W, Krüger B, Thieme F. CO adsorption studies on pure and Ni-covered Cu(111) surfaces. *Surf Sci*. 1986;176:505-529.

6. Boucher MB, Zugic B, Cladaras G, et al. Single atom alloy surface analogs in Pd0.18Cu15 nanoparticles for selective hydrogenation reactions. *Phys Chem Chem Phys*. 2013;15:12187-12196. doi:10.1039/c3cp51538a.

7. Lucci FR, Liu J, Marcinkowski MD, et al. Selective hydrogenation of 1,3-butadiene on platinum – copper alloys at the single-atom limit. *Nat Commun*. 2015;6:8550. doi:10.1038/ncomms9550.

8. Yamamoto T a., Nakagawa T, Seino S, Nitani H. Bimetallic nanoparticles of PtM (M=Au, Cu, Ni) supported on iron oxide: Radiolytic synthesis and CO oxidation catalysis. *Appl Catal A Gen*. 2010;387(1-2):195-202. doi:10.1016/j.apcata.2010.08.020.

9. Haaland DM. Infrared studies of CO adsorbed on Pt/Al2O3: Evidence for CO bonded in 3-fold coordination. *Surf Sci*. 1987;185(1-2):1-14. doi:10.1016/S0039-6028(87)80610-6.

10. Brandt RK, Hughes MR, Bourget LP, Truszkowska K, Greenler RG. The interpretation of CO adsorbed on Pt/SiO2 of two different particle-size distributions. *Surf Sci*. 1993;286(1-2):15-25. doi:10.1016/0039-6028(93)90552-U.

11. Greeley J, Gokhale AA, Kreuser J, et al. CO vibrational frequencies on methanol synthesis catalysts: a DFT study. *J Catal*. 2003;213(1):63-72. doi:10.1016/S0021-9517(02)00040-4.

12. Nishiyama H, Inoue Y. IRAS study of surface acoustic wave effects on CO adsorbed on Cu surfaces. *Surf Sci*. 2005;594(1-3):156-162. doi:10.1016/j.susc.2005.07.021.

13. Oxford SM, Lee PL, Chupas PJ, Chapman KW, Kung MC, Kung HH. Study of Supported PtCu and PdAu Bimetallic Nanoparticles Using In-Situ X-ray Tools †. *J Phys Chem C*. 2010;114(40):17085-17091. doi:10.1021/jp103675n.

14. Chandler B. DRIFTS studies of carbon monoxide coverage on highly dispersed bimetallic Pt-Cu and Pt-Au catalysts. *Catal Today*. 2001;65(1):39-50. doi:10.1016/S0920-5861(00)00543-5.

15. Yang XF, Wang A, Qiao B, Li J, Liu J, Zhang T. Single-atom catalysts: a new frontier in heterogeneous catalysis. *Acc Chem Res*. 2013;46:1740-1748. doi:10.1021/ar300361m.

16. Oxford SM, Lee PL, Chupas PJ, Chapman KW, Kung MC, Kung HH. Study of Supported PtCu and PdAu Bimetallic Nanoparticles Using In-Situ X-ray Tools . *J Phys Chem C*. 2010;114(40):17085-17091. doi:10.1021/jp103675n.

17. Hoffman AS, Fang C-Y, Gates BC. Homogeneity of Surface Sites in Supported Single-Site Metal Catalysts: Assessment with Band Widths of Metal Carbonyl Infrared Spectra. *J Phys Chem Lett*. 2016;7(19):3854-3860. doi:10.1021/acs.jpclett.6b01825.

18. Babucci M, Fang C-Y, Hoffman AS, Bare SR, Gates BC, Uzun A. Tuning the Selectivity of Single-Site Supported Metal Catalysts with Ionic Liquids. *ACS Catal*. 2017;7(10):6969-6972. doi:10.1021/acscatal.7b02429.

19. Qiao B, Wang A, Yang X, et al. Single-atom catalysis of CO oxidation using Pt1/FeOx. *Nat Chem*. 2011;3(8):634-641. doi:10.1038/nchem.1095.

20. Bazin P, Saur O, Lavalley JC, Daturi M, Blanchard G. FT-IR study of CO adsorption on Pt/CeO2: characterisation and structural rearrangement of small Pt particles. *Phys Chem Chem Phys*. 2005;7(1):187. doi:10.1039/b414159h.

21. Castro GR, Doyen G. Electronical and structural effects in CO Chemisorption on Cu3Pt(111). *Surf Sci*. 1994;(307):384.

22. Zhang CJ, Baxter RJ, Hu P, Alavi A, Lee MH. A density functional theory study of carbon monoxide oxidation on the Cu[sub 3]Pt(111) alloy surface: Comparison with the reactions on Pt(111) and Cu(111). *J Chem Phys*. 2001;115(11):5272. doi:10.1063/1.1395626.

23. Mondelli C, Ferri D, Grunwaldt J-D, Ravasio N, Baiker A. Redox properties of supported copper catalysts studied in liquid and gas phase by in situ ATR-IR and XAS. *Catal Today*. 2011;178(1):124-131. doi:10.1016/j.cattod.2011.08.043.

24. Ferri D, Bürgi T, Baiker A. Pt and Pt/Al2O3 Thin Films for Investigation of Catalytic

Solid−Liquid Interfaces by ATR-IR Spectroscopy: CO Adsorption, H2 -Induced Reconstruction and Surface-Enhanced Absorption. *J Phys Chem B*. 2001;105(16):3187-3195. doi:10.1021/jp002268i.

25. Gumuslu G, Kondratyuk P, Boes JR, et al. Correlation of Electronic Structure with Catalytic Activity: H2 –D2 Exchange across CuxPd1– x Composition Space. *ACS Catal*. 2015;5(5):3137-3147. doi:10.1021/cs501586t.

26. Lucci FR, Lawton TJ, Pronschinske A, Sykes ECH. Atomic scale surface structure of Pt/Cu(111) surface alloys. *J Phys Chem C*. 2014;118:3015-3022.

27. Lucci FR, Marcinkowski MD, Lawton TJ, Sykes ECH. H2 Activation and Spillover on Catalytically Relevant Pt-Cu Single Atom Alloys. *J Phys Chem C*. 2015;119(43):24351-24357.

28. Collins DM, Spicer WE. The adsorption of CO, O2 and H2 on Pt. *Surf Sci*. 1977;69:85-113.

Chapter 5. PtCu single-atom alloy catalysts for coke resistant C-H activation and selective dehydrogenation of n-butane

5.1 Introduction

The production of shale gas from hydraulic fracturing has boosted the supply of light alkanes such as ethane and propane in recent years.[1,2] However, there are few low-carbon footprint methods that efficiently convert these gases to more valuable chemicals due to their relative inertness.[3] While steam cracking is the traditional industrial process, it is energy-demanding and less than 60% efficient.[2] Catalytic processes are sought after to potentially improve the energy balance sheet. Facile activation of C-H bonds in alkanes would open new routes to synthesize commodity and fine chemicals.[3–6] There are numerous ways to functionalize alkanes including alkane halogenation/oxyhalogenation, oxidative coupling, and oxidative dehydrogenation.[7–10] This chapter focused on the dehydrogenation of alkanes to produce alkenes, which are precursors to industrially relevant polymers.[1,6,11,12] Preventing coking is indeed an active, yet challenging area of current research.[13] Pt catalysts also suffer from coking and Pt's high price prohibits widespread use.[14–16] Cu catalysts are typically not considered viable due to a high C-H activation barrier on Cu surfaces, but are resistant to coking.[17]

Alloys often exhibit unique properties compared to their constituent metals.[18,19] For example, using a combination of surface science, theory, and catalysis, Besenbacher et al. showed that small amounts of Au dispersed in Ni can suppress carbon deposition in methane

steam reforming by both raising the barrier to C-H activation and decreasing the binding strength of carbon to the surface.[18] We took the opposite approach in this work, using the smallest amount of a catalytic metal (Pt) in the form of single atoms in the surface layer of a more inert host metal (Cu) to facilitate C-H activation while avoiding coking that typically occurs on larger ensembles.[19] These single-atom alloys (SAAs)[20–22] are analogous to single-atom catalysts[23,24], but unlike many single-atom catalysts, reaction at the active site can be understood with atomistic detail on SAAs.

PtCu alloys activate C-H bonds with significantly improved activity over Cu, while avoiding coking that occurs on catalysts with extended Pt ensembles due to Cu's ability to facilitate C-C coupling chemistry. These PtCu alloy nanoparticle catalysts exhibit reaction temperatures significantly lower than Cu under realistic operating conditions. The Pt-Cu SAAs were demonstrated to be highly stable and coke-resistance in butane dehydrogenation reactions.

5.2 Experimental methods

PtCu NP catalysts were prepared as described in chapter 2.[21,25,26] Cu NPs prepared as colloids by reducing $Cu(NO_3)_2$ in aqueous solution with $NaBH_4$ as reducing agent and polyvinylpyrrolidone as capping agent. The resulting copper NPs were deposited onto a silica support (fumed silica, 0.2-0.3 µm average aggregate particle size, surface area 200 m^2/g)

followed by calcination in air at 300 °C.[21,26,27] $Pt_{0.03}Cu$-SAA and $Pt_{0.01}Cu$-SAA were prepared by the galvanic replacement method on the copper NPs.[21,26]

Diffuse reflectance infrared Fourier transform spectroscopy (DRIFTS) and X-ray absorption spectroscopy (XAS) were conducted using the same protocols as described in chapter 3 and 4. DRIFTS was conducted using a Thermo Nicolet iS50 FT-IR equipped with a Harrick DRIFTS cell.[25] The samples were pre-reduced in H_2 at 400 °C *in situ*. Samples were degassed with helium for 15 minutes before introducing CO. After 10 minutes CO exposure, helium was passed through the sample while the IR spectra were collected.

Temperature- programmed- oxidation (TPO) experiments were performed in a packed-bed flow microreactor (L = 22 inch, O.D. = 1/2 inch) following the long-hour butane-D_2 isotope scrambling (B-D scrambling) experiments. The samples were treated in Argon (pure, 50 mL/min) at 300 °C for 2 h prior to the TPO. After cooling to ambient temperature in Argon, 20 % O_2/He (20 mL/min) was introduced to the reactor and allow the system to stabilize for one hour. To perform TPO, the temperature was increased from ambient temperature to 600 °C at 3 °C/min. The gas effluent from the reactor was analyzed by a mass-spectrometer.

TEM was conducted on a JEOL 2010 electron microscope with 200 kV and 107 μA beam emission. The specimens were obtained by adding one drop of ethanol solution of nanoparticles onto a carbon film with a nickel covered microgrid.

B-D scrambling and butane dehydrogenation experiments were performed in a packed-bed flow microreactor (L=22 inch, O.D.=1/2 inch) with 100 mg of catalyst diluted by 1 g of quartz particles. Prior to the introduction of reaction gas mixture, the samples were reduced in

20% H_2/He at 400 °C for 20 minutes and cooled to ambient temperature. After stabilizing in the reaction gas mixture at ambient temperature for 1 hour, the temperature was raised to the desired point. The gas effluent from the reactor was analyzed by a mass-spectrometer. To perform temperature programmed B-D scrambling, the temperature was increased from ambient temperature to 400 °C at 5 °C/min.

For butane dehydrogenation reactions, the samples were reduced in 20% H_2/He at 400 °C for 20 minutes and cooled to ambient temperature. After stabilizing in the reaction gas mixture at ambient temperature for 1 hour, the temperature was raised to the desired point. The gas effluent from the reactor was analyzed by a mass-spectrometer. For the apparent activation energy measurements, the catalysts were tested in steady state at highest temperature followed by decreasing the temperature to the desired points.

5.3 Results and discussion

$Pt_{0.03}$Cu-SAA and $Pt_{0.01}$Cu-SAA NPs were prepared by a galvanic replacement reaction as reported in Lucci et al. and Liu et al.[21,26] and supported on silica (Table 5.1). We conducted extended X-Ray absorption fine structure (EXAFS) and Fourier transform infrared spectroscopy (FTIR) studies to confirm the formation of NPs with isolated Pt atoms.

Table 5.1. Sample Information

Sample	Composition[a]	Preparation Method	Pt Species
Cu-NP	3.6 wt.% Cu on SiO_2	Colloidal	---
Pt-NP	0.5 wt.% Pt on SiO_2	IWI[b]	NPs
$Pt_{0.03}$Cu-SAA	0.25 wt.% Pt, 3 wt.% Cu on SiO_2	Galvanic replacement	Single atoms in Cu surface[c]
$Pt_{0.01}$Cu-SAA	0.1 wt.% Pt, 3.4 wt.% Cu on SiO_2	Galvanic replacement	Single atoms in Cu surface[d]

[a] Determined by ICP-AES.

[b] Incipient wetness impregnation (IWI).

[c,d] Determined by STEM in ref. 9 and EXAFS and CO-IR in this work.

Figure 5.1 and 5.2 show the FTIR spectra for $Pt_{0.01}$Cu-SAA and $Pt_{0.03}$Cu-SAA with CO chemisorption, respectively. The peaks at 2130 to 2112 cm^{-1} are assigned to linearly adsorbed CO on Cu and Pt respectively.[26,28–31] Peaks corresponding to linearly adsorbed CO and bridge CO on extended Pt surfaces are not observed in the SAA samples, which typically appear at 2018-2043 cm^{-1} and 1780-1820 cm^{-1}, respectively.[31–35] This suggests that Pt atoms are fully isolated in the copper surface. The CO peaks observed are not shifted as the CO coverage is changed, which indicates small dipole-dipole interaction because of the high dispersion of individual Pt atoms and low CO coverage on the Cu surface.

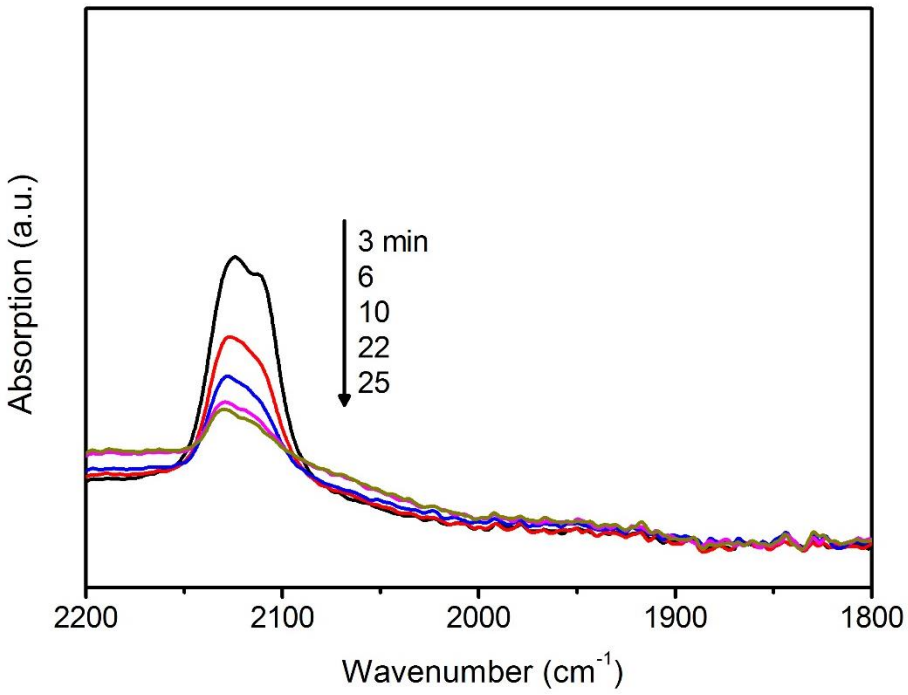

Figure 5.1. FTIR spectra of chemisorbed CO molecule on $Pt_{0.01}Cu$-SAA catalyst. The time values on the graph indicate the time of helium gas purge after CO exposure.

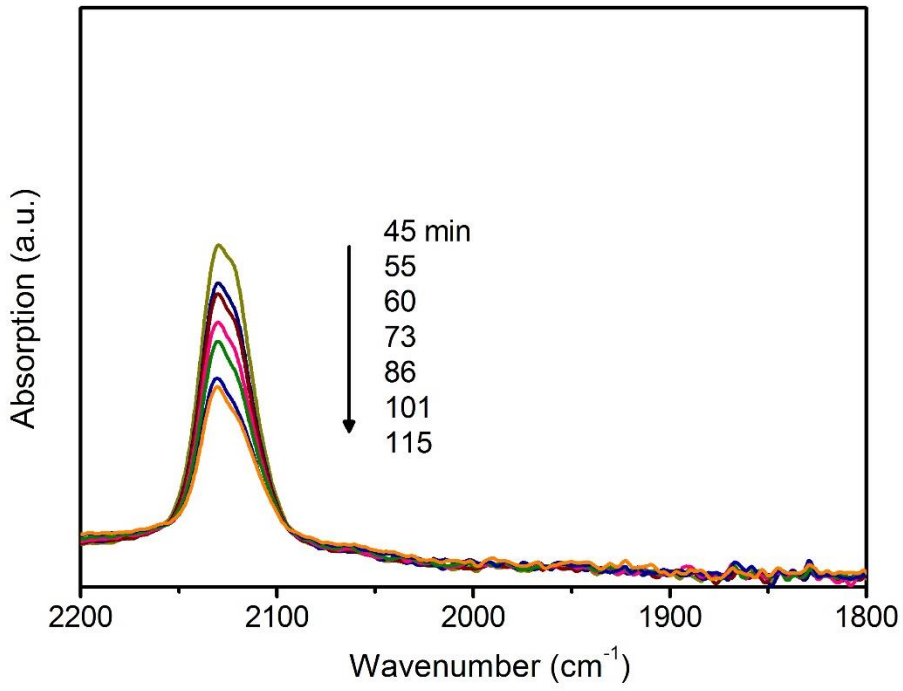

Figure 5.2. FTIR spectra of chemisorbed CO molecule on the $Pt_{0.03}$Cu-SAA catalyst. The time values on the graph indicate the time of helium gas purge after CO exposure.

Figures 5.3 and 5.4 show the EXAFS of $Pt_{0.01}$Cu-SAA, $Pt_{0.03}$Cu-SAA and Pt foil plotted in k-space and Fourier transform space (R-space). The EXAFS $Pt_{0.01}$Cu-SAA and $Pt_{0.03}$Cu-SAA are significant different from that of Pt foil. EXAFS at Pt edge characterize the coordination of Pt atoms, especially in the first shell. $Pt_{0.01}$Cu-SAA and $Pt_{0.03}$Cu-SAA have Pt-Cu interaction peak at lower R value in comparison to that of Pt-Pt interaction peak of Pt foil. EXAFS model fitting suggests there is no Pt-Pt interaction in $Pt_{0.01}$Cu-SAA or $Pt_{0.03}$Cu-SAA in the first coordination shell but only in Pt-Cu interactions (Table 5.2). This further confirms that Pt atoms are fully isolated in the Cu NPs. The first shell bond length (2.59 and 2.61 Å) of SAA NPs is 100% Pt-Cu without Pt-Pt contribution. This is consistent with the formation of SAAs.

Table 5.2. EXAFS model fitting.

Sample	Shell	CN[a]	R[b] (Å)	σ^2 (Å^2)	R-factor
Pt foil	Pt-Pt	12	2.764±0.002	0.004	0.001
$Pt_{0.01}$Cu-SAA	Pt-Pt	0			0.013
	Pt-Cu	10.51±1.62	2.591±0.004	0.005	
$Pt_{0.03}$Cu-SAA	Pt-Pt	0			0.016
	Pt-Cu	10.80±1.75	2.609±0.004	0.006	

[a] CN, coordination number. [b] R, distance between absorber and backscattered atoms. R-factor, closeness of the fit, if < 0.05, consistent with broadly correct models.

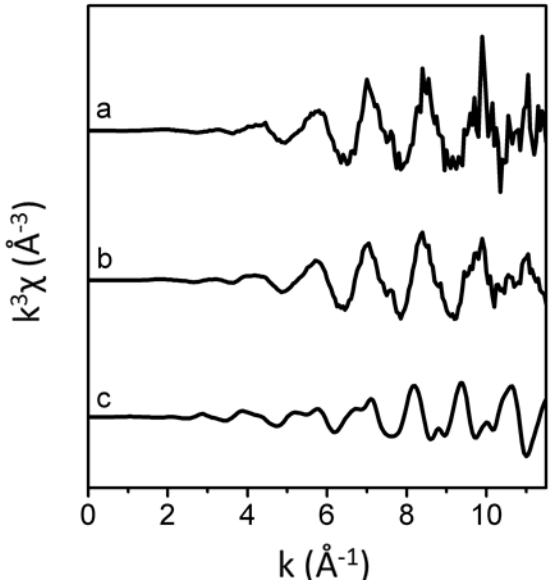

Figure 5.3. *In situ* Pt L_{III} EXAFS of (a) $Pt_{0.01}$Cu-SAA, (b) $Pt_{0.03}$Cu-SAA and (c) Pt foil plotted in k space.

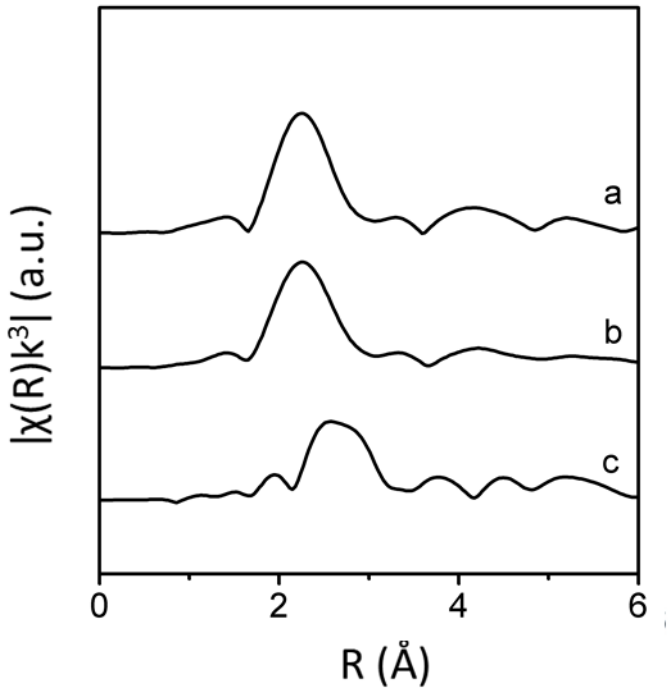

Figure 5.4. Fourier transform of k^3-weighted Pt L_{III} EXAFS of (a) $Pt_{0.01}Cu$-SAA, (b) $Pt_{0.03}Cu$-SAA and (c) Pt foil plotted in R space.

Butane – deuterium scrambling (B-D scrambling)

We compared the performance of Cu NPs and PtCu SAA NP catalysts for B-D scrambling using temperature programmed surface reaction (TPSR) (Figure 5.5). Butane-deuterium isotope scrambling (B-D scrambling) experiments were performed with nanoparticle (NP) catalysts in a flow reactor. The production rate of deuterated butane in B-D scrambling experiments indicates the C-H activation capability of the catalysts as hydrogen (deuterium) dissociation is a facile process under the reaction conditions applied.[21,26] The reaction was operated within the kinetics controlled regime (conversion < 5%), so that the effluent concentration of B-D scrambling products is proportional to the overall C-H activation rate.

The second cycle data were plotted here as there is no activity difference between the second and third cycle. In Figure 5.5, the ratio between mass 59 and 58 reflects the ratio between deuterated butane (C_4H_9D) and butane (C_4H_{10}). $Pt_{0.03}$Cu-SAA and $Pt_{0.01}$Cu-SAA start to convert butane (C_4H_{10}) to deuterated butane (C_4H_9D) at around 250 °C but Cu-NP is active only at temperatures above 500 °C (Figure 5.6). This demonstrates that the activity of B-D scrambling i.e. C-H activation, is significantly improved by the addition of a small amount of isolated Pt atoms into the Cu surface. At the same condition, the silica support is not active for B-D scrambling.

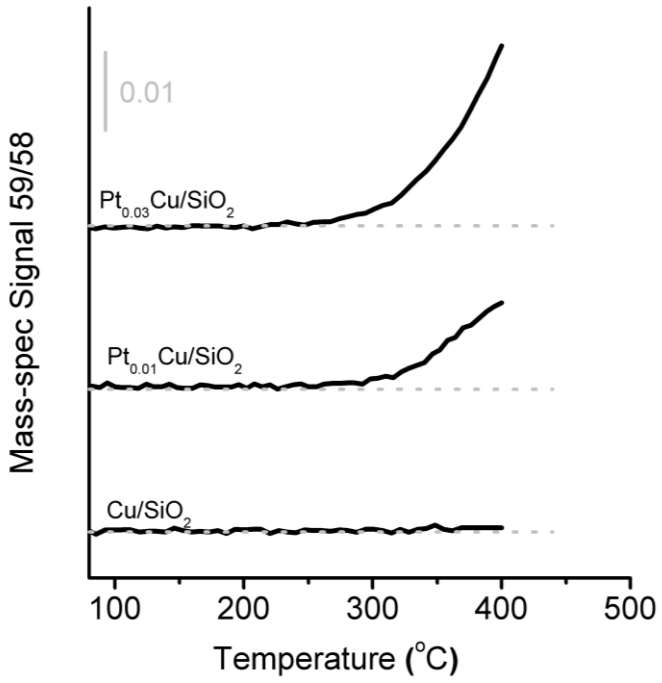

Figure 5.5. Reactor studies of B-D scrambling. TPSR data for the B-D scrambling reaction over $Pt_{0.03}$Cu-SAA, $Pt_{0.01}$Cu-SAA and Cu-NP catalysts, followed by mass spectrometry. (Temperature ramp 5 °C/min). The 59/58 mass ratio indicates the C_4H_9D level. The data are from the second

reaction cycle. Gas composition: 5% butane, 2% deuterium and balance argon. 50 mL/min, 100 mg catalysts, 1 g quartz beads. Collaborative work with Joshua Wimble.[36]

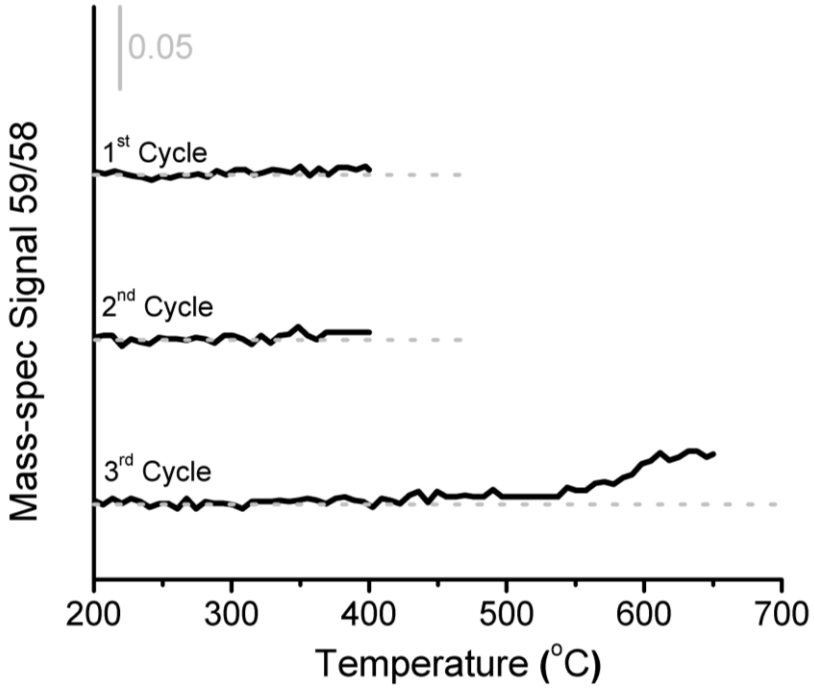

Figure 5.6. Temperature programmed surface reaction data for the B-D scrambling reaction over Cu-NP catalyst. Collaborative work with Joshua Wimble.[36]

Figure 5.7 shows the B-D scrambling TPSR of Pt-NP for the first three cycles up to 400 °C. In the first cycle, Pt-NP begins to catalyze the B-D scrambling around 100 °C. Although the Pt-NP deactivated in the second and third cycles, we can still observe B-D scrambling activity at temperatures higher than 100 °C. Thus, TPSR finds the onset of C-H activation with PtCu-SAA, Cu-NP and Pt-NP at 250, 550, and 100 °C, respectively. This suggests the barriers of C-H

activation on the NP catalysts follow the order: Pt < PtCu-SAA < Cu. This corroborates the trend of C-H activation barriers identified in the model catalyst study[37].

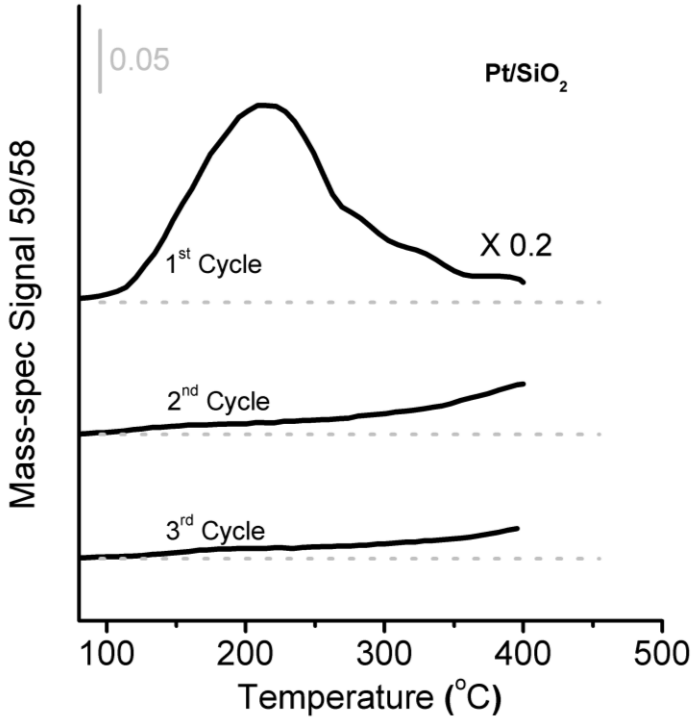

Figure 5.7. Reactor studies of B-D scrambling. TPSR data for the B-D scrambling reaction over Pt-NP catalysts, followed by mass spectrometry. (Temperature ramp 5 °C/min). The 59/58 mass ratio indicates the C_4H_9D level. First, second and third cycles of TPSR are shown. Gas composition: 5% butane, 2% deuterium and balance argon. 50 mL/min, 100 mg catalyst, 1 g quartz beads. Collaborative work with Joshua Wimble.[36]

Monometallic Pt NP catalysts rapidly deactivate during the reaction (Figure 5.7). In the first cycle of TPSR, the production of C_4H_9D 'lights-off' at 100 °C and increases with increasing

temperature up to 230 °C. The production rate of C_4H_9D then drops off after 230 °C indicating significant deactivation, overcoming the effect of temperature increase on reaction rate. The second and third cycles of TPSR show much lower activity compared to the first cycle and the activity decreases cycle by cycle. On the other hand, PtCu-SAAs are very stable. Figure 5.8 shows that $Pt_{0.01}$Cu-SAA catalyzes the B-D scrambling at 360 °C without any deactivation for at least 12 hours. The deactivation of Pt-based catalysts in alkane C-H activation reactions is mainly due to coke formation and sintering of Pt NPs, while the coke formation is the major cause in most cases. However, $Pt_{0.01}$Cu-SAA does not experience any deactivation under the reaction conditions employed.

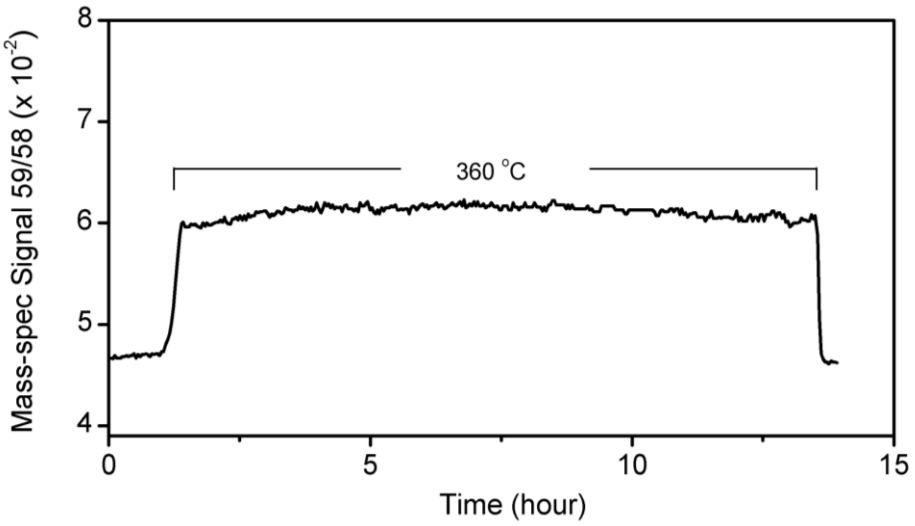

Figure 5.8. Reactor studies of B-D scrambling. 12-hour stability test for the $Pt_{0.01}$Cu-SAA catalyst at 360 °C. The catalyst was at room temperature at the beginning and end of the test. Gas composition: 5% butane, 2% deuterium and balance argon. 50 mL/min, 100 mg catalysts, 1 g quartz beads. Collaborative work with Joshua Wimble.[36]

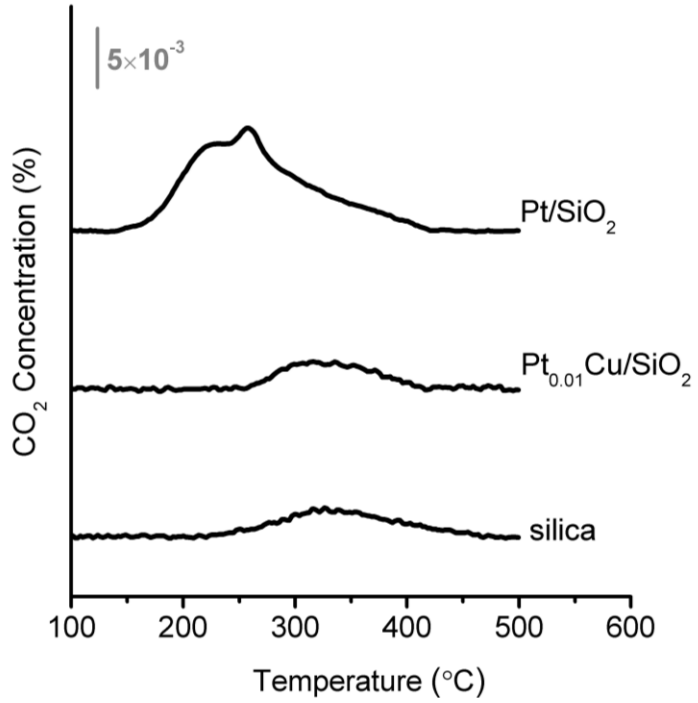

Figure 5.9. Determination of carbon deposition**.** Temperature programmed oxidation (TPO) of (a) Pt-NP, (b) $Pt_{0.012}Cu$-SAA and (c) silica. (a) and (b) were treated in butane-D2 exchange reaction condition at 360 °C for 12 hours. (a), (b) and (c) were treated in argon flow at 300 °C for 2 hours before TPO to desorb the hydrocarbon adsorbates. Collaborative work with Joshua Wimble.[36]

We performed temperature-programmed-oxidation (TPO) on used catalysts to determine whether carbon deposition occurs during B-D scrambling. Pt-NP and $Pt_{0.01}Cu$-SAA were both exposed to B-D scrambling conditions at 360 °C for 12 hours prior to TPO measurements. As shown in Figure 5.9, a broad CO_2 evolution from the used Pt-NP is seen, beginning at 130 °C. At least two different types of carbon are shown, the second matching graphitic carbon oxidation[38], while any adsorbed hydrocarbon species must have desorbed

during the Ar heat treatment. These features are absent on the $Pt_{0.01}$Cu-SAA. The amount of CO_2 produced from this catalyst is essentially the same as that produced from the silica support without any hydrocarbon exposure. Thus, PtCu SAAs are coke- resistant at atmospheric pressure reaction conditions while Pt NPs catalyze carbon formation and deposition, which causes severe deactivation of the catalyst during the B-D scrambling conditions.

In catalysis with exclusively single-atom active sites, a linear relationship between active metal loading and reactivity was reported[39,40]. Here, a linear relationship between the B-D scrambling rate and Pt loading in the catalysts was demonstrated for the PtCu SAA catalysts, as shown in Figure 5.10. This corroborates the fact that Pt atoms are fully isolated in $Pt_{0.01}$Cu-SAA and $Pt_{0.03}$Cu-SAA.

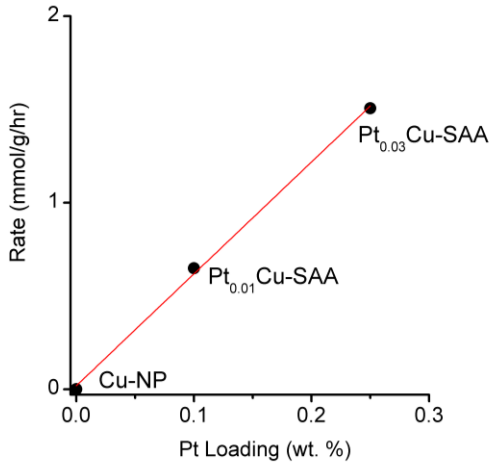

Figure 5.10. B-D scrambling rate as a function of Pt loading in the catalysts. Gas composition: 5% butane, 2% deuterium and balance argon. 50 mL/min, 100 mg catalyst, 1 g quartz beads.

We increased the Pt/Cu ratio to 0.39 in $Pt_{0.39}Cu$ catalyst, which is no longer SAA as indicated by CO-IR and EXAFS model fitting in previous studies[41] that Pt clusters are formed at this Pt loading level. As shown in Figure 5.11, in the first cycle, the reaction rate starts to drop at 390 °C, even with increasing temperature. The B-D scrambling reactivity of the catalyst decreases with cyclic operation. This indicates the deactivation of PtCu bimetallic catalysts when extended Pt ensembles are present.

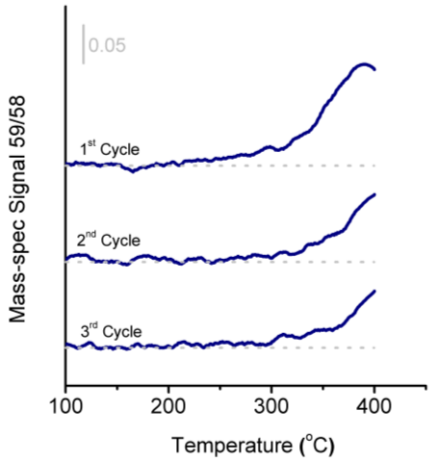

Figure 5.11. Reactor studies of B-D scrambling. TPSR data for the B-D scrambling reaction over $Pt_{0.39}Cu$ followed by mass spectrometry. (5 °C/min) Gas composition: 5% butane, 2% deuterium and balance argon. 50 mL/min, 100 mg sample, 1 g quartz beads.

In model catalyst studies, the Sykes group used methyl groups adsorbed on the single-atom Pt sites in the surface of Cu(111) and demonstrated the C-H activation barrier of them is significantly lower than that on Cu(111).[37] DFT calculation indicates single-atom Pt binds the hydrocarbon intermediates weaker compared to Pt(111) but stronger compared to Cu(111). The strong adsorption of hydrocarbon intermediates on Pt(111) causes the over-

dehydrogenation as the favorable pathway instead of coupling or desorption.[37] Overall, single-atom Pt sites are active for C-H activation but not active in over-dehydrogenation or C-C bond breaking.

Nonoxidative dehydrogenation of butane

Encouraged by the success in the coke resistance B-D scrambling with SAA catalysts, we explored the nonoxidative dehydrogenation of butane with SAA catalysts. At 400 °C, $Pt_{0.01}$Cu-SAA stably converts butane to butene for at least 52 hours without any deactivation (Figure 5.13). An Arrhenius type plot for butane dehydrogenation over $Pt_{0.01}$Cu-SAA and Pt-NP catalysts is shown in Figure 5.12. The apparent activation energy of the reaction over $Pt_{0.01}$Cu-SAA and Pt-NP is 112 and 51 kJ/mol, respectively. The rate limiting step for light alkane dehydrogenation is the first C-H activation. We have found the C-H activation barrier over $Pt_{0.01}$Cu-SAA is higher than that of Pt-NP from the B-D scrambling studies. Thus, the trend we observed in the apparent activation energy of butane dehydrogenation is in agreement with the trend in the C-H activation barrier. The high stability of $Pt_{0.01}$Cu-SAA in butane dehydrogenation conditions is also in agreement with its stability in B-D scrambling conditions.

In the industrial Pt-Sn alloy based catalysts for selective dehydrogenation of light alkanes, Pt is the major active phase and Sn is added to mitigate the coke formation. Due to the breaking of the Pt ensembles and the electronic effect as electrons are transferred to Pt 5d band, the active sites for the cracking and hydrogenolysis are reduced[42–44]. In other studies, addition of a second metal such as Ga, In, Li, Na and K lead to lower acidity of the catalysts,

which results in lower coke formation[45–49]. This thesis reports a novel approach for the alkane dehydrogenation catalysis that the singe atom Pt active sites are formed in the surface of a relatively inert but highly selective metal (Cu). Thus, no active sites for side reactions exist in the first place. And this catalyst is proved to be stable in selective alkane dehydrogenation conditions. Moreover, the single-atom configuration allows the highest material efficiency of precious Pt metal compared to the nanoparticle configurations.

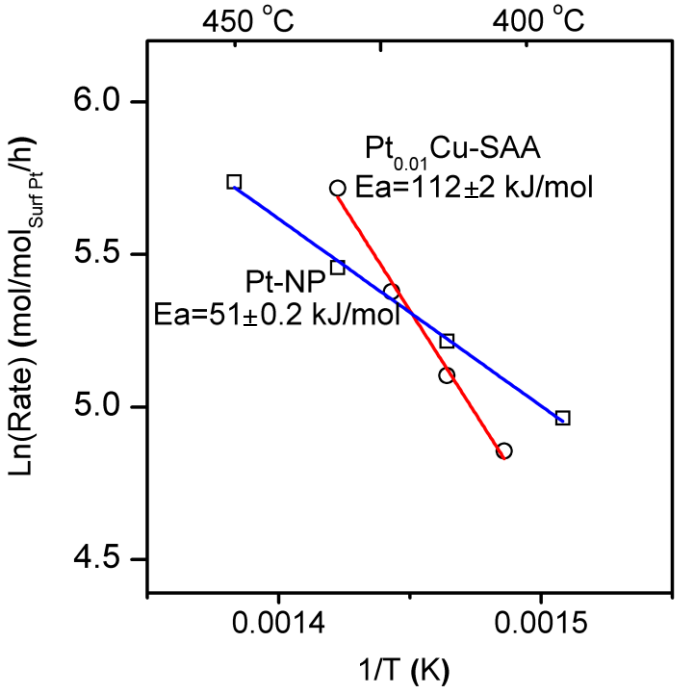

Figure 5.12. Arrhenius- type plot. The reaction rate of butane dehydrogenation was measured between 450 and 390 °C with conversion below 10%. Reaction condition: 2.5% butane, 5% H_2, bal. He. 50 mL/min, 30-80 mg sample.

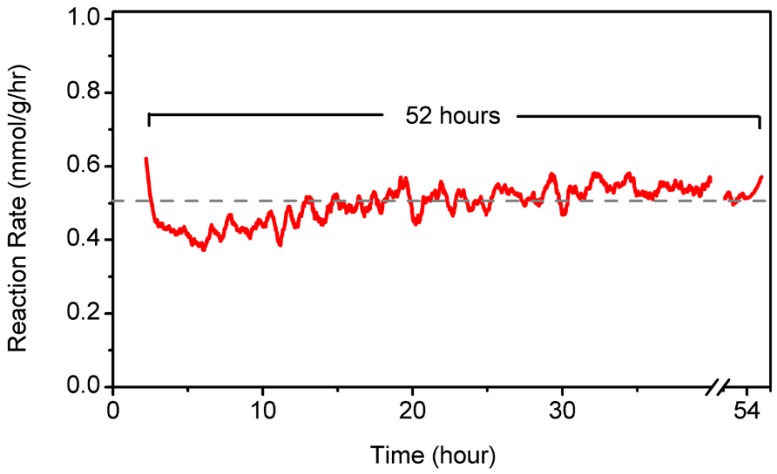

Figure 5.13. Long-term butane dehydrogenation reaction over $Pt_{0.01}Cu$-SAA catalyst. Reaction condition: 2.5% butane, 5% H_2, bal. He. 50 mL/min, 0.1 g catalyst, 400 °C.

The carbon deposition on spent Pt NP and PtCu SAA catalysts after long-hour butane dehydrogenation reactions was followed with TPO experiments, as shown in Figure 5.14. Significant CO_2 peaks were observed on Pt NP, revealing the carbon deposition. There are multiple CO_2 peaks in this TPO profile, at least one of them corresponding to the graphitic carbon. Different from Pt NP, PtCu SAA catalyst only shows minimal carbon deposition, which is essentially the same as that on the bare silica support. These results are in agreement with the stability tests shown in Figure 5.13. PtCu SAA catalyst is highly stable in butane dehydrogenation conditions without coke formation, while monometallic Pt catalyzes the coke formation. The two major mechanisms of the deactivation of Pt catalysts in alkane dehydrogenation reactions are carbon deposition and sintering of Pt nanoparticles. From TEM imaging, we found the particle size of Pt slightly increases from 1.8 to 2.1 nm after being used

in the reaction conditions. Thus, the instability of the monometallic Pt catalysts is mainly due to the carbon deposition.

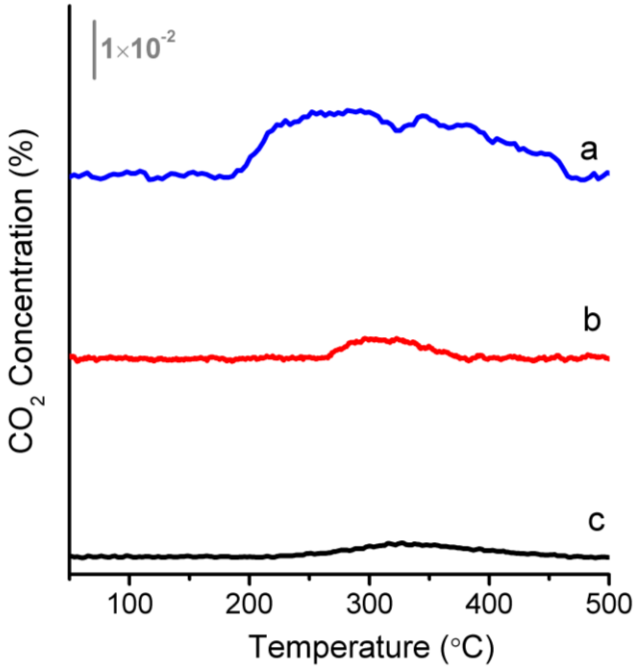

Figure 5.14. Comparing the degree of coking in Pt NP vs PtCu SAA catalysts. Temperature–programmed-oxidation (TPO) of used (a) Pt-NP, (b) $Pt_{0.01}Cu$-SAA and (c) silica. (a) and (b) are spent catalysts after butane dehydrogenation reaction. (a), (b) and (c) were treated in a He flow at 300 °C for 1 h before TPO to desorb the hydrocarbon adsorbates. TPO conditions: 10% O_2/N_2, 50 mL/min, 3 °C/min, 100 mg sample.

To investigate the sintering of PtCu SAA NPs in butane dehydrogenation condition, TEM images were taken for fresh $Pt_{0.01}Cu$-SAA samples reduced in H_2 and $Pt_{0.01}Cu$-SAA used in butane dehydrogenation at 400 °C for 52 hours. The particle size of $Pt_{0.01}Cu$-SAA does not

change, as shown in the TEM images and particle size distribution in Figure 5.15. This confirms the stability of PtCu SAA NPs in butane dehydrogenation conditions.

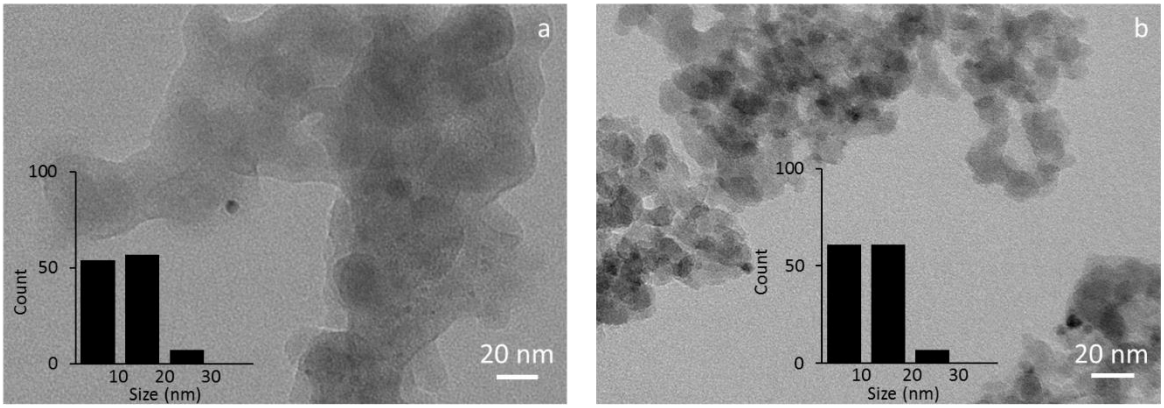

Figure 5.15. TEM images and particle size distribution (insets) of (a) fresh $Pt_{0.01}Cu$-SAA and (b) spent $Pt_{0.01}Cu$-SAA after butane dehydrogenation reaction at 400 °C.

Controlling coke formation is one of the most important considerations C-H bond activation catalysts. A well-known example is coke formation during methane steam reforming over nickel which requires costly regeneration processes to be used at industrial scales. In the same vein, the design of commercial dehydrogenation processes is often dominated by the need to control coke formation on the catalyst surface. The most popular dehydrogenation technology for light alkanes is UOP's Oleflex process which uses a supported Pt on Al_2O_3 catalyst. Here, a complex and high-cost continuous catalyst regeneration is used to burn off coke from the particles followed by treatment with chlorine gas to redisperse the Pt particles. Similarly, CB&I's Catofin process uses a series of fixed bed reactors containing a chromium oxide catalyst. These reactors must be regenerated after only a few minutes on stream in part

due to rapid coke deposition. Clearly, the development of coke resistant C-H bond activation catalysts based on single-atom alloys would have important practical implications for these industries.

Figures 5.16 and 5.17 show the FTIR spectra for used $Pt_{0.01}Cu$-SAA and $Pt_{0.03}Cu$-SAA catalysts, where we cannot find any linearly or bridge adsorbed CO on extended Pt surfaces. This confirms that Pt atoms remain isolated after long term B-D scrambling experiments. These results demonstrate the structural stability of PtCu SAA NPs under atmospheric pressure reaction conditions.

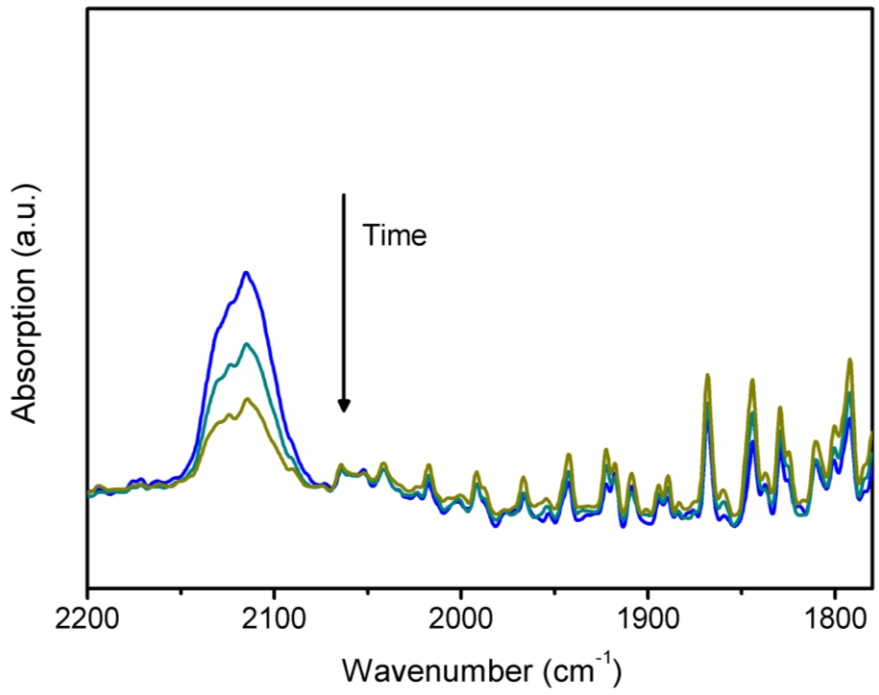

Figure 5.16. FTIR spectra of chemisorbed CO molecule on the used $Pt_{0.01}Cu$-SAA. The time values on the graph indicate the time of helium gas purge after CO exposure.

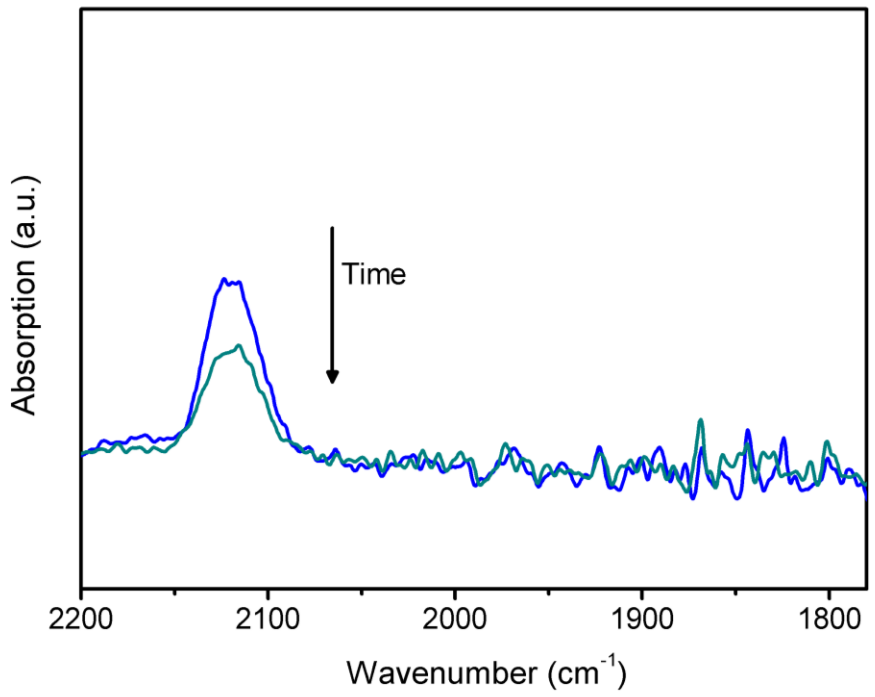

Figure 5.17. FTIR spectra of chemisorbed CO molecule on the used $Pt_{0.03}Cu$-SAA catalyst. The time values on the graph indicate the time of helium gas purge after CO exposure.

5.4 Collaboration: surface science and DFT studies on the C-H activation over PtCu SAA catalysts

The surface science studies on C-H activation over PtCu SAA catalysts were performed in the Sykes lab at Tufts. Methyl iodide (CH_3I) provides a simple method for adding methyl groups to the alloy surfaces and TPR studies of subsequent methane evolution allows us to examine C-H activation energetics. On Cu(111), methane and the larger hydrocarbons desorb at ~450 K. It has been previously demonstrated that the rate limiting step to form these products is the activation of C-H bonds in methyl groups to produce methylene and H_a.[50,51] On the 0.01ML PtCu(111) SAA surface, methane and carbon coupling products desorb at ~350 K, 100 K cooler than on the pure Cu(111) surface. Because the rate limiting step in methane evolution is C-H

activation, this 100 K temperature shift reveals that single Pt atoms in the Cu surface significantly lower the barrier to C-H activation in CH_3. The formation of ethene, ethane and propene implies the Pt-Cu SAA maintains the ability of Cu to avoid coking via C-C coupling. On 1ML Pt-Cu(111), the majority of methane desorbs at ~250 K, and hydrogen from methylene decomposition desorbs at high temperature.

DFT studies were performed at Stamatakis's Lab at University College London. DFT calculations find the strong binding of CHx intermediates to the Pt(111) surface compared to Cu(111) which explains the tendency for coke to form on Pt and the lack thereof on Cu. Interestingly, the Pt-Cu(111) SAA exhibits intermediate barrier heights compared to the two pure metals. Dehydrogenation of CH_x species on Pt-Cu(111) SAA and Cu(111) are endothermic, however the net pathway on Pt(111) is exothermic. These findings explain our experimental observations that the Pt-Cu(111) SAA may readily activate C-H bonds in adsorbed CH_3* while resisting coke formation.

5.5 Summary

The development of coke resistant C-H activation catalysts is an important but difficult task for the field of heterogeneous catalysis. Here we introduced a novel single-atom alloy (SAA) approach in designing Pt- based C-H activation catalysts. In this chapter, C-H activation was examined on PtCu SAAs using supported nanoparticle catalysts in a fixed-bed flow reactor at atmospheric pressure. Our catalytic studies with supported PtCu, Pt, and Cu NPs show that

PtCu-SAAs activate C-H bonds using the B-D scrambling reaction in butane. We find that the PtCu SAAs catalyze the exchange reaction at 250 °C compared to 550 °C on Cu NPs and are stable during the reaction. Pt NPs activate the reaction at temperatures as low as 100 °C, but quickly deactivate due to coking. Moreover, the PtCu SAA catalysts showed high stability and coke resistance in butane dehydrogenation reaction conditions. The PtCu SAA catalysts can stably convert butane to butene at 400 °C for at least 52 hours without any carbon deposition or sintering. The single-atom Pt sites are stable in the reaction condition as indicated by CO-IR and EXAFS results.

We find the C-H activation barrier in butane molecule follows the order of: Pt < PtCu SAA < Cu, which is in agreement with the surface science and DFT results of our collaborators. The apparent activation energy measured for the butane dehydrogenation reaction corroborates this trend. These findings illustrate that PtCu SAAs are promising catalysts for C-H bond activation in small alkane molecules at moderate temperatures and can be further developed as robust catalysts resistant to coking that plagues traditional Pt, Pd and Ni catalysts.

5.6 References

1. Sattler JJHB, Ruiz-Martinez J, Santillan-Jimenez E, Weckhuysen BM. Catalytic dehydrogenation of light alkanes on metals and metal oxides. *Chem Rev*. 2014;114:10613-10653. doi:10.1021/cr5002436.

2. Alper J. *The Changing Landscape of Hydrocarbon Feedstocks for Chemical Production: Implications for Catalysis: Proceedings of a Workshop*. The National Academies Press;

2016.

3. Shilov AE, Shul'pin GB. Activation of C-H bonds by metal complexes. *Chem Rev*. 1997;97:2879-2932.

4. Labinger JA, Bercaw JE. Understanding and exploiting C-H bond activation. *Nature*. 2002;417:507-514. doi:10.1038/417507a.

5. Wencel-Delord J, Glorius F. C–H bond activation enables the rapid construction and late-stage diversification of functional molecules. *Nat Chem*. 2013;5:369-375. doi:10.1038/nchem.1607.

6. Zhao Z-J, Chiu C, Gong J. Molecular Understandings on Heterogeneous Catalytic Dehydrogenation of Light Alkanes. *Chem Sci*. 2015;6:4403-4425. doi:10.1039/C5SC01227A.

7. Lin R, Amrute AP, Pérez-Ramírez J. Halogen-mediated conversion of hydrocarbons to commodities. *Chem Rev*. 2017;117:4182-4247. doi:10.1021/acs.chemrev.6b00551.

8. McFarland E. Unconventional chemistry for unconventional natural gas. *Science*. 2012;338:340-342. doi:10.1126/science.1226840.

9. Gärtner CA, van Veen AC, Lercher JA. Oxidative dehydrogenation of ethane: common principles and mechanistic aspects. *ChemCatChem*. 2013;5:3196-3217. doi:10.1002/cctc.201200966.

10. Schwarz H. Chemistry with methane: concepts rather than recipes. *Angew Chemie - Int Ed*. 2011;50:10096-10115. doi:10.1002/anie.201006424.

11. Guo X, Fang G, Li G, et al. Direct, Nonoxidative Conversion of Methane to Ethylene, Aromatics, and Hydrogen. *Science*. 2014;344:616-620.

12. Schweitzer NM, Hu B, Das U, et al. Propylene Hydrogenation and Propane Dehydrogenation by a Single-Site Zn2+ on Silica Catalyst. *ACS Catal*. 2014;4(4):1091-1098. doi:10.1021/cs401116p.

13. Taccardi N, Grabau M, Debuschewitz J, et al. Gallium-rich Pd-Ga phases as supported liquid metal catalysts. *Nat Chem*. 2017:1-6. doi:10.1038/nchem.2822.

14. Jiang F, Zeng L, Li S, Liu G, Wang S, Gong J. Propane Dehydrogenation over Pt/TiO2-Al2O3 Catalyst. *ACS Catal*. 2015;5:438-447. doi:10.1021/ie800848c.

15. Iglesias-Juez A, Beale AM, Maaijen K, Weng TC, Glatzel P, Weckhuysen BM. A combined in situ time-resolved UV-Vis, Raman and high-energy resolution X-ray absorption spectroscopy study on the deactivation behavior of Pt and PtSn propane dehydrogenation catalysts under industrial reaction conditions. *J Catal*. 2010;276:268-279. doi:10.1016/j.jcat.2010.09.018.

16. Henderson MA, Mitchell GE, White JM. The Chemisorption of Methyl Halides (Cl, Br, and I) on Pt(111). *Surf Sci*. 1987;184:L325-L331.

17. Yang F, Koeller J, Ackermann L. Photoinduced copper-catalyzed C-H arylation at room temperature. *Angew Chem Int Ed*. 2016;55:4759-4762. doi:10.1002/anie.201512027.

18. Besenbacher F, Chorkendorff I, Clausen BS, et al. Design of a Surface Alloy Catalyst for Steam Reforming. *Science*. 1998;279(5358):1913-1915.

doi:10.1126/science.279.5358.1913.

19. Rodriguez JA. Physical and Chemical Properties of Bimetallic Surfaces. *Surf Sci Rep*. 1996;24:223-287. doi:10.1016/0167-5729(96)00004-0.

20. Lucci FR, Marcinkowski MD, Lawton TJ, Sykes ECH. H 2 Activation and Spillover on Catalytically Relevant Pt–Cu Single Atom Alloys. *J Phys Chem C*. 2015;119:24351-24357. doi:10.1021/acs.jpcc.5b05562.

21. Lucci FR, Liu J, Marcinkowski MD, et al. Selective hydrogenation of 1,3-butadiene on platinum–copper alloys at the single-atom limit. *Nat Commun*. 2015;6:8550. doi:10.1038/ncomms9550.

22. Lucci FR, Lawton TJ, Pronschinske A, Sykes ECH. Atomic scale surface structure of Pt/Cu(111) surface alloys. *J Phys Chem C*. 2014;118:3015-3022.

23. Yang XF, Wang A, Qiao B, Li J, Liu J, Zhang T. Single-atom catalysts: a new frontier in heterogeneous catalysis. *Acc Chem Res*. 2013;46:1740-1748. doi:10.1021/ar300361m.

24. Thomas JM, Saghi Z, Gai PL. Can a Single Atom Serve as the Active Site in Some Heterogeneous Catalysts? *Top Catal*. 2011;54(10-12):588-594. doi:10.1007/s11244-011-9677-y.

25. Marcinkowski MD, Liu J, Murphy CJ, et al. Selective formic acid dehydrogenation on Pt-Cu single atom alloys. *ACS Catal*. 2016. doi:10.1021/acscatal.6b02772.

26. Liu J, Lucci FR, Yang M, et al. Tackling CO Poisoning with Single-Atom Alloy Catalysts. *J Am Chem Soc*. 2016;138(20):6396-6399. doi:10.1021/jacs.6b03339.

27. Boucher MB, Zugic B, Cladaras G, et al. Single atom alloy surface analogs in Pd0.18Cu15 nanoparticles for selective hydrogenation reactions. *Phys Chem Chem Phys*. 2013;15:12187-12196. doi:10.1039/c3cp51538a.

28. Greeley J, Gokhale AA, Kreuser J, et al. CO vibrational frequencies on methanol synthesis catalysts: a DFT study. *J Catal*. 2003;213(1):63-72. doi:10.1016/S0021-9517(02)00040-4.

29. Mondelli C, Ferri D, Grunwaldt J-D, Ravasio N, Baiker A. Redox properties of supported copper catalysts studied in liquid and gas phase by in situ ATR-IR and XAS. *Catal Today*. 2011;178(1):124-131. doi:10.1016/j.cattod.2011.08.043.

30. Nishiyama H, Inoue Y. IRAS study of surface acoustic wave effects on CO adsorbed on Cu surfaces. *Surf Sci*. 2005;594(1-3):156-162. doi:10.1016/j.susc.2005.07.021.

31. Oxford SM, Lee PL, Chupas PJ, Chapman KW, Kung MC, Kung HH. Study of Supported PtCu and PdAu Bimetallic Nanoparticles Using In-Situ X-ray Tools. *J Phys Chem C*. 2010;114(40):17085-17091. doi:10.1021/jp103675n.

32. Qiao B, Wang A, Yang X, et al. Single-atom catalysis of CO oxidation using Pt1/FeOx. *Nat Chem*. 2011;3(8):634-641. doi:10.1038/nchem.1095.

33. Chandler B. DRIFTS studies of carbon monoxide coverage on highly dispersed bimetallic Pt-Cu and Pt-Au catalysts. *Catal Today*. 2001;65(1):39-50. doi:10.1016/S0920-5861(00)00543-5.

34. Ferri D, Bürgi T, Baiker A. Pt and Pt/Al2O3 Thin Films for Investigation of Catalytic Solid−Liquid Interfaces by ATR-IR Spectroscopy: CO Adsorption, H2 -Induced

Reconstruction and Surface-Enhanced Absorption. *J Phys Chem B*. 2001;105(16):3187-3195. doi:10.1021/jp002268i.

35. Bazin P, Saur O, Lavalley JC, Daturi M, Blanchard G. FT-IR study of CO adsorption on Pt/CeO2: characterisation and structural rearrangement of small Pt particles. *Phys Chem Chem Phys*. 2005;7(1):187. doi:10.1039/b414159h.

36. Wimble J. Single atom alloy catalysts for C-H bond activation and propane dehydrogenation. 2017.

37. Marcinkowski MD, Darby MT, Liu J, et al. Pt/Cu single-atom alloys as coke-resistant catalysts for efficient C–H activation. *Nat Chem*. 2018;10(3):325-332. doi:10.1038/nchem.2915.

38. Deng W, Flytzani-Stephanopoulos M. On the Issue of the Deactivation of Au–Ceria and Pt–Ceria Water–Gas Shift Catalysts in Practical Fuel-Cell Applications. *Angew Chemie*. 2006;118(14):2343-2347. doi:10.1002/ange.200503220.

39. Yang M, Liu J, Lee S, et al. A common single-site Pt(II)-O(OH)x- species stabilized by sodium on “active” and “inert” supports catalyzes the water-gas shift reaction. *J Am Chem Soc*. 2015;137(10):3470-3473. doi:10.1021/ja513292k.

40. Yang M, Li S, Wang Y, et al. Catalytically active Au-O(OH)x-species stabilized by alkali ions on zeolites and mesoporous oxides. *Science*. 2014;(346):1498-1501.

41. Lucci FR, Liu J, Marcinkowski MD, et al. Selective hydrogenation of 1,3-butadiene on platinum – copper alloys at the single-atom limit. *Nat Commun*. 2015;6:8550.

doi:10.1038/ncomms9550.

42. Nagaraja BM, Shin C-H, Jung K-D. Selective and stable bimetallic PtSn/θ-Al2O3 catalyst for dehydrogenation of n-butane to n-butenes. *Appl Catal A Gen*. 2013;467:211-223. doi:10.1016/j.apcata.2013.07.022.

43. Cortright RD, Hill JM, Dumesic JA. Selective dehydrogenation of isobutane over supported Pt/Sn catalysts. *Catal Today*. 2000;55(3):213-223. doi:10.1016/S0920-5861(99)00249-7.

44. Wu J, Peng Z, Bell AT. Effects of composition and metal particle size on ethane dehydrogenation over PtxSn100−x/Mg(Al)O (70⩽x⩽100). *J Catal*. 2014;311:161-168. doi:10.1016/j.jcat.2013.11.017.

45. Zhang Y, Zhou Y, Shi J, et al. Comparative study of bimetallic Pt-Sn catalysts supported on different supports for propane dehydrogenation. *J Mol Catal A Chem*. 2014;381:138-147. doi:10.1016/j.molcata.2013.10.007.

46. Silvestre-Albero J, Serrano-Ruiz JC, Sepúlveda-Escribano A, Rodríguez-Reinoso F. Modification of the catalytic behaviour of platinum by zinc in crotonaldehyde hydrogenation and iso-butane dehydrogenation. *Appl Catal A Gen*. 2005;292:244-251. doi:10.1016/j.apcata.2005.06.005.

47. Vu BK, Song MB, Ahn IY, et al. Pt–Sn alloy phases and coke mobility over Pt–Sn/Al2O3 and Pt–Sn/ZnAl2O4 catalysts for propane dehydrogenation. *Appl Catal A Gen*. 2011;400(1-2):25-33. doi:10.1016/j.apcata.2011.03.057.

48. Casella ML, Siri GJ, Santori GF, Ferretti OA, Ramírez-Corredores MM. Surface Characterization of Li-Modified Platinum/Tin Catalysts for Isobutane Dehydrogenation. *Langmuir*. 2000;16(13):5639-5643. doi:10.1021/la991437r.

49. Siri GJ, Bertolini GR, Casella ML, Ferretti OA. PtSn/γ-Al2O3 isobutane dehydrogenation catalysts: The effect of alkaline metals addition. *Mater Lett*. 2005;59(18):2319-2324. doi:10.1016/j.matlet.2005.03.013.

50. Chiang C-M, Wentzlaff TH, Bent BE. Iodomethane Decomposition on Cu(110): Surface Reactions of C1 Fragments. *J Phys Chem*. 1992;96:1836-1848.

51. Azizian S, Gobal F. Mechanism of catalytic decomposition of CH3I on the Cu(111) surface: a UBI-QEP approach. *Langmuir*. 2000;16:8095-8099. doi:10.1021/la0003847.

Chapter 6. PdAu single-atom alloy catalysts for selective hydrogenation of 1-hexyne to 1-hexene

6.1 Introduction

Selective hydrogenations of both double and triple carbon-carbon bonds are important for a wide range of industrial processes. Pd, Pt, Ni, and Ru based systems are commonly employed for hydrogenation of alkenes and alkynes due to their high catalytic activity. While these catalysts are highly active, they may not always be selective to the desired products. Among these metals, Pd is the most selective but typically exhibits a decrease in alkene selectivity with alkyne conversion. Therefore, Pd catalysts are commonly used with promoters to improve alkene selectivity; transition metals such as Ag, Rh, Au, Cu, Zn, Cr, and V have been reported to improve selectivity.[1] Another approach to combat this problem is to design catalysts that contain only the Pd ensembles necessary to perform or to assist the reaction of interest.

Individual, isolated Pd atoms in the Cu surfaces, termed single-atom alloys (SAAs), act as sites for hydrogen adsorption, dissociation and spillover onto the otherwise inert Cu surface. The weak binding of the H atom intermediates offered by Cu(111) led to the selective hydrogenation of both styrene and acetylene, as demonstrated by a combination of scanning tunneling microscopy (STM) and temperature programmed desorption/reaction (TPD/R) experiments under UHV conditions.[2] Recently the SAA strategy was applied to the preparation of PdCu alloy nanoparticles (NPs) which are

active for the hydrogenation of phenylacetylene to styrene at ambient temperature with 94% selectivity at all conversions.[3] NP catalysts were prepared by depositing small amounts of Pd into the surface of pre-formed Cu NPs by the galvanic replacement (GR) reaction.

Furthermore, over the last few years, several studies of single Pd atoms stabilized in different matrices for selective hydrogenation reactions have been reported.[4–6] Liu et al. showed single-atom Pd dispersed on ethylene glycolate-stabilized TiO_2 nanosheets are highly active for the hydrogenation of alkenes and aldehydes.[4] Yan et al. showed that atomically dispersed Pd on graphene is selective for the partial hydrogenation of 1,3-butadiene.[5] Vilé et al. reported that single Pd atoms anchored into the cavities of graphitic carbon nitride (g-C_3N_4) have high activity and selectivity for the partial hydrogenation of 1-hexyne.[6,7] Yan et al. attributed the high selectivity to a steric effect induced by the high packing density at the single-atom Pd sites compared to the extended Pd surfaces.[5] Through DFT calculations, Vilé et al. concluded that the weak adsorption of products and the electron deficiency at Pd sites contribute to the high selectivity.[6]

In this chapter, single Pd atoms were incorporated in gold surfaces, and the resulting Pd_1Au SAAs were evaluated for the selective hydrogenation of alkynes, specifically the hydrogenation of 1-hexyne to 1-hexene. Bimetallic PdAu materials of various compositions have been studied extensively for a number of reactions, including selective oxidation[8–11], selective hydrogenation[12–19], the Ullmann reaction[20], vinyl acetate synthesis[21], formic acid decomposition[22], and the direct synthesis of hydrogen peroxide[23–25]. Generally, it is difficult to

elucidate the roles of Pd and Au in the catalytic cycles and their alloying effects due to the presence of many Pd and Au ensembles on the catalyst surfaces. In a few reports, the effect of preparing isolated Pd or Au atoms in the bimetallic PdAu catalysts has been attributed to providing exceptional activity or selectivity because of the unique chemistry of single-atom sites, which also allows for more conclusive mechanistic studies.[8,21,26–28] Pioneering work from the Goodman[21] and Toshima[29] groups has identified Pd or Au single- atom active sites in vinyl acetate synthesis and glucose oxidation, respectively, on catalytic surfaces with well-defined single Pd or Au atom structures. The Mullins group has demonstrated that the PdAu alloy surfaces catalyse the dehydrogenation of formic acid while the extended Pd surfaces catalyse the dehydration of formic acid.[22] Through careful bimetallic nanoparticle synthesis with modified impregnation methodology, Luo et al. prepared Au-Pd random alloy nanoparticles with homogeneous structures and demonstrated the enhancement of hydrogenation activity by the alloying effect.[30]

The selective hydrogenation reactions of alkynes to alkenes are important processes for the production of high purity alkene feedstocks for the polymer industry. Pd is widely used for hydrogenation due to its low hydrogenation activation barrier.[1] While Au NP catalysts are highly selective for partial hydrogenation of alkynes, they are rarely used for these reactions due to the low intrinsic activity of Au.[31] Some studies have used Au as an additive to improve the selectivity of Pd catalysts for partial hydrogenation reactions, while Pd is still the bulk catalyst phase.[12,13,15,17,18,32] Recent work by the Louis and Zhang groups has evaluated various Pd ensembles from clusters to single atoms and suggested that the selectivity increases with the dispersion of Pd in PdAu alloys.[33,34] However, these reports fall short of elucidating the

specific roles of Pd and Au in selective hydrogenation of alkadienes[33] and alkynes[34] and have only investigated the hydrogenation reactions in the gas phase.

In this work, we demonstrate that PdAu SAAs are both active and highly selective for the partial hydrogenation of 1-hexyne in the liquid phase, and attribute these properties to the unique structure of PdAu SAAs.

6.2 Experimental methods

6.2.1 Catalyst Synthesis

PdAu-SAA NPs were prepared using sequential reduction methods as reported in Tedsree et al. with some modifications.[35] First, Au NPs were prepared as follows: 0.3 g $HAuCl_4 \cdot 3H_2O$ and 1.2 g poly(vinylpyrrolidinone) (PVP, MW= 58,000) were mixed in 50 mL ethylene glycol (EG) in a round bottom flask with vigorous stirring. The solution was purged with N_2 for one hour before 0.3 g $NaHCO_3$ was added. The solution was then heated to 90 °C at 5 °C/min with N_2 flowing through the round bottom flask. The solution was held at 90 °C for half an hour before cooling to ambient temperature. The Au NPs were thus obtained. To prepare PdAu-SAA NPs, the desired amount of $Pd(NO_3)_2 \cdot xH_2O$ was dissolved in 1 mL EG and added to the round bottom flask containing the EG-dispersed Au NPs. Under N_2 purge and vigorous stirring, the solution was heated to 90 °C at 5 °C/min and held for 8 h. After the solution was cooled to ambient temperature, 300 mL of acetone was added in order to precipitate the NPs. The acetone-EG solution was centrifuged at 3000 rpm for 10 minutes to separate the NPs. The retrieved NPs were then washed with ethanol and hexane thrice and dried in vacuum overnight. To obtain silica supported Au and PdAu NPs, fumed silica (heat treated in air at

650 °C for 3 h) was introduced into the NP gold and PdAu-SAA solutions in water and stirred overnight. The slurry carrying the supported NPs was centrifuged and dried in vacuum for 24 h then calcined in air at 300 °C. The unsupported Pd-NPs were prepared by the same method with $Pd(NO_3)_2$ precursor.

Pd/C is provided by Sigma-Aldrich (St. Louis, MO). It is 10 wt% Pd on activated carbon support (surface area: 933 m^2/g, pore size: 150-200 Å, pore volume 0.92 ml/g). Pyridine-IR shows peaks at 1588, 1575, 1446 and 1438 cm^{-1}, which suggests Lewis acid sites[36,37]. All peaks disappeared after degassing at room temperature for 60 minutes. The Lewis acid sites are relatively weak.

6.2.2 Catalyst characterization

The NPs were digested with concentrated HCl and H_2O_2 to prepare the samples for inductively coupled plasma atomic emission spectroscopy (ICP-AES) with a Leeman Labs PS1000 instrument. High-resolution transmission electron microscopy (HR-TEM) was conducted on a JEOL 2010 electron microscope with 200 kV and 107 μA beam emission. The samples were obtained by drop casting of the ethanol solution of NPs on carbon film over a copper microgrid.

X-ray photoelectron spectra (XPS) were obtained on a Thermo Scientific K-Alpha system equipped with an Al source and a double focusing hemispherical analyser with a 128-channel detector at a pass energy of 50 eV.

X-ray powder diffraction (XRD) tests were performed on a PANalytical X'Pert Pro instrument. Cu Kα radiation was used as the X-ray source. Data was collected for 2θ between 30° and 70°.

Infrared (IR) spectroscopy was performed in both attenuated total reflection (ATR) and diffuse reflectance infrared Fourier transform spectroscopy (DRIFTS) modes on a Thermo Nicolet iS50 FT-IR.

6.2.3 H_2-D_2 exchange

To measure the hydrogen activation activity of the catalysts, H_2-D_2 exchange reaction was conducted in a packed-bed flow microreactor (L=22inch, O.D.=1/2 inch). The samples were treated in 20% H_2 at 150 °C for 5 minutes prior to the H_2-D_2 exchange experiments. A gas mixture of 10% H_2, 10% D_2 and bal. Ar was introduced to the reactor at a total flow rate of 50 mL/min at ambient temperature. After flowing the gas mixture for 15 minutes, the temperature was raised to desired temperature at 5 °C/min. The gas composition was analysed by a mass-spectrometer.

6.2.4 Partial hydrogenation of 1-hexyne

A stainless-steel Parr reactor was used for the hydrogenation of 1-hexyne. The desired amount of sample was added to 20-80 mL ethanol. The mixture was stirred for half an hour and sonicated for 15 minutes before being loaded into the reactor. Pure hydrogen was bubbled through the solution while stirring for 1 h. 1-hexyne was injected into the solution to reach 1% vol/vol concentration in ethanol. The reactor was then pressurized with pure hydrogen to the desired pressure (5 bar) under stirring at 600 rpm. Liquid-phase specimens were taken from the reactor at different time points.

6.3 Results and discussion

NP preparation and characterization

Table 6.1. NP sample properties

Sample ID	Composition	Pd species
PdAu-SAA	0.4 at.% Pd, 99.6 at.% Au	Single atoms
PdAu-SAA/SiO_2	0.008 wt. % Pd, 3.8 wt. % Au / SiO_2	Single atoms
Pd/C	10 wt. % Pd / C	NPs*
Au/SiO_2	3.8 wt. % Au / SiO_2	--

* Dispersion of Pd is 26%. (Determined by CO chemisorption)

To study the catalytic performance of PdAu SAAs in ambient pressure reaction conditions, we prepared PdAu SAA NPs and other samples, as listed in table 6.1. We followed the sequential reduction (SR) method in ethylene glycol to prepare the PdAu SAA NPs. As reported in the literature, the SR methods are effective in forming core-shell nanoparticles.[35,38] In order to prepare PdAu SAAs, a small amount of Pd species was added onto the pre-formed Au NPs. The Pd to Au atomic ratio was 1/250 as determined by ICP-AES. Pd and Au metals are miscible and their negative mixing enthalpy drives the Pd atoms to disperse well in the surface of the Au NPs.[39] Therefore, at low Pd loadings,

Au NPs with isolated Pd atoms can be formed. The PdAu-SAA NPs were prepared in unsupported form, then a portion of the sample was deposited on silica followed by calcination. The silica-supported samples are denoted as PdAu-SAA/SiO_2.

The ethanol solution of PdAu-SAA NPs exhibited the typical deep red colour of Au NPs (Figure 6.1a). Figures 6.1 (b, d) show TEM micrographs of the as-synthesized PdAu-SAA NPs. The NPs have well defined shapes indicating crystalline structures. Figure 1c shows the particle size distribution with an average particle size of 7.6±1.9 nm. In the zoom-in TEM image (Figure 6.1d), Au(111) lattice spacing of 0.23nm was found. These results confirm the formation of Au NPs and the dilute distribution of Pd atoms within them.

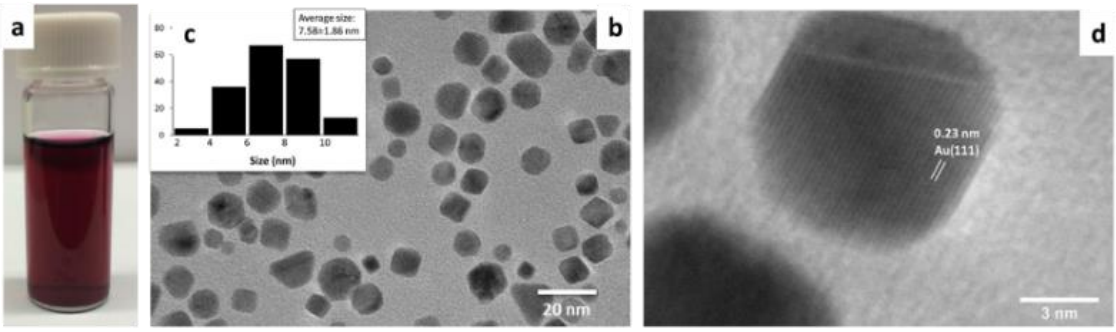

Figure 6.1. (a) Photograph of PdAu-SAA NP solution. (b, d) TEM images and (c) particle size distribution of PdAu-SAA NPs.

The XRD results (Figure 6.2) corroborate the TEM observations. Peaks at 2θ of 38, 45 and 65 degrees indicate only Au diffraction patterns, in agreement with the TEM results. The average crystallite size is 7.6 nm as determined by the band broadening of

the Au(111) and (200) peaks which is very close to the NP diameter found in the TEM measurements.

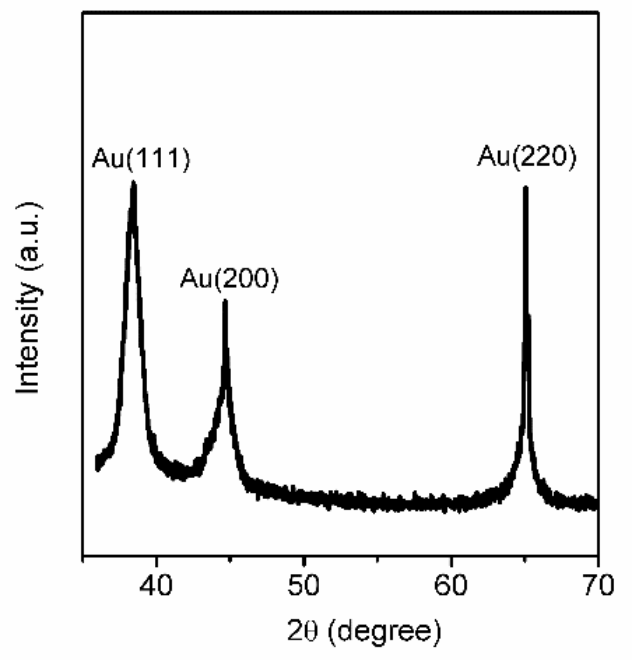

Figure 6.2. Powder XRD of PdAu-SAA/SiO_2.

We performed EDS elemental mapping on PdAu SAAs to characterize the distribution of Pd and Au in the catalysts. As shown in Figure 6.3, EDS elemental mapping over a large area of the sample does not show any monometallic Pd nanoparticles. Pd is in the Au area in all cases. This demonstrates that truly bimetallic PdAu NPs are formed.

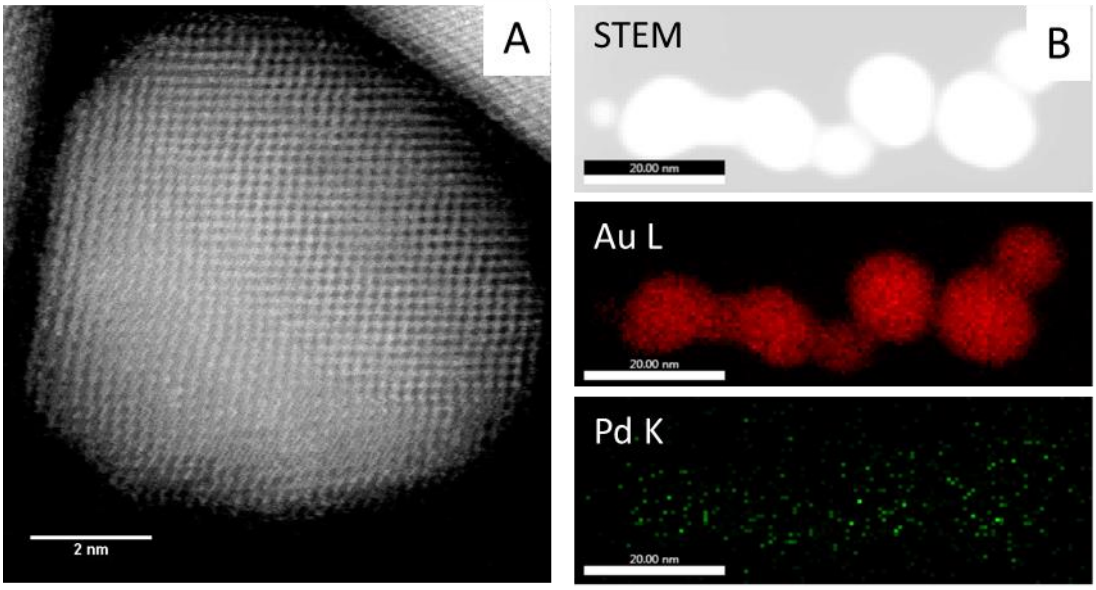

Figure 6.3. Dark field STEM image and Au and Pd EDS maps of PdAu-SAA.

XRD analysis of samples of different Pd/Au ratios were performed. As shown in Figure 6.4, the peaks of $PdAu_3$ and Au phases are very close. We did not observe any $AuPd_3$ or Pd phases in these samples. XRD shows that there are no monometallic Pd nanoparticles, which confirms the effectiveness to form bimetallic nanoparticles by this preparation method. However, XRD alone cannot prove the formation of PdAu alloy phases due to the very close 2θ of $PdAu_3$ and Au peaks.

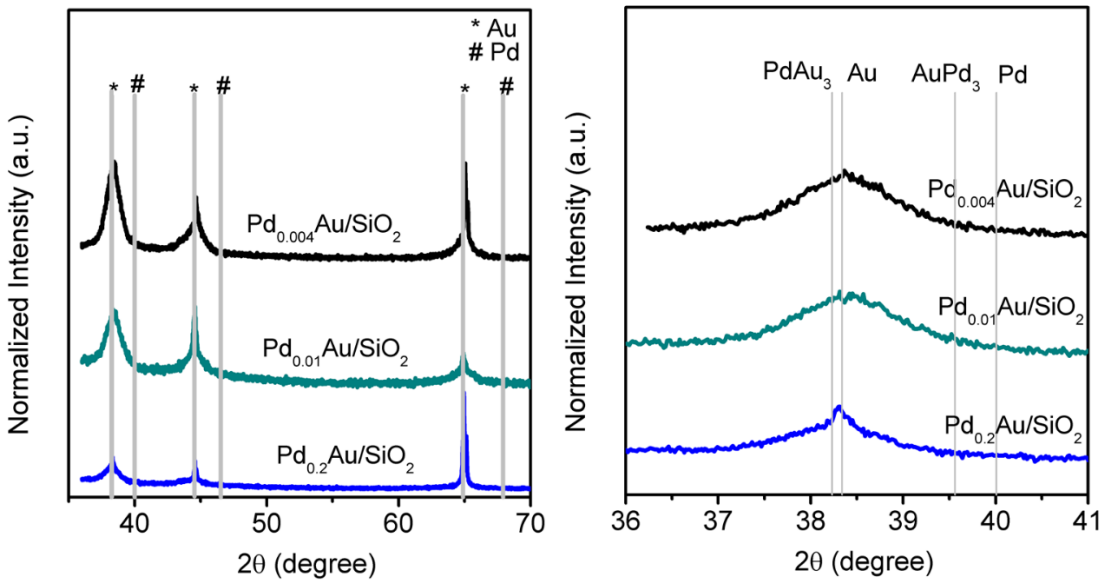

Figure 6.4. Powder XRD of PdAu samples with different Pd/Au ratios.

EDS and XRD confirm the formation of PdAu bimetallic NPs, which also demonstrate the effectiveness of the SR method in preparation of bimetallic NPs. SR method has been applied in the preparation of core-shell structure NPs[38,40], this is the first time it is applied in the preparation of PdAu SAA NPs.

In order to probe the atomic geometry of the Pd ensembles in the surface of the Au NPs we performed CO-IR experiments in the ATR-IR cell with CO in the gas phase.[41,42] Figure 6.5 shows the IR spectra of the carbonyl region for Pd-NP, PdAu-SAA and Au-NP samples. Atop CO on Au and Pd sites was observed at 2099 and 2015 cm^{-1}, respectively, while the stretch frequency at 1935-1920 cm^{-1} corresponds to bridged CO on the extended Pd surfaces.[33,43,44] However, no bridged CO was detected on PdAu-SAAs, which confirms that the Pd atoms are isolated from one another in the surface of the gold NPs. Only

linearly adsorbed CO (atop) on the Au and Pd atoms was found on the SAA samples.[33,45] These results provide strong evidence that the Pd atoms are fully isolated in the surface of PdAu-SAA NPs.

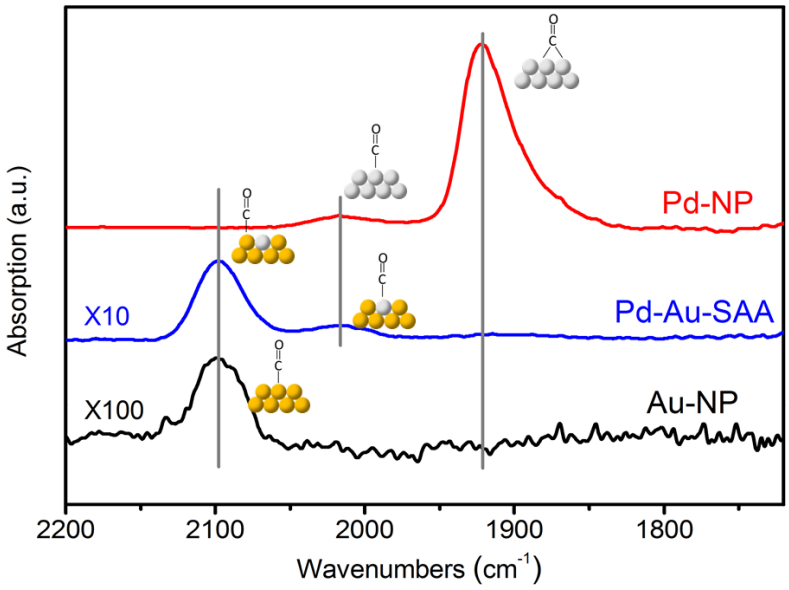

Figure 6.5. ATR-IR spectra of the CO stretch on Pd-NP, Au-NP and PdAu-SAA samples. Spectra were collected at 30 °C with pure CO flowing in the gas phase for Au-NP and PdAu-SAA. The spectra for Pd-NP were collected in H_2/He (20%) gas after CO adsorption.

Catalytic reaction studies

The catalytic performance of PdAu-SAA catalysts for the partial hydrogenation of 1-hexyne was studied in a batch reactor.

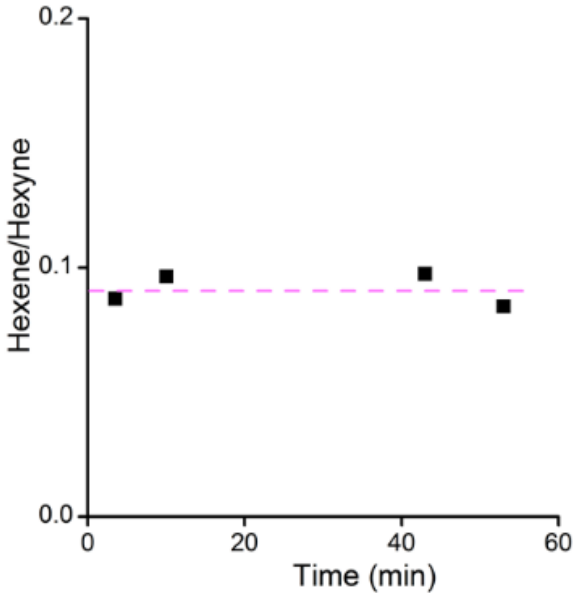

Figure 6.6. Leaching test: 1-hexene/1-hexyne ratio as a function of time. The liquid phase was separated from the reaction mixture after 6-hour reaction. Fresh 1-hexyne was injected and the typical hydrogenation reaction conditions used in this work were applied. (5 bar H_2, 600 rpm, 25 ^oC) The 1-hexene/1-hexyne ratio is plotted here. No conversion of 1-hexyne was observed.

It is clear from Figure 6.6 that the liquid phase of the reaction mixture is not active for hydrogenation of 1-hexyne. In this experiment, the catalyst was filtered out of the solution after 6-hour reaction in the batch reactor. 1-hexyne was re-introduced into the solution but was not converted under the hydrogenation reaction condition, as indicated by the constant 1-hexene/1-hexyne ratio over the course of 60 minutes. Therefore, the PdAu-SAA system is a truly heterogeneous hydrogenation reaction catalyst.

Figure 6.7 shows time-resolved batch reactor data for PdAu-SAA/SiO_2 and Pd/C catalysts at ambient temperature. PdAu-SAA is highly selective in the hydrogenation of 1-hexyne to 1-hexene as the product distribution consists over 85% hexenes (96% 1-hexene and 4% 2-hexene isomers) at full conversion of 1-hexyne. Isomers of 1-hexenes were formed, but less than 4% over the course of the hydrogenation reaction. Similar observations that a small amount of 2-hexene isomers can be formed in the hydrogenation of 1-hexyne have been reported on various supported Pd catalysts.[46–48] By comparison, the monometallic Pd catalysts (10 wt. % Pd on carbon) have less than 10% selectivity to hexenes because they convert most of the 1-hexyne to n-hexane at 100% conversion. This is in agreement with previous reports that monometallic Pd catalysts over-hydrogenate alkynes to undesired alkanes, while single Pd atom catalysts have high selectivity for partial hydrogenation reactions.[3,33]

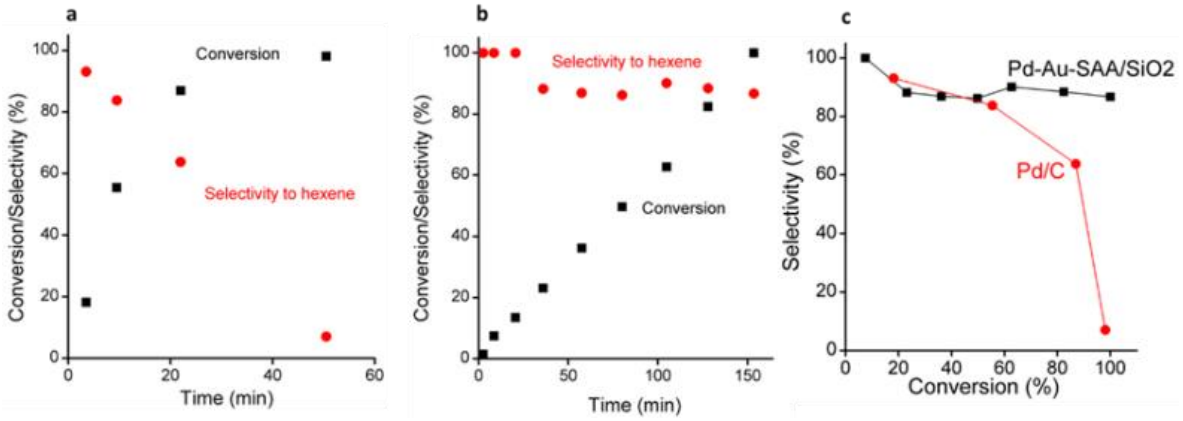

Figure 6.7. Time-resolved batch reactor data for the hydrogenation of 1-hexyne over (a) 10 wt% Pd/C catalysts and (b) PdAu-SAA/SiO_2 catalysts. (c) selectivity to 1-hexene as a function of

conversion. Reaction condition: 1% hexyne-ethanol solution, 5 bar H_2, 600 rpm, 25 ^oC. Same 1-hexyne/Pd ratio was used for hydrogenation reaction with 10wt% Pd/C and PdAu-SAA/SiO_2.

We have demonstrated in prior work that PdCu and PtCu SAAs are highly selective for the partial hydrogenation of alkynes and dienes.[3,49,50] A bifunctional mechanism was verified for those catalysts in which hydrogen is activated at the single Pt atom sites and hydrogen atoms spill over to the copper surface where they are weakly bound and participate in the selective hydrogenation reactions.[2,49] Surface science investigations have found that single Pd atoms facilitate molecular hydrogen dissociation on the otherwise inert Au(111) surface, however, hydrogen spillover from Pd to Au is unfavourable due to weak H-Au binding.[39,51]

The high selectivity of Au catalysts was preserved in PdAu SAA NPs for the partial hydrogenation of alkynes. We propose this is due to the weak adsorption of alkenes on PdAu SAAs as metallic Au is well-known to bind hydrocarbon molecules weakly. However, Pd surfaces strongly bind alkenes and their desorption barrier is higher than their hydrogenation reaction barrier which leads to low selectivity for partial hydrogenation.[52,53] Alloying Pd with Au leads to modification of the electronic structure of Pd atoms: the s and p electron density moves toward Au while d electron density moves toward Pd. So the d band center is shifted away from the Fermi level and the adsorption strength of adsorbates on Pd is weakened.[26,54,55] These electronic effects,

coupled with the ensemble effects that no extended Pd ensembles are present in the surface give exclusively weak adsorption sites.

The reaction rate per surface Pd atom on PdAu-SAA/SiO_2 is lower than that of the monometallic Pd catalysts (Figure 6.8). This might be due to the ligand effects by alloying with Au.

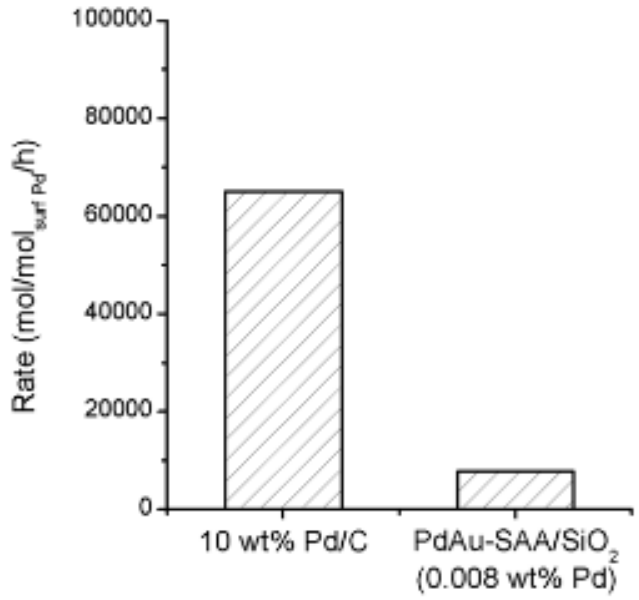

Figure 6.8. Initial reaction rate of hydrogenation of 1-hexyne normalized by amount of surface Pd. (Batch reactor, 1% 1-hexyne-ethanol solution, 5 Bar H_2, 600 rpm, 25 ^oC)

In batch reactor studies, a reaction rate of 3 x 10^4 $mol_{1\text{-hexene}}/mol_{Pd}/h$ was measured at 70 °C and 5 bar H_2 with PdAu-SAA/SiO_2, while the high selectivity to 1-hexene was maintained (Figure 6.9). Vilé et al. tested Pd/mpg-C_3N_4 catalyst under the

same temperature and H_2 pressure in a continuous-flow three-phase reactor and found lower normalized reaction rate (~ 1.5 x 10^3 $mol_{1\text{-hexene}}/mol_{Pd}/h$) but similar selectivity.[56]

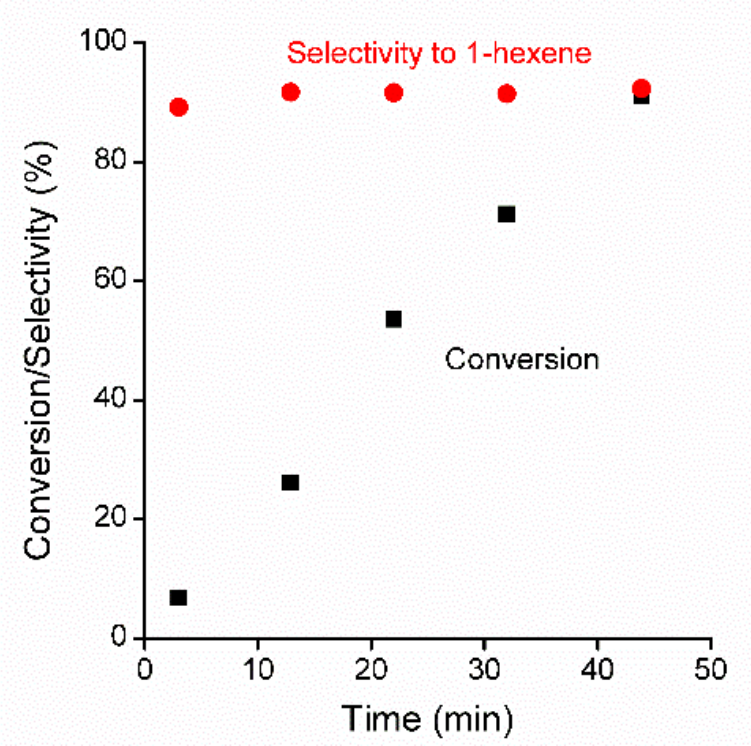

Figure 6.9. Time- resolved batch reactor data of partial hydrogenation of 1-hexyne to hexene over PdAu-SAA/SiO_2 catalysts. 1% hexyne-ethanol solution, 5 bar H_2, 600 rpm, 70 ^oC.

Stability test

The activity of the PdAu-SAA/SiO_2 catalysts is stable at the reaction conditions applied. As shown in Figure 6.10, no decrease of the hydrogenation rate was observed during 3 cycles of 1-hexyne hydrogenation reactions. The high stability of SAA catalysts has been demonstrated in gas phase hydrogenation and dehydrogenation

reactions.[49,57–59] However, this is the first report showing good stability of SAA NPs in liquid phase hydrogenation reactions.

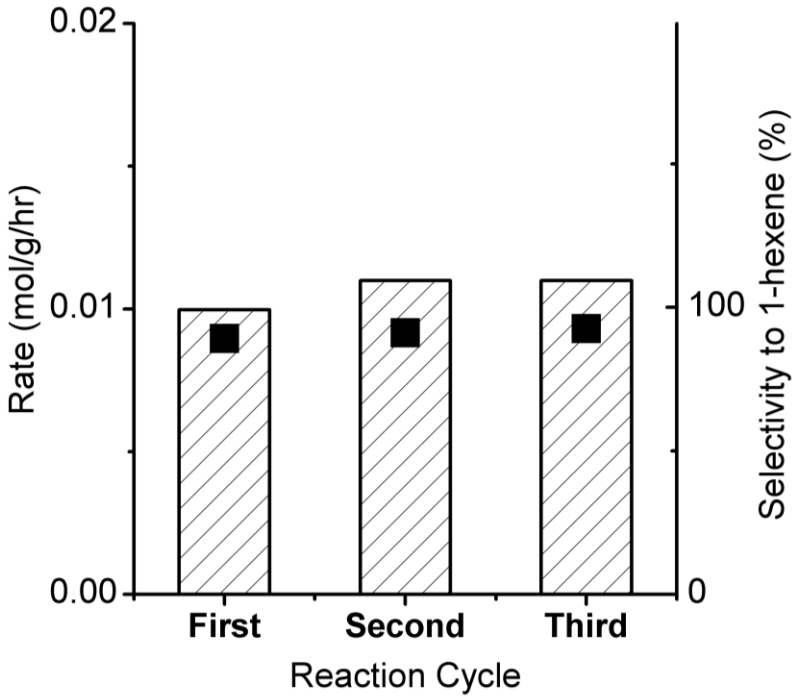

Figure 6.10. Stability test for PdAu-SAA/SiO_2 catalyst. The reaction rate of hydrogenation of 1-hexyne (bars) and selectivity to 1-hexene at 50% conversion (squares) was compared between the first, second and third cycles. (Batch reactor, 1% Hexyne-ethanol solution, 5 bar H_2, 600 rpm, 25 ^oC. ~3h each cycle)

Characterization of used catalysts

We characterized the spent catalysts to examine the stability of the single-atom alloy structure. TEM images of used PdAu-SAA NPs show crystalline samples with an average particle size of 8.3 ±2.0 nm with narrow size distribution (Figure 6.12). The minor increase of the average gold particle size in the used catalyst indicates the PdAu-SAA NPs are stable in the reaction conditions with respect to sintering.

XRD of the used PdAu-SAA/SiO_2 catalysts shows diffraction peaks at 38, 44 and 65 degrees that correspond to metallic Au (Figure 6.13a). The peak intensity of Au(111) is same as that of fresh catalysts, no peak shift was observed compared to the fresh catalysts. Moreover, ICP-AES of the spent catalysts found no change in the elemental catalyst composition.

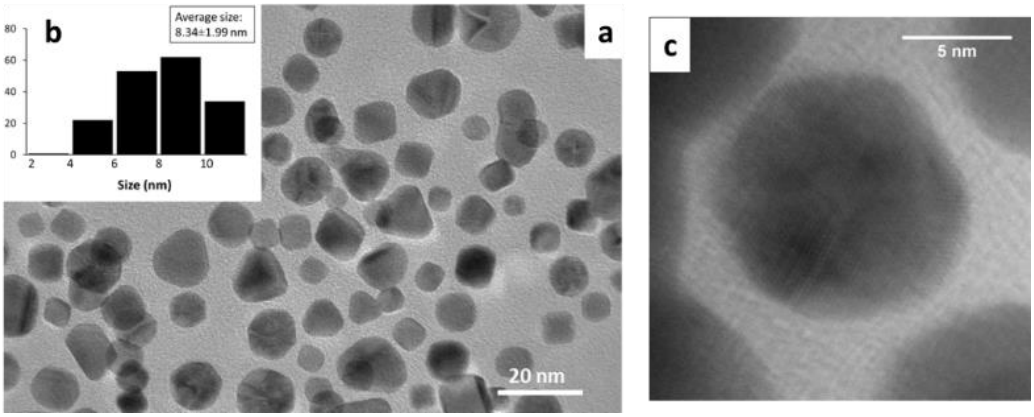

Figure 6.11. (a, c) TEM image and (b) particle size distribution of used PdAu-SAA NPs.

CO-IR for the spent PdAu-SAA NPs shows exclusively atop CO on Pd and Au sites but no bridging CO at lower wavenumbers, which confirms the stability of the single Pd atom sites (Figure 6.12c). XPS of spent PdAu-SAA exhibits an Au $4f_{7/2}$ peak at 83.4 eV

(binding energy) corresponding to metallic Au (Figure 6.12b). This is in agreement with the reported values of Au 4f peaks in bimetallic PdAu NPs.[60] There is indeed a slight negative shift of the binding energy compared to the $4f_{7/2}$ of metallic Au (84 eV). This may be due to the charge transfer between Pd and Au. We were not able to obtain definitive XPS spectra for Pd as the Pd 3d peak overlaps with Au $4d_{5/2}$ and Pd 3p intensity is lower than the detection limit of the instrument. Overall, the characterization of the spent catalysts demonstrates the structural and compositional stability of the PdAu-SAA NPs in hydrogenation reaction conditions, which explains the stability observed in the reaction tests.

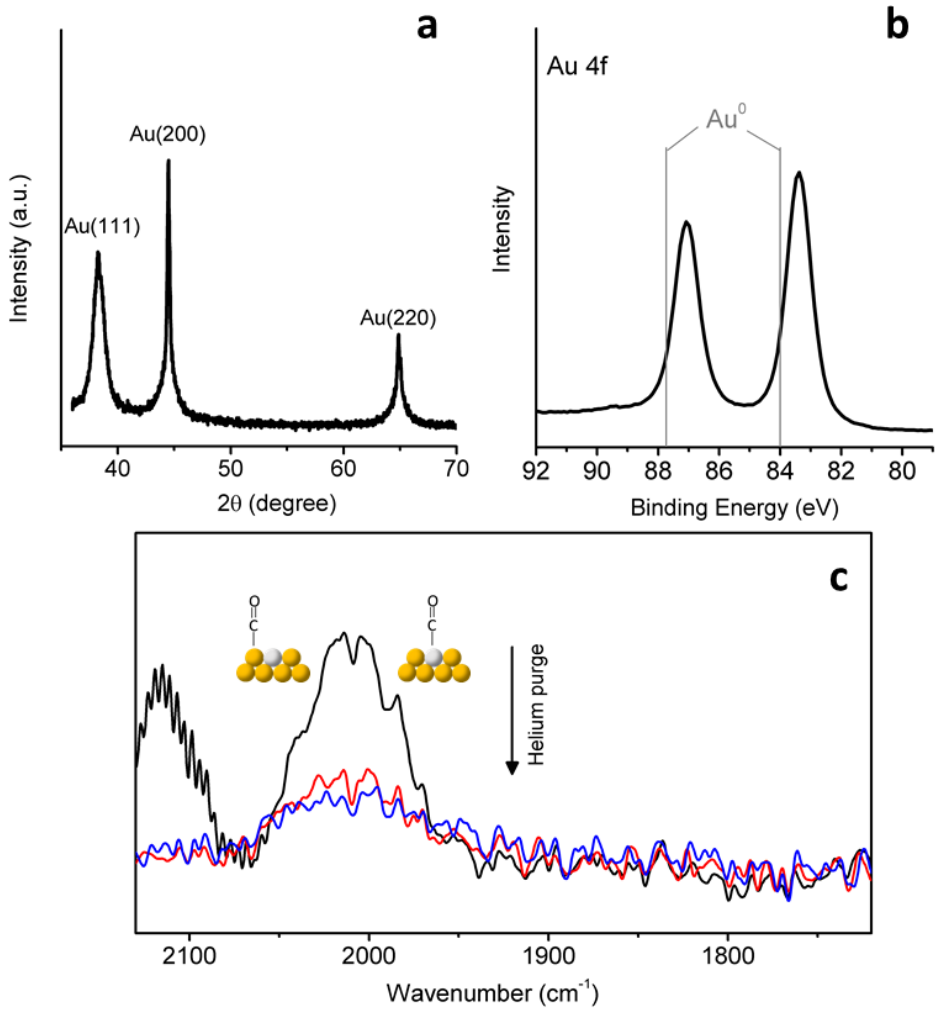

Figure 6.12. Characterization of used PdAu-SAA/SiO_2 catalysts. (a) XRD, (b) XPS and (c) CO-DRIFTS. The tests were performed on spent catalysts without further treatment at ambient temperature.

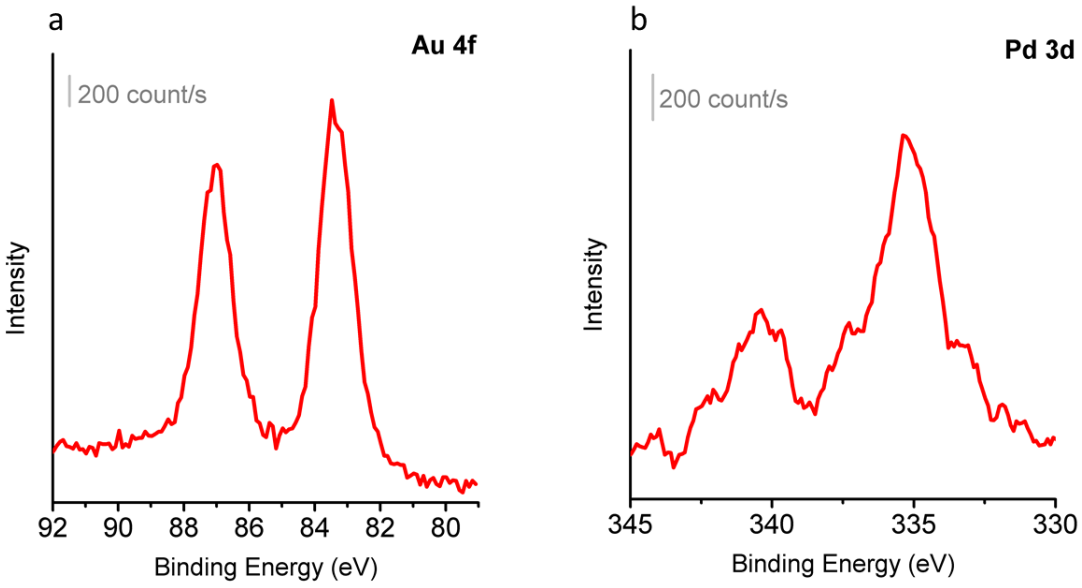

Figure 6.13. XPS of $Pd_{0.2}Au$ bimetallic catalysts.

To investigate the surface composition of PdAu catalysts, we performed XPS on a higher Pd loading sample, which is $Pd_{0.2}Au$. In this sample the bulk Pd to Au ratio is 0.2. As shown in Figure 6.14, both Au and Pd are in the metallic states. The surface Pd/Au ratio calculated with XPS data is 3/2, which indicates the Pd segregates to the surface of PdAu bimetallic NPs.

FTIR studies

To investigate the 1-hexyne hydrogenation on PdAu-SAA catalysts, FTIR spectroscopy was performed with DRIFTS and ATR reaction cells. As shown in Figure 6.14, DRIFTS spectra were collected following a dose of 1-hexyne (2 μL) in the pure hydrogen gas stream. The peaks at 2966, 2941 and 2877-2865 cm^{-1} are assigned to v(C-H) in CH_2 and CH_3 groups. They are very

similar to the same features in the liquid 1-hexyne spectra (Figure 6.16). This shows these is no significant perturbation in the saturated part of the 1-hexyne molecules upon adsorption on the catalysts. The peaks between 3335 and 3296 cm^{-1} are assigned to v(≡C-H). The peaks are broadening after adsorption compared to the liquid 1-hexyne, similar effects were observed on adsorbed phenylacetylene on Pt catalysts before.[61] The peak at 2112 cm^{-1} is assigned to the v(C≡C), while the v(C≡C) of liquid 1-hexyne is at 2119 cm^{-1}.

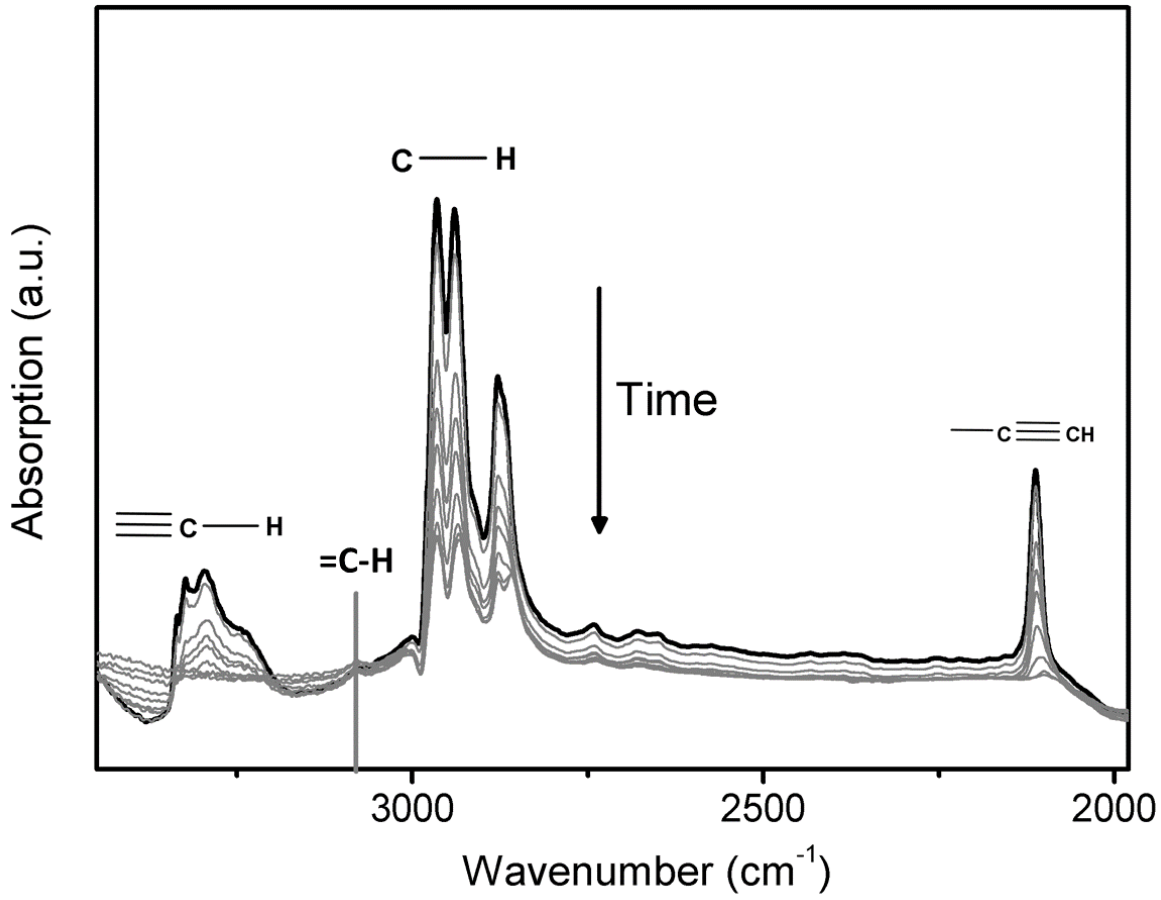

Figure 6.14. DRIFTS spectra recorded when 1-hexyne and H_2 are carried over PdAu-SAA/SiO_2 catalyst.

A peak at 3081 cm^{-1} appears after a short period of time following 1-hexyne dose (Figure 6.15). This peak is assigned to v(=C-H). We find a similar v(=C-H) peak when 1-hexene and helium are carried over PdAu-SAA/SiO_2 catalyst. However, we do not see this peak when 1-hexyne and H_2 are carried over silica support. This is a direct evidence of the conversion of 1-hexyne to 1-hexene at room temperature. The 1-hexene formed on the surface of PdAu NPs has a certain residence time and can be desorbed and re-adsorbed on the PdAu NPs or on the silica support. The v(=C-H) of all these species of 1-hexene can be detected.

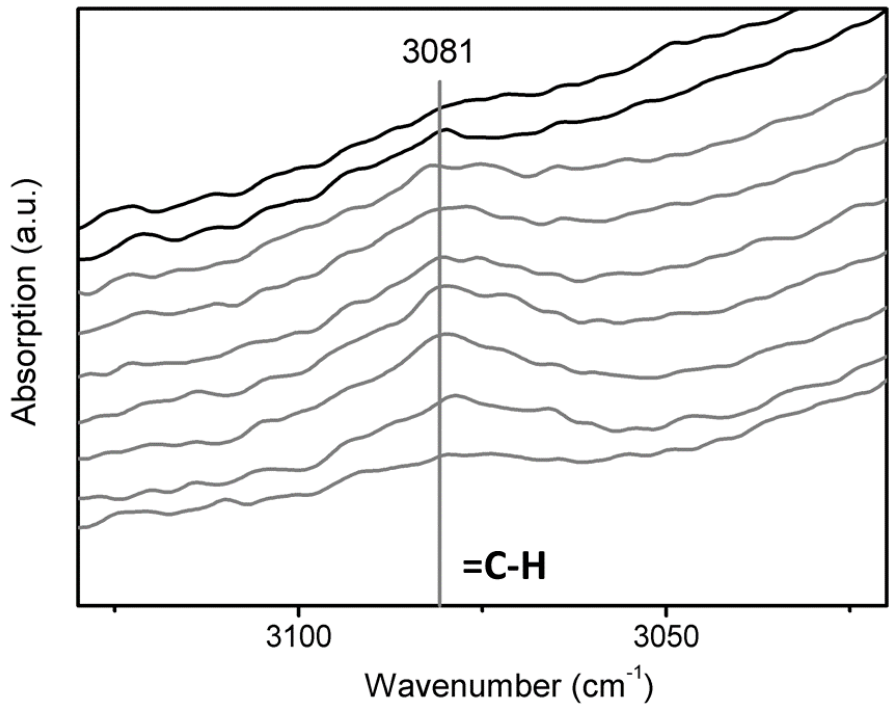

Figure 6.15. DRIFTS spectra between 3130 and 3120 cm^{-1} recorded when 1-hexyne and H_2 are carried over PdAu-SAA/SiO_2 catalyst.

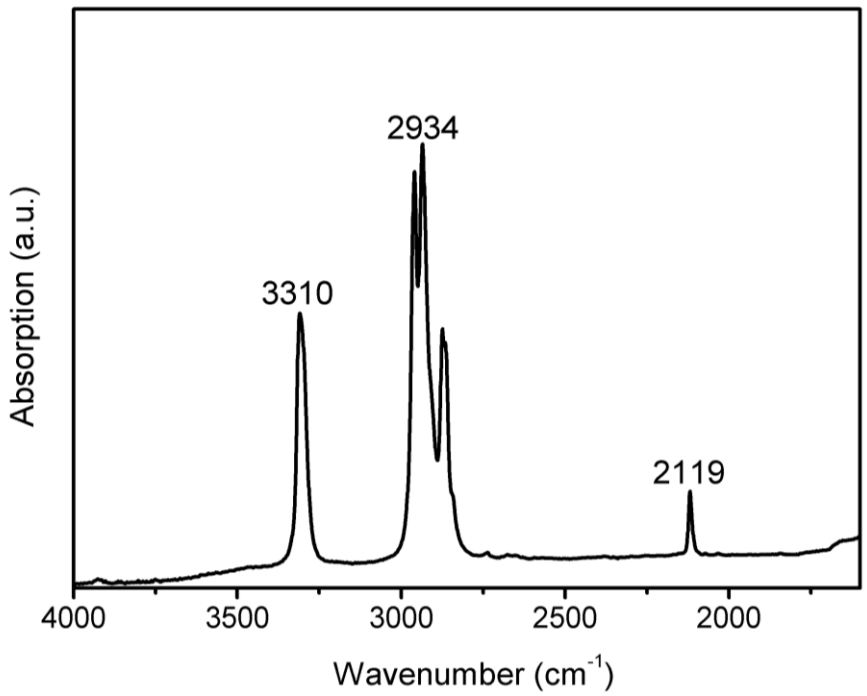

Figure 6.16. IR spectra of liquid 1-hexyne collected with ATR accessory.

As shown in Figure 6.17, we observed a peak centered at around 3580 cm^{-1} and an adjacent negative peak at higher wavenumbers when carrying 1-hexyne and H_2 over PdAu-SAA/SiO_2 catalyst. The 3583 cm^{-1} peak is assigned to a 1-hexyne species π-adsorbed on the OH group of silica.[62] The negative peak has been reported previously, which is likely due to the perturbation of the silanol group on silica.

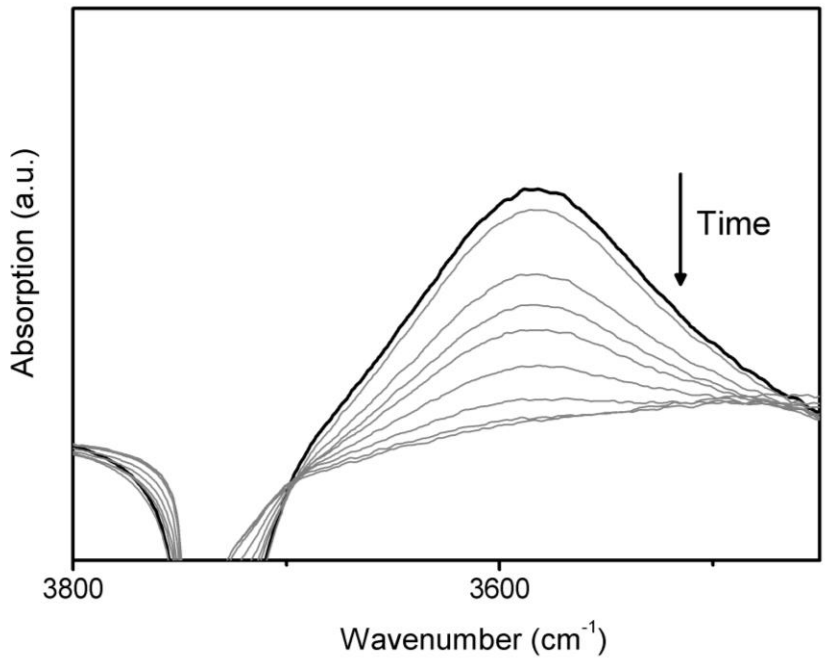

Figure 6.17. DRIFTS spectra between 3800 and 3450 cm^{-1} recorded when 1-hexyne and H_2 are carried over PdAu-SAA/SiO_2 catalyst.

The DRIFTS spectra recorded when carry 1-hexyne and H_2 over silica support are shown in Figure 6.18 and 6.19. The peaks at 2966, 2941, 2879 and 2870 cm^{-1} are assigned to v(C-H). They are at very similar positions as that of PdAu/SiO_2. A peak at 2115 cm^{-1} is assigned to v(C≡C), which is slightly higher (3 cm^{-1}) than that of PdAu/SiO_2. We observed a broad absorption band centered at ~ 3335 – 3316 cm^{-1} ascribed to v(C≡C-H) as shown in Figure 6.19B. At the meantime, multiple peaks are shown for the PdAu/SiO_2 sample (Figure 6.14) at 3335, 3323, 3296 cm^{-1} and a shoulder band at around 3260 cm^{-1} in the v(C≡C-H) region. The differences between them is very likely due to the adsorption on PdAu NPs. We can also see a broad peak around 3700-3500 cm^{-1} corresponding to 1-hexyne species π-adsorbed on the OH group of

silica.[62] This confirms the adsorption of 1-hexyne on silica support. We flow 1-hexyne and H_2 over silica support but did not observe any evidence to show the formation of 1-hexene.

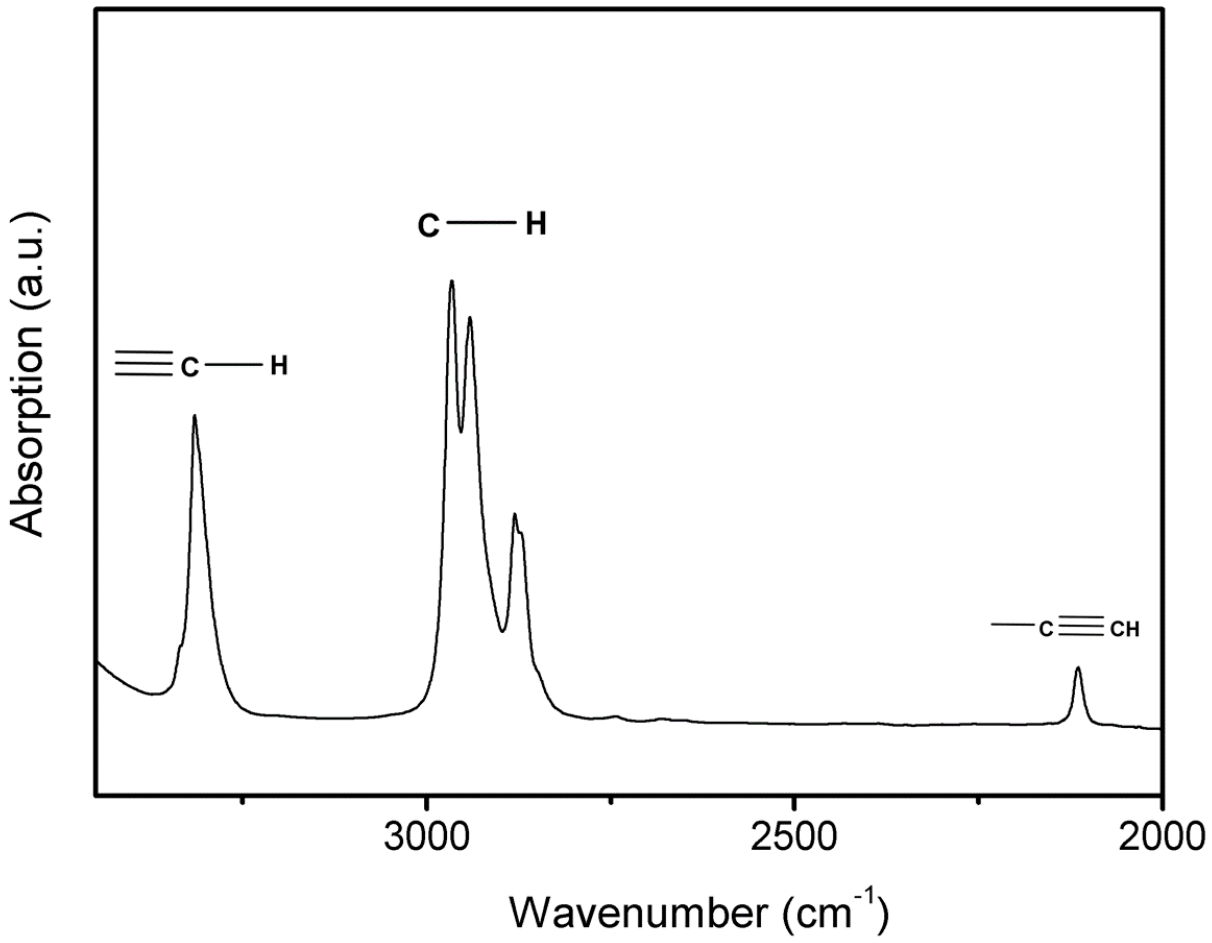

Figure 6.18. DRIFTS spectra between 3450 and 2000 cm^{-1} recorded when 1-hexyne and H_2 are carried over silica.

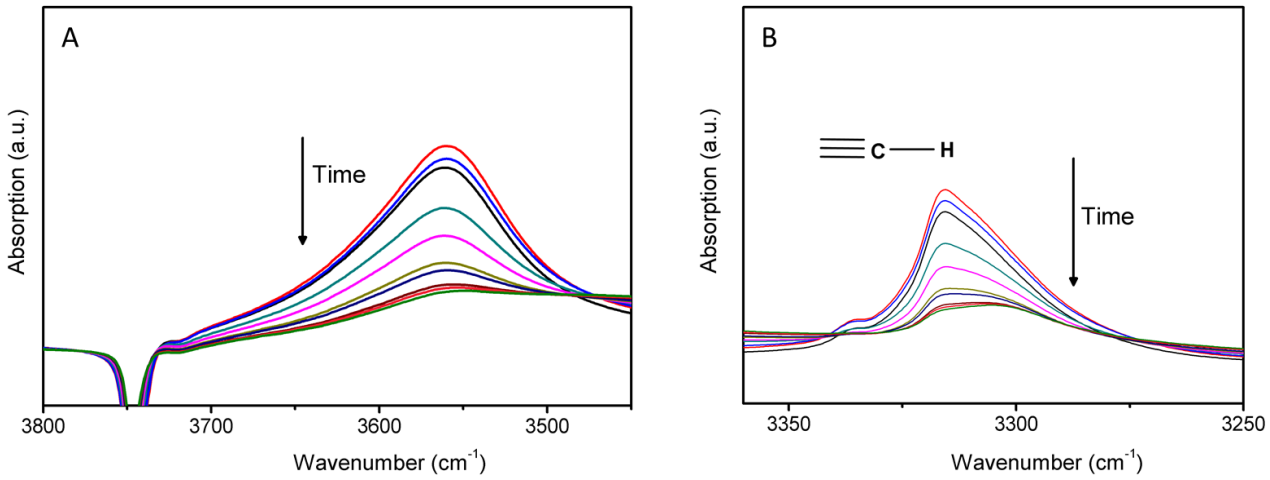

Figure 6.19. DRIFTS spectra between (A) 3800 and 3450 cm^{-1} and (B) 3360 and 3250 cm^{-1} recorded when 1-hexyne and H_2 are carried over silica.

The catalytic performance studies were performed in a batch reactor with liquid phase 1-hexyne and above ambient pressure of H_2. To better mimic the hydrogenation reaction conditions, we used an ATR reaction cell with liquid phase 1-hexyne and 120 psi H_2 applied to the PdAu-SAA catalysts without support.

As shown in Figure 6.20, 6.22 and 6.23, the IR spectra were recorded over the course of the hydrogenation reactions. In the spectra of H_2-hexyne over $Pd_{0.004}Au$-SAA system, the v(≡C-H) is at 3306 cm^{-1}, the v(C-H) are at 2960, 2934, 2902, 2873 and 2864 cm^{-1}, while the v(C≡C) is centered at 2117 cm^{-1}. The peak positions are very similar to that in the DRIFTS studies. The v(C≡C) band is broadened compared to the liquid 1-hexyne (Figure 6.16), which is in agreement with that has been reported in the literature. The peak intensity of v(C≡C) and v(≡C-H) decrease over the time while the peak intensity of v(C-H) essentially unchanged, this captures the

conversion of 1-hexyne in the hydrogenation conditions. The peak at 3080 cm^{-1} is ascribed to v(=C-H), which appears under the reaction condition (Figure 6.21), showing the formation of hexene molecules.

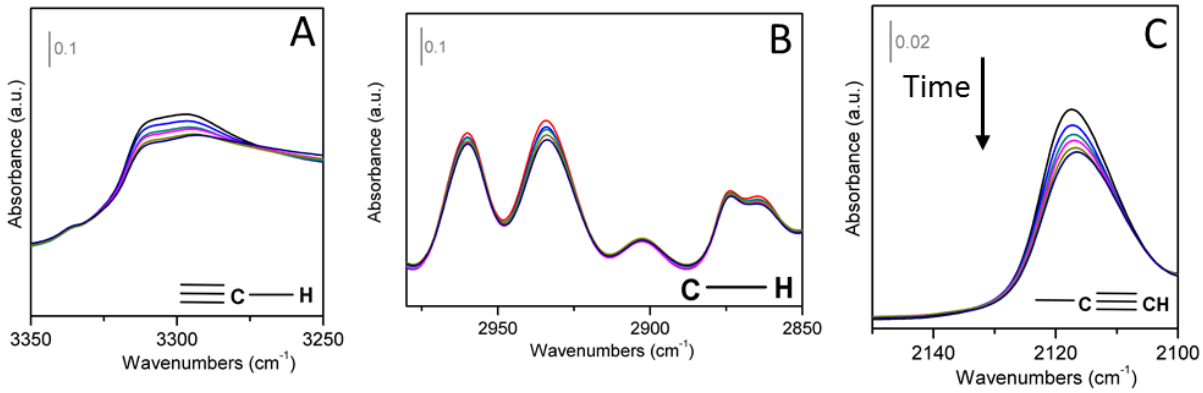

Figure 6.20. ATR-IR collected with 1-hexyne and 120 psi H_2 applied on $Pd_{0.004}Au$-SAA catalysts in the batch mode at room temperature.

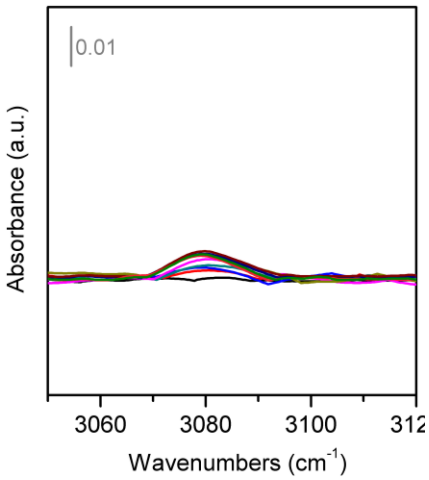

Figure 6.21. ATR-IR collected with 1-hexyne and 120 psi H_2 applied on $Pd_{0.004}Au$-SAA catalysts in the batch mode at room temperature.

We also conducted ATR-IR with a $Pd_{0.01}Au$ sample, which was prepared with the same method as $Pd_{0.004}Au$ -SAA but with higher Pd loadings. CO-FTIR finds no bridge CO adsorbed on this sample. The data are shown in Figure 6.22. The broad band centered at 3306 cm^{-1} is assigned to v(≡C-H), the peaks at 2960, 2933, 2902, 2873, 2862 cm^{-1} are assigned to v(C-H) modes and the peak at 2115 cm^{-1} is ascribed to v(C≡C).

Similarly, we observed the evolution of v(≡C-H), v(C-H) and v(C≡C) over $Pd_{0.2}Au$ sample (Figure 6.23), which is an even higher Pd loading sample that CO-FTIR shows bridge CO.

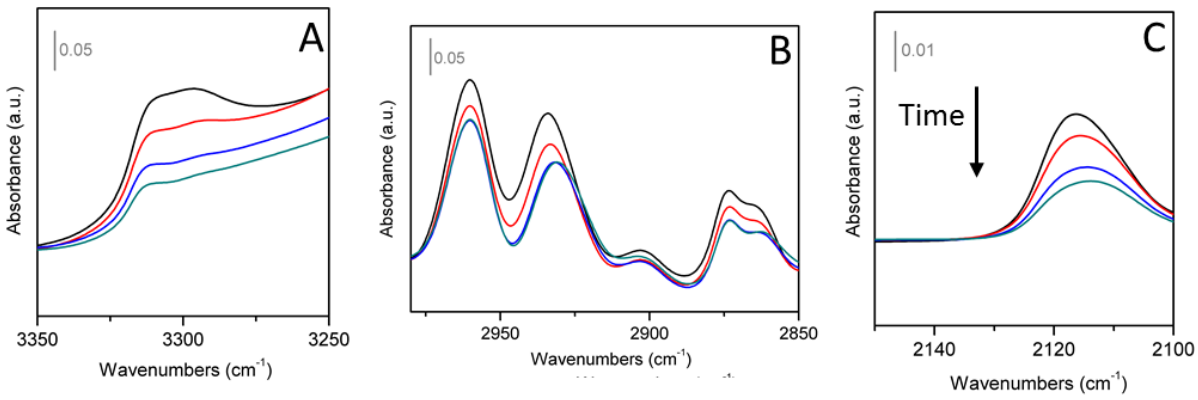

Figure 6.22. ATR-IR collected with 1-hexyne and 120 psi H_2 applied on $Pd_{0.01}Au$ catalysts in the batch mode at room temperature.

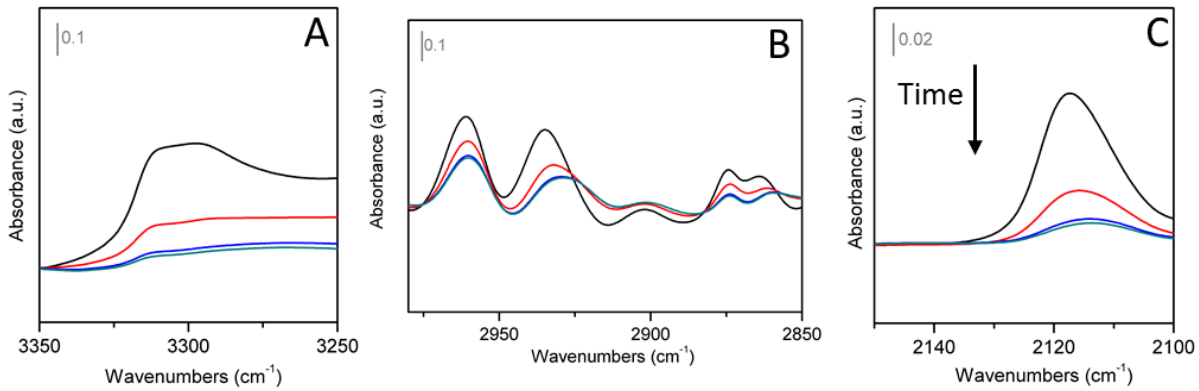

Figure 6.23. ATR-IR collected with 1-hexyne and 120 psi H_2 applied on $Pd_{0.2}Au$ catalysts in the batch mode at room temperature.

The ATR-IR results are in good agreement with the DRIFTS data for 1-hexyne hydrogenation reactions over PdAu catalysts. ATR-IR mimics the batch reactor conditions while DRIFTS is in flow mode. The PdAu SAA catalysts were thoroughly characterized with both techniques. We demonstrated the conversion of 1-hexyne to hexene *in situ*. 1-hexyne adsorbed on the catalysts mainly through the non-dissociative fashion as we did not detect any dissociative adsorbed species through the conversion of 1-hexyne. 1-hexyne can be adsorbed on the silica support but cannot be hydrogenated by the silica.

To quantify the adsorption of 1-hexyne on the PdAu-SAA catalysts, we performed TGA of the catalyst pellets in nitrogen with different 1-hexyne concentrations, as shown in Figure 6.24. It corroborates the FTIR results that 1-hexyne adsorbed on both silica support and PdAu-SAA NPs. At 60 °C, the adsorption of 1-hexyne is much less than at 30 °C.

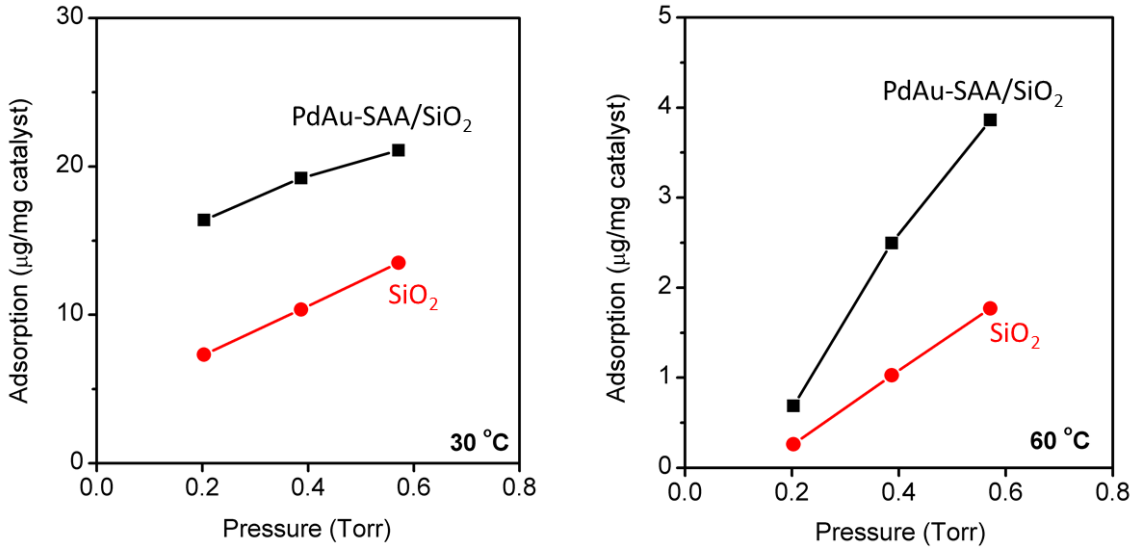

Figure 6.24. 1-hexyne adsorption isotherm at 30 and 60 °C.

Kinetics Studies

Comparing PdAu-SAA NP and Au NP catalysts, we observed a remarkable increase in hydrogenation activity of PdAu-SAA. Figure 6.25 compares the initial reaction rate normalized by the total Au loading between the two catalysts. It shows the reactivity is improved tenfold with the addition of a small amount of Pd (0.4 at.%) to the Au NPs. The rate-limiting step of hydrogenation on Au NPs at ambient temperature is hydrogen activation, and the single-atom Pd sites efficiently catalyse hydrogen dissociation as shown in Figure 6.25B. To confirm this in the PdAu NPs, we performed H_2-D_2 exchange experiments on PdAu-SAA/SiO_2 and Au/SiO_2, where HD production is a reporter of the H_2 activation capability of the catalysts. Figure 6.25B shows the temperature-programmed HD production for both catalysts. At the same Au loading, PdAu-SAA/SiO_2 shows much higher HD production rate than Au/SiO_2. This indicates that single

Pd atoms in the surface of Au NPs effectively catalyze the H_2 activation. The reaction rate per surface Pd atom on PdAu-SAA/SiO_2 is lower than that of the monometallic Pd catalysts.

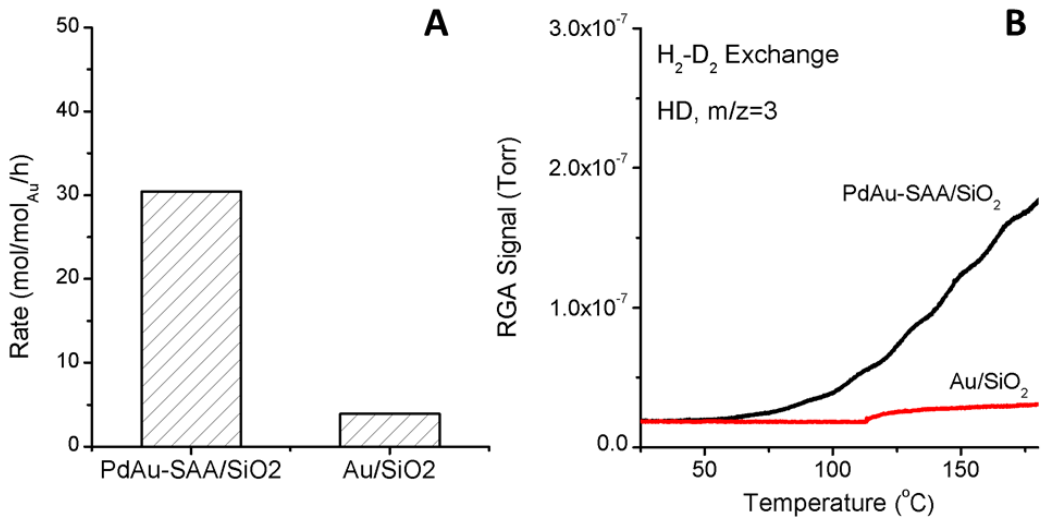

Figure 6.25. Hydrogenation of 1-hexyne. (A) Reaction rate of PdAu-SAA/SiO_2 and Au/SiO_2. Reaction condition: 1% hexyne-ethanol solution, 5 bar H_2, 600 rpm, 25 ^oC. (B) H_2-D_2 exchange TPSR of PdAu-SAA/SiO_2 and Au/SiO_2 catalysts. H_2-D_2 exchange: 10% H_2, 10% D_2, balance Argon, 50 mL/min, 5 °C/min.

Comparing the initial rate over Pd-NP and PdAu-SAA catalysts in Figure 6.26, we found the rate per surface Pd atom was lower on PdAu-SAA. However, the selectivity PdAu-SAA to partial hydrogenation products is significantly higher than that of Pd/SiO_2. The decreased reactivity is likely due to the ligand effects through alloying with Au and the limited availability of adsorbed hydrogen on PdAu-SAA compared to that of Pd-NP.

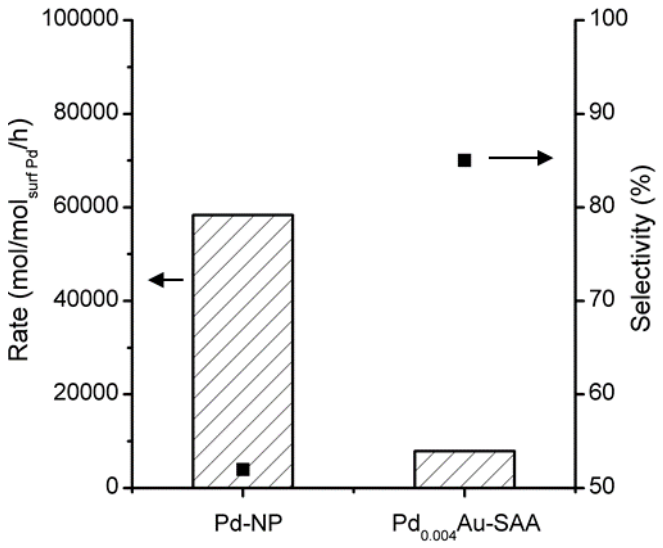

Figure 6.26. 1-hexyne hydrogenation reaction rate and the selectivity to 1-hexene at 100% conversion of 1-hexyne with Pd-NP (5% Pd/SiO_2) and $PdAu\text{-}SAA/SiO_2$ catalysts. Reaction condition: 1% hexyne-ethanol solution, 5 bar H_2, 600 rpm, 25 ^oC.

In Figure 6.27, we compare the hydrogenation rate over Pd/SiO_2 and $PdAu\text{-}SAA/SiO_2$ in an Arrhenius-type plot. The PdAu-SAA shows lower activity per Pd atom than monometallic Pd. The apparent activation energy of monometallic Pd is around 26.7 kJ/mol, while the apparent activation energy of PdAu-SAA is around 41.2 kJ/mol. The difference in apparent activation energy indicates different reaction pathway or rate limiting steps. Considering monometallic Pd catalysts, hydrogenation activation is a facile process, while on the monometallic Au catalysts, the rate limiting step is hydrogenation activation. PdAu-SAA is a novel class of hydrogenation catalysts and its rate limiting step has not yet been determined.

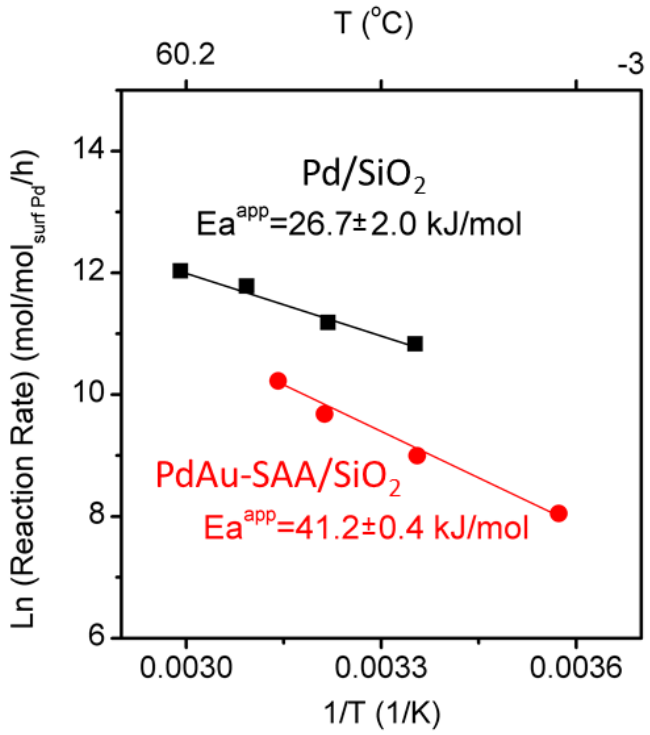

Figure 6.27. Arrhenius type plot of 1-hexyne selective hydrogenation over 5% Pd/SiO_2 and $PdAu\text{-}SAA/SiO_2$ catalysts. Reaction conditions: 1% hexyne-ethanol solution, 5 bar H_2, 600 rpm, 6-70 °C.

To study the rate determining step of hydrogenation over PdAu-SAA catalysts, we performed kinetics isotope effect (KIE) measurements, as shown in Figure 6.28. In this study, either H_2 or D_2 was used in the selective hydrogenation of 1-hexyne at the same experimental conditions. We observed significant KIE with $R_{H2}/R_{D2} = 1.87$. This indicates the hydrogen is involved in the rate limiting step in hydrogenation reactions over these catalysts.

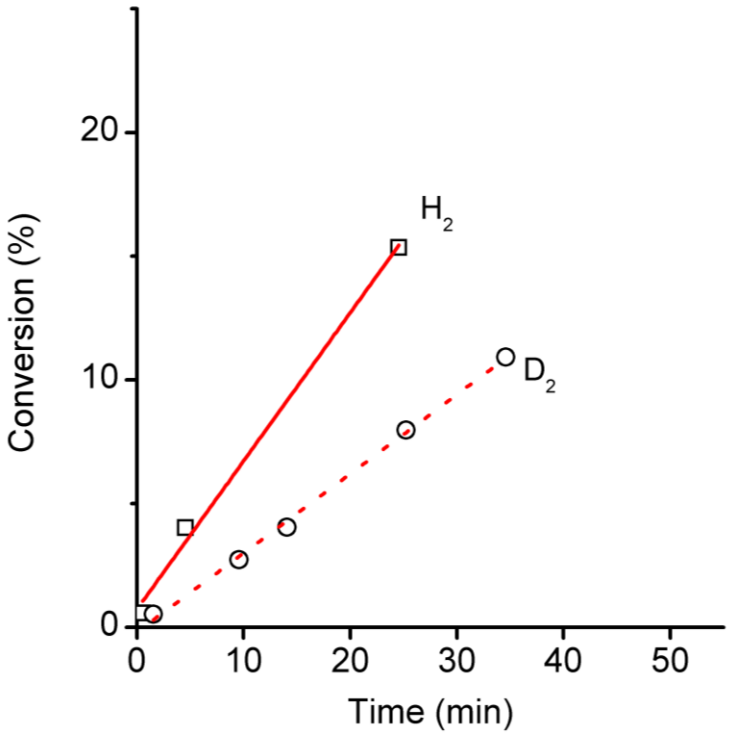

Figure 6.28. KIE measurements. The conversion vs. reaction time for 1-hexyne hydrogenation with PdAu-SAA/SiO_2 catalysts. The initial rate is calculated from the slope of the conversion-time curve. Reaction condition: 1% hexyne-ethanol solution, 5 bar H_2 or D_2, 600 rpm, 25 ^oC.

To further understand the kinetics of 1-hexyne hydrogenation over PdAu-SAA catalysts, we performed reaction order measurements, as shown in Figure 6.29. The reaction rate of 1-hexyne hydrogenation is linearly correlated with the H_2 pressure (Figure 6.29 A), which reveals first order kinetics to H_2.[63,64] While the reaction order to 1-hexyne appears to be zero as the reaction rate is independent of the concentration of 1-hexyne between 0.5 and 1.5% (Figure 6.29 B). Combined with the results of KIE studies, we conclude the rate limiting step in 1-hexyne hydrogenation with PdAu-SAA catalyst is hydrogen activation. These results also corroborate

the surface science TPD results that 1-hexyne adsorbs on the PdAu surface much stronger than hydrogen atoms.

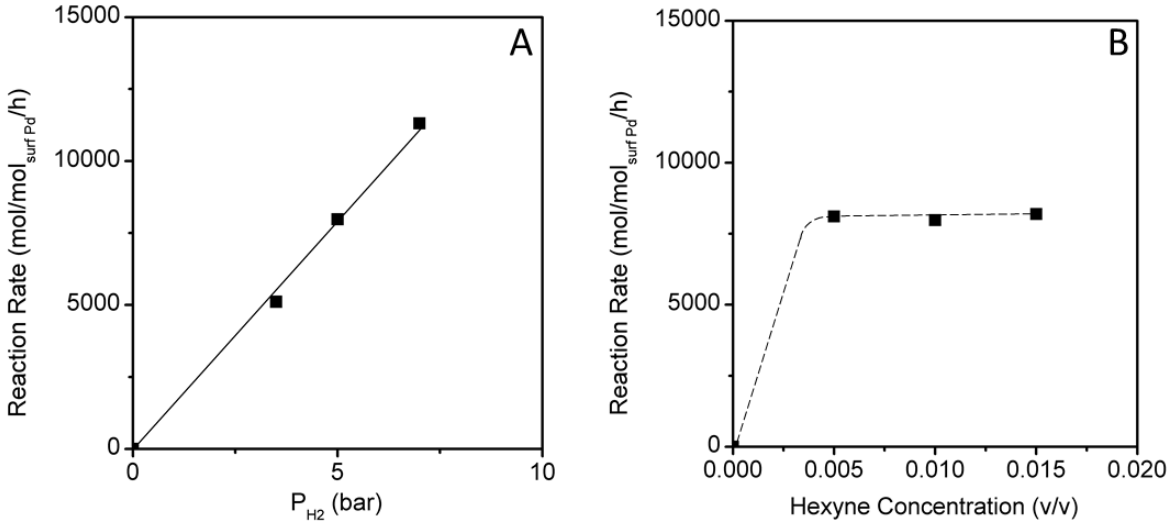

Figure 6.29. Reaction order to H_2 and 1-hexyne. (A) The reaction rate was measured with 1% 1-hexyne and 3-7.5 bar H_2, 600 rpm, 25 ^oC. (B) The reaction rate was measured with 0.5-1.5% 1-hexyne, 5 bar H_2, 600 rpm, 25 ^oC.

We investigated the H_2-D_2 exchange with PdAu SAA catalysts. H_2-D_2 exchange includes two steps, H_2 dissociative adsorption and desorption. Gellman et al. devised a mathematical model to describe the H_2-D_2 exchange on Pd-Cu alloys and fitted their experimental data to the model to calculate the energy barriers. When the H_2 partial pressure is low and conversion of H_2 and D_2 is low, the HD concentration in the outlet is approximately proportional to exp(-E_{ads}/RT). Thus, the apparent activation energy of H_2-D_2 exchange to produce HD can reflect the H_2 activation barrier. As shown in Figure 6.30, the results of steady state H_2-D_2 exchange are put in an Arrhenius-type plot. The apparent activation energy calculated from it is 41.9 kJ/mol,

which is essentially the same as that of apparent activation energy of 1-hexyne hydrogenation over PdAu-SAA catalysts. Thus, the rate limiting step in 1-hexyne hydrogenation is the hydrogenation activation.

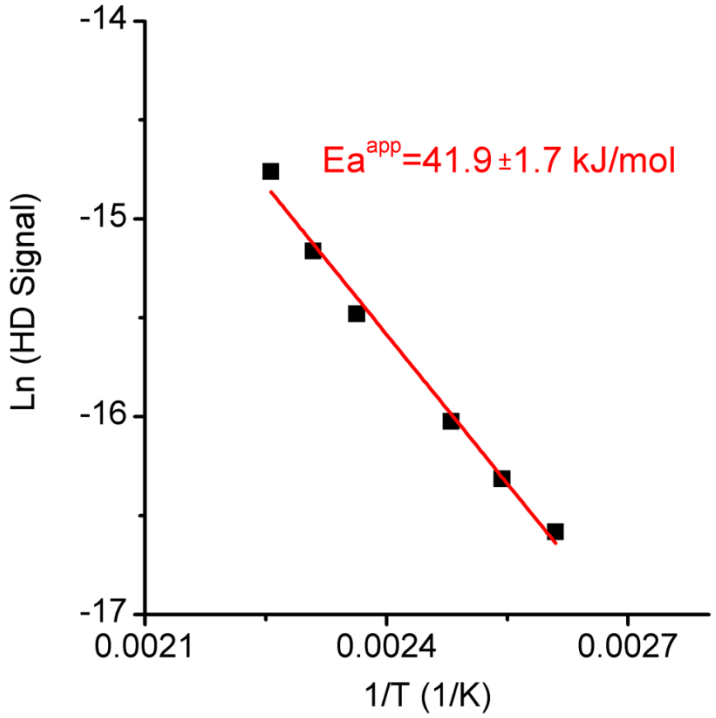

Figure 6.30. Arrhenius-type plot of H_2-D_2 exchange over PdAu-SAA/SiO_2 catalysts. The RGA intensity of HD is proportional to the concentration of HD. Reaction condition: H_2-D_2 exchange: 10% H_2, 10% D_2, balance Argon, 50 mL/min, 170-110 ^oC.

In selective hydrogenation processes, alkyne and alkene hydrogenation are two competing processes. Pd is active for both reactions, but the favorable adsorption of alkyne over alkene leads to selective hydrogenation of alkyne to alkene especially at low

conversion.[38,65,66] But with the increase of alkyne conversion, the alkyne surface coverage is reduced, and the selectivity to alkene is decreased. On the Cu catalysts, the alkene desorption barrier is lower than on Pd and the alkene hydrogenation barrier is higher than on Pd, which results in the desorption of reactively formed alkene instead of over-hydrogenation[52]. Thus, Cu is intrinsically more selective than Pd in hydrogenation reactions. For Au NP catalysts, the low-coordination sites are believed to be the active sites, since the hydrogen activation barrier on Au terraces is too high.[67] The favorable adsorption of alkynes compared to alkenes on the low-coordination Au sites determines the high selectivity of Au catalysts in selective hydrogenation. When single-atom Pd is added to the Au surface, the low-coordination Au sites are no-longer necessary for hydrogenation activation. The hydrogenation chemistry of single Pd atom and the surrounding Au atoms is of great interest in understanding the selective hydrogenation with PdAu-SAA catalysts.

Besides the kinetics studies reported in this thesis, surface science techniques and DFT calculations are employed by our collaborators to investigate the PdAu SAA system for selective hydrogenation of 1-hexyne. DFT calculations indicate the most stable adsorption site of 1-hexyne molecules is the bridged Pd-Au site, while the 1-hexene molecule favorably adsorbs in the atop configuration on the single-atom Pd sites. However, on the Pd surface, 1-hexyne adsorbs at the 3-fold hollow sites and 1-hexene adsorbs atop on one Pd atom. The adsorption sites for 1-hexyne on PdAu-SAA and Pd(111) are different. Moreover, the adsorption strength of 1-hexyne and 1-hexene was calculated with DFT and from TPD results. The values calculated with the two methods are in good agreement with each other. We find the addition of single-atom Pd stabilizes the adsorption of both 1-hexyne and 1-hexene, while the adsorption

strengths of 1-hexyne and 1-hexene are comparable. This indicates the favorable adsorption of 1-hexyne over 1-hexene no longer holds for PdAu-SAA catalysts. In other words, 1-hexyne hydrogenation is not thermodynamically favorable compared to 1-hexene hydrogenation on PdAu-SAA catalysts.

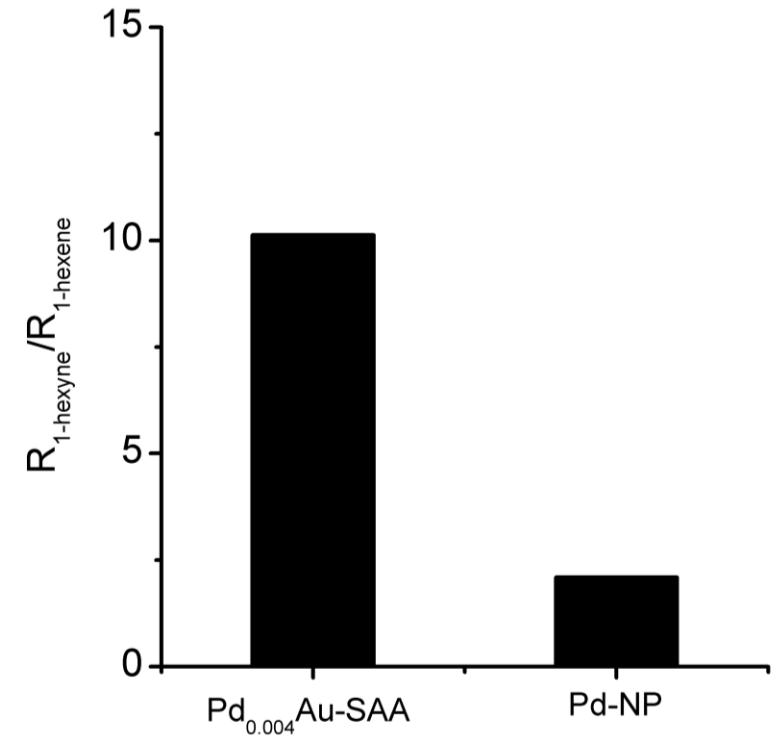

Figure 6.31. Reaction rate ratio of 1-hexyne hydrogenation over 1-hexene hydrogenation of PdAu-SAA/SiO_2 and Pd/SiO_2 catalysts. Reaction conditions: 1% hexane - or hexene-ethanol solution, 5 bar H_2, 600 rpm, 25 ^oC.

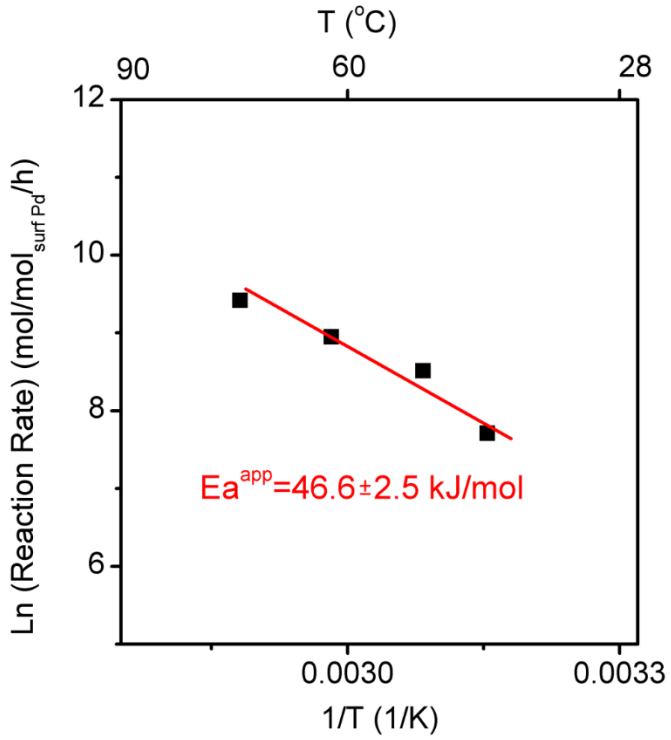

Figure 6.32. Arrhenius-type plot of 1-hexene hydrogenation over PdAu-SAA/SiO_2 catalysts. Reaction condition: 1% hexene-ethanol solution, 5 bar H_2, 600 rpm.

To better understand the hydrogenation selectivity of PdAu-SAA catalysts, we compared the reaction rate of 1-hexyne hydrogenation with that of 1-hexene hydrogenation. As shown in Figure 6.31, the 1-hexyne hydrogenation rate is one-order-of-magnitude higher than that of 1-hexene over PdAu-SAA catalysts, which reveals a highly selective hydrogenation kinetics. However, the difference between 1-hexyne and 1-hexene hydrogenation rate over Pd-NP catalysts is less than that. Indeed, the apparent activation energy of 1-hexene hydrogenation is higher than that of 1-hexyne over PdAu-SAA catalysts, as shown in Figure 6.32.

6.4 Summary

In this work, we have demonstrated that PdAu SAA catalysts have excellent selectivity and stable activity for the hydrogenation of 1-hexyne to 1-hexene. PdAu SAA NPs were synthesized through a sequential reduction approach with a Pd/Au ratio of 1/250, and the exclusive presence of isolated single-atom Pd sites in the surface of Au NPs was confirmed by CO-IR. We found the hydrogenation activity of Au NPs was enhanced 10-fold through addition of this small amount of Pd atoms in the Au surface. This is attributed to the improved hydrogen activation on PdAu SAA NPs. Moreover, high selectivity to 1-hexene was achieved. PdAu SAA NPs retain stable structure and longer-term activity in the hydrogenation reaction in the liquid phase. The properties of the PdAu SAA NPs were rationalized by examining the model catalyst analogues in which a different amount of Pd was alloyed into the surface of Au(111). STM found that Pd atoms were isolated in Au(111) when the Pd coverage was low, while CO- and H_2-TPD showed weaker binding of CO and low-temperature uptake and release of H_2 on the single Pd atom sites as compared to Pd(111). Thus, PdAu SAAs can be used for the selective hydrogenation of alkynes to alkenes and serve as practical stable catalysts for these reactions under industrially relevant conditions. This study also provides a well-defined catalytic material that can be applied in a wide range of reactions including oxidation and dehydrogenation reactions.

The selective hydrogenation of 1-hexyne was investigated with IR in DRIFTS and ATR reaction cells. We observed the adsorption of 1-hexyne on both metal NPs and the silica supports. No IR peaks for dissociative adsorption species were detected. The

conversion of 1-hexyne and formation of 1-hexene were investigated under the reaction condition with liquid phase 1-hexyne and above-ambient pressure hydrogen.

Moreover, we demonstrated a different selective hydrogenation chemistry over PdAu SAA catalysts compared to that of monometallic Pd. DFT calculations reveal 1-hexyne adsorbed on the three-fold sites on extended Pd surface, but on the Pd-Au bridge sites on the surface of PdAu SAA. The two catalysts showed different reactivity, selectivity and apparent activation energy. The role of single-atom Pd in the surface of Au NPs is to activate the hydrogen molecules and stabilize the adsorption of reactant and product molecules, which activate the otherwise inert Au surface for selective hydrogenation of 1-hexyne. Moreover, PdAu SAA catalysts are more active for the 1-hexyne hydrogenation than the 1-hexene hydrogenation, such that PdAu SAAs are demonstrated as a class of highly selective catalysts for alkyne conversion selectively to alkenes.

Overall, this work demonstrates that the SAA approach can be applied in the design of various bimetallic catalysts to achieve high selectivity and reactivity.

6.5 References

1. Chen B, Dingerdissen U, Krauter JGE, et al. New developments in hydrogenation catalysis particularly in synthesis of fine and intermediate chemicals. *Appl Catal A Gen*. 2005;280(1):17-46. doi:10.1016/j.apcata.2004.08.025.

2. Kyriakou G, Boucher MB, Jewell a. D, et al. Isolated Metal Atom Geometries as a Strategy

for Selective Heterogeneous Hydrogenations. *Science*. 2012;335(6073):1209-1212.

3. Boucher MB, Zugic B, Cladaras G, et al. Single atom alloy surface analogs in Pd0.18Cu15 nanoparticles for selective hydrogenation reactions. *Phys Chem Chem Phys*. 2013;15:12187-12196. doi:10.1039/c3cp51538a.

4. Liu P, Zhao Y, Qin R, et al. Photochemical route for synthesizing atomically dispersed palladium catalysts. *Science*. 2016;352(6287):797-801. doi:10.1126/science.aaf5251.

5. Yan H, Cheng H, Yi H, et al. Single-Atom Pd_1/Graphene Catalyst Achieved by Atomic Layer Deposition: Remarkable Performance in Selective Hydrogenation of 1,3-Butadiene. *J Am Chem Soc*. 2015;137(33):10484-10487. doi:10.1021/jacs.5b06485.

6. Vilé G, Albani D, Nachtegaal M, et al. A stable single-site palladium catalyst for hydrogenations. *Angew Chem Int Ed Engl*. 2015;54(38):11265-11269. doi:10.1002/anie.201505073.

7. Vilé G, Albani D, Almora-Barrios N, López N, Pérez-Ramírez J. Advances in the Design of Nanostructured Catalysts for Selective Hydrogenation. *ChemCatChem*. 2016;8(1):21-33. doi:10.1002/cctc.201501269.

8. Zhang H, Watanabe T, Okumura M, Haruta M, Toshima N. Catalytically highly active top gold atom on palladium nanocluster. *Nat Mater*. 2011;11(1):49-52.

9. Xie S, Tsunoyama H, Kurashige W, Negishi Y, Tsukuda T. Enhancement in Aerobic Alcohol Oxidation Catalysis of Au 25 Clusters by Single Pd Atom Doping. *ACS Catal*. 2012;2(7):1519-1523. doi:10.1021/cs300252g.

10. Ab Rahim MH, Forde MM, Jenkins RL, et al. Oxidation of Methane to Methanol with Hydrogen Peroxide Using Supported Gold-Palladium Alloy Nanoparticles. *Angew Chemie*. 2013;125(4):1318-1322. doi:10.1002/ange.201207717.

11. Personick ML, Madix RJ, Friend CM. Selective Oxygen-Assisted Reactions of Alcohols and Amines Catalyzed by Metallic Gold: Paradigms for the Design of Catalytic Processes. *ACS Catal*. 2017;7(2):965-985. doi:10.1021/acscatal.6b02693.

12. Choudhary TV, Sivadinarayana C, Datye AK, Kumar D, Goodman DW. Acetylene Hydrogenation on Au-Based Catalysts. *Catal Letters*. 2003;86(1):1-8. doi:10.1023/A:1022694505504.

13. Pawelec B, Venezia AM, La Parola V, Cano-Serrano E, Campos-Martin JM, Fierro JLG. AuPd alloy formation in Au-Pd/Al2O3 catalysts and its role on aromatics hydrogenation. *Appl Surf Sci*. 2005;242(3-4):380-391. doi:10.1016/j.apsusc.2004.09.004.

14. Sárkány A, Horváth A, Beck A. Hydrogenation of acetylene over low loaded Pd and Pd-Au/SiO2 catalysts. *Appl Catal A Gen*. 2002;229(1-2):117-125. doi:10.1016/S0926-860X(02)00020-0.

15. Piccolo L, Piednoir A, Bertolini J-C. Pd–Au single-crystal surfaces: Segregation properties and catalytic activity in the selective hydrogenation of 1,3-butadiene. *Surf Sci*. 2005;592(1-3):169-181. doi:10.1016/j.susc.2005.07.005.

16. Miura H, Terasaka M, Oki K, Matsuda T. Preparation of Egg-Shell Type Pd-Ag and Pd-Au Catalysts by Selective Deposition and Hydrogenation of 1,3-Butadiene. *Stud Surf Sci*

Catal. 1993;75:2379-2382.

17. Kittisakmontree P, Pongthawornsakun B, Yoshida H, Fujita S, Arai M, Panpranot J. The liquid-phase hydrogenation of 1-heptyne over Pd–Au/TiO2 catalysts prepared by the combination of incipient wetness impregnation and deposition–precipitation. *J Catal*. 2013;297:155-164. doi:10.1016/j.jcat.2012.10.007.

18. Sárkány A, Geszti O, Sáfrán G. Preparation of Pdshell–Aucore/SiO2 catalyst and catalytic activity for acetylene hydrogenation. *Appl Catal A Gen*. 2008;350(2):157-163. doi:10.1016/j.apcata.2008.08.012.

19. Zhang Y, Diao W, Williams CT, Monnier JR. Selective hydrogenation of acetylene in excess ethylene using Ag- and Au–Pd/SiO2 bimetallic catalysts prepared by electroless deposition. *Appl Catal A Gen*. 2014;469:419-426. doi:10.1016/j.apcata.2013.10.024.

20. Zhang L, Wang A, Miller T, et al. E ffi cient and Durable Au Alloyed Pd Single-Atom Catalyst for the Ullmann Reaction of Aryl Chlorides in Water. *ACS Catal*. 2014;4:1546-1553.

21. Chen M, Kumar D, Yi C-W, Goodman DW. The promotional effect of gold in catalysis by palladium-gold. *Science*. 2005;310(5746):291-293. doi:10.1126/science.1115800.

22. Yu W-Y, Mullen GM, Flaherty DW, Mullins CB. Selective Hydrogen Production from Formic Acid Decomposition on Pd–Au Bimetallic Surfaces. *J Am Chem Soc*. 2014;136(31):11070-11078. doi:10.1021/ja505192v.

23. Edwards J, Solsona B, Landon P, et al. Direct synthesis of hydrogen peroxide from H2 and

O2 using TiO2-supported Au–Pd catalysts. *J Catal*. 2005;236(1):69-79. doi:10.1016/j.jcat.2005.09.015.

24. Jirkovský JS, Panas I, Ahlberg E, Halasa M, Romani S, Schiffrin DJ. Single Atom Hot-Spots at Au–Pd Nanoalloys for Electrocatalytic H 2 O 2 Production. *J Am Chem Soc*. 2011;133(48):19432-19441. doi:10.1021/ja206477z.

25. Edwards JK, Solsona B, N EN, et al. Switching Off Hydrogen Peroxide Hydrogenation in the Direct Synthesis Process. *Science*. 2009;323(5917):1037-1041. doi:10.1126/science.1168980.

26. Gao F, Goodman DW. Pd–Au bimetallic catalysts: understanding alloy effects from planar models and (supported) nanoparticles. *Chem Soc Rev*. 2012;41(24):8009. doi:10.1039/c2cs35160a.

27. Hutchings GJ. Nanocrystalline gold and gold palladium alloy catalysts for chemical synthesis. *Chem Commun*. 2008;(10):1148-1164. doi:10.1039/B712305C.

28. Zhang L, Xie Z, Gong J. Shape-controlled synthesis of Au–Pd bimetallic nanocrystals for catalytic applications. *Chem Soc Rev*. 2016;45(14):3916-3934. doi:10.1039/C5CS00958H.

29. Zhang H, Watanabe T, Okumura M, Haruta M, Toshima N. Catalytically highly active top gold atom on palladium nanocluster. *Nat Mater*. 2011;11(1):49-52. doi:10.1038/nmat3143.

30. Luo W, Sankar M, Beale AM, et al. High performing and stable supported nano-alloys for the catalytic hydrogenation of levulinic acid to γ-valerolactone. *Nat Commun*.

2015;6:6540. doi:10.1038/ncomms7540.

31. Jia J, Haraki K, Kondo JN, Domen K, Tamaru K. Selective Hydrogenation of Acetylene over Au/Al2O3 Catalyst. *J Phys Chem B*. 2000;104(47):11153-11156. doi:10.1021/jp001213d.

32. Miura H, Endo K, Ogawa R, Shishido T. Supported Palladium–Gold Alloy Catalysts for Efficient and Selective Hydrosilylation under Mild Conditions with Isolated Single Palladium Atoms in Alloy Nanoparticles as the Main Active Site. *ACS Catal*. January 2017:1543-1553. doi:10.1021/acscatal.6b02767.

33. Kolli N El, Delannoy L, Louis C. Bimetallic Au–Pd catalysts for selective hydrogenation of butadiene: Influence of the preparation method on catalytic properties. *J Catal*. 2013;297:79-92. doi:10.1016/j.jcat.2012.09.022.

34. Pei GX, Liu XY, Wang A, et al. Promotional effect of Pd single atoms on Au nanoparticles supported on silica for the selective hydrogenation of acetylene in excess ethylene. *New J Chem*. 2014;38(5):2043. doi:10.1039/c3nj01136d.

35. Tedsree K, Li T, Jones S, et al. Hydrogen production from formic acid decomposition at room temperature using a Ag-Pd core-shell nanocatalyst. *Nat Nanotechnol*. 2011;6(5):302-307. doi:10.1038/nnano.2011.42.

36. Cao S, Monnier JR, Regalbuto JR. Alkali promotion of alumina-supported ruthenium catalysts for hydrogenation of levulinic acid to γ-valerolactone. *J Catal*. 2017;347:72-78. doi:10.1016/j.jcat.2017.01.009.

37. Garbarino G, Wang C, Valsamakis I, et al. Acido-basicity of lanthana/alumina catalysts

and their activity in ethanol conversion. *Appl Catal B Environ*. 2017;200:458-468. doi:10.1016/j.apcatb.2016.07.010.

38. Henning AM, Watt J, Miedziak PJ, et al. Gold-palladium core-shell nanocrystals with size and shape control optimized for catalytic performance. *Angew Chemie - Int Ed*. 2013;52(5):1477-1480.

39. Lucci FR, Darby MT, Mattera MFG, et al. Controlling Hydrogen Activation, Spillover, and Desorption with Pd-Au Single-Atom Alloys. *J Phys Chem Lett*. 2016;7:480-485. doi:10.1021/acs.jpclett.5b02400.

40. Tedsree K, Li T, Jones S, et al. Hydrogen production from formic acid decomposition at room temperature using a Ag-Pd core-shell nanocatalyst. *Nat Nanotechnol*. 2011;6(5):302-307.

41. Tan S, Sun X, Williams CT. In situ ATR-IR study of prochiral 2-methyl-2-pentenoic acid adsorption on Al2O3 and Pd/Al2O3. *Phys Chem Chem Phys*. 2011;13(43):19573. doi:10.1039/c1cp21660k.

42. Tan S, Williams CT. An In Situ Spectroscopic Study of Prochiral Reactant–Chiral Modifier Interactions on Palladium Catalyst: Case of Alkenoic Acid and Cinchonidine in Various Solvents. *J Phys Chem C*. 2013;117(35):18043-18052. doi:10.1021/jp403273c.

43. Groppo E, Bertarione S, Rotunno F, et al. Role of the Support in Determining the Vibrational Properties of Carbonyls Formed on Pd Supported on SiO2 −Al2 O3 , Al2O3 , and MgO. *J Phys Chem C*. 2007;111(19):7021-7028. doi:10.1021/jp0666434.

44. Cao S, Monnier JR, Williams CT, Diao W, Regalbuto JR. Rational nanoparticle synthesis to determine the effects of size, support, and K dopant on Ru activity for levulinic acid hydrogenation to γ-valerolactone. *J Catal*. 2015;326:69-81. doi:10.1016/j.jcat.2015.03.004.

45. Hugon A, Delannoy L, Krafft J-M, Louis C. Selective Hydrogenation of 1,3-Butadiene in the Presence of an Excess of Alkenes over Supported Bimetallic Gold−Palladium Catalysts. *J Phys Chem C*. 2010;114(24):10823-10835. doi:10.1021/jp100479b.

46. Crespo-Quesada M, Dykeman RR, Laurenczy G, Dyson PJ, Kiwi-Minsker L. Supported nitrogen-modified Pd nanoparticles for the selective hydrogenation of 1-hexyne. *J Catal*. 2011;279(1):66-74. doi:10.1016/j.jcat.2011.01.003.

47. Semagina N, Renken A, Kiwi-Minsker L. Palladium Nanoparticle Size Effect in 1-Hexyne Selective Hydrogenation. *J Phys Chem C*. 2007;111(37):13933-13937. doi:10.1021/jp073944k.

48. Albani D, Vilé G, Mitchell S, et al. Ligand ordering determines the catalytic response of hybrid palladium nanoparticles in hydrogenation. *Catal Sci Technol*. 2016;6(6):1621-1631. doi:10.1039/C5CY01921D.

49. Lucci FR, Liu J, Marcinkowski MD, et al. Selective hydrogenation of 1,3-butadiene on platinum–copper alloys at the single-atom limit. *Nat Commun*. 2015;6:8550.

50. Liu J, Lucci FR, Yang M, et al. Tackling CO Poisoning with Single-Atom Alloy Catalysts. *J Am Chem Soc*. 2016;138(20):6396-6399. doi:10.1021/jacs.6b03339.

51. Yu W-Y, Mullen GM, Mullins CB. Interactions of Hydrogen and Carbon Monoxide on Pd–Au Bimetallic Surfaces. *J Phys Chem C*. 2014;118(4):2129-2137. doi:10.1021/jp411299e.

52. Studt F, Abild-Pedersen F, Bligaard T, Sorensen RZ, Christensen CH, Norskov JK. Identification of Non-Precious Metal Alloy Catalysts for Selective Hydrogenation of Acetylene. *Science*. 2008;320(5881):1320-1322. doi:10.1126/science.1156660.

53. Studt F, Abild-Pedersen F, Bligaard T, Sørensen RZ, Christensen CH, Nørskov JK. On the Role of Surface Modifications of Palladium Catalysts in the Selective Hydrogenation of Acetylene. *Angew Chemie Int Ed*. 2008;47(48):9299-9302. doi:10.1002/anie.200802844.

54. Venezia A, La Parola V, Deganello G, Fierro JLG. Synergetic effect of gold in Au/Pd catalysts during hydrodesulfurization reactions of model compounds. *J Catal*. 2003;215(2):317-325. doi:10.1016/S0021-9517(03)00005-8.

55. Rodriguez J. Physical and chemical properties of bimetallic surfaces. *Surf Sci Rep*. 1996;24(7-8):223-287. doi:10.1016/0167-5729(96)00004-0.

56. Vilé G, Albani D, Nachtegaal M, et al. A stable single-site palladium catalyst for hydrogenations. *Angew Chem Int Ed Engl*. 2015;54(38):11265-11269. doi:10.1002/anie.201505073.

57. Shan J, Lucci FR, Liu J, et al. Water co-catalyzed selective dehydrogenation of methanol to formaldehyde and hydrogen. *Surf Sci*. February 2016. doi:10.1016/j.susc.2016.02.010.

58. Shan J, Janvelyan N, Li H, et al. Selective non-oxidative dehydrogenation of ethanol to acetaldehyde and hydrogen on highly dilute NiCu alloys. *Appl Catal B Environ*.

2017;205:541-550. doi:10.1016/j.apcatb.2016.12.045.

59. Marcinkowski MD, Liu J, Murphy CJ, et al. Selective Formic Acid Dehydrogenation on Pt-Cu Single-Atom Alloys. *ACS Catal*. December 2016:413-420. doi:10.1021/acscatal.6b02772.

60. Chen Y, Wang H, Liu C-J, et al. Formation of monometallic Au and Pd and bimetallic Au–Pd nanoparticles confined in mesopores via Ar glow-discharge plasma reduction and their catalytic applications in aerobic oxidation of benzyl alcohol. *J Catal*. 2012;289:105-117. doi:10.1016/j.jcat.2012.01.020.

61. Liu W, Otero Arean C, Bordiga S, Groppo E, Zecchina A. Selective Phenylacetylene Hydrogenation on a Polymer-Supported Palladium Catalyst Monitored by FTIR Spectroscopy. *ChemCatChem*. 2011;3(1):222-226. doi:10.1002/cctc.201000244.

62. Maetz P, Saussey J, Lavalley JC, Touroude R. Hydrogenation of But-1-yne on Platinum/Silica Catalysts: An in Situ Dynamic Infrared Study. *J Catal*. 1994;147(1):48-56. doi:10.1006/jcat.1994.1113.

63. Horiuti J, Miyahara K. *Ydrogenation of Ethylene on Metallic Catalysts*. US Department of Commerce, National Bureau of Standards; 1968.

64. Bond GC. *Metal-Catalysed Reactions of Hydrocarbons*. Springer US; 2005. doi:10.1007/b136857.

65. Arnold H, Döbert F, Gaube J. Selective Hydrogenation of Hydrocarbons. In: *Handbook of Heterogeneous Catalysis*. ; 2008:3266-3283.

66. Silvestre-Albero J, Sepulveda-Escribano A, Rodriguez-Reinoso F, Anderson JA. Influence of Zn on the characteristics and catalytic behavior of TiO2-supported Pt catalysts. *J Catal*. 2004;223:179-190. doi:10.1016/j.jcat.2004.01.019.

67. Segura Y, López N, Pérez-Ramírez J. Origin of the superior hydrogenation selectivity of gold nanoparticles in alkyne + alkene mixtures: Triple- versus double-bond activation. *J Catal*. 2007;247(2):383-386.

Chapter 7. Conclusions and Recommendations

7.1 Conclusions

This thesis reports the preparation of single-atom alloy (SAA) nanoparticle (NP) catalysts. With well controlled galvanic replacement methods, PtCu SAA NPs were formulated on alumina and silica supports. Using a variety of characterization techniques including EDS, STEM, *in situ* FTIR, XRD, *in situ* XANES and *in situ* EXAFS, the presence of isolated Pt atoms in the surface of Cu NPs was demonstrated. Moreover, the PdAu SAA NP catalysts were prepared with sequential reduction method with silica support or unsupported.

This novel class of catalysts is of great fundamental and practical importance: First, SAA NPs are the ideal platform materials in studying the chemical reactions in the single-atom sites under ambient pressure conditions. Unlike the conventional bimetallic catalysts, where single atoms, clusters and monometallic NPs co-exist, SAA NPs contain only single-atom sites in the surface of the host metal. SAAs indeed effectively bridge the materials gap between NP catalysts and model catalyst single crystals. We and our collaborators performed catalysis, surface science and DFT studies and found good convergence in the results from different sides. This capability enabled us to understand the specific chemical reactions from the molecular level to reactor level.

Second, SAA NP catalysts provide the solutions to many practical challenges in the Pt group metal (PGM) catalysts. PGMs are among the most widely used transition metal catalysts due to their superior catalytic performance for both dehydrogenation and hydrogenation reactions. Despite their favorable reactivity, there are three major drawbacks of PGM catalysts.

First, PGMs, especially Pt and Pd are very expensive, which imposes major limitations on their future role in catalysis. Second, the intrinsic selectivity of monometallic PGMs is low for hydrogenation and dehydrogenation at high conversions. Third, Pt and Pd are susceptible to carbon monoxide (CO) poisoning because CO binds strongly to metallic Pt and Pd. Indeed, SAAs are the hybrid systems containing only the minimum number of Pt (or Pd) sites necessary to perform or to assist a target reaction that retain most of the high activity of Pt (or Pd), at similar high selectivity as that of the host metal (Cu, Au), and increase the PGM tolerance to CO poisoning.

Following the invention of the SAA catalysts, we have applied them in the selective hydrogenation of 1,3-butadiene, CO tolerant H_2 activation, coke resistant selective dehydrogenation of butane, selective hydrogenation of 1-hexyne, selective dehydrogenation of methanol, selective dehydrogenation of ethanol and selective dehydrogenation of formic acid reactions. This thesis reports on the first four reactions among them. For selective hydrogenation and dehydrogenation reactions, the selectivity to partial hydrogenation/dehydrogenation products is very important. SAA catalysts with exclusive single-atom Pt or Pd sites largely avoid the side reactions and prove to be highly selective and stable for these reactions.

In PtCu SAA catalysts, Pt single atoms lower the hydrogen activation and desorption barrier on Cu, and enable the hydrogenation on Cu with spillover of hydrogen. With the addition of a small amount of Pt single atoms in the surface of Cu NPs, the 1,3-butadiene hydrogenation activity is improved more than one order of magnitude, while the high selectivity to butenes is maintained. In the presence of excess propylene, the PtCu SAA catalysts

are still highly selective in 1,3-butandiene hydrogenation to butenes with less than 1% conversion of propylene. Moreover, the PtCu SAA catalysts are highly stable in the hydrogenation reaction conditions.

PtCu SAAs are highly CO tolerant due to the electronic effects in SAAs. The alloying of Pt with Cu alters the electronic properties of Pt leading to weak adsorption of CO. Thus, PtCu SAA catalysts show higher CO tolerance compared to monometallic Pt catalysts from near ambient temperature to 200 °C with CO concentration from 200ppm to 3.3%. For instance, PtCu SAA shows one order of magnitude higher H_2 activation activity than monometallic Pt at 150 °C with 3.3% CO in the gas phase. In the practical low temperature and low CO partial pressure conditions (200 ppm CO, 70 °C), PtCu SAA shows much higher CO tolerance compared to monometallic Pt. Moreover, the interaction between SAA surface and CO molecules was studied with CO-FTIR and corroborative surface science studies. Therefore, the PtCu SAA is a promising candidate for improvement of many CO-poisoned systems, such as fuel cell electrocatalysts.

Pt is the most often used metal catalyst for alkane dehydrogenation reactions in industry, and its alloys with Sn are coke resistant to a certain extent but still need considerable coke removal treatments in the reaction process. In alkane dehydrogenation reactions, the first C-H activation is the rate limiting step. PtCu SAA can combine the C-H activation chemistry of single-atom Pt and the weak bonding nature of the Cu surface, which is ideal for coke resistance C-H activation. Our flow reactor studies demonstrate that with the addition of single-atom Pt in the surface of Cu, the “light off” temperature of C-H activation is lowered by almost 300 °C. Single-atom Pt, the smallest possible and most material efficient Pt ensemble, is enough

to facilitate the C-H activation in the surface of Cu. Moreover, PtCu SAA catalysts show excellent coke resistance in the C-H activation processes. This is indeed due to the highly selective nature of SAA catalysts, while the undesired by-product in this case is carbon coke. On extended Pt surfaces, the strong binding between Pt and reactively formed molecules lead to the over-dehydrogenation and other side reactions. But PtCu SAA binds the molecules weakly, the uphill energy barrier for over-dehydrogenation makes the desorption of the reactively formed molecules more favorable. The PtCu SAA catalysts were applied in the selective dehydrogenation of butane to butene under practical reaction conditions. They showed considerable reactivity with high stability without carbon deposition for at least 50 hours. The apparent activation energy of butane dehydrogenation over PtCu SAA is higher than that of monometallic Pt, indicating different energy landscape of the two catalysts.

In sum, this thesis has investigated the selective hydrogenation, CO-tolerant hydrogen activation and selective dehydrogenation reactions with PtCu SAA catalysts. For both selective hydrogenation and selective dehydrogenation reactions, commercial catalysts based on Pt or Pd are available, where Pt or Pd are in the bulk phase with additives to improve the selectivity or stability. In this thesis, we introduced a new SAA design idea for the selective hydrogenation and dehydrogenation catalysts. The Pt ensembles are designed as single-atom sites and loaded into the surface of Cu to activate the otherwise inert Cu for these reactions. The single-atom Pt can catalyze the rate limiting steps in these reactions but cannot catalyze the undesired side reaction. Although the rate limiting steps in selective hydrogenation and dehydrogenation are H_2 and C-H activation, respectively, which are the two reactions at the two ends of the spectrum of activation barrier, single-atom Pt is effective in both. On the other hand, Cu binds

the reactant and product molecules weakly, which makes it intrinsically selective. PtCu SAA is indeed a bifunctional catalytic system. We postulate that the SAA approach can be applied to a wide range of bimetallic systems for different reactions to design highly selective and stable catalysts. Indeed, the SAA strategy will become important for the "rational catalyst design" tool set.

Furthermore, to demonstrate the applicability of the SAA strategy in other catalytic systems, we designed and prepared PdAu SAA NP catalysts. A sequential reduction method was developed as galvanic replacement is not possible for Pd-Au. We find PdAu SAA catalysts are highly reactive and selective in partial hydrogenation of 1-hexyne to 1-hexene in the liquid phase. They have stable activity and selectivity without leaching. The kinetics studies find that PdAu SAAs have different reactivity, selectivity and apparent activation energy compared to monometallic Pd, revealing different hydrogenation chemistries. The role of single-atom Pd sites is to activate the hydrogen molecules, which is the rate limiting step, and stabilize the adsorption of reactant and product molecules. The surface science and DFT studies were performed to extend the understanding of PdAu SAA catalysts. Their results corroborate the findings in catalysis and *in operando* FTIR studies at ambient and above ambient pressures.

7.2 Recommendations

SAA catalysts based on Pt and Pd have shown promising performance in various selective hydrogenation and dehydrogenation reactions. To investigate Ni based SAA catalysts will be of great interest in decreasing the use of precious metals and providing the high-

performance catalysts for other reactions. Giannakakis et al. has demonstrated NiAu SAAs as the selective and active catalysts for the non-oxidative dehydrogenation of ethanol to acetaldehyde.[1] Resent work by Shan et al. shows the alcohol dehydrogenation reactivity and selectivity of NiCu SAA catalysts. NiCu SAA appears to be more reactive in C-H bond breaking in alcohols compared to PtCu and PdCu SAAs.[2] The NiCu SAA catalysts might be good candidates for a wide variety of selective dehydrogenation and oxidation reactions of hydrocarbons and alcohols. Moreover, DFT calculations performed by Stamatakis et al. show stronger adsorption of CO on Ni based SAAs compared to monometallic Ni, unlike the weaker adsorption on PtCu and PdCu SAAs. This suggests a different alloying effect in Ni-Cu, which might be useful for reactions such as water gas shift and CO oxidation reactions.

I recommend evaluating the reaction network and developing the reaction kinetics models for the selective hydrogenation and dehydrogenation reactions with PtCu SAA catalysts. The activation energy of each elementary steps can also be obtained. Through comparing the reaction mechanisms between PtCu SAA, Cu and Pt catalysts, we will be able to evaluate the structure-function relationship in the SAA catalysts. These results would indicate the nature of the active sites for the different reaction steps and which one is the rate-determining-step. This would extend our understanding of the SAA as a bifunctional catalyst. It would also be useful to identify reactions for which this is not a bifunctional catalyst. I also suggest performing the microkinetic modeling with the DFT-derived parameters to gain insight into the mechanistic aspects of the catalyst activity and guide further improvement of the SAA catalysts.

References

1. Giannakakis G, Trimpalis A, Shan J, et al. NiAu Single Atom Alloys for the Non-oxidative Dehydrogenation of Ethanol to Acetaldehyde and Hydrogen. *Top Catal*. 2018;61(5-6):475-486. doi:10.1007/s11244-017-0883-0.

2. Shan J, Janvelyan N, Li H, et al. Selective non-oxidative dehydrogenation of ethanol to acetaldehyde and hydrogen on highly dilute NiCu alloys. *Appl Catal B Environ*. 2017;205:541-550. doi:10.1016/j.apcatb.2016.12.045.